

Caenorhabditis elegans model of tauopathy

Dissertation

zur Erlangung des Doktorgrades der Naturwissenschaften

vorgelegt im Fachbereich Biologie
der Fakultät für Mathematik, Informatik und Naturwissenschaften
der Universität Hamburg

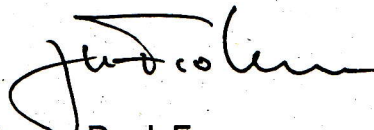
von

Pir Ghulam Jeelani
aus Jammu und Kashmir, India

Hamburg
März, 2013

Genehmigt vom Fachbereich Biologie
der Fakultät für Mathematik, Informatik und Naturwissenschaften
an der Universität Hamburg
auf Antrag von Professor Dr. E. MANDELKOW
Weiterer Gutachter der Dissertation:
Professor Dr. M. KNEUSSEL
Tag der Disputation: 14. Dezember 2012

Hamburg, den 30. November 2012

A handwritten signature in black ink, appearing to read 'J. Fromm', is positioned above the printed name.

Professor Dr. J. Fromm
Vorsitzender des Promotionsausschusses
Biologie

Table of Contents

1	Introduction.....	1
1.1	Protein misfolding diseases.....	1
1.2	Alzheimer disease (AD)	3
1.3	Tau: A microtubule-associated protein	5
1.3.1	Localization and functions of Tau protein	5
1.3.2	Isoforms of Tau	8
1.4	Frontotemporal dementia and Parkinsonism linked to chromosome 17 (FTDP-17).....	10
1.5	Tau aggregation.....	12
1.6	Tau phosphorylation	13
1.7	Other modifications of Tau protein.....	16
1.8	Tau degradation	18
1.9	Amyloid-β cascade hypothesis	20
1.10	Connection between Aβ and Tau	22
1.11	<i>Caenorhabditis elegans</i> as a model organism	23
1.12	<i>C. elegans</i> life cycle	25
1.13	Evolution of <i>C. elegans</i> and its significance in biomedical studies.....	27
1.14	Tau like protein in <i>C. elegans</i>.....	29
1.15	Human tauopathy models in <i>C. elegans</i>	30
1.15.1	Kraemer B.C. et al., 2003	30
1.15.2	T. Miyasaka et al., 2005.....	31
1.15.3	R. Brandt et al., 2007	32
2	MATERIALS AND METHODS	35
2.1	Materials	35
2.1.1	Chemicals.....	35
2.1.2	Enzymes.....	35
2.1.3	Antibodies	35
2.1.4	Molecular weight markers	36
2.1.5	Kits	36
2.1.6	Vectors.....	36
2.1.7	Bacterial strains for cloning.....	37
2.1.8	Antibiotics	37
2.1.9	Bacterial media	37

2.1.10	<i>C. elegans</i> media, buffers and chemicals	37
2.1.11	Cell culture media and reagents	39
2.1.12	Software	39
2.1.13	List of equipments	39
2.1.14	List of buffers	40
2.2	Methods.....	41
2.2.1	Molecular biological methods.....	41
2.2.2	<i>C. elegans</i> methods	50
2.2.3	Biochemical methods	60
3	RESULTS	65
3.1	Single worm PCR confirms the presence of transgenes.....	65
3.2	Western blot analysis for tau-transgenic expression.....	67
3.3	2.5% perchloric acid extraction of tau.....	68
3.4	Full-length tau along with the F3 fragment leads to uncoordinated phenotype	69
3.5	Pro-aggregant strain shows a relatively delayed clearance of food.....	71
3.6	Pro-aggregant worms have a shorter life-span	72
3.7	Full-length tau along with the F3 fragment leads to aggregation (ThS Staining).....	73
3.8	Pro-aggregation tau combination leads to the deposition of aggregates right at day 1 of adulthood.....	74
3.9	RNAi against tau ameliorates the phenotype	76
3.10	Aggregation increases with age more prominently in pro-aggregant line	77
3.11	Full-length tau along with the F3 fragment leads to gaps in the motor neurons	79
3.12	Tau is phosphorylated to a higher extent in the pro-aggregant <i>C. elegans</i> line	81
3.13	Pro-aggregant animals accumulate higher oligomeric species	84
3.14	Accumulation of synaptobrevin-1 in the presynaptic areas of the pro-aggregant line	86
3.15	Mitochondria get mislocalized in the DA9 motor neuron of the pro-aggregant line	88
3.16	Defective axonal transport in the mechanosensory neurons of the pro-aggregant line	90
3.17	Compound treatment	92

3.18	bb14, BSc3094 and cmp16 lead to an amelioration of the phenotype in the pro-aggregant strain	94
3.19	Methylene blue	96
3.20	Trehalose treatment ameliorates the phenotype of pro-aggregant line, decreases the aggregation load by inducing autophagy	98
4	Discussion	103
4.1	Phenotypic characterization of <i>C. elegans</i> Tau-transgenic lines	103
4.2	Pro-aggregation strain shows appearance of higher oligomeric Tau species along with accelerated aggregation at an early age.....	107
4.3	Pro-aggregation Tau species reduce the lifespan in <i>C. elegans</i>	109
4.4	Full-length V337M Tau but not the seeding F3ΔK280 fragment is highly phosphorylated in the pro-aggregation strain	110
4.5	Inhibitor compounds of Tau aggregation protect against Tau-induced toxicity.....	112
4.6	Trehalose induces autophagy and relieves the worms from Tau-aggregation induced toxicity.....	114
5	Summary	117
6	Bibliography	119
7	Appendix	157
8	Acknowledgment.....	177

1 Introduction

1.1 Protein misfolding diseases

Proteins need to adopt their native functional conformational states to ensure that the cells and organisms function properly. The acquisition of this three-dimensional functional conformational state of a protein, primarily determined by its amino-acid sequence, is supervised by Chaperone proteins (Soto, 2003). However, under certain conditions a specific peptide or protein may aggregate due to its failure to adopt its native functional conformational state leading to its loss of function. The tightly folded globular proteins require substantial unfolding to become amyloidogenic. However, in case of intrinsically disordered proteins or polypeptides, the first and critical step in the aggregation is partial folding (Uversky, 2008). This results in a partially folded conformation with hydrophobic surface patches that favors self-association. Such aggregate-prone conformations can polymerize to form fibrillar or amorphous aggregates, or soluble oligomers. Under these conditions, there is a reduction in the quantity of the protein that is available to play its normal role. This transition of proteins from their soluble forms into highly ordered fibrillar aggregates can give rise to pathological conditions generally referred to as protein misfolding diseases. A few exceptions are when functional proteins occur in the amyloid state, like the egg stalk of the green lace-wing fly (Geddes et al., 1968), the Pmel17 protein associated with skin pigmentation (Kelly and Balch, 2003), and a large number of secretory hormones (Maji et al., 2009). Protein misfolding diseases can be broadly grouped into neurodegenerative diseases, in which aggregation occurs in the brain, non-neuropathic localized amyloidosis, in which aggregation is restricted to a single type of tissue other than the brain, and nonneuropathic systemic amyloidosis, in which aggregation occurs in multiple tissues. Neurodegenerative diseases present neuronal pathologic forms in which there is a progressive loss of structure or function of neurons, ultimately leading to their death. Some of these neurodegenerative diseases such as Alzheimer and Parkinson diseases are predominantly sporadic, however several cases of hereditary forms have also been reported (Chiti and Dobson, 2006). Some of the proteins that aggregate in

neurodegenerative diseases are listed in table 1. The aggregates of Tau, a highly soluble microtubule-associated protein, occur in a group of neurodegenerative diseases such as progressive supranuclear palsy, corticobasal degeneration, Pick disease, and frontotemporal dementia and parkinsonism linked to chromosome 17 (FTDP-17). These diseases, together with AD are collectively known as tauopathies. Although aggregation of Tau has been studied in great detail, particularly in AD and FTDP-17 (Esmali-Azad et al., 1994); the exact mechanism underlying this process still remains a mystery.

Table 1 Human diseases associated with formation of extracellular amyloid deposits or intracellular inclusions with amyloid-like characteristics

Disease	Aggregating protein or peptide	Number of residues ^a	Native structure of protein or peptide ^b
Neurodegenerative diseases			
Alzheimer's disease ^c	Amyloid β peptide	40 or 42 ^f	Natively unfolded
Spongiform encephalopathies ^{c,e}	Prion protein or fragments thereof	253	Natively unfolded (residues 1–120) and α -helical (residues 121–230)
Parkinson's disease ^c	α -Synuclein	140	Natively unfolded
Dementia with Lewy bodies ^c	α -Synuclein	140	Natively unfolded
Frontotemporal dementia with Parkinsonism ^c	Tau	352–441 ^f	Natively unfolded
Amyotrophic lateral sclerosis ^c	Superoxide dismutase 1	153	All- β , Ig like
Huntington's disease ^d	Huntingtin with polyQ expansion	3144 ^g	Largely natively unfolded
Spinocerebellar ataxias ^d	Ataxins with polyQ expansion	816 ^{g,h}	All- β , AXH domain (residues 562–694); the rest are unknown
Spinocerebellar ataxia 17 ^d	TATA box-binding protein with polyQ expansion	339 ^g	α + β , TBP like (residues 159–339); unknown (residues 1–158)
Spinal and bulbar muscular atrophy ^d	Androgen receptor with polyQ expansion	919 ^g	All- α , nuclear receptor ligand-binding domain (residues 669–919); the rest are unknown
Hereditary dentatorubral-pallidoluysian atrophy ^d	Atrophin-1 with polyQ expansion	1185 ^g	Unknown
Familial British dementia ^d	ABri	23	Natively unfolded
Familial Danish dementia ^d	ADan	23	Natively unfolded

^aData refer to the number of residues of the processed polypeptide chains that deposit into aggregates, not of the precursor proteins. ^bAccording to Structural Classification Of Proteins (SCOP), these are the structural class and fold of the native states of the processed peptides or proteins that deposit into aggregates prior to aggregation. ^cPredominantly sporadic, although in some cases hereditary forms associated with specific mutations are well documented. ^dPredominantly hereditary, although in some cases sporadic forms are documented. ^eFive percent of the cases are transmitted (e.g., iatrogenic). ^fFragments of various lengths are generated and have been reported to be present in ex vivo fibrils. ^gLengths shown refer to the normal sequences with nonpathogenic traits of polyQ. ^hLength shown is for ataxin-1 (Adapted from Chiti and Dobson, 2006).

1.2 Alzheimer disease (AD)

The name Alzheimer disease (AD) comes from a German psychiatrist and pathologist Dr. Alois Alzheimer, who in 1907 described the case of a 51 year old female patient's death in a completely demented state (Alzheimer, 1907). AD, an irreversible progressive neurodegenerative disorder, is the leading cause of dementia among older people. An impaired memory is a general and a popular concept associated with Alzheimer disease; however, a number of other changes occur in the brain function in the patients suffering from this devastating disease. These ultimately result in inattention, disoriented behavior, altered personality, difficulty in speaking and comprehension, and impaired gait and movement (Tabert et al., 2005; Waldemar et al., 2007). About 50% of the people with dementia suffer from AD. The risk of getting AD increases as one gets older (beyond age 65) (Giacobini, 2000). In 2010, there were more than 30 Million people suffering with Alzheimer disease but it is anticipated that by 2015 over 35 Million people worldwide will be suffering from this disease. Traditionally thought to be a disease of the developed nations owing to a larger proportion of elderly people, however, this notion is changing as the developing countries are undergoing a demographic transition towards more elderly population. By 2050, 59 percent of the world's Alzheimer cases will live in Asia. Global Alzheimer disease has increased manifold and is expected to cross US\$ 19 Billion by 2015. These astonishing figures underscore a need to develop a strategy in order to curb this devastating disease. A major risk factor for AD is age; however, family history, genetic predisposition and environmental factors are important factors. (Gatz et al., 1997). Alzheimer disease can be of two basic types: the sporadic AD (SAD), which is late in onset (>65 years) and has not been linked to any mutation. In contrast, several mutations have been linked to the other type called familial AD (FAD) which has an early onset (<40 years) (Campion et al., 1999; Chartier-Harlin et al., 1991; Murrell et al., 1991) and can be seen in patients as young as 25 (Miklossy et al., 2003). AD is however not a single-gene disorder, but involves mutations and polymorphisms in multiple genes on several chromosomes. It is associated with gene mutations on chromosomes 1, 14, and 21. Most of the FAD cases are caused by mutations in two genes namely presenilin 1 (PS1) and presenilin

2 (PS2) (Rogaev et al., 1995; Sherrington et al., 1995). In AD, no mutation has been identified in the gene, MAPT which codes for Tau protein.

In its initial phases, the disease causes damage to specialized structures in the brain like entorhinal cortex, hippocampus and basal forebrain that play a critical role in memory (alzforum 2012). At the cellular level, the brains of AD patients are characterised by the accumulation of two main types of protein aggregates: extracellular neuritic amyloid plaques composed mainly of a 40- or 42-residue peptide – amyloid- β protein ($A\beta$) (Glennner and Wong, 1984b; Kosik, 1992; Masters et al., 1985) and intracellular neurofibrillary tangles comprising of hyperphosphorylated Tau ((Grundke-Iqbal et al., 1986) (Goedert et al., 1996b; Lee, 1993; Mandelkow, 1999; Mandelkow and Mandelkow, 1998) (**Fig 1.1**).

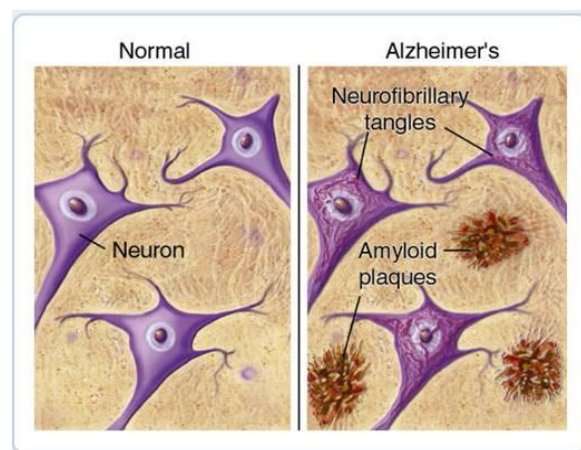


Figure 1.1: Pathological hallmarks of Alzheimer disease. Amyloid plaques are extracellular deposits of a 40- or 42-residue peptide called amyloid- β protein ($A\beta$) in the brain parenchyma and around the cerebral vessel walls, while tangles composed of twisted fibers of Tau protein build up intracellularly in the degenerating neurons. The plaques and tangles get deposited in structures in the brain that play a critical role in memory and then spread to other regions. The plaques and tangles contribute to the degradation of the neurons in the brain and are the main hallmark of Alzheimer's disease. (Figure reproduced from <http://www.ahaf.org/alzheimers/about/understanding/plaques-and-tangles.html>).

The disease slowly progresses and destroys large areas of the brain, leaving its victims with little comprehension or unawareness. As the disease advances, patients become bedridden, unable to restrain natural discharges and unable to feed themselves. The patients survive from 2 to 15 years after the onset of symptoms, but some may survive as long as 20 years. In spite of the fact that both the tangles and plaques are found in conjunction, it is difficult to correlate the appearance and

distribution of A β deposits with the progression of the disease; however, the appearance and distribution of tangles can well be correlated ("Braak stages") (Braak and Braak, 1991).

1.3 Tau: A microtubule-associated protein

1.3.1 Localization and functions of Tau protein

Tau protein was discovered in 1975 in Marc Kirschner's laboratory at Princeton University (Weingarten et al., 1975) in an attempt to search for factors that promote the self-assembly of tubulin into microtubules. However, Tau only gained interest when it was found to be a subunit of protein aggregates called neurofibrillary tangles, one of the major hallmarks of Alzheimer disease (AD) (Brion et al., 1985; Grundke-Iqbal et al., 1986) and has since then remained in the limelight. MAPs like Tau consist of two other proteins MAP2 (Lewis et al., 1988) and MAP4 (Chapin and Bulinski, 1991) occur throughout much of the animal kingdom namely: *Caenorhabditis elegans* (Goedert et al., 1996a; McDermott et al., 1996), *Drosophila* (Cambiazio et al., 1995; Irminger-Finger et al., 1990), goldfish (Liu et al., 1997), bullfrog (Yin et al., 1995), rodents (Kosik and Finch, 1987; Lee et al., 1988), bovine (Himmler, 1989; Himmler et al., 1989), goat (Nelson et al., 1996), monkeys (Nelson et al., 1996), and human (Goedert et al., 1989a; Goedert et al., 1989b).

The gene encoding Tau protein is expressed predominantly in the neurons of the central nervous system (CNS) and the peripheral nervous system (PNS) (Andreadis et al., 1992). Tau is ubiquitously expressed in immature neurons. But as the neurons mature, its localization gets restricted almost entirely to the axonal compartment. Furthermore, there is a shift toward higher-molecular-weight isoforms and reduced phosphorylation (Drubin and Kirschner, 1986; Kosik et al., 1989). In spite of this, low levels of Tau can still be found in other neuronal compartments after maturation, for example, the nucleus (Loomis et al., 1990; Sultan et al., 2011) and dendrites (Papazosomenos and Binder, 1987), and in other brain cells, notably oligodendrocytes (Goldbaum et al., 2003; LoPresti et al., 1995). Furthermore, the presence of low Tau mRNA and Tau protein in astrocytes as well as in oligodendrocytes has also been reported (LoPresti et al., 1995; Shin et al., 1991). In

addition to this, Tau mRNA and proteins can also be detected in several peripheral tissues such as heart, kidney, lung, muscle, pancreas, testis, as well as in fibroblasts where its function is not clear (Gu et al., 1996; Ingelson et al., 1996; Vanier et al., 1998). In muscle fibers Tau forms aggregates in inclusion body myositis (Askanas and Engel, 2008).

Although it remains to be known as what causes Tau to be specifically sorted into the axon, several mechanisms have been proposed, for example, selective protein transport into axons, selective degradation in dendrites (Hirokawa et al., 1996; Nakata and Hirokawa, 2003), selective axonal transport of Tau mRNA (Aronov et al., 2002), selective up-regulation of translation in axons (Morita and Sobue, 2009) and more recently the presence of a selective barrier in the axon hillock which prevents the reentry/missorting of Tau back into the soma (Li et al., 2011). This is of considerable importance as missorting of Tau into the somatodendritic compartment is recognized as one of the earliest signs of neurodegeneration in AD and in mouse models (Braak and Braak, 1994; Coleman and Yao, 2003). An insult to the neurons triggered by various factors like A β , glutamate, oxidative stress leads to the missorting of Tau into dendrites. This in turn, causes a decay of dendritic spines mediated by Ca²⁺ influx through NMDA receptors and hence a decay of neuronal communication (Mattson, 2004; Shankar et al., 2007; Zempel et al., 2010).

Tau regulates the assembly of microtubules by binding to them and stabilizing them. Microtubules are protein polymers of the cytoskeleton that play a role in diverse cellular functions like stabilizing cell shape, mitosis, and as tracks for intracellular transport by motor proteins (Garcia and Cleveland, 2001; Hirokawa, 1993, 1994). The evidence that support the role of Tau in regulating assembly, stabilization, and bundling of microtubules came from the experiments whereby purified bovine brain Tau protein microinjected into rat fibroblasts deficient in endogenous Tau lead to an increased microtubule mass and enhanced microtubule stability (Drubin and Kirschner, 1986). Additionally, neurons treated with antisense oligonucleotides to Tau mRNA (siRNA) to block expression of Tau fail to extend axon-like processes (Caceres and Kosik, 1990; Caceres et al., 1991). This suggests a role of Tau protein in the establishment of neuronal polarity by stabilizing the

microtubules specifically in a particular compartment during development (Caceres and Kosik, 1990; Caceres et al., 1991). The above mentioned functions of Tau are a result of direct interactions of Tau with microtubules and can be modulated by Tau and its phosphorylation (Brandt et al., 2005; Dolan and Johnson, 2010) depending on how dynamic the microtubules are needed in a particular compartment of the cell. Furthermore, over-expression of Tau in Chinese hamster ovary (CHO) cells causes a change in cell shape, retarded cell growth and an altered distribution of various organelles known to be transported via microtubule-dependent motor proteins (Ebner et al., 1998). These findings were further consolidated with the experiments in differentiated N2a cells, whereby over expression of Tau led to disappearance of mitochondria from the neurites (Ebner et al., 1998; Stamer et al., 2002). The above mentioned functions of Tau with regard to microtubules are consequences of indirect interactions and these interactions affect the binding of other proteins that may or may not interact with the microtubules by themselves. Some of the examples are the spacing of the microtubules to establish a clear zone in order to ensure smooth transport in cells (Umeyama et al., 1993) and, inhibition of microtubule dependent transport by motor proteins as a result of a competition between motors (kinesin, dynein) and MAPs (including Tau) for binding sites on the microtubule surface (Dixit et al., 2008; Seitz et al., 2002; Stamer et al., 2002).

Cell biologists wanted to elucidate the function of Tau further by producing mice lacking Tau protein. To their surprise, the nervous system of Tau-deficient mice looked normal immunohistologically with no major changes. But there was a significant decrease in the microtubule stability and organization in some small-calibre axons. It should be noted that the lack of Tau was associated with an increase in microtubule-associated protein 1A (MAP1A) expression, possibly fulfilling the function of Tau (Harada et al., 1994). Furthermore, the mice exhibited muscle weakness and disturbances in memory (Ikegami et al., 2000). In one more example where the authors knocked out Tau, the mice were viable and did not show any macroscopic abnormalities. Again the lack of Tau was associated with an increase in microtubule-associated protein 1A (MAP1A) levels at birth which declined with age. In contrast to the previous studies, the primary neuron cultures from this Tau-deficient mouse showed some abnormalities. The neurons showed slowed

maturation with reduced neurite length throughout all developmental stages and reduced axon length of stage 3 neurons (Dawson et al., 2010). Importantly, all these abnormalities shown by the primary neuronal cultures obtained from this Tau-deficient mouse were restored back to normal after crossing this Tau-deficient mouse with human Tau-transgenic mouse (Dawson et al., 2010). These results suggest that Tau plays an essential role in axonal growth and neurite extension.

A careful observation of the developing brains after Tau knockdown in a recent study, however, revealed some important roles for Tau in the developing cerebral cortex. A successful knockdown of Tau achieved by Tau shRNA electroporation into the brains of E14 mouse embryos *ex vitro* resulted in an inhibition of neuronal migration in the developing cortex. Furthermore, some of the Tau knocked down postnatal brain neurons which were able to migrate and reach the cortical plate, nevertheless, exhibited smaller somas and poorly developed dendrites which were not able to make proper connections (Sapir et al., 2012), pointing to some developmental defects. In summary these data show that although MAPs may be redundant in their function, upregulation of MAP 1A in Tau-deficient mice (Harada et al., 1994; Dawson et al., 2010) does not restore the normal function as it relates to axonal and neurite extension in culture.

1.3.2 Isoforms of Tau

Human Tau is encoded by a single gene located on the long arm of chromosome 17 (17q21) (Neve et al., 1986), however, alternative splicing generates six Tau isoforms (Goedert et al., 1989a) (**Fig 1.2**). The six Tau isoforms differ in the presence of three (3R Tau) or four (4R Tau) repeats of 31 or 32 amino acids in the carboxy-terminal half, as well as in the presence or absence of inserts of 29 or 58 amino acids in the amino terminal region (Goedert et al., 1989a; Goedert et al., 1988). The tandem repeats in the carboxy-terminal half are encoded by exons 9, 10, 11, and 12, and it is the alternative splicing of exon 10 that results in the generation of E10 + 4R Tau and E10 - 3R Tau mRNAs and their corresponding 4R and 3R Tau isoforms, respectively. This consecutive repeat region was thought to constitute the microtubule binding domain of Tau protein (Butner and Kirschner, 1991; Goedert and Jakes, 1990; Goode and Feinstein, 1994). However, Gustke et al in 1994 extensively studied the

interaction of various Tau domains with respect to microtubules. They found that the flanking regions (the proline-rich domain P upstream of the repeats and the fifth repeat P3 downstream) of Tau act like jaws and strongly enhance the binding of Tau repeat region to microtubules. Thus a well defined microtubule binding domain of Tau protein consists of the repeat domain plus the flanking regions (Gustke et al., 1994). The 4R Tau has a much higher affinity for microtubules and therefore, plays a

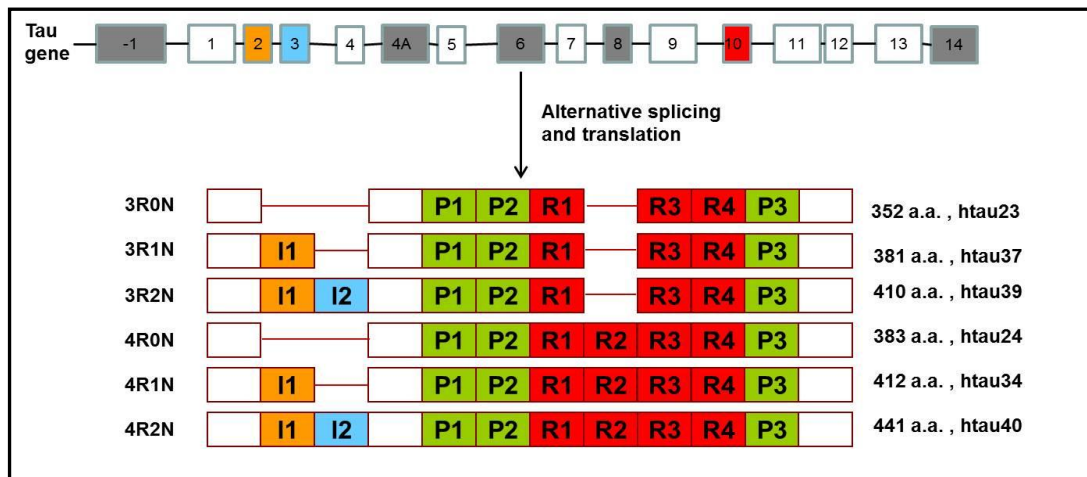


Figure 1.2: Six Tau isoforms are generated by alternative splicing of a single human Tau gene. The gene encoding Tau is a multi-exon gene that undergoes alternative post-transcriptional splicing of exons 2 (shown in orange), 3 (shown in blue) and 10 (shown in red) to yield six isoforms in the brain. The exons shown in dark grey do not appear in the translated protein. Exons 9-12 encode microtubule-binding repeat domains, and the exclusion or inclusion of exon 10 results in Tau with three (3R) or four (4R) microtubule-binding domains, respectively (shown as red boxes) (Figure reproduced from (Gustke et al., 1994), with modifications).

greater role in regulating the microtubule dynamics than 3R Tau (Goode and Feinstein, 1994). The alternative splicing of the six brain Tau isoforms is developmentally regulated. Developing brains require highly dynamic microtubules which may be achieved by expressing only the shortest isoforms which explains why the fetal human brains have only the three repeat Tau isoform without amino-terminal inserts (Ikegami et al., 2000). The adult CNS contains the following Tau isoforms in order of abundance: Tau with one amino-terminal insert (1N Tau, 50%), Tau with no amino-terminal insert (0N, 40%) and Tau with two amino-terminal inserts (2N, 10%). The ratio between 4R and 3R Tau isoforms has been found to be 1 (Hong et al., 1998). Only three 4R Tau isoforms are known to be expressed in the adult rodent brain, while a 3R0N or fetal Tau isoform is expressed in the developing CNS of rodents (Gotz et al., 1995; Kampers et al., 1999). In addition to these, a higher

molecular weight Tau protein (~110 kDa) appears in the peripheral nervous system. This Tau protein, referred to as big Tau, results due to the inclusion of E4a exon (Couchie et al., 1992; Georgieff et al., 1991; Goedert et al., 1992).

1.4 Frontotemporal dementia and Parkinsonism linked to chromosome 17 (FTDP-17)

Tauopathies are a group of neurodegenerative disorders characterized by the presence of intracellular Tau inclusions (Lee et al., 2001). Among the MAP proteins in the brain, Tau has received a tremendous attention because of its role in AD and other tauopathies. Tauopathies depict a range of clinical manifestations including memory and language impairments, behavioral and psychiatric abnormalities, extrapyramidal signs, and motor deficits (Foster et al., 1997). In spite of the distinct hallmark brain lesions shown by the patients suffering from this group of heterogeneous dementias and movement disorders, the affected patients share a common neuropathology characterized by abundant neuronal and to a lesser extent glial fibrillary lesions composed of hyperphosphorylated Tau proteins and are associated with a remarkable loss of neurons in affected regions (Reed et al., 1997; Reed et al., 1998; Spillantini et al., 1998a; Spillantini et al., 1998b). Whether Tau protein is causal to the disease or just an effect of some disease process was debatable until 1998, when several mutations in the gene encoding Tau protein were discovered in frontotemporal dementia and parkinsonism linked to chromosome 17 (FTDP-17), thereby confirming a causative role of Tau in neurodegeneration (Hutton et al., 1998; Poorkaj et al., 1998; Spillantini et al., 1998a). Tau is now regarded as one of the risk factors in PSP, PD and others (Hardy and Singleton, 2008). More than 40 different mutations in the Tau gene are known to occur in FTDP-17 (Goedert and Spillantini, 2001; Poorkaj et al., 1998). These mutations include either missense, deletion or silent mutation in the coding region (**Fig 1.3**) or intronic mutations located close to the splice-donor site of the intron following the alternatively spliced exon 10 (R2) (van Swieten and Spillantini, 2007).

Tau mutations in FTDP-17 may act by two mechanisms. First, they may affect the alternative splicing of exon 10 resulting in a change of the ratio of 4R: 3R Tau. These mutations comprise a mixture of coding changes within exon 10 (N279K, delK280, L284L, N296N/H, delN296, P301L/S, G303V, and S305S/N) and also intronic mutations close to the 5' splice site of exon 10 (at positions +3, +11, +12, +13, +14, +16, +19, and +29) (Wszolek et al., 2006). Second, the mutations (missense and deletions) may directly cause deficits in the abilities of Tau to bind to microtubules (MTs) and promote assembly and stability of MTs. This has been linked to several Tau gene missense mutations including: G272V, delK280, P301L, P301S, V337M, G389R, and R406W using *in vitro* studies (D'Souza et al., 1999; Hasegawa et al., 1998; Hong et al., 1998). Recombinant G272V, N279K, Δ K280, P301L, V337M, and R406W mutant Tau proteins show an enhanced filament formation in the presence of

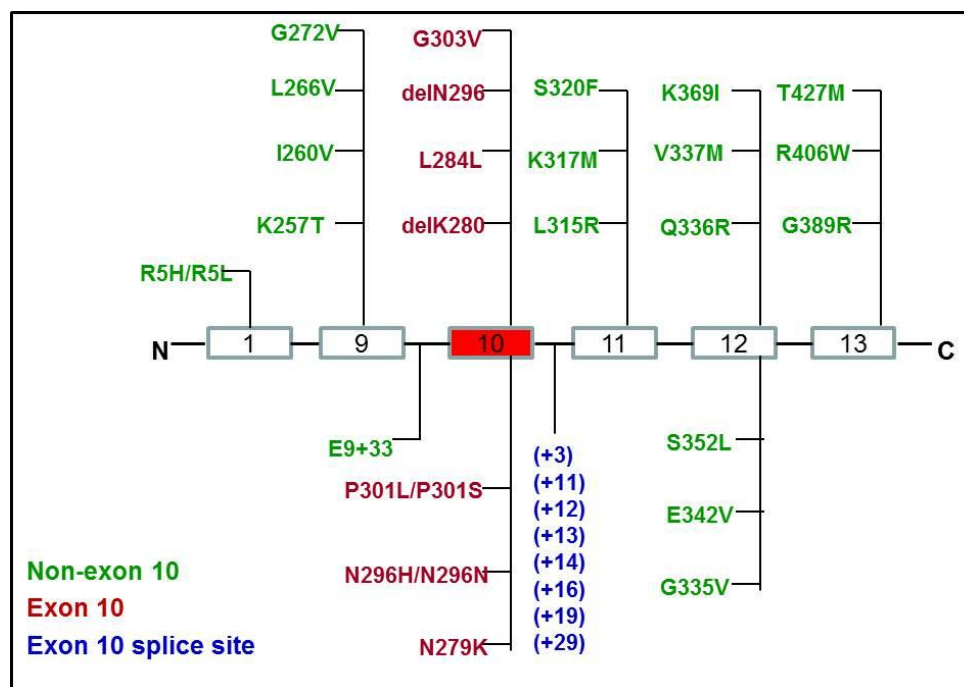


Figure 1.3: Tau gene mutations in FTDP-17. Known Tau mutations that occur in FTDP-17 are shown. Mutations affect either the splicing of exon 10 (altering the ratio of 3R and 4R Tau isoforms) or the function of Tau (mostly by increased aggregation tendency or reduced microtubule affinity) (reproduced from (Schneider and Mandelkow, 2008)).

heparin compared to wild type Tau protein (Arrasate et al., 1999; Barghorn et al., 2000; Nacharaju et al., 1999). Moreover, mutations such as V337M and R406W in exons other than those in exon 10 promote Tau aggregation which is composed of all

six isoforms, whereas other exon 10 mutations (P301L) increase 4R Tau in insoluble FTDP-17 brain fractions (Clark et al., 1998; Hong et al., 1998). Mutations such as Δ K280 and P301L moderately decrease the affinity of Tau to microtubules, however, strongly enhance the aggregation of Tau into PHFs (Barghorn et al., 2000; Schneider and Mandelkow, 2008). Furthermore, polyanions like RNA was shown to induce the assembly of all the six full-length isoforms of Tau, with three repeat constructs being the most efficient at polymerization. RNA induces polymerization by the formation of intermolecular disulphide bridges between Cys³²² in the third repeat of Tau (Kampers et al., 1996). Mutations in the intronic sequence adjacent to the stem loop structure in exon 10 have been identified that increase soluble 3R Tau by altering the Tau splicing, leading to increased Tau proteolysis and neuronal apoptosis without deposition of insoluble Tau aggregates (Stanford et al., 2003).

1.5 Tau aggregation

Tau shows no tendency to aggregate under physiological conditions because of its highly soluble nature (Wille et al., 1992). Despite this fact, Tau aggregates are found in several brain diseases collectively termed as tauopathies, including AD (Lee et al., 2001) but the mechanism of Tau aggregation still remains to be known. *In vitro* studies have shown that Tau aggregation is a multiple step process which involves the formation of an oligomeric nucleus (rate-limiting nucleation step) followed by an elongation step whereby protein subunits add to this nucleus (Friedhoff et al., 1998). Two hexapeptide motifs [PHF6 (VQIVYK) and PHF6* (VQIINK)] within the repeat domains of Tau which have the highest propensity for β -structure are responsible for the Tau aggregation and during the aggregation process a transition from random coil to β -structure takes place (Barghorn et al., 2000; von Bergen et al., 2000). Tau aggregation can be suppressed by the introduction of two proline residues within these hexapeptide motifs (I287P and I308P), which produce kinks in the chain due to the cyclic structure of proline and hence act as β -breakers (von Bergen et al., 2001). Furthermore, the deletion mutation Δ K280 which enhances this β -propensity promotes Tau aggregation (Barghorn et al., 2000; Khlistunova et al., 2006). Although it is not clear why a soluble protein like Tau forms insoluble fibers in various

neurodegenerative diseases, various posttranslational modifications of Tau discussed below play a role.

1.6 Tau phosphorylation

Tau phosphorylation, the most common posttranslational modification of Tau is regulated by the balanced activities of various kinases and phosphatases. **Fig 1.4** shows the number of potential amino acid residues that could be phosphorylated in Tau. The role of phosphorylation on Tau aggregation has received the most attention over the years but still remains to be a controversial field. For example, each Tau molecule in AD brain is associated with eight or more phosphates compared with only ~ two in normal adult brains (Kopke et al., 1993), but a normal fetal brain also shows high phosphorylation status (~four), and likewise it is high in hibernating animals (Hartig et al., 2007). There are a number of potential Phosphorylation sites on Tau and majority of them are found to be phosphorylatable by multiple kinases (>45) (Hanger et al., 2007). A subset of sites has gained prominence because they are recognized by antibodies raised against AD Tau in a phosphorylation-dependent manner. They include PHF1 (pS396 + pS404) (Greenberg and Davies, 1990), several of the AT series of antibodies (Biernat et al., 1992; Goedert et al., 1994), for example, AT8 (pS202 + pT205), AT180 (pT231 + pS235), AT270 (pT181) and AT100 (pT212 + pS214), and Sternberger monoclonal antibodies of the SMI series (e.g., SMI31, 33, 34; (Lichtenberg-Kraag et al., 1992).

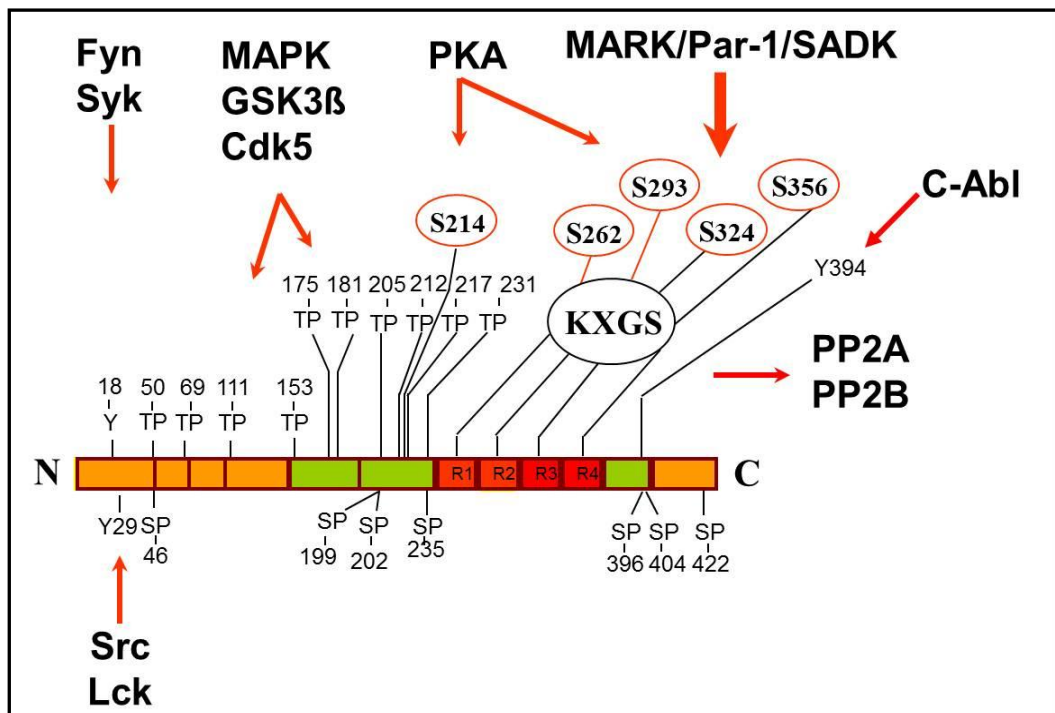


Figure 1.4: Tau phosphorylation sites. Phosphorylation sites in full length Tau (hTau40) isoform are targets of various kinases and phosphatases. Phosphorylations at SP/TP motifs by kinases like GSK3 β , CDK5 and MAPK have transitional effect on Tau-microtubule affinity. PKA, MARK and SADK phosphorylate KXGS motifs and S214. SFKs phosphorylate tyrosine residues at position 18, 29 and 394. Potential phosphatases that can dephosphorylate Tau include PP2A and PP2B. (Figure reproduced from (Schneider and Mandelkow, 2008).

Kinases that phosphorylate Tau can be divided into three classes: (i) Proline-Directed Protein Kinases (PDPKs) which phosphorylate SP or TP motifs. Examples include: GSK3 β (Glycogen Synthase Kinase-3 β) (Ishiguro et al., 1993; Mandelkow et al., 1992), CDK5 (Cyclin-Dependent Kinase 5) (Baumann et al., 1993) and MAPKs (Mitogen-Activated Protein Kinases) (Drewes et al., 1992; Lu et al., 1993) which phosphorylate SP/TP motifs in the flanking regions of the repeat region of Tau. (ii) Non PDPKs. PKA (Protein Kinase A), MARK (Microtubule Affinity Regulating Kinase) (Drewes et al., 1997) and SADK (Synapses of Amphids Defective Family Kinases) (Kishi et al., 2005) are non PDPKs which target KXGS motifs in the repeat domain and other sites. (iii) Protein kinases specific for tyrosines. SFKs (Src Family Kinases) such as Src (Lee, 2005), Lck (Williamson et al., 2002), Syk (Lebouvier et al., 2008), Fyn (Lee et al., 1998; Lee et al., 2004) and c-Abl Kinase (Derkinderen et al., 2005) target Tau tyrosine residues at Y18, Y29 and Y394.

Phosphorylations at SP/TP motifs have only a weak influence on Tau-microtubule interactions (Biernat et al., 1993; Drechsel et al., 1992; Schneider et al., 1999), however, they are of diagnostic value because these phosphorylation sites are elevated in Alzheimer Tau (Morishima-Kawashima et al., 1995). It is assumed that hyperphosphorylation at SP or TP motifs may lead to aggregation, but the issue is controversial since non-phosphorylated Tau in the presence of polyanions can also aggregate and form filaments (von Bergen et al., 2000; Wille et al., 1992). The KXGS motifs in the repeat domain (S262, S293, S324, S356) can be phosphorylated by MARK (alias Par-1), PKA, SADK (alias BRSK), CamKII (Drewes et al., 1997). PKA additionally phosphorylates S214 (Brandt et al., 1994; Illenberger et al., 1998; Zheng-Fischhofer et al., 1998). Tau phosphorylation in KXGS motifs strongly decreases the Tau-microtubules affinity, as recognized by antibody 12E8; however, it does not eliminate this binding (Seubert et al., 1995). Phosphorylation at these sites occurs early in the AD process (Augustinack et al., 2002) as well as in Tau inducible transgenic mice (Eckermann et al., 2007). It is assumed that phosphorylation drives Tau into aggregation, and certain highly phosphorylated states of Tau might be prone to aggregation (Iqbal et al., 2008); on the contrary, phosphorylation at certain sites (e.g., KXGS motifs) inhibits aggregation (Schneider et al., 1999). Tau is dephosphorylated by PP2A (Protein Phosphatase 2A), PP2B (Protein Phosphatase 2B, calcineurin) and PP-1 (Protein Phosphatase-1) (Drewes et al., 1993; Gong et al., 1994; Sontag et al., 1996; Sun et al., 2003). In short, equilibrium exists in the action of various kinases and phosphatases in a cell and under certain conditions; this equilibrium gets shifted specifically to one direction. Thus, hyperphosphorylation can be ruled out as being an absolute indicator of a disease state. As far as the phosphorylation and disease are concerned, Tau can be thought of getting protected against aggregation while bound to the microtubules, but not when detached by phosphorylation. The cartoon below explains the mechanism underlying the role of Tau in neurodegeneration (**Fig 1. 5**).

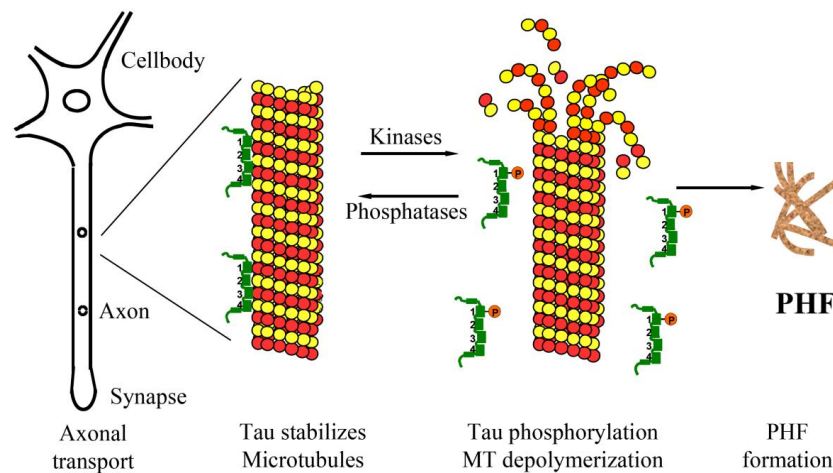


Figure 1.5: Tau hypothesis of AD. Hyperphosphorylation of Tau due to the disturbances in the regulation of activity of kinases and phosphatases results in the detachment of Tau from microtubules. Subsequent failure of microtubule stabilization causes inhibition of axonal transport. Hyperphosphorylated Tau which is detached from MTs is now free to aggregate into PHFs. PHFs, in turn can further augment the obstruction of axonal transport. All these things cause neuronal dysfunction and ultimately lead to neurodegeneration (reproduced from (Mandelkow and Mandelkow, 1998).

1.7 Other modifications of Tau protein

Tau undergoes another major modification in the form of proteolytic cleavage. The natively unfolded nature of Tau and the presence of a number of potential cleavage sites (See Fig 1.6) make Tau an easy substrate to multiple proteases. Proteolysis might yield breakdown products that could be toxic in various ways. For example, caspases cleave Tau in the tail ends (behind D421 or behind D13) (Gamblin et al., 2003; Horowitz et al., 2004; Rissman et al., 2004) perturbing the paperclip folding of Tau (Jeganathan et al., 2006) resulting in the release of products which are more vulnerable to aggregation. Calpains can cleave Tau at a number of sites (Canu and Calissano, 2003; Park and Ferreira, 2005). A 17 kDa Tau fragment has been a centre of focus. *In vitro* digestion of recombinant Tau by calpain was reported to generate this 17 KDa fragment which could subsequently be blocked upon treatment with calpain inhibitor. This 17 kDa Tau fragment was thought to induce apoptosis in cerebellar macroneurons and was assigned to residues from 73-315 of Tau, based on antibody reaction assays (Canu et al., 1998). However, the exact N- and C-terminal ends were unambiguous. Furthermore, pre-aggregated A β treatment of cultured neurons was also reported to generate a 17 KDa Tau fragment through the activation

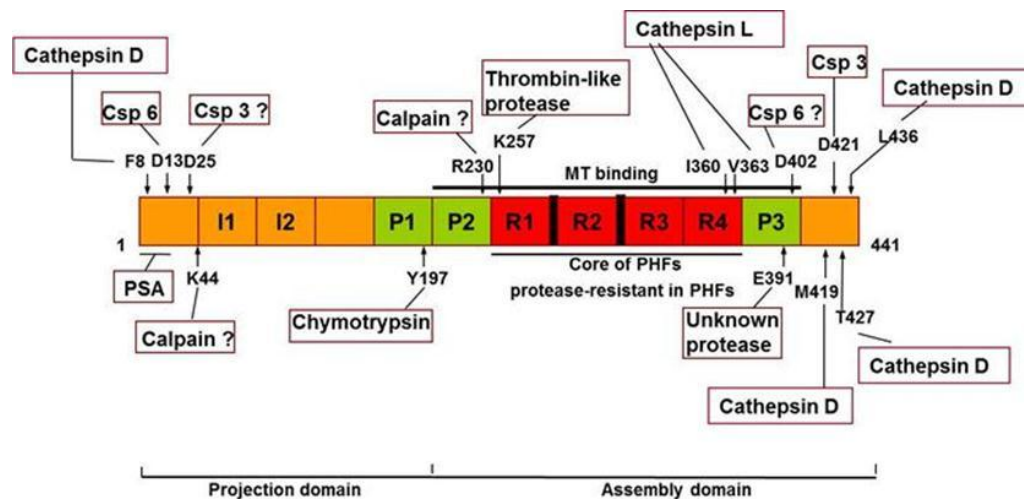


Figure 1.6: Diagram of proteolytic cleavage sites on Tau. Tau is divided into an N-terminal projection domain and a C-terminal assembly domain containing the microtubule-binding elements, based on the cleavage by chymotrypsin after Y197 (Steiner et al., 1990). The repeat domain of Tau (R1-R4) represents the core of PHFs and is highly protease-resistant in PHFs (von Bergen et al., 2006; Wischik et al., 1988a). The microtubule (MT) binding region of Tau contains the repeat domains plus the flanking proline-rich domains P2 and P3 (Gustke et al., 1994; Preuss U et al., 1997). Cleavage sites after D13 by caspase 6 (Horowitz et al., 2004), D421 by caspase 3 (Gamblin et al., 2003; Rissman et al., 2004), F8, M419, T427, L436 by cathepsin D (Kenessey et al., 1997), I360, V363 by cathepsin L (Wang et al., 2007) and K257 by an unknown thrombin-like cytosolic protease (Khlistunova et al., 2006; Wang et al., 2007) were validated by N-terminal protein sequencing or mass spectrometry. Cleavages after D25 (putative caspase 3 cleavage site) (Rohn et al., 2002), D402 (putative caspase 6 cleavage site) (Guo et al., 2004) and E391 were determined with site-directed antibodies. E391 is cleaved by an unknown protease (Novak et al., 1993; Wischik et al., 1988b). Cleavage after K44 and R230 was proposed from putative calpain cleavage sites found on Tau according to the P2-P1 rule (Park and Ferreira, 2005). PSA stepwise removes residues from the N-terminus of Tau (Karsten et al., 2006) (reproduced from Wang et al., 2010).

of calpain (Park and Ferreira, 2005). Based on the potential calpain cleavage sites on Tau and the apparent molecular weight, the 17 kDa Tau fragment was assumed to be Tau₄₅₋₂₃₀. Tau₄₅₋₂₃₀ over-expression induced apoptosis in CHO cells or cultured neurons. Based on these findings, it was proposed that the A β -induced neurodegeneration is mediated by this 17 kDa Tau₄₅₋₂₃₀ fragment (Park and Ferreira, 2005). The role of N-terminal part of Tau in neurodegeneration is also highlighted by the finding that this region of Tau is essential for prefibrillar A β induced microtubule disassembly in cultured cells (King et al., 2006). However, until now the presence of the 17 kDa calpain-induced Tau fragment has not been detected in AD brains so the proposition, that, the Tau fragment is the mediator of A β -induced neurodegeneration is highly controversial. The proposition received a setback by the recent work of Garg et al. 2011. They reported the generation of a metastable fragment A125-R230 that spans several PXXP motifs and therefore has the potential of scavenging SH3-containing proteins including tyrosine kinases (Garg et al., 2011).

They demonstrated that the "17 kDa" fragment is actually much smaller, containing residues 125-230 with an apparent molecular weight of 10.7 kDa. In addition, the fragment could be generated by other cell stressors as well. Finally, they showed in various cell lines that the overexpression of neither Tau₍₄₅₋₂₃₀₎ nor Tau₍₁₂₅₋₂₃₀₎ fragment is toxic. A third type of cleavage occurs by PSA (puromycin-sensitive aminopeptidase), discovered by a genomic screen for modifiers of tauopathy in flies (Karsten et al., 2006). Finally, expression of Tau repeat domain containing the FTDP-17 mutation (K18ΔK280) leads to the formation of PHF like aggregates in an inducible N2a cell model. In addition, the repeat domain is cleaved sequentially to generate three small fragments (F1, F2, and F3) derived from the same N-terminal cleavage site between K257 and S258 (thrombin-like protease) but different C-terminal tails (Cathepsin L) (Wang et al., 2009). Of these, F2 and F3 are prone to aggregation and form sarkosyl insoluble aggregates. Furthermore, the first cleavage at K257 by an unknown thrombin-like protease seems to be important not only for the aggregation of K18Δk280 but also for the two subsequent cleavages as a mutation (K257A) at this site abolishes the proteolytic processing of the repeat domain. The shortest fragment (S258-I360) named "F3" has the highest propensity for aggregation. It is sufficient to nucleate and co-aggregate with endogenous Tau (Wang et al., 2007). Nitration and glycation are the other posttranslational modifications of Tau in AD. Nitration of Tau is a salient feature of diverse tauopathies (Horiguchi et al., 2003) and antibodies specific to nitrated Tau can stain AD brains but not the normal brains (Reynolds et al., 2007). Glycation is a consequence of oxidative damage and cross-linking, which accumulates once the tangles are formed (Yan et al., 1994).

1.8 Tau degradation

Proteostasis, defined as a state of dynamic equilibrium in which protein synthesis and folding is balanced with degradation, is necessary to maintain a healthy proteome in a cell (Balch et al., 2008). The equilibrium maintains a specific protein level necessary for the proper functioning of the cell and any disturbance in this equilibrium could have profound effects. As far as the degradation of Tau protein is concerned, both proteasome and autophagy have been found to contribute to this

process. The proteasome may play a role in regulating Tau turnover because it degrades misfolded proteins which otherwise would form potentially toxic aggregates (Benaroudj et al., 2001; Ciechanover, 2001; Kisselev et al., 1998; Kisselev et al., 1999; Tofaris et al., 2001; Touitou et al., 2001). 20S proteasome has been found to contribute to Tau degradation through Trypsin-like activity (Cardozo and Michaud, 2002). Experiments with Tau transfected SH-SY5Y cells showed that inhibition of the 20S proteasome catalytic core by Lactacystin can inhibit Tau degradation (David et al., 2002). Furthermore, the direct degradation of unfolded recombinant Tau by the 20S proteasome *in vitro* in an ubiquitin-independent and bi-directional manner leads to the formation of stable intermediates during degradation process (~27 kDa and 17 kDa fragments) (David et al., 2002). Since AD brains have been shown to have a decreased proteasomal activity, this could contribute to accumulation of aggregates including Tau filaments (Keller et al., 2000; Lopez Salon et al., 2000). Corresponding to this, the proteasome system has been shown to be inhibited by the binding of PHF-Tau to the 20S core proteasome in human brain tissue (Keck et al., 2003). Molecular chaperones bind Tau protein and target it for degradation via proteasomal system, thereby preventing its aggregation and toxicity. Several studies have shown that phosphorylated Tau can be ubiquitinated by the CHIP-Hsc70 complex and targeted for proteasome degradation (Petrucelli et al., 2004; Shimura et al., 2004). All these studies suggest Tau as a proteasomal substrate. However, other studies contradict these findings (Brown et al., 2005; Delobel et al., 2005; Feuillette et al., 2005). Tau phosphorylated at the KXGS motifs in the repeat domain is not degraded via proteasome pathway (Dickey et al., 2007). Furthermore, proteasomal inhibitors such as MG132 and epoxomicin have no effect on the clearance of Tau aggregates detected in the sarkosyl insoluble fraction from the cells (Wang et al., 2009).

The other route for Tau degradation is through the autophagy-lysosomal system, which includes three main pathways for the delivery of cargo to lysosomes: macroautophagy, microautophagy and chaperone-mediated autophagy (CMA) (Santambrogio and Cuervo, 2011). Induction of autophagy has been shown to protect against the accumulation of proteins (Nixon et al., 2005). Macroautophagy induced by rapamycin has been shown to degrade detergent-insoluble mutant Tau protein (hTau40/P301L) (Berger et al., 2006), while blockage of macroautophagy by 3-

methyladenine (a PI3K-type III inhibitor which can be used to block macroautophagy) (Seglen and Gordon, 1982) slows down Tau degradation (Hamano et al., 2008). A recent study reported the macroautophagy mediated degradation of both soluble and insoluble mutant Tau (Tau_{RD}/ΔK280) (Wang et al., 2009). CMA is a type of lysosomal degradation that degrades cytosolic proteins containing a specific pentapeptide motif KFERQ (Dice, 1990) and since there are two CMA-targeting motifs (³³⁶QVEVK³⁴⁰ and ³⁴⁷KDRVQ³⁵¹) present in the C-terminal repeat domain of Tau, this makes Tau a good candidate for this type of degradation. Indeed, Wang et al (2009) reported that the CMA machinery contributes to the delivery of a mutant Tau construct to the lysosomes. Furthermore, recent findings that trehalose mediated induction of autophagy can reduce the endogenous Tau levels in primary neurons and insoluble Tau aggregates in a tauopathy cell model (Kruger et al., 2011) further consolidate these results.

1.9 Amyloid-β cascade hypothesis

The accumulation of β-amyloid peptide (Aβ) is a primary pathological hallmark of AD brains. Aβ accumulates into amyloid plaques extracellularly (diffuse and later neuritic) and, to a lesser extent, in blood vessels. Aβ was first sequenced in 1984 from the meningeal blood vessels of AD patients and individuals with Down's syndrome (Glenner and Wong, 1984a) and in 1985, it was found to be the primary component of the senile plaques of AD brain tissue (Masters et al., 1985). Aβ is a normal product of the APP metabolism generated by the cleavage of APP by proteases called the α-, β-, and γ- secretases and is produced throughout life (Haass et al., 1992; Seubert et al., 1992; Shoji et al., 1992); In the normal brain, most APP is processed in a non-amyloidogenic secretory pathway involving the cleavage of APP by α-secretase (Selkoe, 1994) that prevents the formation of potentially amyloidogenic fragments. However, in AD brains APP gets cleaved predominantly by the β-, and γ- secretases leading to the generation of amyloidogenic Aβ. Various mutations discovered in the APP gene that are known to cause AD favor the processing of APP by the amyloidogenic pathway (Cai et al., 1993; Citron et al., 1992; Suzuki et al., 1994). In addition to this, APP mutations within the Aβ sequence increase the self-aggregation of Aβ into amyloid fibrils (Wisniewski et al., 1991). All these findings led John Hardy

and David Allsop in 1991 to formulate the Amyloid hypothesis of Alzheimer's disease. According to this hypothesis, the initiating event in AD is the accumulation of A β caused by APP mismetabolism and the rest of the pathological events including the formation of neurofibrillary tangles (NFTs) are downstream of this cascade. A schematic view of this hypothesis is given in **Fig 1.7** below:

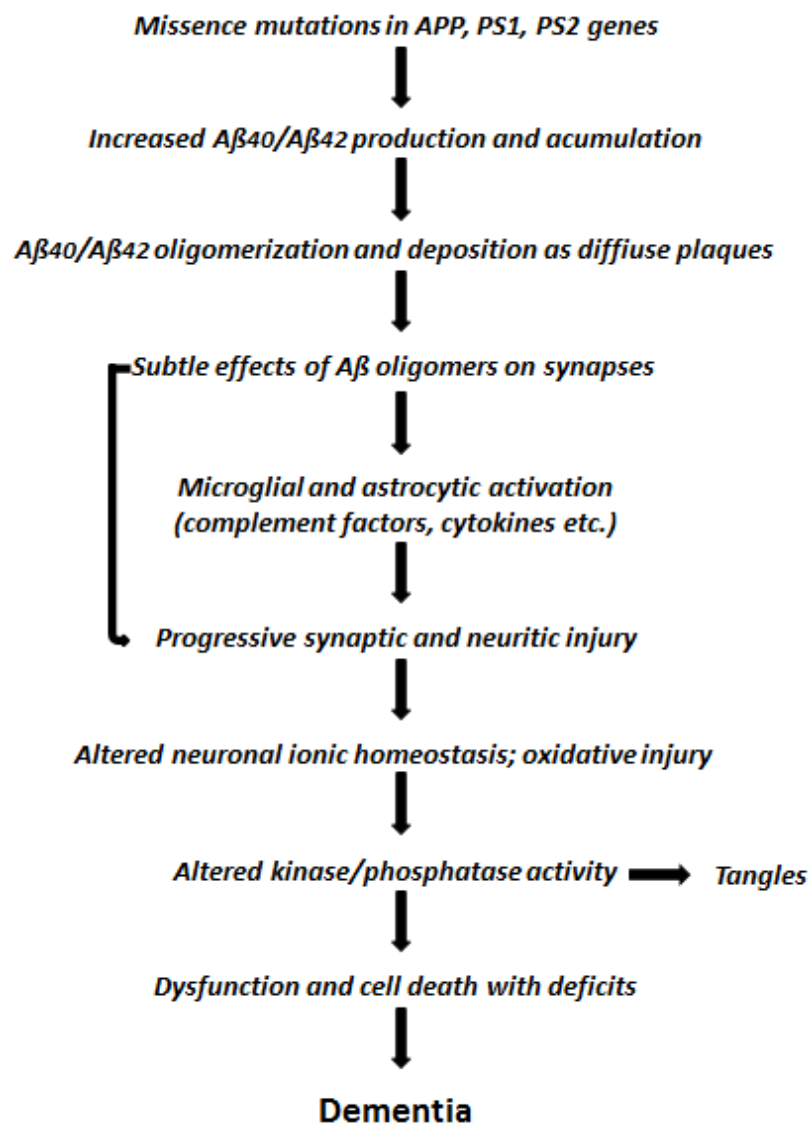


Figure 1.7: Amyloid cascade hypothesis of AD. Shown here is the sequence of pathogenic events that finally lead to AD. A β oligomers can have an additional effect by causing injury to the synapses and neurites of brain neurons directly as shown by the curved arrow (reproduced from (Hardy and Allsop, 1991)).

1.10 Connection between A β and Tau

The two main hallmarks of AD are extracellular amyloid plaques and intracellular NFTs. Although the connection between the two proteins A β and Tau which form these two types of aggregates, respectively, is still not clear, studies from the recent years have provided some clue about the relationship between the two and their hierarchy in the cascade of events that lead to Alzheimer's disease.

Earlier work by Rapoport and his coworkers provided the first evidence of a direct relationship between Tau and A β when they found that cultured hippocampal neurons from Tau knockout mice were resistant to A β -induced neurodegeneration. Furthermore, Tau knockout neurons possessed more dynamic microtubules as seen by increased tubulin tyrosination (a marker of unstable microtubules) (Schulze and Kirschner, 1987), suggesting that neurons may compensate for A β -induced neurodegeneration by having more dynamic microtubules (Rapoport et al., 2002). Meanwhile, immunotherapy studies on triple transgenic mice (3xTg-AD), which develop both the hallmark lesions of AD, surfaced in 2004. In this study, it was found that the administration of antibodies against A β in the hippocampus reduces not only the extracellular A β plaques and intracellular A β load but more importantly, this immunotherapy also led to the clearance of early Tau pathology. Furthermore, after 30 days of post injection, A β deposits were the first to reemerge. Therefore, this study established a hierarchy between A β and Tau as the immunotherapy against Tau did not have any effects on either of the hallmark lesions (Oddo et al., 2004).

Further studies showed that the reduction in endogenous Tau in hAPP mice (Mucke et al., 2000) can prevent behavioral deficits, without affecting the APP metabolism (Roberson et al., 2007). In addition to these studies, Tau which is an axonal protein was recently assigned a dendritic function of targeting the kinase Fyn to the dendrite. It was shown that in Tau knockout mice and mice expressing only the amino-terminal projection domain (Δ Tau74), which is totally excluded from the dendrites, have reduced synaptic localization of Fyn. Reduced Fyn localization to synapses, in turn, reduces the A β -induced toxicity as the premature lethality, memory deficits and seizure susceptibility presented by APP23 mice were mitigated

upon their crossing with Δ Tau74 mice or Tau knockout mice (Ittner et al., 2010). All these studies propose an effective strategy to treat the Alzheimer's disease by reducing the Tau levels. In contradiction to this, transgenic mice expressing hAPP with Swedish mutation in a Tau knockout background showed neurite degeneration, increased A β peptide deposits and severe cognitive deficits (Dawson et al., 2010). Additional reports from Tau knockdown studies show that neuronal migration in the developing cortex becomes perturbed and the postnatal brain neurons undergo morphological defects upon Tau knockdown (Sapir et al., 2012). Hence, the proposition that a reduction of Tau presents an effective strategy to combat this disease remains controversial and needs further careful evaluation.

1.11 *Caenorhabditis elegans* as a model organism

Caenorhabditis elegans (*C. elegans*) is a free living soil nematode (roundworm) that feeds on microbes, mainly bacteria. Under natural conditions *C. elegans* exists in two sexes: hermaphrodite and male. Hermaphrodites are self-fertilizing organisms with 5 autosomal chromosomes and 2 sexual chromosomes (XX). Males have 5 autosomal chromosomes and are hemizygous for the sex chromosome (XO). Males show a low spontaneous occurrence (0.1%) in a population by spontaneous nondisjunction in the hermaphrodite germ line. However, this frequency can approach up to 50% through mating between males and hermaphrodites (Altun & Hall, 2008a). In the laboratory *C. elegans* can be maintained in Petri dishes on the surface of an agar medium or in liquid cultures with *Escherichia coli* (*E. coli*) as the food source. One of the important property of *C. elegans* is its ability to withstand ultra-low temperatures that allows the strains to be cryopreserved for long periods of time (typically 25-30 years), by freezing in ultra-low freezers at -80°C.

C. elegans genome roughly codes for 20,000 genes (Claverie, 2001). Out of these, 83% have clear homologs in the human genome as inferred by a comparative analysis of expressed sequence tags (ESTs) (Lai et al., 2000; Rubin et al., 2000). This high degree of homology has earned *C. elegans* a high status among the most privileged model organisms to study the genetics of human hereditary diseases. It has a relatively small genome of roughly 97 million base pairs which is approximately 20X bigger than that of *E. coli* and about 1/30 of that of human. The

popularity of *C. elegans* as a model system received a major boost when its genome was sequenced in 1998, also making it the first multicellular organism (and only the second eukaryote, after *Saccharomyces cerevisiae*) for which a complete genome sequence was obtained (The *C. elegans* Sequencing Consortium, 1998). The achievement of this big feat was well described by Robert Waterston when he said, "*This is a tremendously gratifying moment and more of a beginning than an end. We have provided biologists with a powerful new tool to experiment with and learn how genomes function. We'll be able to ask and answer questions we could never even think about before.*" All the information regarding *C. elegans* genome is available online from the website <http://wormbase.org/> (Chen et al., 2005). *C. elegans* has a simple body plan. Its transparent body throughout life allows a detailed anatomical observation of the whole animal through microscopy. The hermaphrodite body consists of exactly 959 somatic cells whereas the male bears 1031 somatic cells. A complete and well-defined cell lineage, which is invariable between animals, makes it possible to follow the fate of each single cell throughout its whole life (Brenner, 1973, 1974; Byerly et al., 1976; Lewis and Fleming, 1995; Sulston et al., 1983; Wood, 1988).

One of the most important advantages of *C. elegans* which adds more to its versatility as a tool for biological research is the ease with which the function of a single gene can be reduced or eliminated by RNAi. This allows biologists to see how that reduction affects the development of the worm. Notably, this gene silencing in *C. elegans* is systemic. Administration of gene-specific double-stranded RNA (dsRNA) into one tissue not only leads to the silencing of that gene in that particular tissue but in other tissues as well. Furthermore, the silencing effect is inherited and persists in the offspring after the double-stranded RNA that initiated the silencing has disappeared (Fire et al., 1998). This systemic nature of RNAi has made it possible to initiate RNAi by soaking animals in dsRNA (Maeda et al., 2001; Tabara et al., 1998) or by growing worms on bacteria expressing dsRNA (Timmons et al., 2001; Timmons and Fire, 1998). Subsequent work led to the discovery of a transmembrane protein SID-1 required cell-autonomously for systemic RNAi. SID-1 is thought to act as channel for dsRNA, siRNAs, or some other RNAi signals (Winston et al., 2002). The RNAi-induced gene silencing shows some limitations when it comes to neurons. However, recent genome wide screens have deciphered

few mutations which can increase the neuronal RNAi sensitivity. Notable among these mutations are *eri-1*, an endogenous inhibitor of RNAi and *lin-15b*. *lin-15b* is implicated in chromatin remodeling and also enhances the response to dsRNA (Kennedy et al., 2004; Sieburth et al., 2005; Wang et al., 2005). Presently a combination of both of these mutations is used for most of the neuronal RNAi studies owing to their additive effect on the RNAi sensitivity.

The small size of about 1 mm in length of adult individuals, its short life cycle of 3 days, its short lifespan of 14 days under laboratory conditions, an inexpensive handling, a compact genome, stereotypical development, ease of propagation and the ease with which it can be manipulated makes it one of the most prominent model organism in genetics and molecular biology.

1.12 *C. elegans* life cycle

The life cycle of *C. elegans* comprises three major stages; embryogenesis, larval development, and adulthood (**Fig 1.8**). The fertilization of the egg in the hermaphrodite uterus marks the beginning of embryogenesis. The embryo gets laid at approximately 30 cell stage (at gastrulation), undergoes organogenesis and the young larva (stage L1) finally hatches from the egg. The hatched nematode passes four larval stages (L1, L2, L3, and L4) before reaching the adulthood. Shifts between the different stages are marked by molting processes during which the new cuticle surrounding the animal replaces the old one.

Under unfavorable conditions, the L2 larva may enter an arrested state called the dauer larva. Unfavorable conditions may be determined by scarcity of food resources, overcrowded population (which causes the release of a pheromone) or an adverse environment in general. During the dauer larval stage, the animal stops feeding indefinitely and reduces movements compared to a non-stressed animal. Apart from a change in morphology this particular larval stage has a lifespan that is overwhelmingly longer than the adult worm (Cassada and Russell, 1975). However, upon return of the favorable conditions, the dauer state ends and it starts feeding again finally molting to the L4 stage. The last molt after the L4 stage leads to an adult animal. Adult animals reach sexual maturity and start laying eggs in case of

hermaphrodites or search for mates in the case of males. Under standard laboratory conditions, *C. elegans* reproductive life cycle from egg to fertile animal takes about three days. Having reached fertility, the adult hermaphrodite animal remains fertile for 3-4 days, has a lifespan of 10-15 days and generates about 300 progenies (Altun & Hall, 2008a). Figure 8 depicts the life-cycle of *C. elegans*.

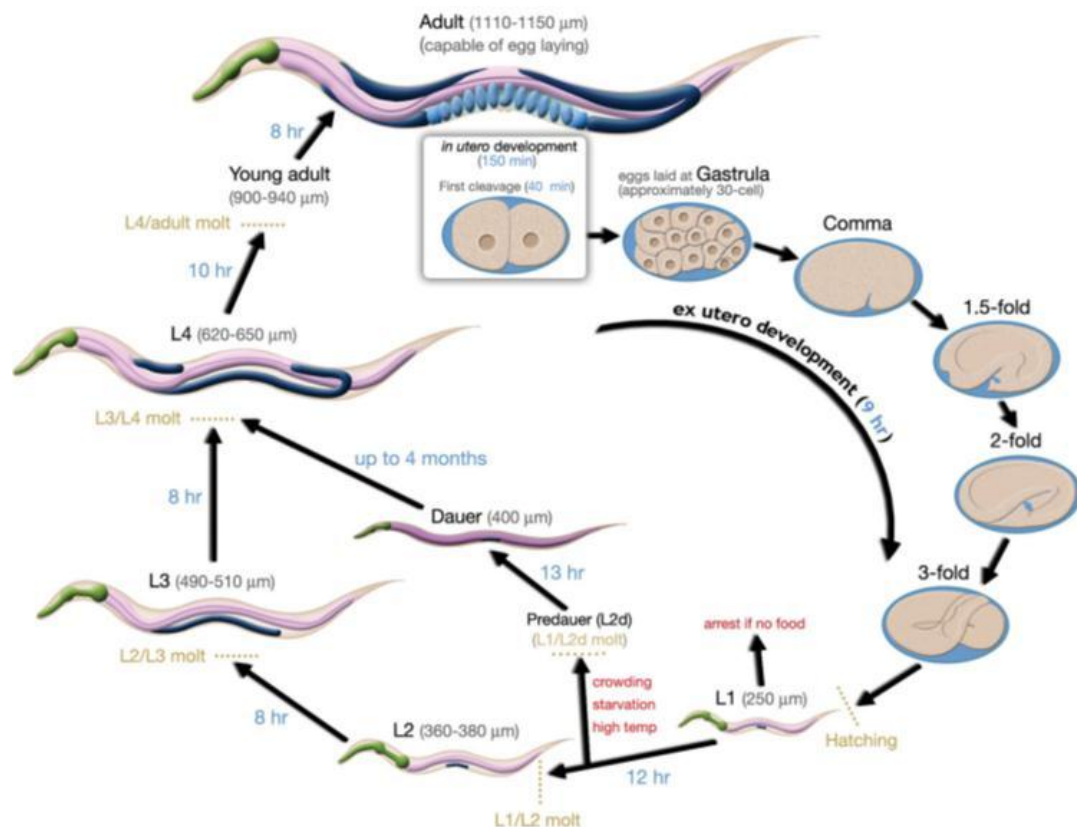


Figure 1.8: Life cycle of hermaphrodite *C. elegans* at 22°C. The embryo is laid outside when it reaches approximately the 30 cell stage. The embryo outside the body undergoes major changes until hatching, finally releasing an L1 larva. Before reaching the adulthood, the larva undergoes post hatching development through four larval stages: L1, L2, L3, and L4. A conditional developmental choice before the L1/L2 molt is offered by the dauer larva stage. The names of the stages and the dimension in μm of the animal are indicated in black. The time required for the transition from one stage to the next is expressed in hours (hr) and specified in light blue (Adapted from Altun & Hall, 2008a).

An adult hermaphrodite becomes mature and starts laying its first eggs at approximately 45-54 hours post-hatching at 22°C-25°C, thereby completing its reproductive life cycle (Byerly et al., 1976; Lewis and Fleming, 1995). The adult hermaphrodite can remain fertile for a period of about 4 days during which it can produce about 300 progeny through self-fertilization. This number can reach up to

1200-1400 if mating with a male occurs. After this fertile period is over, the adult hermaphrodite can live for an additional 10-15 days. After crossing the L4 stage, males can successfully mate for 6 days and can father about 3000 progeny (Hodgkin, 1988).

A total of 1090 somatic cells are generated during hermaphrodite development, out of these 131 undergo programmed cell death at characteristic times (Driscoll, 1995) leaving a total of 959 somatic cells in the adult hermaphrodite. Out of these 959 somatic cells, 302 are neurons and 95 are body wall muscle cells (White 1988). On the other hand, the adult male has relatively more cells with a total number equal to 1031 somatic cells, out of which 381 are neurons (extra neurons in males play a role in mating) (White 1988).

1.13 Evolution of *C. elegans* and its significance in biomedical studies

C. elegans has gained a huge popularity since its introduction as a model organism to understand the fundamentals of animal genetics, development and behavior by Sydney Brenner (Brenner, 1974). The scientific classification of *C. elegans* is given below:

Scientific classification	
Kingdom:	Animalia
Phylum:	Nematoda
Class:	Secernentea
Order:	Rhabditida
Family:	Rhabditidae
Genus:	Caenorhabditis
Species:	<i>C. elegans</i>
Binomial name	
<i>Caenorhabditis elegans</i>	
Maupas E., 1900	
(http://en.wikipedia.org/wiki/Caenorhabditis_elegans)	

In order to extend the biological findings from the model organisms such as fruitfly *Drosophila melanogaster* and the nematode *C. elegans* to higher vertebrates like man, it is necessary to know the similarities between the species involved. Although a clear consensus regarding the relationship between the three species is lacking, however,

two hypotheses exist at the moment. The first hypothesis called "Coelomata hypothesis", is based on the assumption that the mesoderm-lined body cavity or coelom, found in arthropods and vertebrates, as well as in other phyla, has a common origin. From this perspective, arthropods and vertebrates cluster together on one branch of the phylogenetic tree and the nematodes, which do not have a true coelom, on the other branch. The second hypothesis, namely "Ecdysozoa hypothesis" is based on the similarity between animals undergoing molting of their cuticle, a process called ecdysis. According to this hypothesis, nematodes and arthropods, since both of them undergo ecdysis, are closer and thereby have been clustered on one branch whereas, vertebrates which do not undergo any such phenomena diverge to another branch.

Analysis of the 18S rRNA, *Hox* genes and myosin gene sequences along with the presence of an epitope recognized by an anti-horseradish-peroxidase antibody, peculiar to ecdysozoan nervous systems, support this hypothesis (Telford, 2004). However a comparative genomic analysis, made possible with the availability of fully sequenced genome for all the three species, support the Coelomata hypothesis. Although more phylogenetic data are required to reinforce this hypothesis, it is currently assumed that arthropods such as fruitflies are evolutionarily and genetically closer to vertebrates than to nematodes (**Fig 1.9**) (Blair et al., 2002; Fitch, 2005; Telford, 2004).

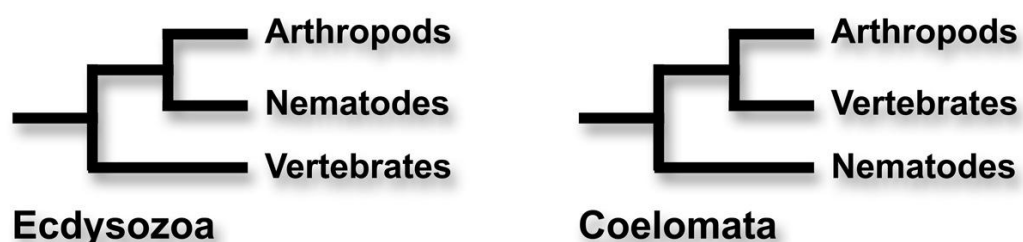


Figure 1.9: The two cladistics trees suggested by recent evolutionary analyses. The ecdysozoa hypothesis maintains a closer relationship between arthropods and nematodes based on the molting process common to both groups. However, the coelomata hypothesis based on the early formation of a coelomic body cavity during embryogenesis joins arthropods with vertebrates. The latter hypothesis has gained more ground recently and was reinforced by comparative genomics data (Adapted from (Blair et al., 2002).

Coelomata hypothesis suggests that *C. elegans* evolved faster and diverged utterly in the past from the phylogenetic branches that later developed to the arthropod and

the vertebrate clades. In other words, nematodes and vertebrates share a common ancestor. It is from this perspective that *C. elegans* has been able to make a place among the highly privileged model organisms relevant for biomedical research. Molecular or physiological features, which are shared between vertebrates and nematodes, could therefore be derived either by common ancestry or by convergent evolution. If the shared characteristics originated before the separation of the nematodes from the vertebrate and arthropod clades, their conservation reflects their importance for the processes they control. This suggests that conserved features could underlie basic biological mechanisms developed early in the evolutionary history. From this perspective, *C. elegans*'s place in the evolutionary tree offers a privileged insight into crucial mechanisms that build metazoans bodies, associate to diseases, and underlie aging processes.

1.14 Tau like protein in *C. elegans*

A true homolog of Tau is absent in *C. elegans*, however, a protein was identified which shares 50% sequence identity within the microtubule tandem repeats with mammalian Tau, MAP2, and MAP4 and thereby named 'protein with Tau-like repeats' (PTL-1) (Goedert et al., 1996a; McDermott et al., 1996). The *ptl-1* primary transcript, like human Tau, is alternatively spliced to give rise to two isoforms PTL-1A and PTL-1B with 4 and 5 repeats respectively (Goedert et al., 1996a; McDermott et al., 1996). Like human Tau, PTL-1B with 5 repeats is much more effective in promoting the microtubule assembly than the 4 repeat isoform PTL-1A. The protein is expressed in the embryonic epidermis and in mechanosensory neurons in *C. elegans*, where microtubules have to play an essential functional role. Expression of PTL-1 facilitates microtubule assembly in *ptl-1* transfected COS cells (Goedert et al., 1996a). Both the isoforms share similarities with human Tau in several other important respects including size, amino acid content, charge distribution, predicted secondary structure, hydrophobicity, and flexibility. In addition, both proteins contain several potential glycosylation sites and numerous phosphorylation sites (McDermott et al., 1996). Knockout of *ptl-1* resulted in a reduction in the number of viable progeny which was, however, incompletely penetrant; surviving animals showed a reduced degree of mechanosensory response. Furthermore, *ptl-1* knockout

animals showed enhanced defects in the background of *mec-12* and *mec-7*, which encode alpha and beta tubulin subunits, respectively (Gordon et al., 2008). All these results confirm two main roles of PLT-1: elongation during development and mechanosensation in larval and adult animals; both roles may require PTL-1 to provide structural support for microtubules. Taken together, these results show that Tau-like proteins evolved early and might be present in many different phyla, making *C. elegans* a powerful system amenable to genetic, molecular, and cellular analysis in which to study the functions of this important class of proteins.

1.15 Human tauopathy models in *C. elegans*

Several human Tau transgenic *C. elegans* models have been generated in the recent years. They are based on the overexpression of wild-type human fetal or adult Tau, as well as human Tau containing different mutations. A brief description of these models is given below:

1.15.1 Kraemer B.C. et al., 2003

C. elegans Tau transgenic models from Kraemer et al were based on the overexpression either the wild type human 4R1N Tau or the FTDP-17 human Tau mutants (V337M and/or P301L) in all the neurons using the pan neuronal *aex-3* promoter. These transgenic lines show two major phenotypes. First, the transgenic animals were uncoordinated and showed reduced motility. Second, the transgenic animals showed a progressive axonal degeneration whereby gaps appeared in the axonal bundles of the dorsal and ventral nerve cords. The phenotype was much more severe in the mutant Tau transgenic animals. All these Tau transgenic lines accumulated insoluble Tau, albeit at later stages of adulthood (Kraemer et al., 2003). They further went on to identify genes participating in Tau neurotoxicity by conducting a forward genetic screen for mutations that ameliorate Tau-induced uncoordinated motion. Two suppressors were isolated, *sut-1* and *sut-2*.

sut-1, which encodes an RNA and snRNP-binding protein (MacMorris et al., 2007), is localized predominantly in the nucleus (Kraemer and Schellenberg, 2007). *sut-1* mutants show a partial suppression of Tau-induced toxicity and decreased

levels of Tau (Kraemer and Schellenberg, 2007). Furthermore, SUT-1 was found to interact with UNC-34/Mena/Enabled and double mutants of *unc-34/Mena/Enabled-sut-1* produced enhanced Tau-induced toxicity, suggesting that *unc-34* is either needed for the *sut-1* suppression or acts in a parallel pathway to affect motility (Kraemer and Schellenberg, 2007). It is interesting to note that in mammals, Mena binds Fe65 (Ermekova et al., 1997) and forms a complex with APP (Sabo et al., 2001). However, it is not known whether all these four proteins (SUT-1, UNC-34/Mena/Enabled, FEH-1/Fe65, and APL-1) together also form a complex.

sut-2 encodes a protein with a novel sub-type of CCCH zinc finger motif (Guthrie et al., 2009), similar to the zinc fingers contained within Nab2 in yeast and ZC3H14 in humans (Kelly et al., 2007) and is identical to the mammalian SUT-2 (MSUT-2) (Guthrie et al., 2011). Interaction studies showed that SUT-2 binds with ZYG-12, a HOOK cytoskeletal linker protein necessary for the attachment between centrosomes and the nucleus (Guthrie et al., 2009), suggesting its role in Tau movement. However, till date the exact mechanism of *sut-1* and *sut-2* mediated suppression of Tau-induced toxicity remains unclear.

1.15.2 T. Miyasaka et al., 2005.

They generated transgenic lines overexpressing either wild type human 4R0N Tau or the FTDP-mutants (P301L and R406W) in six mechanosensory neurons involved in touch response namely ALML/R, AVM, PLML/R and PVM. Reduced touch sensitivity in animals reflects loss-of-function of the touch neurons. The worms expressing Tau lost their sense of touch and it became worse with age. Worms showed swollen neuronal cell bodies with thinner, kinked and tortuous axons often associated with broken microtubules. The neurodegeneration induced by Tau expression in touch neurons was found to be non-apoptotic as the animals in the *ced-3* or *ced-4* background, both of which are deficient in a functional caspase, did not improve their touch response. Furthermore, the expression of human HSP70 significantly improved the touch response in mutant Tau-Tg lines but not in the WT4R worms.

1.15.3 R. Brandt et al., 2007

They generated Tau transgenic *C. elegans* with a pan neuronal expression of wild type fetal human Tau (352 aa) and a pseudohyperphosphorylated (PHP) Tau (in which the amino acids S198, S199, S202, T231, S235, S396, S404, S409 and S413 were changed to glutamate to mimic the AD-relevant tau phosphorylation). Additionally they used TauAla10 (in which the same codons were changed to alanine and hence makes it resistant to phosphorylation) as a control to the PHP Tau. Both wild type and PHP Tau induced a progressive age-dependent uncoordinated locomotion in the absence of neuronal degeneration. However, only PHP Tau induced a defective pattern of motor neuron development as could be seen by the presence of gaps in the dorsal nerve cord, commissures on the wrong side and local broadening of axons.

In this work, we have taken advantage of *C. elegans* to study the toxic effects of Tau aggregation by manipulating its nervous system for the expression of aggregation prone human Tau protein.

Aim of this study

Tau, a microtubule associated protein tau (MAPT), is predominantly expressed in neurons where its main function is to stabilize microtubules, particularly in axons (Binder et al., 1985). Under physiological conditions, tau is a highly soluble protein and its binding to the microtubules is regulated by phosphorylation and other posttranslational modifications (Alonso et al., 1994, 1996; Bancher et al., 1991; Biernat et al., 1993; Bramblet et al., 1993; Drechsel et al., 1992; Gong et al., 2000; Horiguchi et al., 2003; Iqbal et al., 1986; Iqbal et al., 1994; Lindwall and Cole, 1984; Liu et al., 2000, 2002a, 2002b; Morishima and Ihara, 1994; Morishima-Kawashima et al., 1993; Munch et al., 2002; Papasozomenos, 1989; Sato et al., 2001; Wang et al., 1995, 1996; Yoshida and Ihara, 1993). However, in Alzheimer disease and other tauopathies, tau becomes abnormally hyperphosphorylated and forms insoluble aggregates intracellularly (Goedert et al., 1992a; Goedert et al., 1989a; Grundke-Iqbal et al., 1986a; Grundke-Iqbal et al., 1986b; Lichtenberg-Kraag et al., 1992). Mutations in Tau protein like the deletion of Lysine-280 (hTau40ΔK280) are found in patients with Frontotemporal Dementia with Parkinsonism linked to chromosome 17 (FTDP-17). This mutation decreases the microtubule affinity and enhances the self-aggregation propensity of tau (Barghorn et al., 2000; Rizzu et al., 2000). In addition to this, there are two hexapeptide motifs ²⁷⁵VQIINK²⁸⁰ and ³⁰⁶VQIVYK³¹¹ (von Bergen et al., 2000) in the 2nd and 3rd repeat domain respectively, of a 4-repeat tau. These hexapeptide motifs have the highest propensity for beta-structure and are known to drive and stabilize Tau aggregation. However, if the two isoleucine residues in these hexapeptide motifs are substituted with amino acid proline (I287P and I308P), the aggregation is inhibited. Proline has a cyclic structure which produces kinks in the beta-sheet and hence acts as beta-sheet breaker (von Bergen et al., 2001). Furthermore, it has been shown in N2a cells that Tau repeat domain undergoes a stepwise proteolysis leading to the formation of a highly aggregation prone fragment F3 (Wang et al., 2007). This fragment has been shown to act as a seed, which promotes the aggregation of the full length tau protein.

The aim of the present study was the generation of a *C. elegans* model of tauopathy based on Tau aggregation, with a well-defined and a severe phenotype

early in its life. We achieved this by expressing a highly amyloidogenic pro-aggregant F3ΔK280 fragment along with full length human tau V337M in the nervous system of *C. elegans*. As a control we expressed the anti-aggregant F3ΔK280PP along with full length human tau V337M.

This model helped us to study the influence of the tau aggregation process and tau aggregates on cell toxicity and degeneration within the context of the whole organism. Given the adult lifespan of approximately 2 weeks under normal conditions, *C. elegans* allows experiments to be designed and carried out quite rapidly compared with other model systems. The *C. elegans* system has well-established techniques for forward and reverse genetics, a wide range of mutants, and a fully sequenced genome, all of which could help us to find genetic modifiers of tauopathy.

Another important aim was to test compounds that are known to have dissolving activity on protein aggregates in general and on tau aggregates in particular *in vitro*. *C. elegans* offers extra advantage for drug testing due to its ability to grow in liquid cultures, which facilitates their entry into the worm. At the same time, testing these drugs in the context of the whole organism would allow us to nullify any off-target effects of these drugs. This will, in turn, help extrapolate the *in vitro* results of these drugs to higher organisms. Owing to its simplicity and ease of handling in the laboratory, this *C. elegans* model would offer us rapid and high-throughput screening of new compounds.

2 MATERIALS AND METHODS

2.1 Materials

2.1.1 Chemicals

All the high quality chemicals were purchased from Sigma-Aldrich, Calbiochem, Serva, Gerbu, Applichem, Amersham pharmacia biotech, Fluka, Roth, New England biolabs, Qiagen.

2.1.2 Enzymes

Restriction endonucleases	New England Biolabs
BSA	New England Biolabs
Fast Digest enzymes	Fermentas
T4 DNA ligase	New England Biolabs
Quick DNA ligase	New England Biolabs
Pfu ultra DNA polymerase	Stratagene
Taq Polymerase	New England Biolabs
50X dNTPs master mix	Invitex
MgCl ₂	Merck-Novagen
Pwo Master Mix	Roche diagnostic
Proteinase K	Invitrogen

2.1.3 Antibodies

AT100	Pierce
CP13	Davies
Calreticulin	Sigma
Mitotracker	Invitrogen
LC3-II	Nova
K9JA	DAKO
AT8	Pierce
12E8	Elan Pharmaceuticals

PHF1

Peter Davies

The antibodies against epitopes on Tau used are illustrated in the following figure:

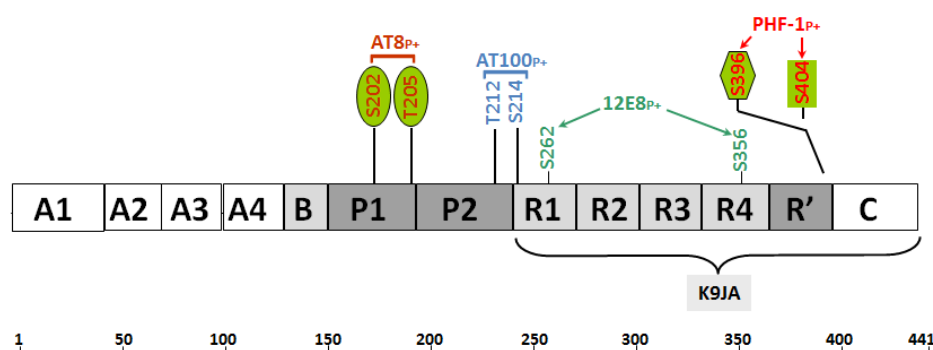


Fig 2.1: Diagram illustrating epitopes of Tau antibodies.

2.1.4 Molecular weight markers

Protein Magic marker	Fermentas
Unstained protein molecular weight marker	Fermentas
Page Ruler prestained protein ladder	Fermentas
Smart ladder	Fermentas

2.1.5 Kits

ECL western blotting detection kit	Amersham
Sire directed mutagenesis kit	Stratagene
Nucleospin Extract II elution kit	Macherey-Nagel
GenElute plasmid miniprep kit	Sigma-Aldrich
Nucleobond xtra midi EF	Macherey-Nagel
Zero Blunt TOPO PCR cloning kit	Invitrogen
Effectene transfection kit	Qiagen
Multisite Gateway Three-Fragment Vector Construction Kit	Invitrogen

2.1.6 Vectors

L4440

pPD30.38
 pDONR221
 p mec7
 pRab3
 pBI-5
 p unc-25
 pPD49.26 Paex3

2.1.7 Bacterial strains for cloning

XL-2 Blue	Stratagene
TOP-10	Invitrogen
XL-10 Gold	Stratagene
DH5 α library efficiency	Invitrogen

2.1.8 Antibiotics

Carbenicillin	Carl Roth
Kenamycin	Sigma aldrich
Tetracycline	Sigma aldrich
Hygromycin	PAA
G418	Biochrom AG
Penicilin/Streptomycin	PAA

2.1.9 Bacterial media

LB medium	Carl Roth GmbH
-----------	----------------

2.1.10 *C. elegans* media, buffers and chemicals

NGM (Nematode Growth Medium)	3 g/l NaCl, 17 g/l Agar (Serva), 2.5 g/l Bactopeptone (Becton, Dickinson and company), 5 μ g/ml Cholesterol (Sigma), 1 mM CaCl ₂ , 1 mM MgSO ₄ , 5 mM KH ₂ PO ₄ (pH 6.0), 20 μ g/l Nystatin (Roth)
------------------------------	--

NGM for RNAi feeding experiments	As NGM plus 1mM IPTG; and 100 µg/ml antibiotics (ampicillin or carbenicillin)
S Medium	1l S Basal, 10 ml Potassium citrate pH 6, 10 ml trace metals solution, 3 ml 1M CaCl ₂ , 3 ml 1M MgSO ₄ , add components under sterile conditions; do not autoclave.
Freezing buffer	0.1 M NaCl, 50 mM KH ₂ PO ₄ , pH 6.0; 30% (w/v) glycerol; 1 M NaOH; add optional 0.1 M MgSO ₄
M9 Buffer	3 g/l KH ₂ PO ₄ , 6 g/l Na ₂ HPO ₄ , 5 g/l NaCl; pH 6.0; add 1 mM MgSO ₄
Bleach solution:	1ml 5% bleach, 0.5 ml 5N NaOH
Worm lysis buffer (WLB)	10 mM Tris, pH 8.2; 50 mM KCl; 2.5 mM MgCl ₂ ; 0.45% NP40; 0.45% Tween 20; 0.01% gelatine; 0.5 mg/ml Proteinase K
S Basal	5.85g/l NaCl, 1g/l K ₂ HPO ₄ , 6g/l KH ₂ PO ₄ , 1 ml cholesterol (5 mg/ml in ethanol), sterilize by autoclaving
1M Potassium citrate pH 6.0	20 g/l citric acid monohydrate, 293.5 g/l tri-potassium citrate monohydrate, sterilize by autoclaving
Trace metals solution	1.86 g/l disodium EDTA, 0.69 g/l FeSO ₄ ·7H ₂ O, 0.2g/l MnCl ₂ ·4H ₂ O, 0.29 g/l ZnSO ₄ ·7H ₂ O, 0.025 g/l CuSO ₄ ·5H ₂ O, sterilize by autoclaving
2'-deoxy-5-fluorouridine (FUdR)	Sigma-Aldrich GmbH
Nystatin	Sigma-Aldrich GmbH

2.1.11 Cell culture media and reagents

MEM with earle's salts	PAA
Dubecco's PBS	PAA
Fetal calf serum	Sigma
Non-essential amino acids	PAA
Trypsin-EDTA	PAA

2.1.12 Software

Vector NTI	Invitrogen
AIDA	Fuji
LSM5 Image processing software	Zeiss
ZEN	Zeiss
Graph Pad Prism	Graph Pad Software, California, USA
EndNote X4	Thomson Reuters, UK

2.1.13 List of equipments

Centrifuges and sonicators

Centrifuge 5415 D	Eppendorf
MIKRO 200R	Hettich
Centrifuge 5810 R	Eppendorf
TL-100 ultracentrifuge	Beckman Coulter
Sonorex RK102	Bandelin
Sonoplus (sonotrode 73)	Bandelin

Spectrophotometers

Ultrospec 3000 pro	Amersham pharmacia biotech
Ultrospec 3100 pro	Amersham biosciences
Nanodrop (ND-1000)	peQLab Biotechnologie GmbH

Microscope

LSM510 microscope	Zeiss
LSM700	Zeiss

Miscellaneous equipment

PCR machine	Eppendorf
Analytic balances, BP 310S and PT 1200	Sartorius
BioDoc Analyze Transilluminator	Biometra
ABI PRISM 310 genetic analyser	PE Applied Biosystems
Fujifilm LAS3000 camera	Fuji
Fujifilm LAS4000 camera	Fuji
TECAN infinite M200 plate reader	Safire
Mixing Block MB-102	BIOER
Microwave oven	BOSCH
37°C Incubator/shaker	INFORS HT
Ultra-centrifuge tubes	Beckman
Micro-dialyser Tubes (3000 KDa)	Millipore

2.1.14 List of buffers

1X SDS Running Buffer	0.025 M Tris-HCl, 0.192 M Glycine, 0.1% SDS
10X Blotting Buffer	480 mM Tris-HCl, 390 mM Glycine, 50% Methanol, 1% SDS
10X TBST	100 mM Tris-HCl pH 7.5, 1.5 M NaCl, 5% Tween 20
1X TAE	40 mM Tris-Acetate pH 8.0, 2 mM EDTA
6X DNA Loading Buffer	10 mM Tris-HCl pH 7.6, 0.03% Bromophenol blue, 0.03% Xylene cyanol FF, 60 mM EDTA, 60% Glycerol

5X SDS Sample Buffer	1.25 M Tris-HCl pH 6.8, Glycerol, 50% SDS, 0.25% Bromophenol blue
2X SDS Sample Buffer	0.5 M Tris-HCl pH 6.8, Glycerol, 10% SDS, 0.1% Bromophenol blue
RAB	100mM Mes/1mM EGTA/0.5mM MgSO ₄ /20mM NaF
RIPA	150mM NaCl/1% Nonidet P-40/0.5% deoxycholate/0.1% SDS/50mM Tris, pH 8.0
BUFFER H	10 mM Tris-HCl (pH 7.4), 0.8 M NaCl, 1 mM EGTA, and 10% sucrose. Protease inhibitors (end conc.): 1 mM benzamidine, 10 µg/ml aprotinin, 10 µg/ml pepstatin, 10 µg/ml leupeptin. Phosphatase inhibitor (final conc): 2µM OA (Okadaic acid)

2.2 Methods

2.2.1 Molecular biological methods

2.2.1.1 Preparation of HT115 competent cells for RNAi in *C. elegans*

5 ml Lb medium was inoculated with bacteria from glycerol stock (gift from Dr. Daniele Bano) and incubated at 37°C O/N in *E. coli* shaker. 500 µl from this O/N culture was used to inoculate 50 ml fresh LB medium and allowed to grow at 37 °C with constant shaking. The culture was taken out when the cell density reached 0.45 – 0.5 at A₆₀₀ (3 – 4 hrs). The bacterial culture was allowed to cool down on ice (~ 10 min.). The bacteria were collected by centrifugation at 4000 g for 10 min. After removing the supernatant, the bacterial pellet was resuspended carefully in half of the original volume (25 ml) of sterile 100 mM CaCl₂ and incubated on ice for 15 min.

The bacteria were again collected by centrifugation at 4000 g for 5 min. at 4°C and supernatant was again removed. The bacterial pellet was finally resuspended very carefully (after CaCl₂ treatment the bacteria become very fragile) in 1/15 original volume (3.5 ml) of 50 mM CaCl₂ and 100 µl of this bacterial suspension was portioned in pre-chilled Eppendorf tubes. The tubes were incubated on ice in cold room for 3 hrs before transformation. The rest of the tubes were frozen in liquid nitrogen and stored at - 80°C.

2.2.1.2 Site directed mutagenesis

Site directed mutagenesis was performed using the QuikChange site-directed mutagenesis kit (Stratagene). The components of the reaction mixture were as follows:

10X Reaction mixture	2 µl
dsDNA template (25 ng/µl)	1 µl
Reverse primer (10 pmol/µl)	1 µl
Forward primer (10 pmol/µl)	1 µl
dNTP mix (2.5 mM)	1 µl
Pfuturbo DNA polymerase (2.5 U/µl)	0.5 µl
H ₂ O to a final volume of	20 µl

Cycling parameters:

Cycles	Temperature	Time
1	95 °C	30 seconds
12	95 °C	30 seconds
	55 °C	1 minute
	68 °C	2 minutes/Kb of plasmid length

Following temperature cycling, reaction was placed on ice for 2 minutes.

2.2.1.3 Digesting the products

0.5 µl of the DpnI restriction enzyme (10 U/µl) was added to the amplification reaction. Reaction mixture was gently and thoroughly mixed by pipetting up and

down several times. The mixture was centrifuged for 1 minute and incubated at 37°C for 1 hour to digest the parental supercoiled dsDNA.

2.2.1.4 Agarose gel electrophoresis

1% agarose gels were prepared to separate the particular DNA size fragments. Agarose was dissolved in 1X TAE by heating for a minimum time required. While the agarose solution was cooling, the comb was placed above the plate. Warm agarose solution was poured into the mould by taking care that no air bubble was entrapped in the gel. Gel was allowed to solidify and thereafter comb was removed carefully. Gel was mounted in the electrophoresis tank filled with 1X TAE. DNA samples were mixed with 0.20 volume of the 6X DNA gel loading buffer (10 mM Tris-HCl pH 7.6, 0.03% Bromophenol blue, 0.03% Xylene cyanol FF, 60 mM EDTA, 60% Glycerol) and loaded into the slots of the submerged gel along with the DNA marker (Smart ladder, Eurogentec). Electrophoresis was done at 100V for 30-90 minutes. After electrophoresis, the gel was stained in ethidium bromide solution (80 µl of 1% ethidium bromide + 200 ml of H₂O) for 10-15 minutes at room temperature and then washed in H₂O for 10 minutes at room temperature. Photography was performed under transilluminator (BioDoc Analyze, Biometra).

2.2.1.5 Restriction digestion

1 µg of DNA sample was mixed with 1U of enzyme with appropriate 10X NEB buffer in a total reaction volume of 20 µl and incubated at 37 °C for 1 hour. Afterwards, 10 µl of reaction mixture was mixed with 0.20 volume of 6X DNA gel loading buffer and loaded onto 1% agarose gel for electrophoresis at 100V.

2.2.1.6 DNA extraction from agarose gel

Appropriate DNA fragments were excised under UV light using a sterile scalpel and were transferred to a sterile 1.5 ml microcentrifuge tubes. The elution of DNA was performed using the Nucleospin Extract II elution kit.

2.2.1.7 Ligation

Ligation of DNA fragments was performed with T4 DNA ligase (NEB). The reaction was set up as following:

Vector (100 ng)	2 µl
Insert	300 ng
10X Quick ligase buffer	2 µl
T4 DNA ligase	1 µl
BSA	0.5 µl
H ₂ O to a final volume of	20 µl

The ligation mixture was incubated at 16 °C temperature overnight and then cooled in ice before transformation.

2.2.1.8 Chemical transformation

2 µl of ligation mixture was added to 50 µl of XL-2 blue competent cells (Stratagene). Cells were incubated on ice for 30 minutes, heat shocked for 45 seconds at 42 °C, then immediately transferred to ice and incubated for 2 minutes. Afterwards, 200 µl of prewarmed SOC medium was added to cells. Cells were shaken horizontally at 37 °C for 1 hour. 10-50 µl from transformation reaction was spreaded on a prewarmed selective plate and incubated overnight at 37 °C.

2.2.1.9 Analysis of positive clones

6-7 single colonies were picked and incubated overnight in 5 ml LB medium containing selective antibiotic. Mini plasmid DNA preparation was done using GenElute plasmid miniprep kit (Sigma-Aldrich). Analysis of the clones was carried out by restriction endonuclease digestion and DNA sequencing. Thereafter, one positive clone was inoculated to 100 ml LB medium containing selective antibiotic and cultured at 37 °C overnight. Midi plasmid DNA preparation was done using Nucleobond xtra midi EF (Macherey-Nagel).

2.2.1.10 Estimation of DNA concentration using spectrophotometric method

Nucleic acids absorb light in the UV range due to the presence of purine and pyrimidine bases in their structures. DNA have absorption maximum at or near 260 nm. For checking the purity of nucleic acid sample, absorption is measured at 260

nm as well as 280 nm. The ratio of 260 to 280 nm absorption should be between 1.8 and 2.0 for pure nucleic acids sample.

On an average, if absorbance (optical density) of a DNA sample at 260 nm is 1, it has 50 µg/ml DNA (light path = 1 cm). For smaller size oligonucleotides, it is 35 µg/ml.

1 µl of DNA sample was diluted in 119 µl of H₂O, mixed and absorbance was measured at 260 nm and 280 nm.

2.2.1.11 Sanger method of DNA sequencing (Dideoxynucleotide chain termination method)

DNA sequencing reactions were performed using Sanger's method (Sanger et al., 1977). It is a fluorescent dye labeling method and is also called as enzymatic DNA sequencing. The components of the reaction mixture were as follows:

Terminator ready reaction mix	8 µl
dsDNA	500 ng
Primer (10 pmol/µl)	1 µl
H ₂ O to a final volume of	20 µl

Cycling parameters:

Step	Temperature	Time	Cycles
Denaturation	96 °C	10 seconds	25X
Annealing	50 °C	5 seconds	
Extension	60 °C	4 minutes	

20 µl of the PCR product was added to 35 µl of 95% ethanol and the sample was incubated on ice for 10 minutes. Then the sample was centrifuged at 14,000 rpm, 4 °C for 20 minutes. Supernatant was discarded and pellet was air dried. Pellet was then resuspended in 75 µl of HPLC-grade ddH₂O, heated at 80 °C for 2 minutes. Sequencing was performed using ABI PRISM 310 Genetic Analyzer (PE Applied Biosystems).

2.2.1.12 Zero blunt TOPO PCR cloning

2.2.1.12.1 Principle

The plasmid vector (pCR™4Blunt-TOPO®) is supplied linearized with Vaccinia virus DNA topoisomerase I covalently bound to the 3' end of each DNA strand (referred to as "TOPO®-activated" vector). Topoisomerase I from Vaccinia virus binds to duplex DNA at specific sites and cleaves the phosphodiester backbone after 5'-CCCTT in one strand (Shuman, 1991). The energy from the broken phosphodiester backbone is conserved by formation of a covalent bond between the 3' phosphate of the cleaved strand and a tyrosyl residue (Tyr-274) of topoisomerase I. The phospho-tyrosyl bond between the DNA and enzyme can subsequently be attacked by the 5' hydroxyl of the original cleaved strand, reversing the reaction and releasing topoisomerase (Shuman, 1994). TOPO® Cloning exploits this reaction to efficiently clone PCR products.

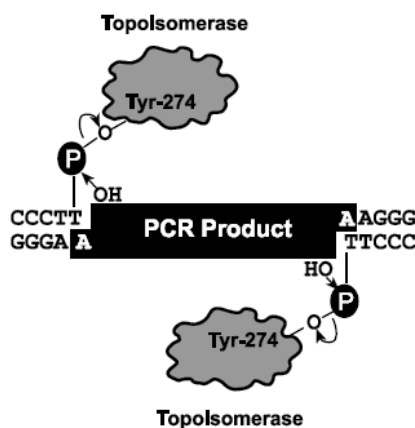


Figure 2.2: Schematic view of TOPO blunt end ligation.

Topoisomerase binding to double-stranded DNA leads to the cleavage of phosphodiester backbone, the energy released is used in the formation of a bond between the 3' phosphate of the cleaved strand and a tyrosyl residue of topoisomerase I. The reaction is reversed when the 5' hydroxyl of the original cleaved strand attacks the new phospho-tyrosyl bond, thereby releasing the topoisomerase I (adapted from Zero Blunt end TOPO cloning manual, Invitrogen).

TOPO PCR cloning was performed using the Zero Blunt TOPO PCR cloning kit (Invitrogen).

2.2.1.12.2 Producing blunt-end PCR products

The components of the reaction mixture were as follows:

dsDNA template (500 ng)

Reverse primer (10 pmol/μl)	1 μl
Forward primer (10 pmol/μl)	1 μl
Pwo Master Mix	25 μl
H ₂ O to a final volume of	50 μl

Amplification was done using the following cycling parameters:

[†]Melting temperature was calculated for each oligonucleotide primers pair.

[§]Elongation time depends on the expected size of the fragment.

Step	Time	Temperature	Cycles
Initial denaturation	2 minutes	95 °C	1X
Denaturation	30 seconds	95 °C	30X
Annealing	30 seconds	T _m [†] °C	
Extension	X [§] minutes	72 °C	
Final Extension	10 minutes	72 °C	1X

The melting temperature (T_m) of the oligonucleotide primers (see **Appendix 6.3**) was calculated either by using the Vector NTI program or according to the following empirical equation (Newton & Graham, 1997):

$$T_m = [(number\ of\ A + T) \times 2\ ^\circ C] + [(number\ of\ G + C) \times 4\ ^\circ C]$$

After producing blunt-end PCR product, agarose gel electrophoresis was done to verify the quality and quantity of PCR product.

2.2.1.12.3 TOPO cloning reaction

The following reagents were used to set up the TOPO cloning reaction:

Fresh PCR product	2 μl
Salt solution	1 μl
PCR II-Blunt-TOPO	1 μl
H ₂ O to a final volume of	6 μl

Reaction was mixed gently and incubated for 5 minutes at room temperature before transformation into a competent bacterial strain (TOP-10 or XL-10 Gold).

Ten colonies were picked and inoculated for plasmid preparation. The plasmids were digested with EcoR I sites flanking the PCR product insertion to allow screening of positive clones. Once a positive clone was identified, the TOPO vector containing the gene of interest and the appropriate destination vector(s) (for vectors see Appendix 6.4) were cut with the appropriate endonuclease enzyme(s) using the temperature and buffer as recommended on <http://www.neb.com/nebecomm/products/protocol445.asp> and http://www.fermentas.com/en/support/ApplicationProtocols/?country_code=DE for conventional restriction enzymes from NEB and Fastdigest enzymes from Fermentas respectively. After restriction the vector DNA was subsequently dephosphorylated with alkaline phosphatase (Roche Diagnostics, Mannheim, Germany) according to manufacturer's instructions in order to avoid religation. Ligation reaction was prepared as described in **section 2.2.1.7** and used for transformation in chemically competent cells.

2.2.1.13 Gateway cloning

The Gateway™ technology (Invitrogen, Karlsruhe, Germany) is a universal cloning method that makes it possible to clone a desired insert into multiple vector backbones. The system is based on the site-specific recombination properties of the recombinase from bacteriophage lambda (Landy, 1989).

In Gateway™ cloning technology a single cloning event can lead to the generation of a construct (entry clone) from which the fragment of interest can be subcloned to a vast array of vectors. A whole array of vectors is now available for the functional and biochemical analysis of specific DNA sequences and their products, thanks to the lambda recombination system. Using the Gateway™ technology the fragment of interest, once properly cloned, will always keep the same orientation and reading frame allowing directional cloning and easy tagging with the tag of interest. Gateway™ cloning is based on Lambda recombination that occurs between site-specific attachment (att) sites. The att sites integrated in the vector serve as the binding site for recombination proteins and have been well-characterized (Weisberg et al., 1983). There is no loss of genetic material during recombination and the recombination reaction perfectly combines the replacement of a given sequence in

the vector of interest with the inserted sequence without the need for canonical ligation or restriction steps (**Fig. 2.4**).

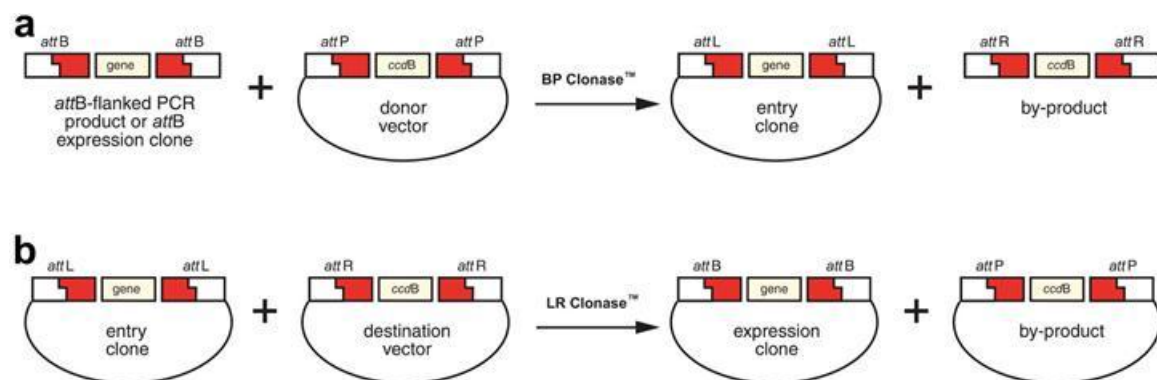


Figure 2.4: Schematic view of the BR and LR reaction occurring during the Gateway™ cloning. **(a):** Schematic view of the generation of an entry vector. A PCR fragment flanked by the two *attB* sites is combined with the donor vector. A recombination event takes place in presence of BP clonase generating an entry clone with the fragment of interest and a by-product composed of the *ccdB* cassette flanked by two *attR* sequences. **(b):** Schematic view of the generation of an expression clone. An entry clone flanked by the two *attL* sites recombine with the *attR* sites of the destination vector in presence of LR clonase forming an expression clone and a by-product. Note that the expression clone insert is flanked by two *attB* sites allowing a recloning in a donor vector (adapted from Gateway™ technology manual).

First of all a PCR amplified insert was generated using specific primers containing a 50 adaptor region called *attB* site (**Fig. 2.4 a**) in order to perform the first BP reaction. The reaction occurred in a total volume of 50 μ l. The PCR product was purified according to the following protocol:

25 μ l PCR product was mixed with 75 μ l TE buffer, pH 8.0 and 50 μ l 30% PEG 8000/30 mM $MgCl_2$, vortexed and centrifuged for 20 minutes at RT as recommended in the Gateway™ technology manual. The supernatant was removed carefully and the pellet dissolved in 25 μ l of TE, pH 8.0. The purified PCR product was checked on agarose gel for purity before performing the recombination reaction.

7 μ l of the purified linear PCR product were incubated with 1 μ l of the donor vector (150 ng/ μ l) with the *attP* sites and 2 μ l of BP Clonase II Enzyme. The mixture was vortexed briefly and incubated at 25°C overnight. The BP reaction led to the integration of the fragment into the donor vector by specific recombination of the *attB* cassette of the insert with the *attP* cassette of the donor vector. For easy selection of true recombinants the donor vector contained the toxic *ccdB* cassette that allowed a negative selection of the bacteria transformed with donor vectors that do not come

from a recombination event. Once the insert was integrated into the donor vector, the new clone was referred to as "entry clone".

In the whole process of recombination a by-product containing the ccdB cassette flanked by two attR sequences was generated (**Fig. 2.4a**). This newly generated entry clone was used for bacterial transformation and transformed cells were selected for the antibiotic resistance carried by the donor vector. The entry clone was transformed for amplification in bacterial cells as described in section 2.2.1.8 and purified as described in section 2.2.1.6. After purification the new construct was stored in TE buffer at -20°C.

Once an entry clone is generated, the Gateway™ technology allows the insertion of the fragment of interest into the functional vector of choice through an LR reaction.

2.2.2 *C. elegans* methods

2.2.2.1 Maintenance of *C. elegans* strains

Animals were maintained on NGM agar plates (Ø 3.5 cm, 5 cm, or 9 cm) seeded with *E. coli* OP50 as previously described (Brenner, 1974). The basic culture methods were performed as described elsewhere (Lewis and Fleming, 1995; Stiernagle, 2006). NGM plates with worms were kept in cardboard boxes at 15, 20, or 25°C.

2.2.2.2 Freezing of *C. elegans* strains

Slow freezing at -80°C allows storing of *C. elegans* strains for a long time period at cryogenic temperatures. When needed, a 9 cm plate was grown until fully covered by slightly starved L1 and L2 stage animals. After washing the worms off the plate with M9 medium (**section 2.1.11**), they were placed in a 15 ml tube. Animals were washed two times by spinning at 1,000 g at 4°C for 2 minutes and changing the M9 buffer twice. Finally the worm suspension was mixed 1:1 with freezing buffer (**section 2.1.11**) and aliquots of 1 ml were transferred into cryovials (Thermo Fisher Scientific, Langenselbold, Germany). Six cryovials were placed in Styrofoam boxes and placed in an ultra-low temperature freezer at -80°C overnight. The following day a control vial was thawed and the content placed in a fresh NGM plate seeded with

OP50. When the rescue of freezed worms exceeded hundred units the freezing procedure was considered successful. In this case four of the five remaining vials were kept at -80°C and 1 stored as backup in liquid nitrogen.

2.2.2.3 Out crossing of *C. elegans* strains

All not out crossed mutant strains obtained by external laboratories or produced from our lab were backcrossed at least five times with the *C. elegans* N2 wild type animals in order to eliminate possible unwanted secondary mutations from the genome. L4 stage hermaphrodites and males were placed in small plates in a ratio of 1 to 5, respectively and transferred into a fresh small plate after 24 hours. The eggs laid in the first 24 hours were discarded due to the high probability of self-fertilization. F1 progeny obtained by eggs laid in the following 24 hours was controlled for a ratio of hermaphrodites to males of 1:1, which was considered as a successful cross. About 20 young F1 hermaphrodite animals were singled out in separate plates at the L4 stage to test the F2 generation. The F2 progeny was analyzed in detail to confirm the success of the cross. Depending on the features of the mutant involved, the genotype of the F2 generation was analyzed by SW-PCR (**section 2.2.2.4**), fluorescent marker, or the combination of these methods. Once the correct F2 worms were identified a final confirmation of F3 worms completed the crossing experiment.

2.2.2.4 Worm lysis for single worm PCR (SW-PCR)

To determine the genotype of the worms via PCR, single worms were transferred into single PCR reaction tubes with 4 µl lysis buffer (**section 2.1.11**). The tubes were incubated at -80°C for 40 minutes then heated to 65°C for 40 minutes and to 95°C for 10 minutes and kept on ice until the time of usage. The worm lysate was then used directly for the specific PCR reaction. PCR settings were optimized according to the characteristics of the primers and the length of the fragment of interest.

2.2.2.5 Decontamination and synchronization of *C. elegans* strains

For the decontamination or synchronization of *C. elegans* strains, worms were treated with alkaline hypochlorite. To obtain a synchronized population, well fed

worms from one to two 10 cm plates were rinsed off with M9 buffer into a 15 ml falcon tube. The animals were washed by spinning at 1,300 g at 4°C for 30 seconds exchanging the M9 buffer once. After the second centrifugation the M9 buffer was eliminated up to 3.5 ml and 1.5 ml of bleaching solution was added. The falcon tube was shaken vigorously by vortexing intermittently for 10 minutes to destroy the cuticle of gravid animals and allow the release of eggs. After 10 minutes of vigorous shaking, eggs and worm debris were pelleted by centrifugation at 1,300 g at 4°C for 30 seconds. The hypochlorite was then replaced by fresh M9 medium. After at least four washing steps the eggs were resuspended in fresh M9 medium and transferred into a new falcon tube. After 2 more washing steps, eggs were incubated overnight in M9 medium. On the following morning synchronized L1 worms were ready to be used for subsequent analysis.

2.2.2.6 Generation of Tau transgenic *C. elegans* strains for muscle expression

All extra chromosomal transgenic strains were generated as previously described (Mello et al., 1991). For the expression of tau in body wall muscles, pPD30_38 vector was used which contains the unc-54 promoter (myosin heavy chain). Following Tau chimeras were generated for expression in muscle cells:

pPD30_38:htau40Dk280

pPD30_38:htau40Dk280PP

pPD30_38:K18Dk280

pPD30_38:K18Dk280PP

pPD30_38:F3Dk280

pPD30_38:F3Dk280PP

The method consisted of the co-injection of the expression plasmid of interest and a marker plasmid into the germ line of a young hermaphrodite adult worm and the observation of the following generations. The concentration of DNA mixture used in the microinjection was:

Tau constructs	1.0ng/ μ l
Mcherry marker	20ng/ μ l
Salmon sperm DNA	100ng/ μ l

Worms bearing the transgenic marker gene were kept for further analysis. Single worm PCR was used to detect the presence of transgene using the Htau Fwd (JB 307) and Htau Rev (JB 308) primers (see Appendix 6.3). The transgenic strains and the transgenic arrays generated were named individually so that the history of each transgenic line was clearly identified. The transgenic lines generated for the study of tauopathy in the body wall muscles are listed below:

Ex[pPD30_38::Htau40ΔK280;Pmyo-2:mcherry]

Ex[pPD30_38::Htau40ΔK280PP;Pmyo-2:mcherry]

Ex[pPD30_38::K18ΔK280;Pmyo-2:mcherry]

Ex[pPD30_38::K18ΔK280PP;Pmyo-2:mcherry]

Ex[pPD30_38::F3ΔK280;Pmyo-2:mcherry]

Ex[pPD30_38::F3ΔK280PP;Pmyo-2:mcherry]

Integration of all the above mentioned extrachromosomal arrays was carried out using the Cesium source at ZKF. 30 grays were applied on the plates. The penetrance of all our lines was approximately 10 % before integration. After the integration, the F3 generation had more than 75 % penetrance (25% the homozygous, 50% the hetero, plus the background penetrance for the non-integrated). Following three integrated lines were obtained in the first shot:

Int[pPD30_38::Htau40ΔK280;Pmyo-2:mcherry]

Int[pPD30_38::F3ΔK280;Pmyo-2:mcherry]

Int[pPD30_38::F3ΔK280PP;Pmyo-2:mcherry]

2.2.2.7 RNA interference (RNAi) feeding experiments

For RNAi against tau we decided to clone the tau repeat fragment F3ΔK280 which would serve to silence both the full length pro- and anti-aggregant tau variants and their repeat fragments. cDNA encoding F3ΔK280 was cloned into L4440 feeding vector (Timmons and Fire, 1998) at the MCS using NheI and XbaI restriction sites. The L4440 plasmid has an IPTG inducible T7 promoter on both ends of the construct leading to the transcription of the sense and antisense strand of the inserted DNA under IPTG induction (see Appendix 6.4). The ingested dsRNA triggers the knock-down of the gene of interest in *C. elegans*. The bacterial strain of choice for the RNAi experiments was *E. coli* HT115 (DE3) (Fire et al., 1998).

In practice, the RNAi experiments were conducted on NGM agar plates. Synchronized L1 larvae obtained by bleaching **as described in section 2.5.6** were poured onto RNAi plates.

For the preparation of RNAi plates, cultures of HT115 (DE3) bacteria containing the RNAi clone of interest were grown overnight in LB medium containing 12 µg/ml tetracycline and 50 µg/ml carbenicillin. After overnight incubation the bacterial culture was diluted 1:1 in fresh LB medium with the aforementioned antibiotics. The expression of the RNAi construct was induced in the 1:1 diluted culture for 6 hours with 1 mM IPTG. After the period of induction the bacteria were plated on NGM plates containing 1 mM IPTG and 100 µg/ml carbenicillin or ampicillin, and dried. As negative and positive controls bacteria transformed with the empty vector L4440.

2.2.2.8 2'-deoxy-5-urouridine (FUdR) treatment

FUdR was solved in ddH₂O to obtain a 100 mM stock solution. The stock solution was applied to the *E. coli* seeded NGM plates to obtain a final concentration of 100 µM. For experimental analysis, late L4 worms were placed on FUdR plates and allowed to grow for one day before being transferred to the normal NGM plates.

2.2.2.9 Sucrose flotation of worms

To clean off the worms from the bacteria and the dead animals, worms were collected from 10cm NGM plates in 0.1M NaCl, transferred to a 15ml tube. The tube was vortexed briefly (the broken NGM chunks will stick to the sides of tube, while the worms stay in liquid) and the liquid transferred to a new tube. The worms were then pelleted at 3000rpm for 1 min. The liquid was removed and the pellet washed 1X with 10ml cold (4°C) 0.1M NaCl. Worms were pelleted again at 3000 rpm. Worms were resuspended in 5ml cold 0.1M NaCl and an equal vol (5ml) ice cold 60% sucrose was added and mixed quickly.

The liquid was layered with 2ml ice cold 0.1M NaCl on top of the sucrose and spun at 3000rpm for 5min. Live worms were collected at the interface of 0.1M NaCl and sucrose. The ~2.5 ml upper phase was transferred to a new 15ml tube containing 10ml M9 buffer and pelleted at 3000rpm.

2.2.2.10 PERCHLORIC ACID EXTRACTION OF TAU

Worms were collected from the NGM plates and cleared off from bacteria/dead animals by sucrose floatation as mentioned above. Worms were lysed in 3 times (wt/vol) of 2.5% perchloric acid (HClO_4) by sonication on ice (6x 10 s with 10 s breaks on ice, 40% amplitude). The lysate was incubated on ice for 20 min and centrifuged for 10 min at 10 000 g (Mikro 200R, Hettach). The supernatant was dialyzed overnight at 4°C in micro dialyzer tubes (Millipore) against 5% formic acid and recentrifuged. The resulting supernatant was concentrated using a speed vacuum apparatus and run on a 17% PAGE for western blot analysis (Goedert et al., 1990).

2.2.2.10.1 Sequential extraction of Tau (method 1)

Dead animals and bacteria were removed by flotation on a 30% sucrose solution. The entire extraction procedure was carried out on ice and centrifugation steps were at 4°C except the last step with 70% formic acid. To extract the different tau fractions (Ishihara, T. et al., 1999), worm pellets after sucrose separation were directly resuspended in an equal amount (wt/vol) of high salt RAB buffer (100 mM Mes, 1 mM EGTA, 0.5 mM MgSO_4 , 20 mM NaF). Worms were lysed by sonication (6 x10s, 10s break) on ice, and homogenates were centrifuged at 40,000 x g for 40 min. The supernatant constitutes the RAB fraction. The pellet was reextracted with 1 M sucrose in RAB buffer and centrifuged 20 min at 40,000 x g, and the supernatant was discarded. The pellet was extracted with RIPA buffer (150 mM NaCl, 1% Nonidet P-40, 0.5% deoxycholate, 0.1% SDS, 50 mM Tris, pH 8.0) and centrifuged at 40,000 x g for 20 min. The supernatant is the RIPA fraction. The pellet left after RIPA extraction was dissolved in 70% formic acid (FA) and centrifuged at 13,000 x g for 15 min. The supernatant is the FA fraction. All buffers contained Complete Protease Inhibitor mixture 3x (Sigma P8340) and 0.5 mM PMSF.

2.2.2.10.2 Sequential extraction of Tau (method 2)

Dead animals and bacteria were removed by flotation on a 30% sucrose solution. The entire extraction procedure was carried out on ice and centrifugation steps were at 4°C except the last step with 70% formic acid. To extract the different tau fractions

(Ishihara et al., 1999), worm pellets after sucrose separation were directly resuspended in an equal amount (wt/vol) of high salt RAB buffer (100 mM Mes, 1 mM EGTA, 0.5 mM MgSO₄, 20 mM NaF). Worms were lysed by sonication (6 x10s, 10s break) on ice, and homogenates were centrifuged at 40,000 x g for 40 min. The supernatant constitutes the RAB fraction. The pellet was reextracted with 1 M sucrose in RAB buffer and centrifuged 20 min at 40,000 x g, and the supernatant was discarded. The pellet was extracted with RIPA buffer (150 mM NaCl, 1% Nonidet P-40, 0.5% deoxycholate, 0.1% SDS, 50 mM Tris, pH 8.0) and centrifuged at 40,000 x g for 20 min. The supernatant is the RIPA fraction. The pellet was resuspended in RIPA buffer and centrifuged at 40,000 x g for 20 min and supernatant added to the first RIPA fraction. The final pellet left after the second RIPA extraction was washed in 1ml of RIPA buffer to remove all the soluble tau stuck on the tubes. The washed pellet was finally extracted with 70% formic acid (FA) and centrifuged at 13,000 x g for 15 min. The supernatant is the FA fraction. All buffers contained Complete Protease Inhibitor mixture 3x (Sigma P8340) and 0.5 mM PMSF. So compared to the first method, here two steps each of RAB and RIPA extractions along with additional washings are carried out to dissolve all the salt soluble and membrane-associated detergent soluble Tau. This in turn, reduces the contamination of RAB and RIPA fractions going into the insoluble fraction dissolved by 70% formic acid.

2.2.2.10.3 Sarkosyl extraction

Before starting the 1.5 ml eppendorf tubes were weighed. Worms in 15 ml tubes were washed until the solution was clean and transparent. The worms were then transferred into the 1.5 ml eppendorf tubes and the tubes weighed again. The worm pellets were resuspended in 3 vol (w/v) homogenization buffer consisting of 10 mM Tris HCl (pH 7.4), 0.8 M NaCl, 1 mM EGTA, 5 mM EDTA, 5 mM NaF, 100 nM okadaic acid, 1 mM orthovanadate, 5 mM microcystin, 3x Complete Protease Inhibitor mixture, and 10% sucrose. The worm pellets were lysed by sonication (9 x 10 s, 10 s break, BANDELIN SONOPULS HD3200, sonotrode: MS73) on ice and later incubated on ice for 20 min. The worm lysates were centrifuged at 14000 rpm (Eppendorf centrifuge) for 20 min. at 4°C to remove the debris. The supernatants were added to new tubes (supernatant 1). The worm debris was rehomogenized with equal volume of the original worm pellet and centrifuged at 14000 rpm for 20

min at 4°C to collect the supernatant 2. The supernatant 2 was combined with supernatant 1. The worm debris left after the second extraction was boiled in 2x sample buffer (w/v of the original worm pellet) and equal volume from each sample was loaded onto the gel. The final volume of the supernatant (1+2) was measured and brought to final 1% N-lauroyl-sarcosinate and 10µg/ml β-mercaptoethanol was added (we keep a 10% N-lauroyl-sarcosinate solution and the ratio of 10% N-lauroyl-sarcosinate to supernatant 1+2 is 1:9). The cell lysates were incubated for 1 h at room temperature while shaking and centrifuged at 100,000 x g for 35 min at 4°C (Rotor TLA100.3). The supernatants were transferred to new tubes and the pellets washed carefully with 100µl 1x TBS 3 times. In the 3rd 1x TBS wash, the pellets were centrifuged briefly for 10 min at 100,000 x g at 4°C to remove any soluble tau from the tube surface and the remaining supernatants were carefully removed. The pellet was resuspended in 50 mM Tris-HCl (pH 7.4), 0.5 µl/mg of starting worm pellet (this will be sarkosyl- insoluble tau). To the aliquots of supernatant (sarkosyl soluble tau) and pellets (sarkosyl-insoluble tau) equal volume of 2x SDS sample buffer was added. The samples were loaded on SDS PAGE in the ratio of 1:3 (soluble to insoluble).

2.2.2.10.4 Compound treatment

E. coli OP50 were grown overnight at 37°C in LB media, pelleted by centrifugation, frozen at -70°C, and then resuspended at a final OD of 1.5 (595 nm) in nematode S-medium (Wood, 1988). Compounds dissolved in the corresponding solvents (100% dmso in case of bb14, BSc3094, compound 16, Anle 138b and Anle 138c or 1x PBS in case of methylene blue and trehalose) were diluted into *E. coli* suspension to the desired concentrations. 1% dmso was used as a control in case of the compounds which were dissolved in dmso and the final concentration of dmso in the compound treated samples was also adjusted to 1% (Anle138 b and c precipitated in the liquid media; therefore, the two compounds were tested in the solid medium by dissolving the compounds in the NGM to their desired concentration before pouring the plates). 5 ml of the final mixture was added per well in a 6-well polystyrene plate and synchronized pro-aggregation L1 larvae collected overnight were added to the wells containing the desired compounds. The worms were allowed to grow at 20°C with constant shaking until day 4 of adulthood and harvested for the protein extraction.

2.2.2.10.5 Thrash Assay

The "thrashing assay", is used as a measure of motility in the genetic model organism *Caenorhabditis elegans* as well as in parasitic nematodes. In this assay, the nematodes are placed in liquid and the frequency of lateral swimming ("thrashing") movements is estimated. A thrash is defined as the change in direction at the mid-body, so that when a thrash is completed both the tail and the head point in the same direction.

It is used as an index of the effects of drugs, chemicals or mutations on motility and has proved to be useful. For thrash assays, compounds were diluted to the desired concentrations into S-medium containing OP-50 at a final OD of 0.5 (595 nm). 200µl of the final solution was added per well of a 96-well polystyrene plate and synchronized L1 larvae obtained by bleaching as described in section 2.2.2.5 were added to each well with/without compounds. The worms were allowed to grow in this medium up to day 3 of adult stage, at which the worms were transferred to NGM plates containing the same concentration of the respective compounds and allowed to acclimatize for 1 hour before analyzing them for the thrashes. For thrash assays, single worms were randomly picked and placed in 20 µl drop of M9 buffer, allowed to recover for 1 min. Thrashes were recorded using Cell^A soft Imaging system with Olympus SC30 camera mounted on an *Olympus SZH10 Zoom Stereo Microscope*.

2.2.2.10.6 Autophagy Flux

For flux experiment, FUdR-sterilized 1 day old adults were grown in OP50 suspension in four separate wells, two without trehalose and two with trehalose (200mM), of a 6-well polystyrene plate. The worms were allowed to grow at 20°C with constant shaking until day 4 of adulthood. Worms at this stage in two of the four wells, one with trehalose and one without trehalose were treated with 150mM NH₄Cl for a period of 8hrs and harvested later. For efficient sonication and in order to avoid foam formation, worm pellets were sonicated in an equal volume (wt/vol) of lysis buffer without detergent (50mM Tris-HCl, pH 7.4, 10% glycerol, 20mM NaF, 1mM sodium orthovanadate, 150mM NaCl, 3x Complete Protease Inhibitor mixture (Sigma P8340), 5µM okadaic acid, 1mM PMSF). The lysate was mixed with the same amount (wt/vol) of lysis buffer containing 2x detergent (50mM Tris-HCl, pH 7.4,

10% glycerol, 2% NP40, 20mM NaF, 1mM sodium orthovanadate, 150mM NaCl, 3x Complete Protease Inhibitor mixture (Sigma P8340), 10mM CHAPS, 5 μ M okadaic acid, 1mM PMSF), vortexed briefly and incubated on ice for 30 min. The lysate was centrifuged at 50,000 x g for 20 min and supernatant checked for LGG2 levels (MAP1LC-3 ortholog in *C. elegans*) (Alberti et al., 2010).

2.2.2.10.7 Food clearance assay

E. coli OP50 were grown overnight at 37°C in LB media, pelleted by centrifugation, frozen at -70°C, and then resuspended at a final OD of 0.5 (595 nm) in nematode S-medium (Wood, 1988) (supplemented with 100x streptomycin/penicillin, Invitrogen). 200 μ l of the final mixture was added per well in a 96-well polystyrene plate.

Approximately, 20-30 synchronized L1 larvae collected overnight were added to the wells. Micro titer plates containing animals were incubated at 20°C with constant shaking. The absorbance (OD 595nm) was measured daily using TECAN. The mean O.D. was calculated for each day from triplicate samples.

2.2.2.10.8 Statistical analyses

One-way ANOVA was applied to test statistical differences between independent groups within the same experiment. Statistical significance was tested with Newman-Keuls, Tukey, and Bonferroni post tests. Two-tailed unpaired Student's t-test was used to examine direct differences between independent groups and to validate ANOVA results. Statistical analysis of survival curves for the lifespan experiments were conducted by use of the Logrank (Mantel-Cox) test.

2.2.2.11 Biochemical Assays

For solubility assays, cells were collected by centrifugation at 1,000 x g for 5 min. The levels and solubility of different tau constructs were determined by sarkosyl extraction or sequential extraction using buffers of increasing stringency (RAB, RIPA, and FA). Soluble and insoluble fractions were analyzed by Western blotting. In case of sarkosyl fractions, the amount of material loaded for supernatant and sarkosyl-insoluble pellet represented \approx 0.5 and 15% of the total material present in the

supernatant and pellet, respectively (the ratio between supernatant and sarkosyl insoluble pellet was always 1:30). For quantification of tau levels, the Western blots were probed with pan-tau antibody K9JA (DAKO, Glostrup, Denmark) and analyzed by densitometry.

2.2.2.12 Immunofluorescence

Inducible N2a cells were transfected with pBI5 plasmids encoding tau fragments mentioned above. After 1 day, cells were induced to express tau with 1 µg/ml doxycycline for 2–3 days. The cells on the coverslips were fixed with 4% paraformaldehyde in PBS for 15min, then permeabilized with 80% MeOH for 6min at -20°C, blocked with 10% goat serum (PBS) for 30 min. Samples were incubated with antibody K9JA against tau and/or antibody against calreticulin for ER localization in 5% goat serum (PBS). The secondary antibodies (anti-rabbit antibody labeled with Cy5 and anti-chick antibody labeled with Cy3) were also diluted with 5% goat serum in PBS and incubated for 45 min. The cells were incubated with DAPI in PBS for 5 min for nuclear staining and afterwards washed twice with PBS, once with water, and mounted. For mitochondrial localization, cells on the coverslips were incubated with Mitotraker in PBS for 45 minutes before fixation. Confocal microscopy was done with a LSM510 microscope (Zeiss, Oberkochen, Germany) and LSM700 (Zeiss).

2.2.3 Biochemical methods

2.2.3.1 Sodium dodecyl sulfate polyacrylamide gel electrophoresis (SDS-PAGE)

SDS-PAGE for separation of proteins was performed according to a modified protocol (Laemmli, 1970; Matsudaira and Burgess, 1978). Sodium dodecyl sulfate, an anionic detergent, is used to completely suppress the native charge on the proteins. It gives them a large negative coat of detergent molecules. The SDS also interacts with the hydrophobic core of proteins, it causes a rapid and irreversible unfolding that linearizes the polypeptide chains which all now have a roughly equivalent charge/mass ratio. Therefore, in SDS-PAGE, the separation of proteins is on the basis of molecular weight (size) of the proteins.

A system with vertically oriented glass plates with 1 mm spacer in between was used for casting gels. Separating gel (small pore size gel) and stacking gel (large pore size gel) were prepared as first described by Ornstein, 1964.

Composition of separating and stacking gel:

Components	Separating gel	Separating gel	Stacking gel (4%) (ml)
	10% (ml)	17% (ml)	
40% Acrylamide/ Bis acrylamide (37.5:1)	15	25.6	5.4
Tris HCl (1.0 M, pH 8.8)	22	22	-
Tris HCl (0.25 M, pH 6.8)	-	-	27
10% SDS	0.6	0.6	0.54
TEMED	0.12	0.12	0.108
10% APS	0.065	0.065	0.065
H ₂ O	22	11.5	20.9

First the separating gel was poured between glass plates and a layer of isopropanol was applied onto it. After polymerization of separating gel, the layer of isopropanol was removed and polymerized gel was washed with H₂O. Then the stacking gel was poured on the top of the polymerized separating gel and the comb was inserted. When the gel solution got solidified, the gel was placed in the electrophoresis chamber filled with the 1X SDS running buffer and comb was removed. Protein sample to be electrophoresed was mixed with 6X SDS sample buffer containing 1.25 M Tris-HCl, pH 6.8, Glycerol, 50% SDS and 0.25% Bromophenol blue and denatured completely by heating at 95 °C for 5 minutes. Then the denatured protein samples were loaded along with molecular weight marker proteins and electrophoresis was performed at 150 volts.

Phosphate-buffered saline (PBS)	140 mM NaCl, 2.7 mM KCl, 10 mM Na ₂ HPO ₄ 1.8 mM KH ₂ HPO ₄ , pH 7.3
PBST	0.1% (v/v) Tween-20 in PBS
Blocking buffer	5% milk powder in PBST
Glycine stripping solution	0.2 M glycine pH 2.8, 0.5 M NaCl
SDS stripping solution	16 mM Tris-HCl pH 6.8, 2% SDS, 0.1 M β-mercaptoethanol

2.2.3.4 Stripping of nitrocellulose membranes

Removal of antibodies from a blot was done under mild conditions to reduce the background for incubation with another primary antibody, either from a different species or for a protein of clearly distinct size than in the first decoration. After washing the membrane in PBST, it was incubated 5-20 min in glycine stripping solution. The solution was neutralized with 1 M Tris-HCl pH 8.5, followed by several washes in PBST. If it was crucial to remove antibodies completely, the blot was incubated in SDS stripping solution for 30 min, tightly closed, on a wheel at 50°C, followed by several washes in PBST. Decoration of the membrane was done as described above, starting from the blocking step again.

2.2.3.5 Estimation of protein using bicinchoninic acid (BCA)

The macromolecular structure of protein, the number of peptide bonds and the presence of four particular amino acids (Cysteine, Cystine, Tryptophan, Tyrosine) are responsible for color development with BCA. Accordingly, protein concentrations generally are determined and reported with reference to standards of a common protein such as bovine serum albumin (BSA).

A series of dilutions of known concentration were prepared from the standard protein BSA and assayed alongside the protein sample of unknown concentration.

Standard (Volume in µl)

H ₂ O	25	20	15	10	0
BSA (1 µg/µl)	0	5	10	15	25

Just before use, BCA reagent was prepared by mixing one part of copper sulfate (Sigma-Aldrich) with 50 parts of BCA (Sigma). The aliquot and water was taken upto 25 μ l, and to it, 200 μ l of BCA reagent was added. After mixing, it was incubated at 37 °C for 30 minutes in dark. Thereafter, the absorbance was measured at 562 nm using TECAN infinite M200 plate reader.

3 RESULTS

3.1 Single worm PCR confirms the presence of transgenes

The presence of well-established forward and reverse genetic tools, a wide range of mutants and a fully sequenced genome along with the relative ease and speed with which the genetic modifiers of disease phenotype can be discovered makes *C. elegans* an excellent model to study the human diseases. Furthermore, given the ease with which *C. elegans* can be grown in liquid cultures which facilitates uptake of substances from the aqueous medium makes it ideal for a high throughput pharmacological screening. Several tauopathy models of *C. elegans* have been described before (Brandt et al., 2009; Kraemer et al., 2003; Miyasaka et al., 2005). Only one of these models accumulates tau aggregates and hence develops defects at a very late stage in their life. Previous studies have shown that the proteostasis regulation which is important for cellular maintenance gets disrupted as the organism ages. For example, the protein degradation machinery which takes care of the damaged proteins and helps in recycling them becomes less efficient with age (Cuervo and Dice, 2000; Tonoki et al., 2009), levels of molecular chaperones which guide the proper folding of the nascent polypeptide chains or misfolded proteins change with age (Lund et al., 2002). In addition, proteins undergo increased irreversible modifications like oxidation and nitration with age which in turn disrupts their recycling (Squier, 2001). Furthermore, in *C. elegans* several hundreds of proteins have been identified which become prone to aggregation with age (David et al., 2010). Keeping all these things in mind, a general phenomenon of aging can contribute to a disease phenotype that appears at a later stage in the life-span of an organism like *C. elegans* which has such a short life-span of approximately 2 weeks. Therefore, in order to perfectly model a human disease in *C. elegans*, it becomes necessary to have a disease phenotype as early in its life-span as possible. Here we wanted to develop a model system having tau aggregates very early in its life so as to uncouple a disease phenotype with a natural decline in the proteostasis with age. This would allow us to attribute the phenotype solely to the presence of tau transgenes in the worm which will finally pave the way for this novel tauopathy model to be used to find the

modifiers of tauopathy by genetic screening. Last but not least, this model would help us to screen for new compounds against tau aggregates, in addition to those already tested in the *in vitro* studies on tau aggregates (Ballatore et al., 2007; Bulic et al., 2009; Pickhardt et al., 2007). In order to achieve this, we co-expressed in a single line the highly amyloidogenic pro-aggregant F3 fragment containing Δ K280 mutation known to accelerate the aggregation of the full-length tau protein by

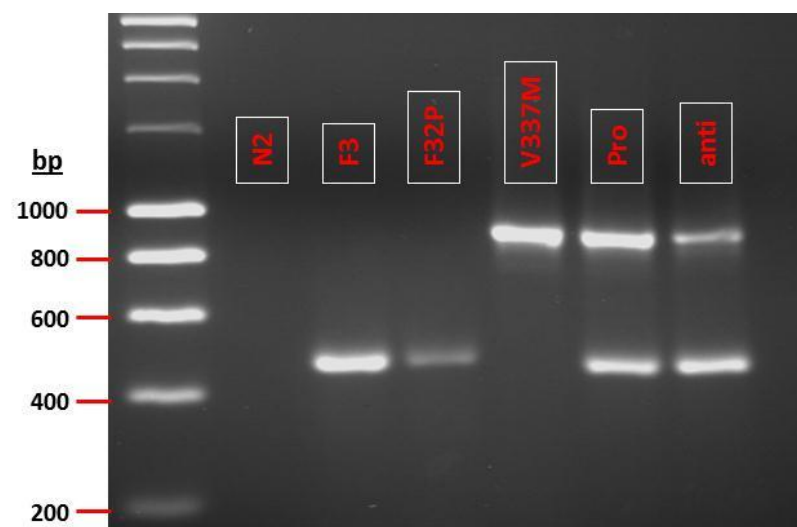


Figure 3.1: Single worm PCR analysis to detect the presence of transgenes. Single Tau-transgenic F3, F32P and FL Tau $V337^M$ strains show only one band corresponding to F3 Δ K280, F3 Δ K280PP and FL Tau $V337^M$, while double tau-transgenic pro-aggregant and anti-aggregant strains show two bands corresponding to FL Tau $V337^M$ and F3 Δ K280 or F3 Δ K280PP respectively. N2 wild type non-transgenic laboratory strain serves as a control.

forming seeds (Wang et al., 2007) with a well characterized Δ K280 mutation (Eckermann et al., 2007; Khlistunova et al., 2006; Mocanu et al., 2008; Sydow et al., 2011) along with the full-length $V337^M$ tau. This was achieved by crossing a strain expressing the tau repeat fragment F3 Δ K280 panneuronally driven by *Rab-3* promoter with the already published CK10 strain expressing the full-length $V337^M$ tau also panneuronally driven by *aex-3* promoter (Kraemer et al., 2003). As a control, we crossed the CK10 strain with a strain expressing the anti-aggregant repeat fragment of tau F3 Δ K280PP, containing two additional proline residues within the hexapeptide motifs (I287P and I308P). The presence of additional prolines produces kinks in the peptide chain due to the cyclic nature of amino acid proline which in

turn destabilizes the amyloid sheet and hence inhibits the aggregation (von Bergen et al., 2001).

To confirm the presence of tau transgenes in our tau-tg model, we designed the reverse primer which binds to the repeat region of tau and hence would act as a common primer for both the transgenes (the full-length tau^{V337M} and the F3ΔK280/F3ΔK280PP repeat fragment) in a double tau-tg *C. elegans* line. The forward primers for the two transgenes were selected from their respective promoter regions (Paex-3 for full-length and pRab-3 for F3ΔK280/F3ΔK280PP fragment). The result is that a single tau-tg line would yield a single band and a double tau-tg line would yield two bands corresponding to the two transgenes in a single PCR amplification reaction as shown in Fig 3.1.

3.2 Western blot analysis for tau-transgenic expression

In order to observe the expression of tau transgenes in Tau-transgenic worms, worm

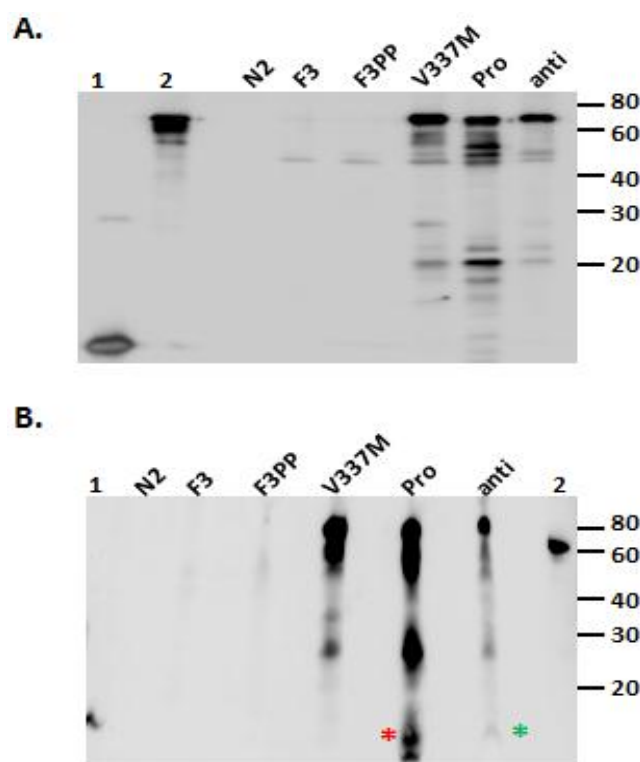


Figure 3.2: Tau expression by immunoblotting using K9JA pan tau antibody. Packed mixed stage worm pellets after boiling in 2X SDS sample buffer (A) or 2.5% perchloric acid extraction (B) were analyzed. Perchloric acid samples were analyzed by running on an 8-20% gradient gel to facilitate the detection of the F3ΔK280/F3ΔK280PP fragments. Lanes 1 and 2 denote recombinant F3ΔK280 and htau40ΔK280 proteins respectively. N2 is wild type non-transgenic control worm, F3 is single transgenic line expressing F3ΔK280, F3PP is single transgenic line expressing F3ΔK280PP, V337M is single transgenic line expressing FL Tau^{V337M}, Pro denotes double transgenic pro-aggregant strain and anti stands for double transgenic anti-

aggregant strain. A thick band corresponding to F3ΔK280 in case of pro-aggregant strain (*) and a faint band (*) corresponding to F3ΔK280PP in case of anti-aggregant strain can be seen after 2.5% perchloric acid extraction only. However, no F3ΔK280 and F3ΔK280PP bands were detected in the single transgenic F3 and F3PP strains.

pellets were boiled in 2 X sample buffer and the supernatant after centrifugation was loaded onto a 17%-PAGE gel and blotted with K9JA antibody. Western blot analysis showed the FL tau^{V337M} bands in the FL tau^{V337M}, pro-aggregant and anti-aggregant strains. However, there were no traces of the repeat fragments, F3ΔK280 in the pro-aggregant line and F3ΔK280PP in the anti-aggregant line, as well as in the F3 and F3PP single transgenic lines (**Fig 3.2 A**).

3.3 2.5% perchloric acid extraction of tau

The continued search for the repeat fragments in the two double-tg lines prompted us to exploit a very unusual property of tau, which is its solubility in perchloric acid. The perchloric acid solubility of tau has been used to isolate and purify tau from other proteins from crude brain extracts (Lindwall and Cole, 1984). We extracted tau protein from mixed stage adult animals from each tau-transgenic line (**Fig 3.2B**). Using this extraction method, we were able to isolate not only the FL tau^{V337M} but also the repeat fragments F3ΔK280 and F3ΔK280PP in the pro- and anti-aggregant strains respectively (lanes 6 and 7 marked by red and green asterisks for pro- and anti-aggregant strains respectively). However, in the single transgenic F3ΔK280 and F3ΔK280PP lines we could not find any protein, probably due to the degradation of these small fragments when expressed alone.

To verify that the tau transgene arrays are expressed at similar levels, we performed the perchloric acid extraction of tau from L4 larval stage and day 3 adult animals from each tau-transgenic strain. We analysed two independent strains from the pro-aggregant and anti-aggregant lines (strains A and strain B in each case) for protein expression. Western blot analysis verified that the transgenes were expressed at comparable levels (**Fig 3.3**). Since the Tau expression levels were similar in the strain A and strain B from each double Tau-tg animals, we decided to analyse only one strain for the further experiments.

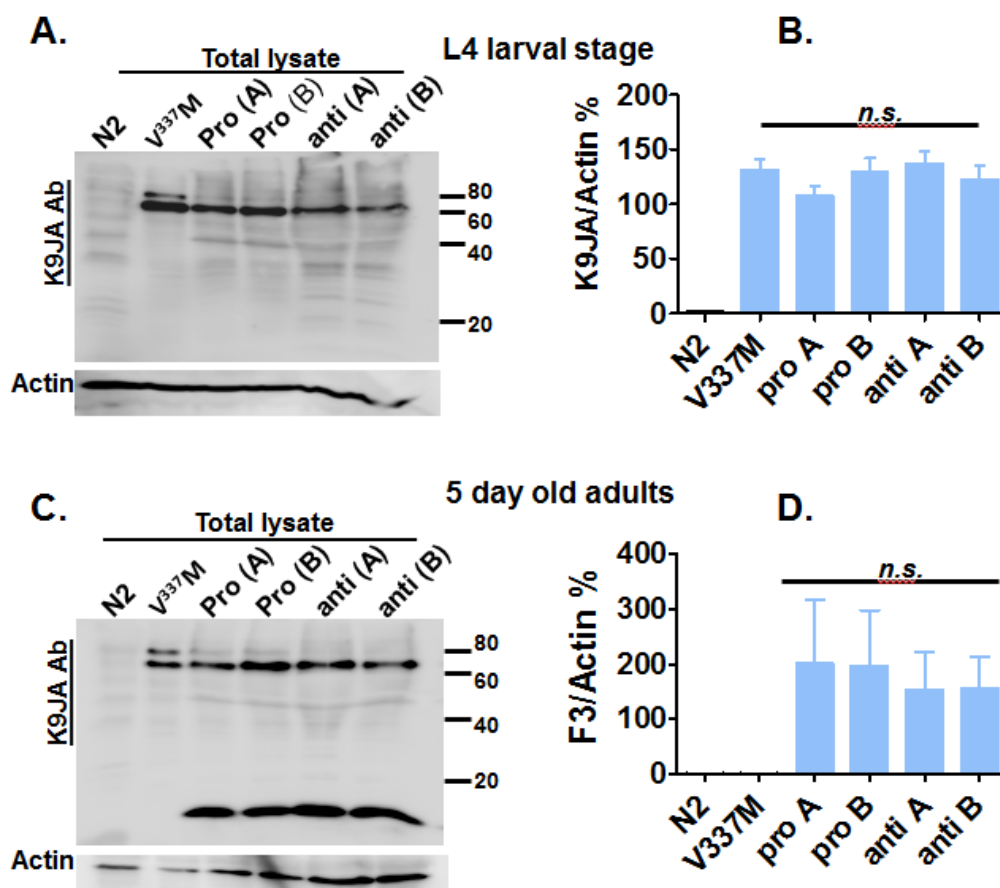


Figure 3.3 (A): Western blot of total lysates from synchronized L4 larvae using 2.5% perchloric acid extraction. K9JA pan tau antibody, which recognizes the Tau repeat domain (RD) and thus detects both full length (FL) Tau and F3ΔK280/F3ΔK280PP fragments, was used to probe the blots. Anti-actin antibody was used as loading control. L4 larvae extracts did not show the F3 fragment but total levels of Tau expression were similar among all the different transgenic lines (normalization to actin). **(B):** quantification of the blot is shown here. The error bars denote standard error of the mean (s.e.m.) from three repetitions of the experiment, and differences were considered non-significant ($p>0.05$) after performing one-way ANOVA. **(C): Western blot of total lysates from synchronized day 5 old adults using 2.5% perchloric acid extraction.** Both FL Tau ^{V337M} and F3ΔK280/F3ΔK280PP fragments were detected with K9JA antibody. The independently integrated strains express the F3 fragment at comparable levels (normalization to actin). **(D):** Shown here is the quantification of the F3 signals. The error bars denote s.e.m. from three repetitions of the experiment, and differences were considered non-significant ($p>0.05$) after performing one-way ANOVA.

3.4 Full-length tau along with the F3 fragment leads to uncoordinated phenotype

The pro-aggregant combination resulted in a strong phenotype characterized by a strong uncoordinated locomotion, which was clearly seen right from the L1 larval stage. On a solid NGM, the pro-aggregant worms moved sluggishly with recurrent tail dragging and were unable to perform a normal sinusoidal movement. The recurrent tail dragging was seen in almost all the pro-aggregant worms after

reaching 3 days of adulthood. In liquid, wild type *C. elegans* thrash rapidly and the uncoordinated pro-aggregant worms thrash slowly. The thrashes can be followed by looking at the change in the direction at the mid-body so that when a thrash is completed, both the head and the tail point in the same direction. However, the pro-aggregant line often kept its tail coiled and showed movements only in the head when compared to the wild-type strain, the FL tau^{V337M} strain or the anti-aggregant line (3 day old video 1). We quantified the thrashes at day 1, day 3 and day 5 of the adult stage, pro-aggregation strain depicted far less thrashes at all of the stages observed (**Fig 3.4**). Beyond day 5 of adulthood, it became difficult to analyze the thrashes made by the pro-aggregant strain as they hardly moved when placed in a liquid drop.

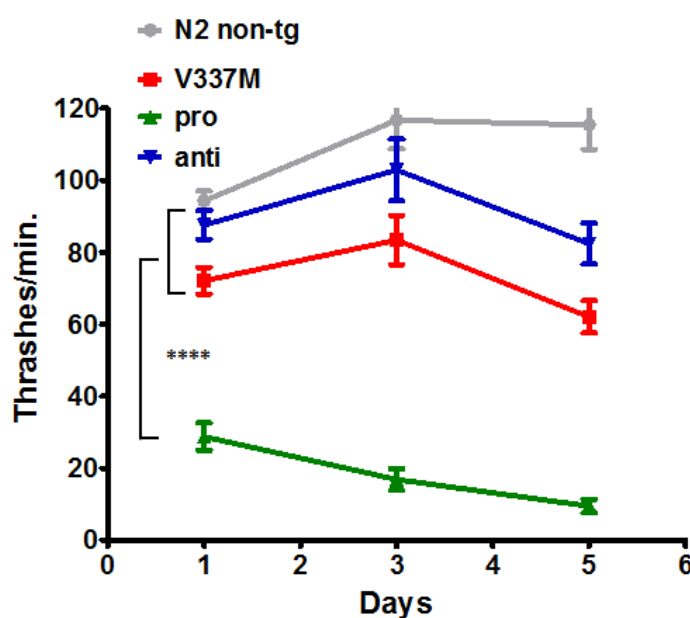


Figure 3.4: Locomotion defects (uncoordinated motion) upon pan-neuronal expression of pro-aggregant human Tau transgenes. Thrash assay was used as readout. Pro-aggregant animals are severely uncoordinated and show less thrashes at all three stages analyzed. The severity of uncoordinated phenotype increases with age. Each point is the mean thrashing rate for 20 developmentally synchronized non-transgenic N2, single-transgenic FL Tau ^{V337M}, pro-aggregant and anti-aggregant animals. Error bars denote SEM. Two-way ANOVA with Bonferroni correction was used for comparison (**** $P < 0.0001$).

When a wild type N2 *C. elegans* is gently touched at the head, it normally reacts by moving backwards quickly resulting in 3-4 sinusoidal waves. A 3 day old adult worm from the tau^{V337M}-tg line and the anti-aggregant line showed no noticeable defects and reacted normally to the gentle touch as did the wild-type *C. elegans*; however, by this age almost all the pro-aggregant animals reacted sluggishly to this

gentle touch with no or very slow backward movement, if at all (video 2). All these phenotypic defects became more severe with age.

3.5 Pro-aggregant strain shows a relatively delayed clearance of food

C. elegans has a short life cycle of roughly 54 hrs at 20°C and can be easily grown in liquid culture. The quality of producing young can be followed up by monitoring the

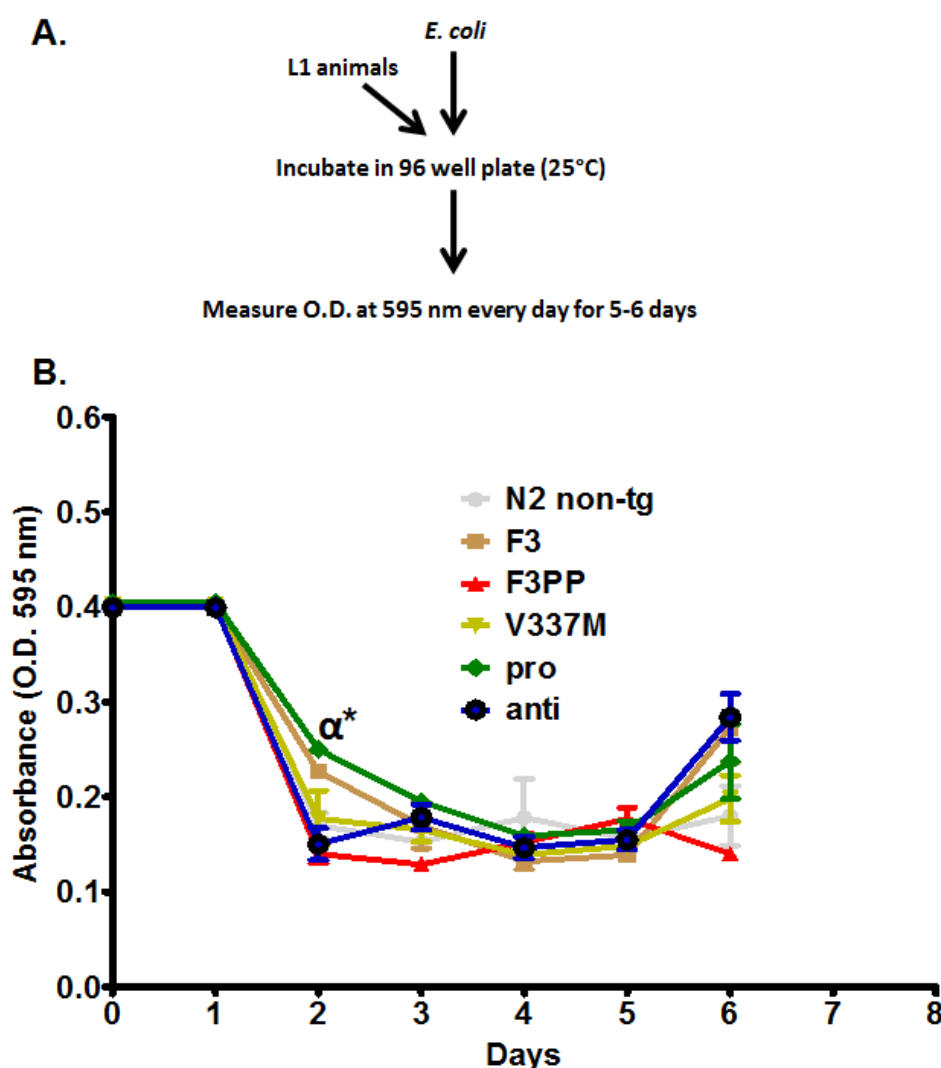


Figure 3.5: Food clearance assay (A): Flow diagram of the food clearance assay. 30 L1 larval stage animals from each strain synchronized overnight were incubated at 25°C in *E. coli* OP-50 at a final OD (A595) of 0.4 in 96 well micotiter plate wells. Three replicates were kept for each strain and the OD of the microtiter plate was measured daily for 6 days. **(B):** The mean OD is calculated for each day from triplicate samples for each strain and plotted over time. Error bars represent SEM. Pro-aggregant worms show delayed food clearance compared to the wild-type and the anti-aggregant strains until 2nd day of incubation ($\alpha^*p < 0.05$) but the differences became insignificant afterwards ($p > 0.05$ after performing one-way ANOVA).

rate at which the limited food source (*E. coli* suspension) is consumed. Each individual is capable of producing hundreds of progeny that rapidly consume the limited *E. coli* supply. As a result, the OD of wells decreases as they reproduce. Any interruption in their growth, survival or fecundity would result in a reduction of the rate at which food is cleared. Here we wanted to see if there is an effect on the fecundity by the over expression of different combinations of tau compared to the wild type N2 strain and single transgenic FL Tau^{V337M} strain. The pro-aggregant strain showed a relatively delayed clearance of *E. coli* suspension compared to the other strains, however, the difference became statistically insignificant after the 2nd day of incubation (Fig 3.5). From this experiment, we can infer that the expression of different combinations of tau transgenes do not have a huge impact on the pharyngeal pumping and fecundity. Furthermore, the type and level of toxicity due to the expression of transgenes is different and cannot be compared to those of toxic compounds like LiCl (Voisine et al., 2007).

3.6 Pro-aggregant worms have a shorter life-span

The pro-aggregant combination of tau transgenes appeared to reduce the life-span of the worms as was apparent during the routine handling of these animals. We thereby performed a survival rate assay to quantify this difference in the life-span.

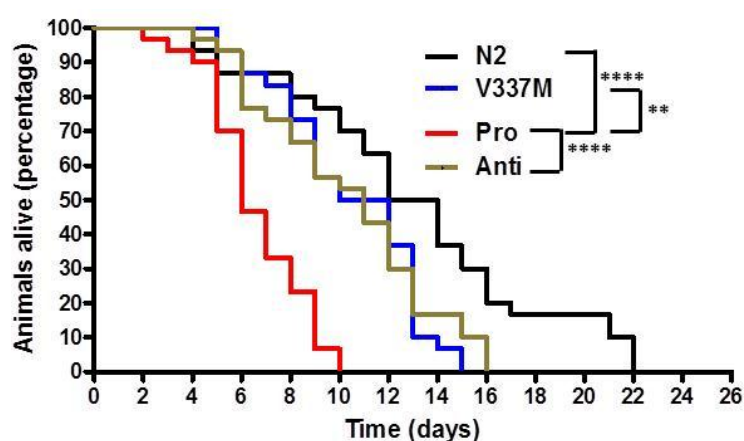


Figure 3.6: Aging graph of *C. elegans*. Shown here are the survival curves of the Tau-transgenic strains versus wild-type N2 strain. The percentage of surviving animals at each day of adulthood is presented. Tau-transgene expression leads to a reduction in the life-span of worms. Pro-aggregant animals have the shortest life-span compared to the FL Tau^{V337M} and anti-aggregant animals. However, all of them live shorter compared to the wild type non-transgenic N2 strain. Chi square Log-rank (Mantel Cox) Test was used for comparison (** $P < 0.01$, **** $P < 0.0001$).

In order to prevent the spawning of progeny, the worms were sterilized by incubating on NGM plates containing 75 μ M FUdR after they had crossed the L4 larval stage. We found that the pro-aggregant animals lived significantly shorter (**Fig 3.6**). Whether this reduced life span of pro-aggregant animals is related to the insulin growth factor (IGF)-1-like signalling (IIS) pathway (Kenyon et al., 1993) needs to be investigated.

3.7 Full-length tau along with the F3 fragment leads to aggregation (ThS Staining)

Whole worm immunostaining using K9JA pan Tau antibody was used to confirm the

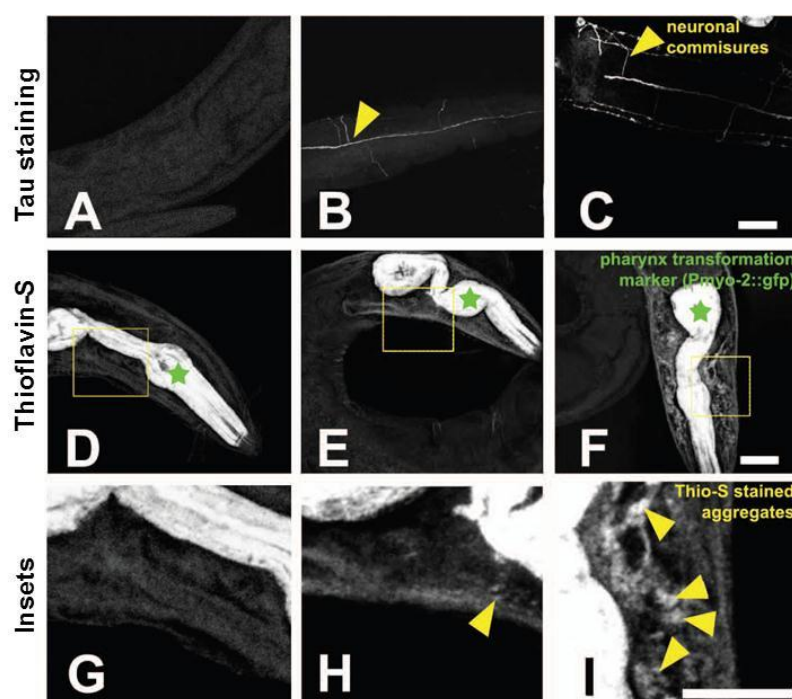


Figure 3.7: Panneuronal expression of FL Tau V337M along with F3 Δ K280 leads to deposition of aggregates in *C. elegans*. (A-C): Tau transgene expression in the nervous system detected with K9JA as primary antibody and Alexa488 goat anti-rabbit secondary antibody. Neuronal structures were stained in the anti-aggregant (B) and pro-aggregant (C) Tau transgenic strains (marked with yellow arrowheads), while faint background staining is observed in non-transgenic controls (A). (D-F): Maximal Intensity Projections (MIP) of the head region of worms stained with Thioflavin-S to image Tau aggregates. The strong signal in the pharynx of the animals (marked with a green star) was the result of expression of the transformation marker (*Pmyo-2::gfp*), which is excited by the FITC laser used for Thioflavin visualization. Wild type strain (transformation marker only) in (D) shows only background staining, the anti-aggregant strain (E) shows very few spots, and the pro-aggregant strain in (F) shows extensive decoration with spots around the nerve ring area. (G-I): Zoomed in images from K-M, corresponding to the dotted rectangle region. Yellow arrowheads point to exemplary Thioflavin-S stained Tau aggregates. Scale bar in all the above pictures is 20 μ m (adapted from Fatouros C and Pir GJ et al., *HMG*, 2012).

expression of Tau in the nervous system (**Fig 3.7A-C**). In order to visualize the tau aggregates in the worm, Thioflavin-S (ThS) staining was used. ThS is known to bind amyloid structures irrespective of the source of protein and has been used to detect the presence of protein aggregates (Link, 1995; Minniti et al., 2009). ThS was applied on synchronous young adult populations of pro-aggregant and anti-aggregant worms, as a control worms expressing only the transformation marker were used. The pro-aggregant animals showed an intense ThS staining in the nerve cord where most of the neurons in *C. elegans* make connections, while the anti-aggregation animals hardly showed any staining (**Fig 3.7D-I**).

3.8 Pro-aggregation tau combination leads to the deposition of aggregates right at day 1 of adulthood

We hypothesized that the early onset of phenotype seen in the pro-aggregant animals right from the first larval stage would be because of the presence of highly amyloidogenic pro-aggregant repeat fragment F3ΔK280, which would accelerate the aggregation of the full-length tau ^{V337M} by forming seeds. Thereby, we collected a synchronous 1 day old adult population of the worms to observe the presence of tau aggregates at such an early stage. Proteins such as tau, amyloid-β, polyQ-Ht and α-synuclein, which have implications in various neurodegenerative diseases, are known to form aggregates that remain insoluble in strong-detergent buffers (DiFiglia et al., 1997; Kawarabayashi et al., 2001; Lee et al., 1999; Spillantini et al., 1997). However, the aggregates formed by these proteins can be solubilized by formic acid or urea and analyzed by SDS-PAGE gels. We sequentially extracted soluble Tau from the tau-transgenic *C. elegans* lines using buffers of higher stringency leaving behind the highly insoluble tau aggregates, which were extracted using formic acid. In striking contrast to FL tau ^{V337M} and anti-aggregant strains, when tau is co expressed with pro-aggregant repeat fragment F3ΔK280 in the pro-aggregant line, both components begin to aggregate and appear in both the detergent soluble as well as the detergent insoluble fractions, starting at day 1 of the adulthood (**Fig 3.8, top panel_K9JA**). Furthermore, the pro-aggregant F3ΔK280 in the pro-aggregant line appears only in the detergent insoluble FA fraction, in contrast to the anti-aggregant repeat fragment F3ΔK280PP in anti-aggregant line which appears solely in the

soluble RAB fraction by this age. However, only full-length $V337^M$ tau is phosphorylated at the KXGS motif (**Fig 3.8, mid panel_12E8**). Furthermore, tau aggregates were also phosphorylated at the S396 and S404 epitopes (**Fig 3.8, lower panel_PHF-1**). Taken together the data indicate that the F3ΔK280 forms seeds and thereby, initiates and accelerates the aggregation of full-length tau, resulting in the rapid appearance of aggregates early in the life of the pro-aggregant line. At the same time, it also confirms that the aggregation of the full-length tau initiated by F3ΔK280 is not unique for the WT full-length Tau, ΔK280 mutant form of full-length tau or the P301L mutant form of full-length tau (Wang et al., 2007), but extends to the FL Tau $V337^M$ mutant as well.

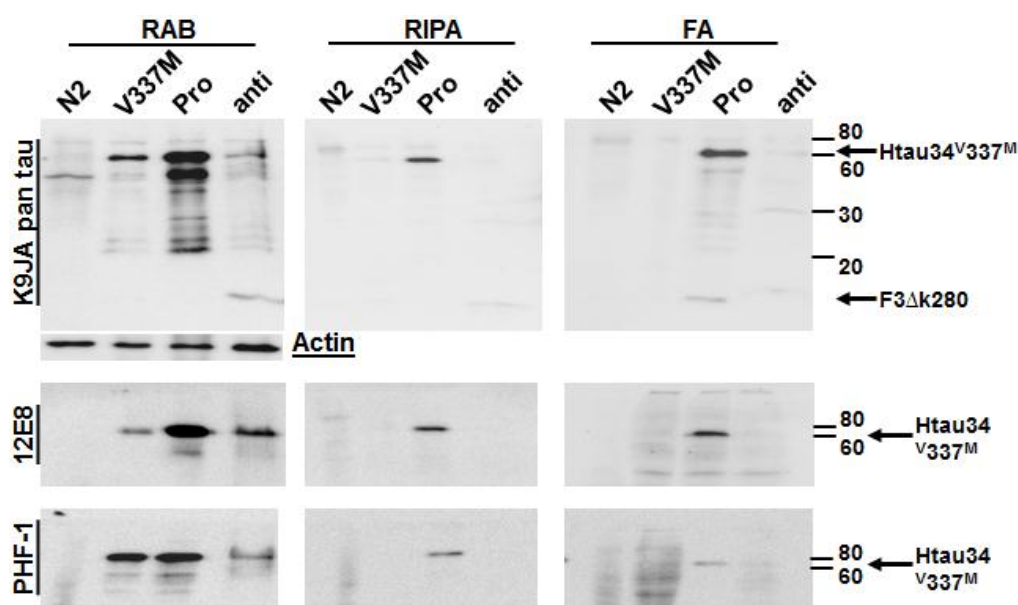


Figure 3.8: Insoluble Tau aggregates accumulate in the pro-aggregant strain starting at day 1 of adulthood. Tau was sequentially extracted from equivalent amounts of packed 1-day-old adults using buffers of increasing stringency and blotted with pan Tau antibody K9JA (upper panel), pS262 antibody 12E8 (middle panel) and pS396, pS404 antibody PHF-1 (lower panel). Anti-actin antibody served as a loading control. After sequential extraction of tau from 1-day-old adult transgenic *C. elegans* strains (with laboratory N2 wild type strain as control), only the pro-aggregant strain (lane 3) showed detergent soluble (RIPA) and detergent insoluble tau aggregates solubilized with 70% formic acid (FA). FL Tau $V337^M$ but not the F3ΔK280 fragment is phosphorylated at the KXGS motif (12E8 panel) and the S396 and S404 epitopes (PHF-1 panel). In the pro-aggregant strain, F3ΔK280 appears only in the detergent insoluble fraction (lane 3 of the FA fraction in the top panel). In contrast, F3ΔK280/2P in the anti-aggregant strain appears solely in the soluble fraction (lane 4 of the RAB fraction, top panel).

3.9 RNAi against tau ameliorates the phenotype

In order to make sure that the phenotypic defects seen in our transgenic line are due to toxicity mediated by tau aggregation so that any attribution of toxicity to the other

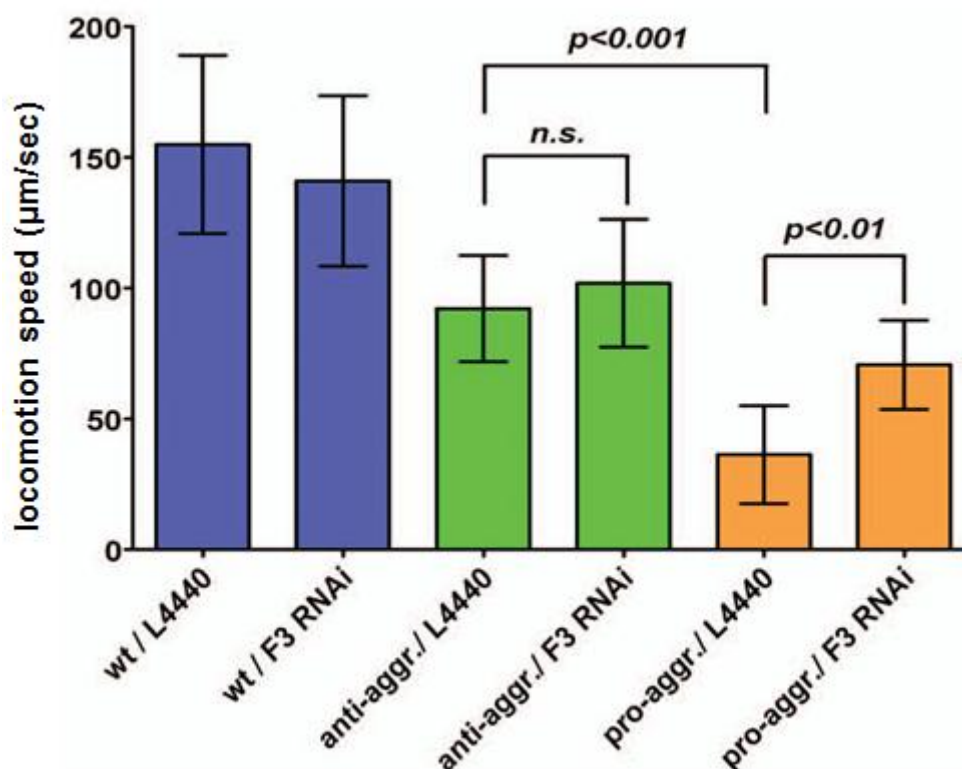


Figure 3.9: RNAi against tau ameliorates the phenotype in pro-aggregant animals. Bar diagram plotting the mean locomotion speed of day 1 adult animals on an empty NGM agar plate grown either on L4440 (empty vector) or F3ΔK280 RNAi expressing HT115 bacteria. Error bars denote the standard deviation (adapted from Fatouros C and Pir GJ et al., *HMG*, 2012).

side-effects caused by the insertion and integration of transgenes into the main chromosome could be nullified, RNAi against tau was performed in the tau transgenic strains. Unfortunately, not all the tissues are equally sensitive to RNAi in *C. elegans*. Nervous system in *C. elegans*, in general, is refractory to RNAi in a wild-type genetic background, however, a few mutations have been discovered which enhance the RNAi sensitivity in neurons (Samuelson et al., 2007; Simmer et al., 2002). Therefore, in order for systemic RNAi to be effective in the neurons where the tau transgenes are expressed, all the transgenic strains were crossed into a neuronal RNAi sensitizing background [strain *eri-1 (mg366)IV;lin-15B(n744)X* (Samuelson et al., 2007)]. Upon RNAi against F3ΔK280, the pro-aggregant worms showed a considerable improvement in the motility (speed=70.7±17 μm/sec for RNAi treated

versus 36.4 ± 18 for control), while the anti-aggregant worms showed no difference upon treatment (**Fig 3.9**). From these experiments it can be concluded that the pro-aggregant F3 Δ K280 combination with FL Tau^{V337M} leads to accelerated formation of insoluble tau species and increased toxicity associated by early uncoordinated locomotion, whereas the FL Tau^{V337M} alone or the anti-aggregant combination does not.

3.10 Aggregation increases with age more prominently in pro-aggregant line

Since the defects in the locomotion enhanced progressively with age and the pro-aggregant strain showed much stronger and more severe phenotype than the anti-aggregant strain and the FL Tau^{V337M} strain, we looked at the aggregates by sequentially extracting tau from 7-day old adult worms. At first we performed a two-step extraction whereby, we extracted the soluble Tau using high salt buffer and the worm pellet left after first extraction step was dissolved directly in formic acid to isolate the remaining tau protein which would eventually be considered as insoluble tau (**Fig 3.10**).

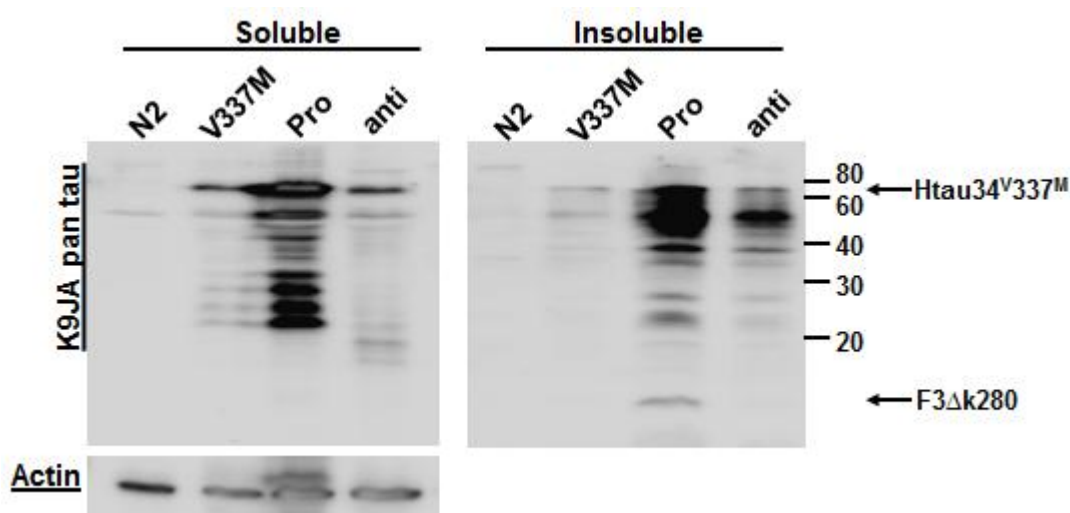


Figure 3.10: Tau solubility using two-step protocol. Tau was extracted from equivalent amounts of packed mixed stage *C. elegans* transgenic strains (with laboratory N2 strain as control) and immunoblotted with K9JA pan tau antibody, which recognizes the Tau repeat domain and thus detects both full length V337M Tau and F3 Δ K280/ F3 Δ K280PP fragments. Anti-actin antibody served as a loading control.

However, to gain more insight into the different species of aggregated tau we performed the 3 step extraction, thereby dividing the aggregated tau into one that is

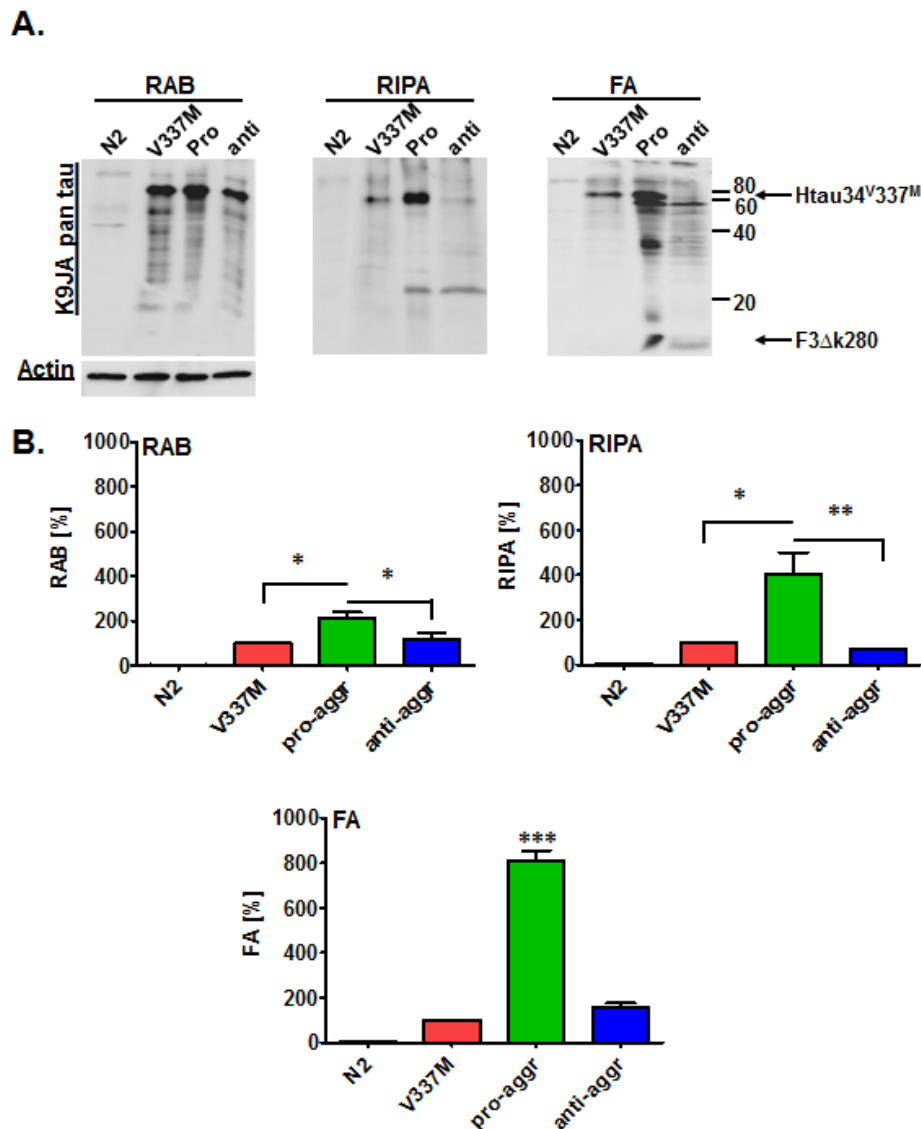


Figure 3.11: Western blot of sequentially extracted of Tau from 7-day-old adult animals using the old protocol (see methods section 2.2.2.10.1). Samples were blotted using pan Tau K9JA antibody and anti-actin antibody was used as a loading control. Equal amount of protein was loaded and normalized against FL Tau V337M sample. The pro-aggregant shows approximately 2-fold soluble (RAB blot), 4-fold detergent soluble (RIPA blot) and 8-fold detergent insoluble Tau (FA blot), as quantified from 3 independent experiments (One-Way ANOVA, * $p < 0.05$, ** $p < 0.01$, *** $p < 0.001$).

detergent soluble (RIPA fraction) and one that is detergent insoluble (FA fraction). By following the protocol published earlier, we found both the detergent soluble and the detergent insoluble aggregates even in the FL Tau^{V337M} strain which corroborated well with the earlier reports for the FL Tau^{V337M} strain (Kraemer et al., 2003) (**Fig 3.11A**), but the pro-aggregant strain showed ~4-fold more aggregates compared to the FL Tau^{V337M} strain (**Fig 3.11B**). However, a small modification of the protocol whereby the samples were extracted with RIPA buffer twice with additional washing steps (see section 2.2.2.10.2), yielded detergent insoluble tau only in the

pro-aggregant strain (**Fig 3.12**). Taken together, the pro-aggregant repeat fragment F3ΔK280 nucleates in *C. elegans* neurons and provides seeds that leads to the accelerated aggregation of the full-length V337M Tau. The accelerated aggregation, in turn, leads to a well-defined and easily distinguishable phenotype early in the life-span of this *C. elegans* tauopathy model. This makes it an ideal model for the genetic screening and last but not least, the compound screening.

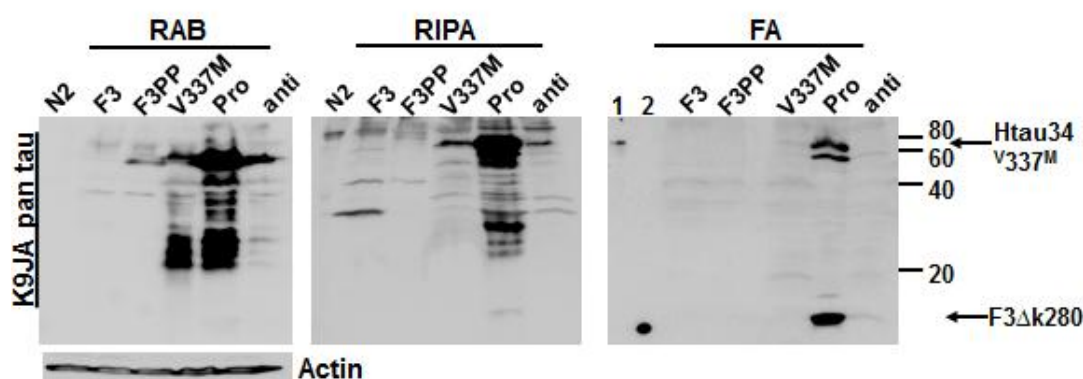


Figure 3.12: Sequential extraction of Tau from 7-day-old adult animals using the modified protocol (for protocol see methods section 2.2.2.10.2). Equal amount of protein was loaded and immunoblotted using K9JA pan tau antibody. Anti-actin antibody served as a loading control. Single transgenic F3ΔK280 (F3) and F3ΔK280PP (F3PP) show no bands. FL Htau34 V337M strain (V337M) and anti-aggregant strain (anti) show the detergent soluble tau (lanes 4 and 6 of the RIPA fraction) but the detergent insoluble aggregates (solubilized with 70% formic acid) consisting of the FL Htau34 V337M along with a proteolytic fragment and the F3ΔK280 appear only in the pro-aggregant strain (lane 6 of the FA fraction). Lanes 1 and 2 represent the htau40ΔK280 and F3ΔK280 recombinant proteins.

3.11 Full-length tau along with the F3 fragment leads to gaps in the motor neurons

To determine whether the severe phenotypic defects observed in the pro-aggregant strain are a consequence of the defects in the neuronal development and connectivity, the motor neurons of the tau transgenic strains were examined. GABAergic motor neurons were visualized by crossing the tau lines with *juIs73:[Punc-25::gfp]*III reporter strain (Lundquist et al., 2001) expressing GFP in the

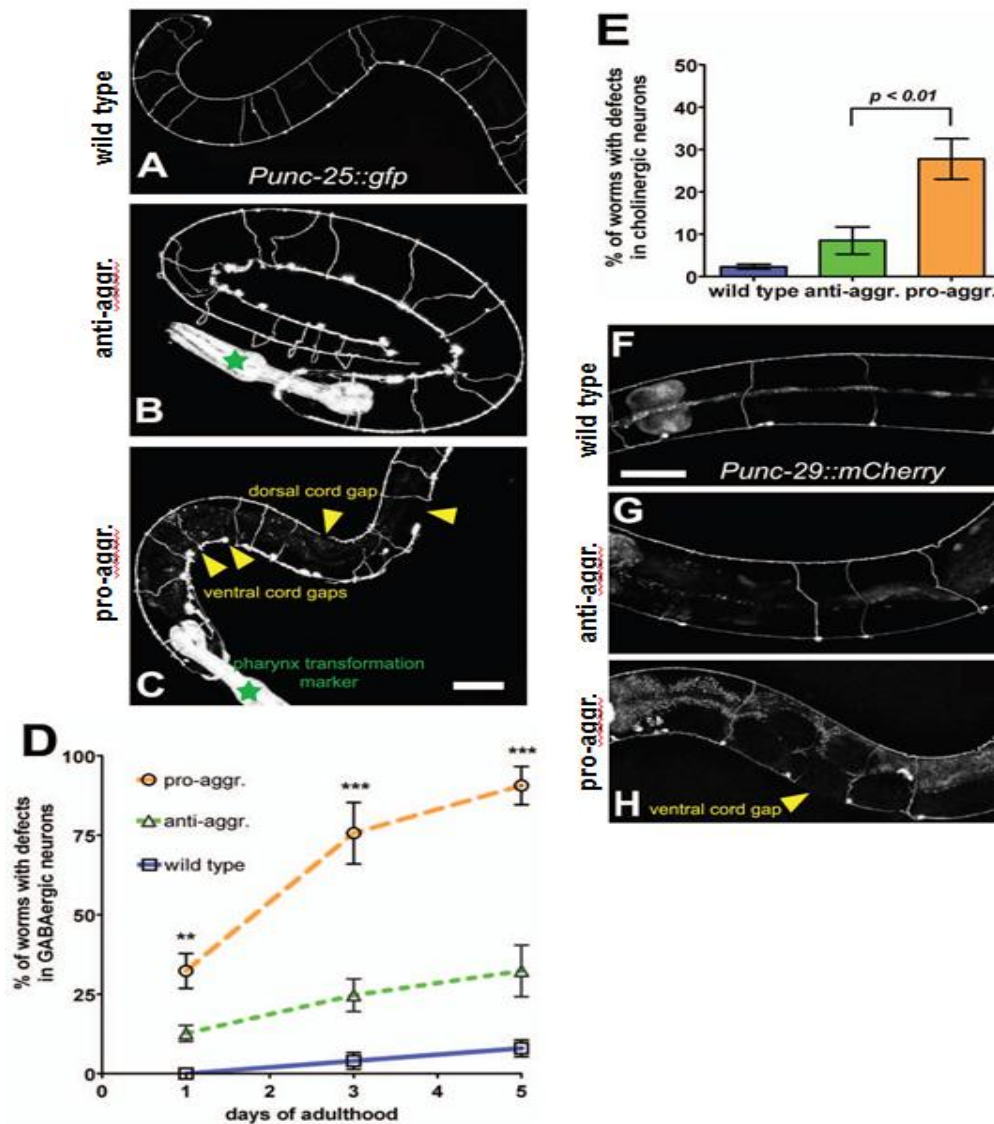


Figure 3.13: Pro-aggregant transgenic *C. elegans* show structural defects in the GABAergic and cholinergic motor neurons. (A): Wild type example of the *Punc-25::gfp* reporter which stains GABAergic motor neurons. (B): Anti-aggregant GABAergic reporter strain (C) Pro-aggregant GABAergic reporter strain. All depicted worms are day 1 adults. The individual figures are Maximum Intensity Projections (MIP) and the yellow arrowheads point to axonal gaps along the ventral or dorsal cord. Green stars denote the pharynx which expresses the GFP transformation marker. Scale bars are 20 μ m. (D): Graph plotting the percentage of animals having axonal gaps at day 1, day 3 and day 5 of adulthood. Progressive accumulation of defects is observed for the pro-aggregant strain (2-way ANOVA, ** for $p < 0.01$, *** for $p < 0.001$ regarding the comparison or the pro- vs the anti-aggregant strain at the different time points). (E): Percentage of day 1 adult worms showing axonal gaps in the cholinergic motor neurons (*Punc-29::mCherry* reporter). Three times more pro-aggregant animals have axonal gaps compared to anti-aggregant animals. (F-H): Representative MIP pictures of the mid-body cholinergic motor nervous system of (F) wild type *Punc-29::mCherry* reporter, (G) anti-aggregant strain and (H) pro-aggregant strain with a ventral axonal gap (yellow arrowhead). Scale bars here are 20 μ m. In summary, the pro-aggregant worms show high occurrence of neuronal structural damage and progressive degeneration (adapted from Fatouros C and Pir GJ et al., *HMG*, 2012).

GABAergic inhibitory neurons. The pro-aggregant strain showed frequent structural defects in the form of axonal gaps and varicosities both in the ventral and the dorsal nerve cord, starting at day 1 of adulthood, which coincided well with the presence of

detergent insoluble tau aggregates in the pro-aggregant strain at day 1 of adulthood. In contrast, the anti-aggregant strain did not show severe morphological defects (**Fig 3.13 A-C**). The structural defects rose with age, so that almost 100% of the pro-aggregant worms showed axonal gaps by day 5 of adulthood (**Fig 3.13 D**). By that age, only 30% of the anti-aggregant reporters developed such defects.

To further consolidate these results, the cholinergic motor neurons which provide the activating signals to the neuromuscular junctions in coordination with the GABAergic inhibitory neurons on the opposite side (Schultheis et al., 2011) were also examined. For this purpose, an extrachromosomal array which marks the cholinergic neurons [*Punc-29::mCherry*] was introduced into the tau lines to help visualize the dorsal and ventral nerve cords of young adult animals for structural defects. Wild-type reporter strain and the anti-aggregant strain hardly showed any structural defects (%age of worms with gaps for wild type is 2.3 ± 0.5 and 8.5 ± 3.5 for the anti-aggregant) (**Fig 3.13 F-G**). In striking contrast to this, the pro-aggregant strain showed frequent gaps (%age = 27.8 ± 4.8 for day 1 adults), similar to what was observed in the GABAergic neurons (**Fig 3.13 H**). These data further support the fact that the pro-aggregation but not the anti-aggregation Tau combination is toxic for the neurons.

3.12 Tau is phosphorylated to a higher extent in the pro-aggregant *C. elegans* line

Abnormal pathological fibres in many neurodegenerative tauopathies are primarily composed of hyperphosphorylated tau (Buee et al., 2000; Gamblin et al., 2003) and this phosphorylation of tau has been suggested to play a role in its aggregation (Iqbal et al., 2005; Kosik and Shimura, 2005). We therefore examined the phosphorylation status of the sequentially extracted tau in our tau transgenic *C. elegans* lines. As a control of protein concentration, we used the pan-tau antibody K9JA which detected both the proteolytic repeat fragments (F3ΔK280 in pro- and F3ΔK280PP in anti-aggregant strain) as well as the full-length tau^{V337M} (**Fig 3.14_upper pannel**). Both high salt soluble and detergent soluble tau from the three transgenic lines were phosphorylated at 5 epitopes examined. However, three epitopes pSer202 (Ab CP13),

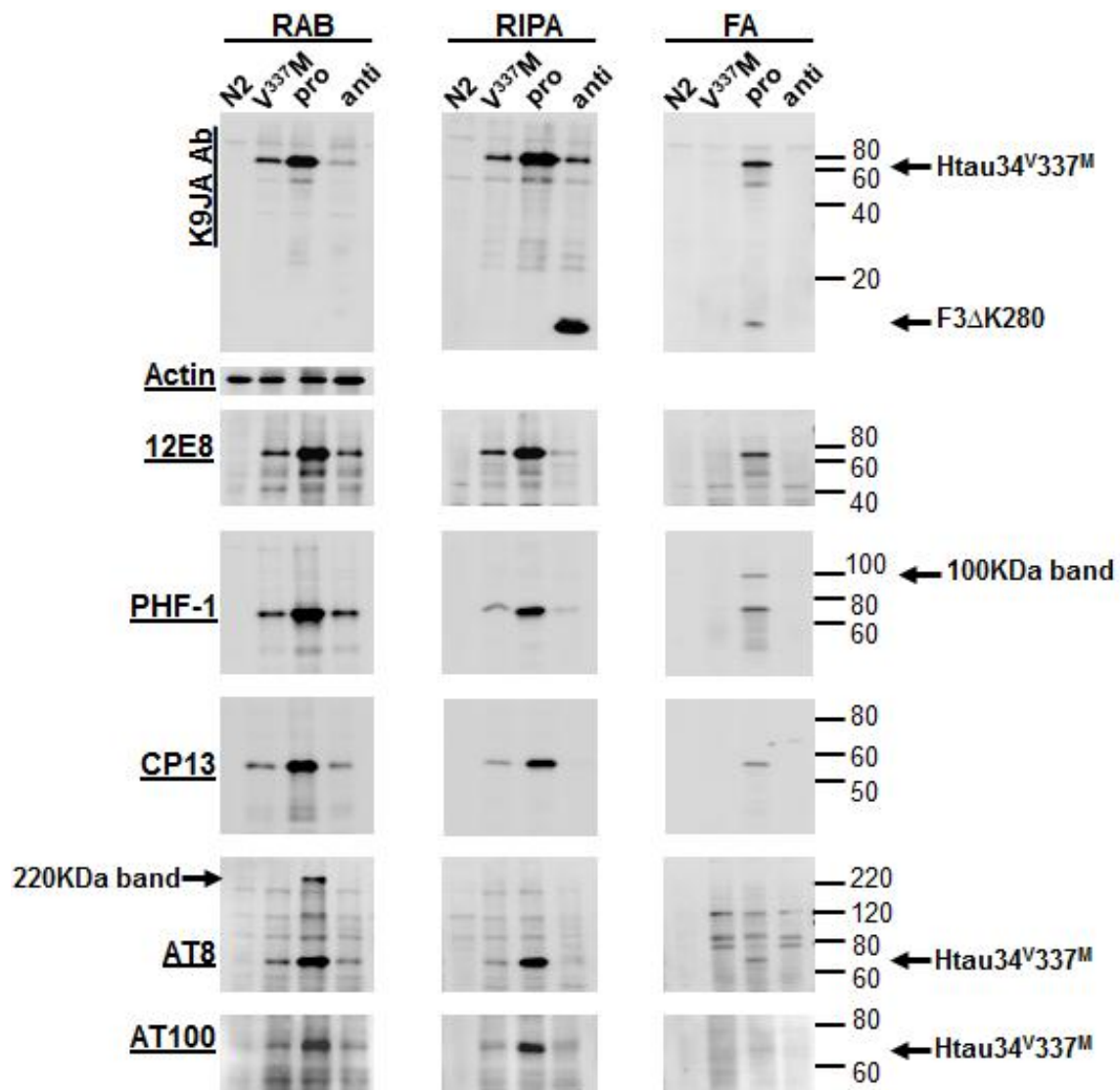


Figure 3.14: Pro-aggregant strain shows a pronounced hyperphosphorylation of tau. Tau was sequentially extracted using buffers of increasing stringency and blotted against the respective antibodies. Anti-actin antibody served as a loading control. RAB (soluble Tau) and RIPA fractions (detergent soluble Tau) from all transgenic strains were phosphorylated at all sites examined with the respective phosphorylation-specific antibodies (12E8 for S262; PHF-1 for S396 and S404; CP13 for S202; AT8 for S202, and T205; AT100 for T212 and S214) with the exception that no phosphorylation at the CP13, AT8 and AT100 epitopes was observed in the anti-aggregant strain. Furthermore, the detergent insoluble Tau (FA fraction) of the pro-aggregant strain was phosphorylated at all sites, except T212 and S214 (AT100 epitope). In addition, PHF-1 antibody detects a >100-kDa band in the FA fraction of this strain indicating the presence of highly insoluble hyperphosphorylated aggregates. AT8 also detects a ≈220-kDa band in the soluble fraction of the same sample, probably representing intermediate oligomers. In short, insoluble Tau in the pro-aggregant strain becomes hyperphosphorylated at multiple epitopes.

pSer202, pThr205 (Ab AT8) and pThr212, pSer214 (Ab AT100) showed reduced phosphorylation in the FL tau^{V337M} strain compared to the pro-aggregant strain. Furthermore, detergent soluble RIPA fraction from the anti-aggregant strain did not

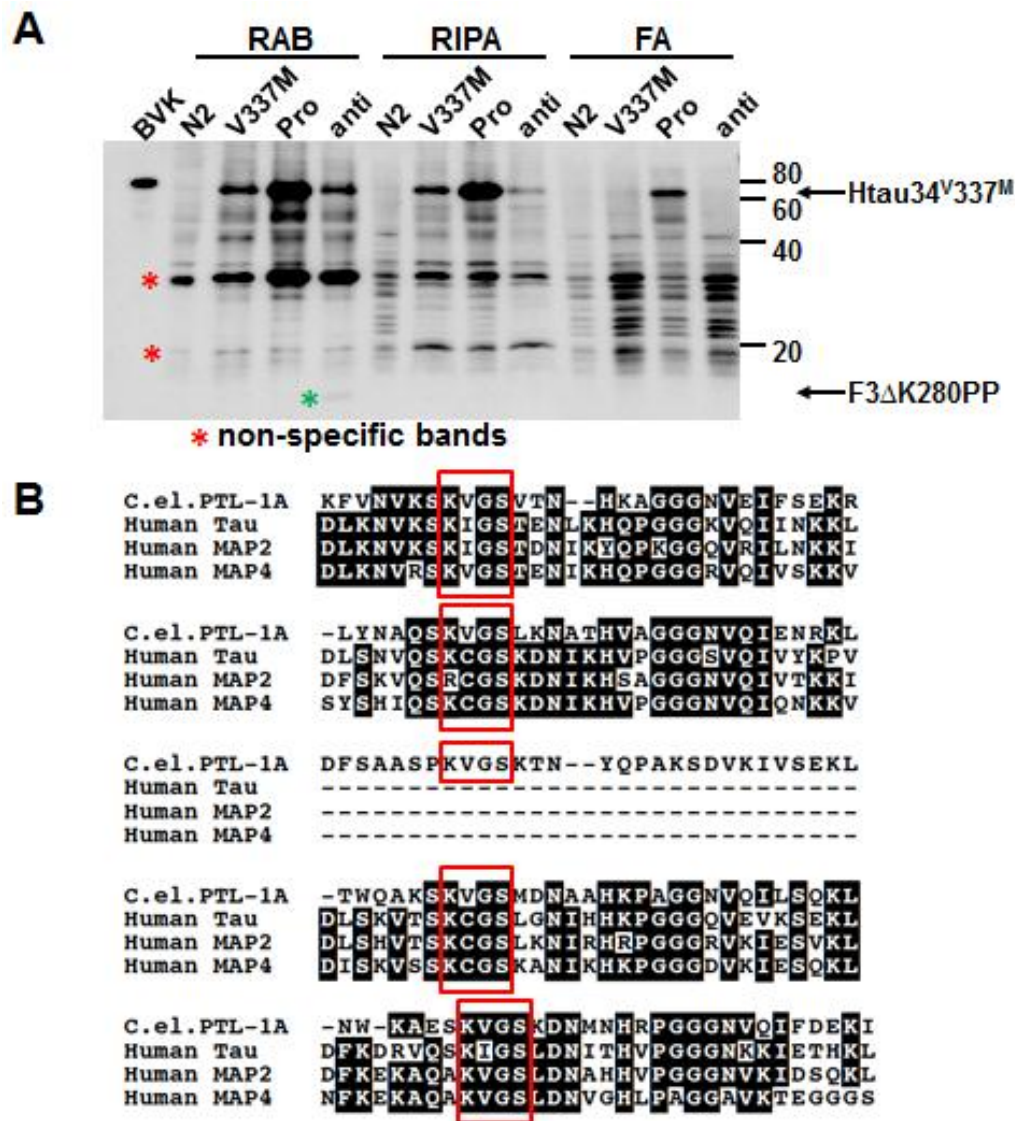


Figure 3.15: (A): Sequentially extracted Tau using buffers of increasing stringency was immunoblotted using 12E8 antibody. The 12E8 antibody against tau phospho-epitope S262 detects bands (marked by red asterisk *) common to all the strains including the wild type laboratory N2 strain. The pro-aggregant repeat fragment F3ΔK280 is not phosphorylated at this epitope, however, anti-aggregant strain shows a faint band (marked by green asterisk *) corresponding to F3ΔK280PP in the soluble RAB fraction. **(B):** Sequence alignment of the repeat domains from PTL-1A, Human Tau, Human MAP2 and Human MAP4 proteins showing homologous regions highlighted in black. The KXGS motifs (in red squares) are conserved throughout [adapted from (Goedert et al., 1996a)].

show any phosphorylation at the three epitopes vis-a-vis pSer202 (Ab CP13), pSer202, pThr205 (Ab AT8) and pThr212, pSer214 (Ab AT100). Detergent insoluble tau (solubilized in 70% formic acid FA) only from pro-aggregant strain was phosphorylated at all these sites except At100 (pSer214). In addition, AT8 detected a band of ≈220 KDa in the soluble RAB fraction of pro-aggregant strain (**Fig 3.14 5th panel**) showing the presence of some intermediate oligomers in the process of

aggregation. Furthermore, PHF-1 (pSer396/pSer404) also detected a higher band of >100 KDa in the detergent insoluble FA fraction (**Fig 3.14_3rd panel**) of pro-aggregant strain, again confirming the presence of phosphorylated higher oligomeric Tau species in the pro-aggregant animals.

It is important to note that the antibody against 12E8 phospho-epitope (pS262) detected two additional bands of ~20 KDa and >30 KDa. These two bands were common to all the strains including the wild type non-transgenic N2 strain (shown by red asterisks in **(Fig 3.15 A)**). It has already been reported that Human Tau and *C. elegans* PTL-1 (protein with Tau like repeats) share ~50% homology in the repeat domain (Goedert et al., 1996a; Goedert et al., 1996b). In particular the KXGS motif, which contains the phosphorylation specific epitope recognized by 12E8, is present in the PTL-1 repeat domain of *C. elegans* (**Fig 3.15 B**). It is reasonable to predict that this epitope could also be a target for phosphorylation and therefore, we assume these bands to be the proteolytic fragments of endogenous MAP in *C. elegans*. In summary tau of the soluble and insoluble fraction was phosphorylated to a higher degree in the pro-aggregant strain compared to the FL tau^{V337M} strain and the anti-aggregant strain.

3.13 Pro-aggregant animals accumulate higher oligomeric species

One of the hallmarks of AD and other tauopathies is that tau protein gets accumulated in NFTs consisting of insoluble twisted filaments made of hyperphosphorylated tau (Mandelkow and Mandelkow, 1998). These insoluble twisted filaments can be isolated from the brains of patients with AD based on sarkosyl insolubility (Greenberg and Davies, 1990). In order to observe the presence of NFTs in our *C. elegans* Tau-transgenic lines, we allowed a synchronous population of tau lines to grow for 9 days and used them to isolate tau based on sarkosyl insolubility. The pro-aggregant line showed only traces of FL monomeric ^{V337M} Tau in the sarkosyl insoluble fraction (**Fig 3.16**). Interestingly, we found a higher band of >220 KDa in the soluble fraction of 9-day old adult pro-aggregant worms. This band persists in the worm debris even after two extraction steps with high salt buffer (**Fig 3.16_Debris blot**); showing the presence of higher oligomeric Tau species in the

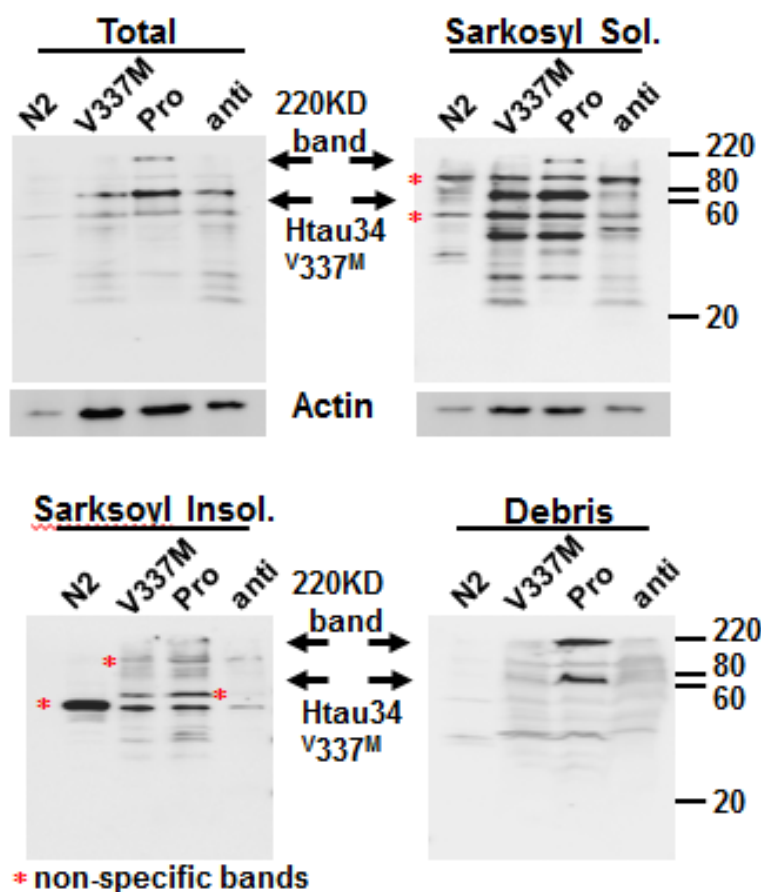


Figure 3.16: Blots of sarkosyl extracted Tau from synchronized 9-day old adult worms with pan Tau antibody K9JA. Proteins were extracted from equal amount of well-packed worm pellets on the basis of their solubility in sarkosyl and blotted. Anti-actin antibody served as a loading control. The worm debris which remained after sarkosyl extraction, were dissolved in 2X sample buffer and loaded onto the gel (Debris-blot). Even after two extractions with high salt buffer, the debris still contained a visible amount of Tau in case of pro-aggregant samples. This consisted of FL Tau V337M and a higher molecular weight band of ~220 KDa representing some kind of oligomeric Tau species (lane 3 of Debris-blot). This indicates the presence of highly insoluble Tau aggregates in pro-aggregant worms. In the sarkosyl-soluble fraction (sarkosyl sol. blot), the same ~220 KDa band can be seen in the pro-aggregant strain only (lane 3). A faint signal corresponding to the same band can also be seen in the sarkosyl-insoluble fraction of pro-aggregant strain (shown by green asterisk in the sarkosyl insol. blot). Asterisks mark non-specific bands common to all the strains including the laboratory N2 wild type strain. In summary, the pro-aggregant strain shows accumulation of highly aggregating Tau species in the form of monomers and higher molecular weight oligomers. These data corroborate the notion that Tau displays increased aggregation when combined with the amyloidogenic F3ΔK280 fragment in the pro-aggregant strain, whereas combination with the non-amyloidogenic F3ΔK280/2P fragment, or FL Tau V337M alone, do not aggregate to such extent.

pro-aggregant worm which cannot be solubilized with high salt buffer used in the Davies preparation. A portion of this high molecular weight band also showed up in the sarkosyl insoluble fraction of the pro-aggregant line. Here again we found some bands running lower than the full length tau in all the strains including the wild-type strain as was the case with the 12E8 antibody (see Fig 3.15A). We assume that because of a different procedure adopted to isolate the insoluble tau using sarkosyl,

the endogenous MAP proteins like PTL-1, which share about 50% homology with the repeat fragment of human tau, may get degraded and in the process might expose the epitopes in the repeat region to a highly specific pan-tau antibody like K9JA. This is, however, not the case with the sequential extraction of tau using RAB, RIPA and FA (as seen in the blots earlier) whereby, the lysates are not incubated at room temperature. Taken together the data confirm that the presence of the pro-aggregant repeat fragment F3ΔK280 potentiates the aggregation of FL V337^M Tau in the pro-aggregant strain, resulting in the rapid appearance of higher molecular weight soluble Tau oligomeric species.

3.14 Accumulation of synaptobrevin-1 in the presynaptic areas of the pro-aggregant line

So far we have described our *C. elegans* tauopathy model that recapitulates the cellular pathology observed in mammalian tauopathy models like the accumulation of hyperphosphorylated Tau aggregates. Earlier studies have linked hyperphosphorylation and aggregation of Tau to axonal transport defects, synaptic malfunction and degeneration (Morris et al., 2011). We therefore next set out to examine the morphology of the synapses, in particular the pre-synaptic areas of the motor neurons. To examine the synapse morphology in the Tau-transgenic strains, a reporter gene *nls52:[Punc-47::snb-1::gfp]* (Weimer et al., 2003) expressing GFP fused to Synaptobrevin-1 (SNB-1::GFP) from the motor neuron-specific promoter was used. Dorsal nerve cord in the posterior gonadal arm was selected to quantify the GFP fluorescence (**Fig 3.17 A-C**). The wild type reporter strain showed a regular punctate pattern of SNB-1::GFP along the neural cord (**Fig 3.17 D**) as has been described before also (Nonet, 1999). The anti-aggregant strain also showed a similar pattern (**Fig 3.17 E**). On the contrary, the pro-aggregant strain displayed a discontinuous punctate pattern and staining was generally more diffuse in pre-synaptic areas,

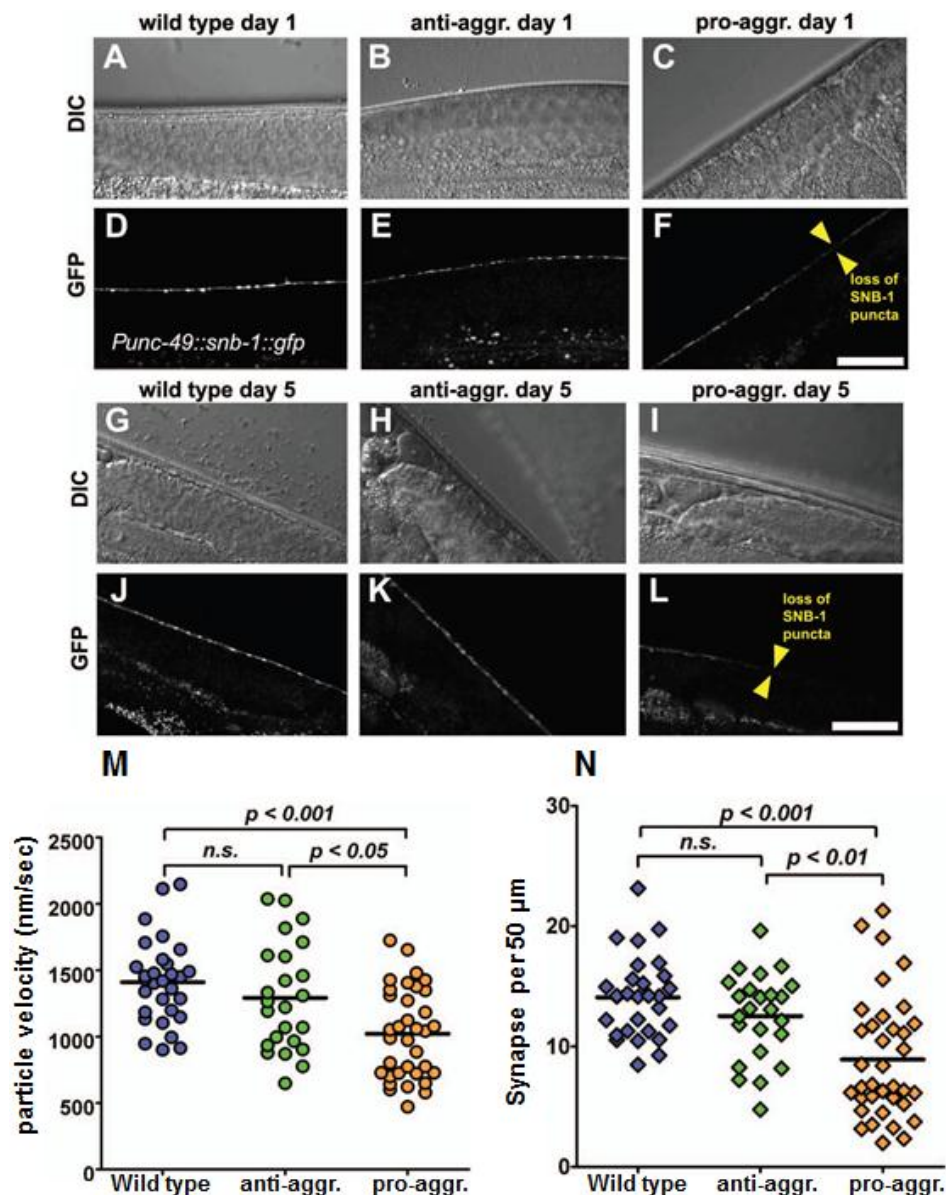


Figure 3.17: Pro-aggregant animals display defective presynaptic structures and organization already at early adulthood that deteriorates with age. (A-C): DIC images of the dorsal region above the posterior gonadal arm (where the imaging of the dorsal neural cord is performed) of (A) wild type, (B) anti-aggregant and (C) pro-aggregant animals expressing the *Punc-49::snb-1::gfp* reporter. (D-F): Maximal Intensity Projections (MIP) of the SNB-1::GFP fluorescent puncta (pre-synaptic termini) along the dorsal neural cord corresponding to the regions shown in the DIC pictures above. Note that for the pro-aggregation example, the SNB-1::GFP puncta are weaker and more diffuse (region between the yellow arrowheads). (G-I): Similar to (A-C) but shown for animals at day 5 of adulthood. (J-K): The MIP of the SNB-1::GFP puncta along the dorsal cord correspond to the regions shown in (G-I). Note the complete absence of SNB-1::GFP puncta in the right part of the MIP from the pro-aggregation animal (region between arrowheads). Scale bars are 20 μm. Pre-synaptic termini in the pro-aggregant strain often show diffuse structure and progressively vanish. (M): Scatter plot of the mean fluorescent intensity of SNB-1::GFP puncta (Arbitrary Units), as measured from the MIP images for each animal. The line denotes the mean (n.s. for non-significant). Kruskal-Wallis ANOVA (non-parametric) with Dunn's post hoc test was used for comparisons. (N): Scatter plot showing the number of SNB-1::GFP puncta (synapses) per 50 μm of dorsal cord, calculated from the same images that were used for the puncta intensity quantification graph in (D). Kruskal-Wallis ANOVA with Dunn's post hoc test was used for comparisons. This figure demonstrates the extent of synaptic loss in the pro-aggregant worms. Synaptobrevin-1 puncta on the dorsal cord are both less intense and less numerous compared to wild type or anti-aggregant strain (adapted from Fatouros C and Pir GJ et al., *HMG*, 2012).

which serves as an indicator for synaptic transport defects or synaptic loss (**Fig 3.17 F**). In older animals, this phenotypic pattern deteriorated further (**Fig 3.17 G-L**). Quantification of the mean fluorescence intensity of SNB-1::GFP puncta from more than 25 animals of each genotype showed a reduction in the puncta intensity of the pro-aggregant strain (mean intensity \pm s.d.= 1022 ± 330 arbitrary units, AU) compared to both wild type (1410 ± 300 AU) and anti-aggregant (1292 ± 400 AU) strains (**Fig 3.17 M**). Moreover, the density of puncta (number of puncta per $50 \mu\text{m}$) was also reduced (**Fig 3.17 N**). Specifically, pro-aggregant worms had 8.9 ± 5.1 puncta per $50 \mu\text{m}$, whereas wild type had 14.1 ± 3.3 and the anti-aggregants had 12.5 ± 3.5 . These alterations in intensity and density of staining can very well represent the alterations in presynaptic structures, as previously correlated by others (Jin, 2002; Nonet, 1999). Thus, the over expression of amyloidogenic Tau species causes extensive progressive synaptotoxicity in this *C. elegans* Tauopathy model.

3.15 Mitochondria get mislocalized in the DA9 motor neuron of the pro-aggregant line

Most of the mammalian neurodegenerative models depict a perturbation of mitochondrial transport and the subsequent energy crisis is known to contribute to neurodegeneration (Lasagna-Reeves et al., 2011; Morris et al., 2011; Schon and Przedborski, 2011; Thies and Mandelkow, 2007). In order to examine this neuronal mitochondria mislocalization phenotype in our Tauopathy model, the reporter strain *wyEx2709* [*Pitr-1::TOM-20^{1-54aa}::yfp*] (Klassen et al., 2010), which labels mitochondria only in the DA9 neuron close to the posterior end of the animal was used. DA9 is a well-defined neuron which possesses a soma located at the ventral side near the anus, and extends a dendrite anteroventrally, and an axon towards the dorsal cord which then extends anteriop dorsally. This anteriop dorsol region typically displays a regular distribution of mitochondrial particles in a wild-type background (Klassen et al., 2010) (**Fig 3.18 A**), extending to the distal axonal segment. The vertical axonal part is asynaptic and has few mitochondria (Klassen et al., 2010). When this *WyEx2709* strain was crossed into the pro-aggregant strain, this regular mitochondrial distribution was found to be distorted. Few or no mitochondrial

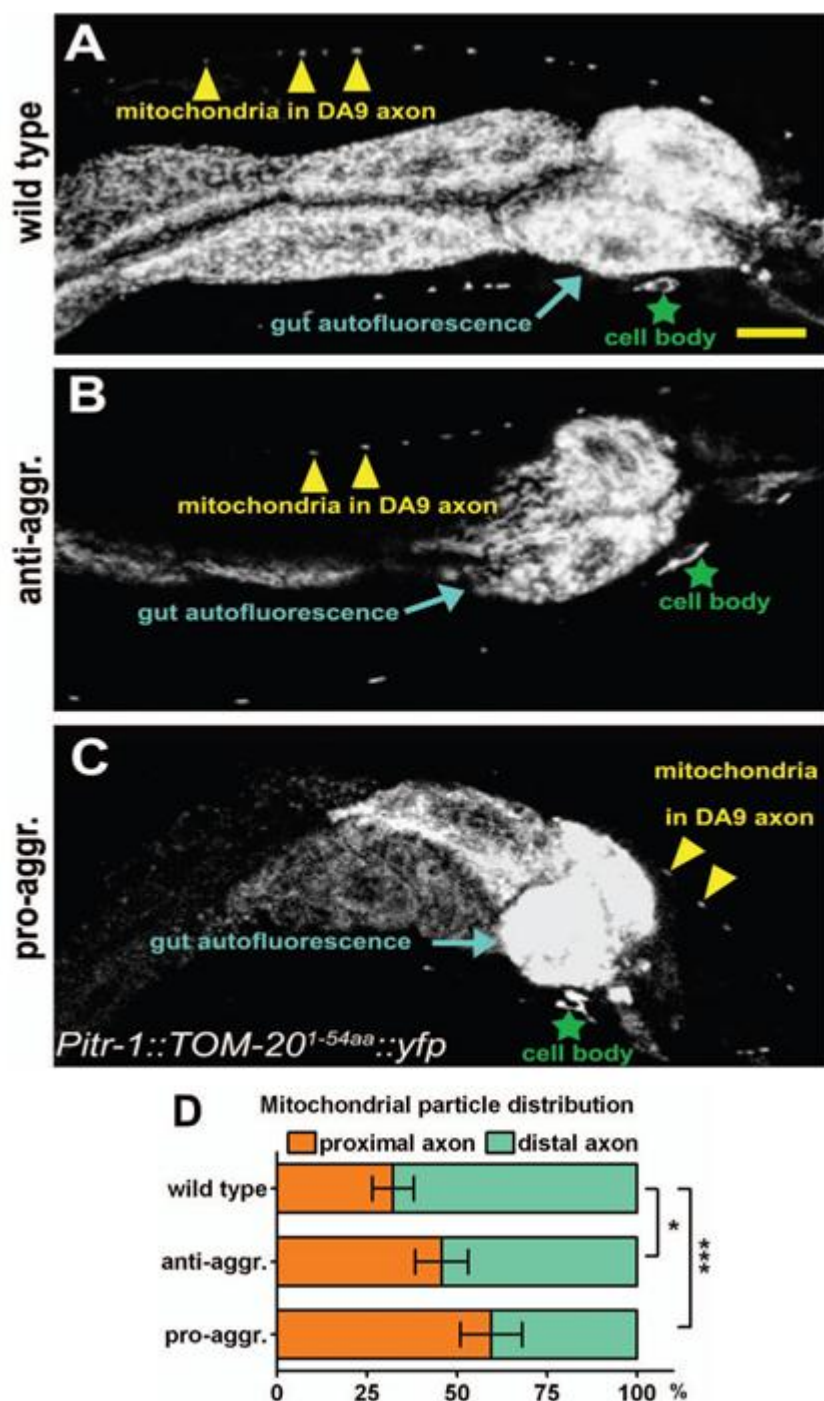


Figure 3.18: Mitochondria mislocalize to the proximal axonal segment of the DA9 neuron in pro-aggregation strain. (A): MIP of the YFP fluorescence from the tail region of a *Pitr-1::TOM-20^{aa1-54}::yfp* wild type reporter worm, showing the distribution of labeled mitochondrial particles along the DA9 neuron. The cell body (labeled by a green star) is located ventrally, extending a dendrite towards the anterior and an axon to the dorsal cord which then extends anteriorly (yellow arrowheads point to representative labeled mitochondria). The big fluorescent mass in the middle is the autofluorescence of the gut. Scale bar is 10 μ m. (B): MIP of the YFP fluorescence from the tail region of an anti-aggregant worm. YFP-labeled mitochondria (arrowheads show representative mitochondria) are distributed along the dorsal axon, similar as in wild type. (C): MIP of the YFP fluorescence from the tail region of a pro-aggregant worm. Note the defective distribution of YFP labeled mitochondria along the DA9 neuron (the yellow arrowheads point to mitochondria in the proximal axon, the distal segment is devoid of puncta). (D): Stacked bar diagram showing the distributions (percentage) of mitochondrial YFP particles in the proximal and distal axonal

segments (the axon was arbitrarily divided in two parts of equal length for this analysis, see also Fig. S3). Relatively more mitochondria cluster in the proximal axon of the pro-aggregant Tau transgenics. While in the wild type reference strain, around 60 % of the total axonal mitochondria are in the distal axonal part, in the pro-aggregant strain the situation is reversed, with 60% being in the proximal axonal segment. The anti-aggregants show an intermediate phenotype. 15 to 20 animals from each strain were used for quantification and error bars denote the standard deviation. Chi-Square Test with Yates' correction was used for comparisons. In this figure, the lack of mitochondria in the distal axonal segment of the pro-aggregants' DA9 neuron is highlighted (adapted from Fatouros C and Pir GJ et al., *HMG*, 2012).

particles were detected in the distal axonal segment (**Fig 3.18 C**) whereas the anti-aggregant strain upon crossing with *WyEx2709* strain showed only a moderate perturbation (**Fig 3.18 B**). Quantification showed that almost 60% of the axonal mitochondria accumulated in the proximal region and typically did not reach the more distal parts of the axon in the pro-aggregant worms. In contrast, only 32% and 45% of the axonal mitochondrial population was localized to the proximal axonal segment of wild type and anti-aggregant animals, respectively (**Fig 3.18 D**). It is not clear whether the absence of mitochondria in the distal axonal region arose from a severe transport problem or from axonal retraction, reminiscent of the axonal gaps in **Figure 3.13**. The results further support the notion that a highly amyloidogenic Tau species is detrimental for neurons, whereas the non-amyloidogenic species does not cause severe problems.

3.16 Defective axonal transport in the mechanosensory neurons of the pro-aggregant line

Since the pro-aggregant animals depicted a mitochondrial mislocalization phenotype, the next step was to examine if the axonal transport of mitochondria is affected. The strain *jsls609* expresses GFP with a mitochondrial localization signal (MLS) in the six mechanosensory neurons of *C. elegans*. The strain was crossed with our Tau mutants, creating the pro-aggregant and the anti-aggregant mitochondrial marker strains. Mitochondrial movements were quantified by performing single plane live imaging of the middle axonal segment of the PLML or PLMR neurons in immobilized worms. The PLM axon closer to the microscope objective was selected

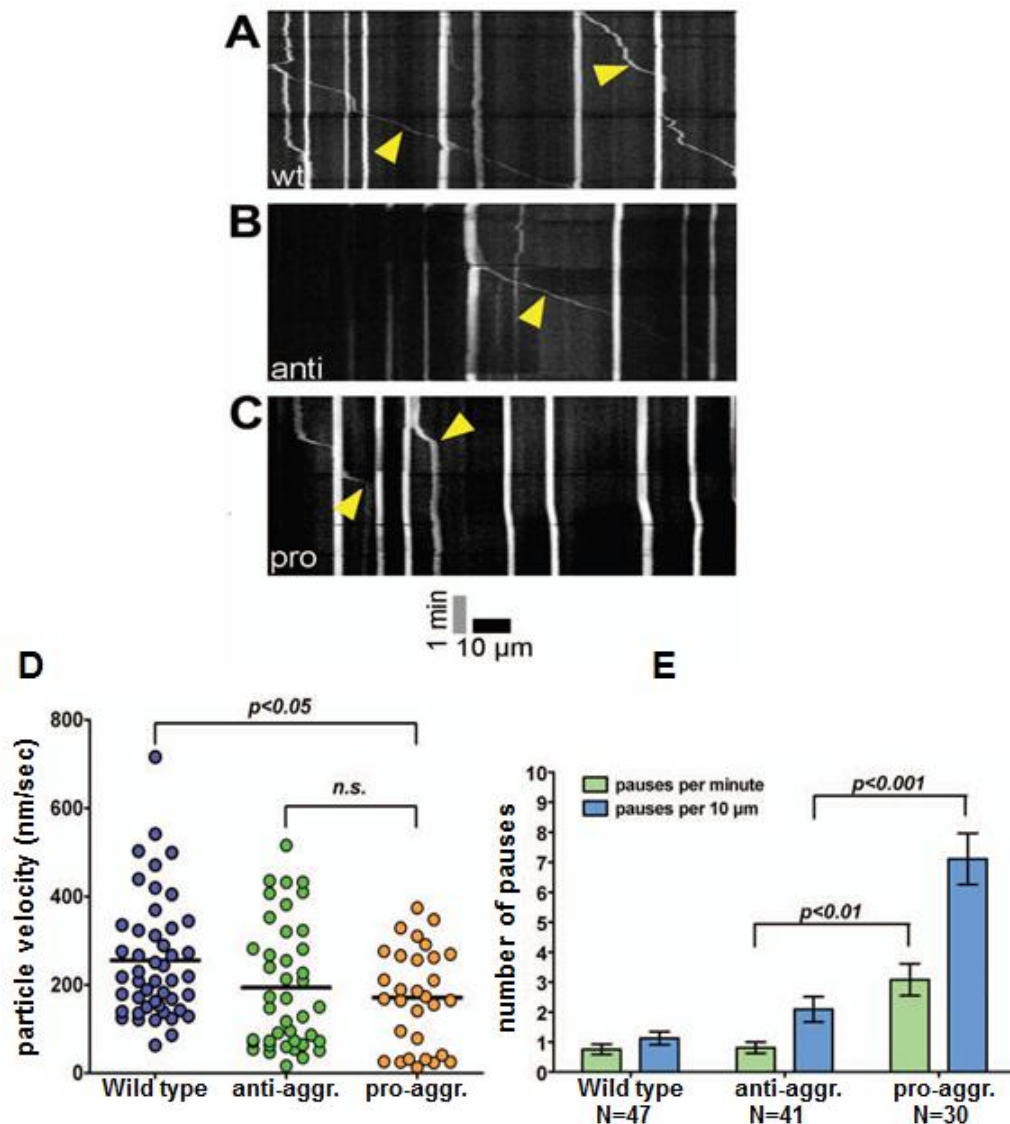


Figure 3.19: Pro-aggregant Tau transgenic worms show defective mitochondrial transport in the axons of mechanosensory neurons. Representative kymographs of PLM axons of pro-, anti-aggregant animals and wild type derived from time-lapse imaging are shown. Vertical lines represent stationary/docked mitochondria and oblique lines (labeled by arrowheads) represent the tracks of moving mitochondria. The slope of this track is an indicator of velocity. Anterograde movements: slope declines to the right, in retrograde movements to the left. The kymograph space and time scale is shown at the bottom. (A): A kymograph recorded from a day 1 adult wild type animal. (B): A kymograph recorded from a day 1 adult animal of the anti-aggregant strain. Note the oblique line in the middle which shows the track of a fast moving mitochondrial particle (arrowhead). (C): A kymograph recorded from a day 1 adult animal of the pro-aggregant strain. Note that the two particles in motion make long pauses (oblique lines become vertical, labeled by yellow arrowheads) and their track displacement is rather limited. (D): Scatter plot of the mean velocities of mitochondrial particles that were manually tracked from 20 time lapse videos that were analyzed for each strain. Instantaneous velocity values that were < 10 nm/sec were not included in the calculation of the means for this plot, as these frames were classified as pause events that were separately analyzed (see next graph). (E): Bar diagram for the quantification of pausing frequency in relation to time and distance parameter. The number of pausing events is significantly increased in the pro-aggregant strain. Error bars account for standard error of the mean (s.e.m). In summary, the axonal transport of mitochondria in pro-aggregant worms does not run smoothly due to increased pause events, although instantaneous velocities *per se* are not substantially different from those seen in the anti-aggregant worms (adapted from Fatouros C and Pir GJ et al., *HMG*, 2012).

for analysis. At least 20 time lapse acquisitions were collected for each strain, the representative examples of each strain are shown as kymographs in **Figures 3.19A-C**. The mean velocity of the continuously moving particles was calculated by manually tracking each moving GFP particle with ImageJ (**Fig 3.19 D**). The pro-aggregant strain showed lower mitochondrial velocity than the wild type (mean \pm s.d. = 171 ± 111 nm/sec versus 256 ± 117 nm/sec), whereas the anti-aggregant strain (194 ± 131 nm/sec) did not substantially differ from wild type (**Figure 3.19 D**). However, there was a striking difference in the mitochondrial pausing frequency between pro-aggregant and the other two strains. The pro-aggregant strain showed approximately four times more frequent pause events compared to the anti-aggregant (**Fig 3.19 E**). The data suggests that there is a reduced mitochondrial transport in the axons of the pro-aggregant strain. In summary, our Tau transgenic strains recapitulate most of the phenotypic defects found in the mammalian neurodegenerative models and further consolidates the notion that the amyloidogenic properties of Tau can block axonal transport of mitochondria.

3.17 Compound treatment

Compounds had no effect on the wild-type N2 strain

Having developed a worm model with a well characterised phenotype very early in its life-span, which shows pathology reminiscent of the cellular pathology, observed in patients with tauopathy, we next set out to test various compounds which are known to have anti-aggregation properties. Some of these compounds have already been tested in vitro (Ballatore et al., 2007; Bulic et al., 2010; Bulic et al., 2009; Pickhardt et al., 2007). These compounds were tested by supplying them in the liquid culture so as to facilitate their entry into the worm through all three entry routes reported so far namely: ingestion, uptake through the skin and uptake via exposed sensory neuronal endings (Choy et al., 2006; Perkins et al., 1986; Smith and Campbell, 1996). Given the fact that drugs can have off-target effects when studied within the context of a whole organism, we tested these compounds first on the wild type N2 strains in order to make sure that there are no off-target effects and any

amelioration in the phenotype could be attributed to the anti-aggregation quality of these drugs.

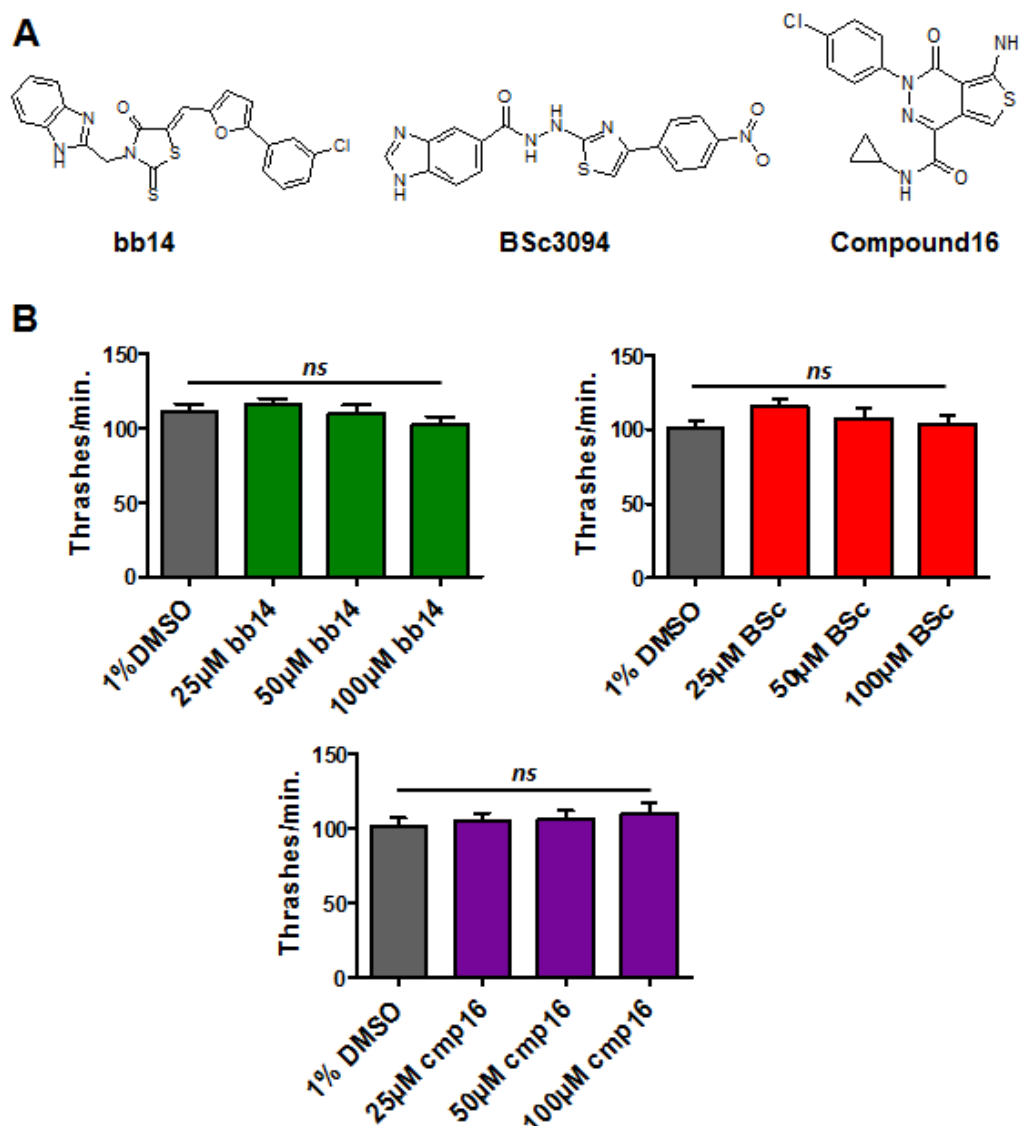


Figure 3.20: Compound treatment of wild type N2 strain. (A): Structure of the compounds. bb14 is a Rhodanine derivative and BSc3094 belongs to the phenylthiazolyl-hydrazide class of compounds while compound 16 (cmp16) belongs to the aminothienopyridazine (ATPZ) class of tau inhibitors (5-Amino-3-(4-chlorophenyl)-N-cyclopropyl-4-oxo-3,4-dihydrothieno[3,4-d]pyridazine-1-carboxamide). (B): Compound treatment in liquid culture was started at the L1 larval stage until day-3 of adulthood and the thrash assay was used as readout. bb14, BSc3094 and cmp16 had no effect on the wild type N2 strain at the three concentrations used.

We first started with bb14, BSc3094 and compound 16. The compound bb14 is a Rhodanine derivative and, BSc3094 is a phenylthiazolyl-hydrazide derivative. They were the two most promising hit compounds obtained in a mammalian cell model of tau toxicity (Pickhardt et al., 2007). Compound 16 (cmp16) belongs to the aminothienopyridazine (ATPZ) class of tau inhibitors (5-Amino-3-(4-chlorophenyl)-

N-cyclopropyl-4-oxo-3,4-dihydrothieno[3,4-d]pyridazine-1-carboxamide and was the most prominent tau aggregation inhibitor compound published in a recent *in vitro* screen (see figure 3.20 A for structure). It is also able to cross the blood brain barrier that makes it a good choice for the clinical applications (Ballatore et al., 2010). The worms were allowed to grow in liquid culture supplied with drugs at three different concentrations: 25 μ M, 50 μ M and 100 μ M in DMSO. 1% DMSO was used as a control and thrash assay was used as the readout of the phenotype. The drugs did not have any effect on the thrashes made by wild type worms at any of these concentrations (Fig 3.20 B) which confirms that the drugs have no apparent side-effects.

3.18 bb14, BSc3094 and cmp16 lead to an amelioration of the phenotype in the pro-aggregant strain

Now that the drugs did not have any effect on the wild type strain we finally went on to test these compounds on the pro-aggregant strain in these three concentrations.

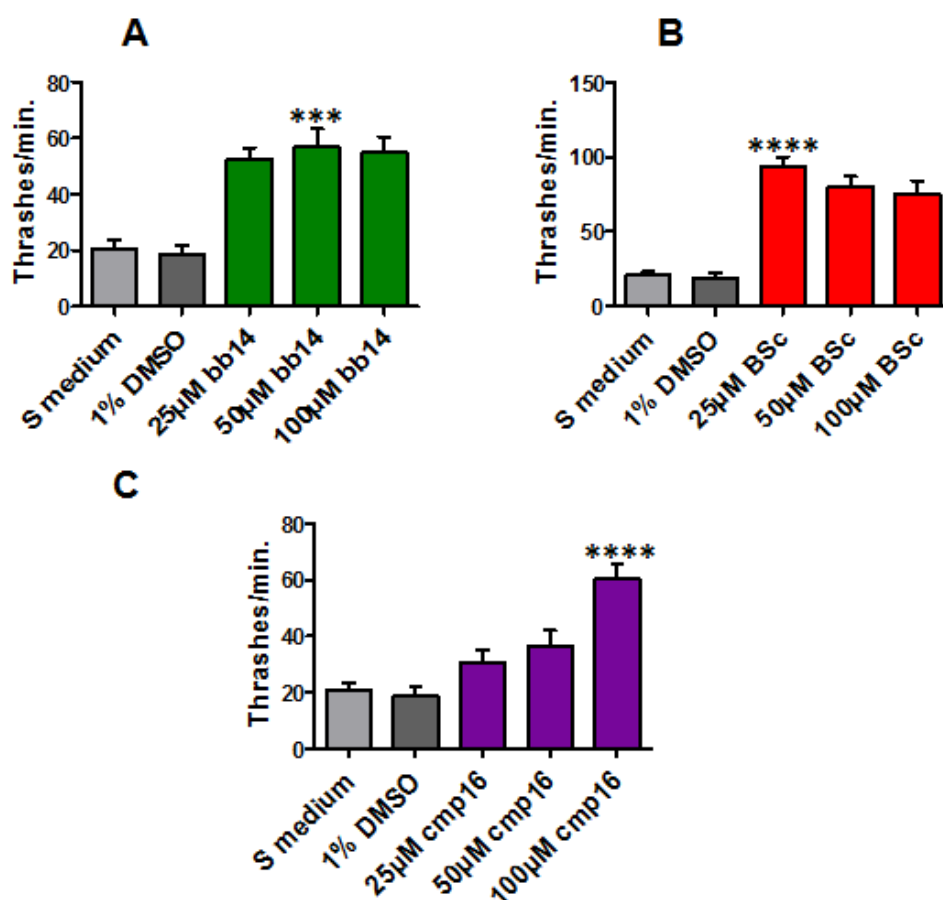


Figure 3.21: Treatment of pro-aggregant strain with the anti-aggregation compounds can ameliorate the phenotype. Bar diagram plotting the thrashing rates of synchronized day-3-old adult pro-aggregant animals

either untreated in S medium and 1% DMSO as controls or treated with compounds at three different concentrations. The error bars denote the SEM. bb14 at 50 μ M (A), BSc3094 at 25 μ M (B) and compound 16 at 100 μ M (C) increased the thrash rates by ~ 3 , ~ 5 and ~ 3 times respectively. Unpaired t test was implemented for comparisons (** stands for $p < 0.001$, *** stands for $p < 0.0001$ in the comparisons between untreated pro-aggregant (S medium or 1% DMSO) and compound treated pro-aggregant at the best concentrations).

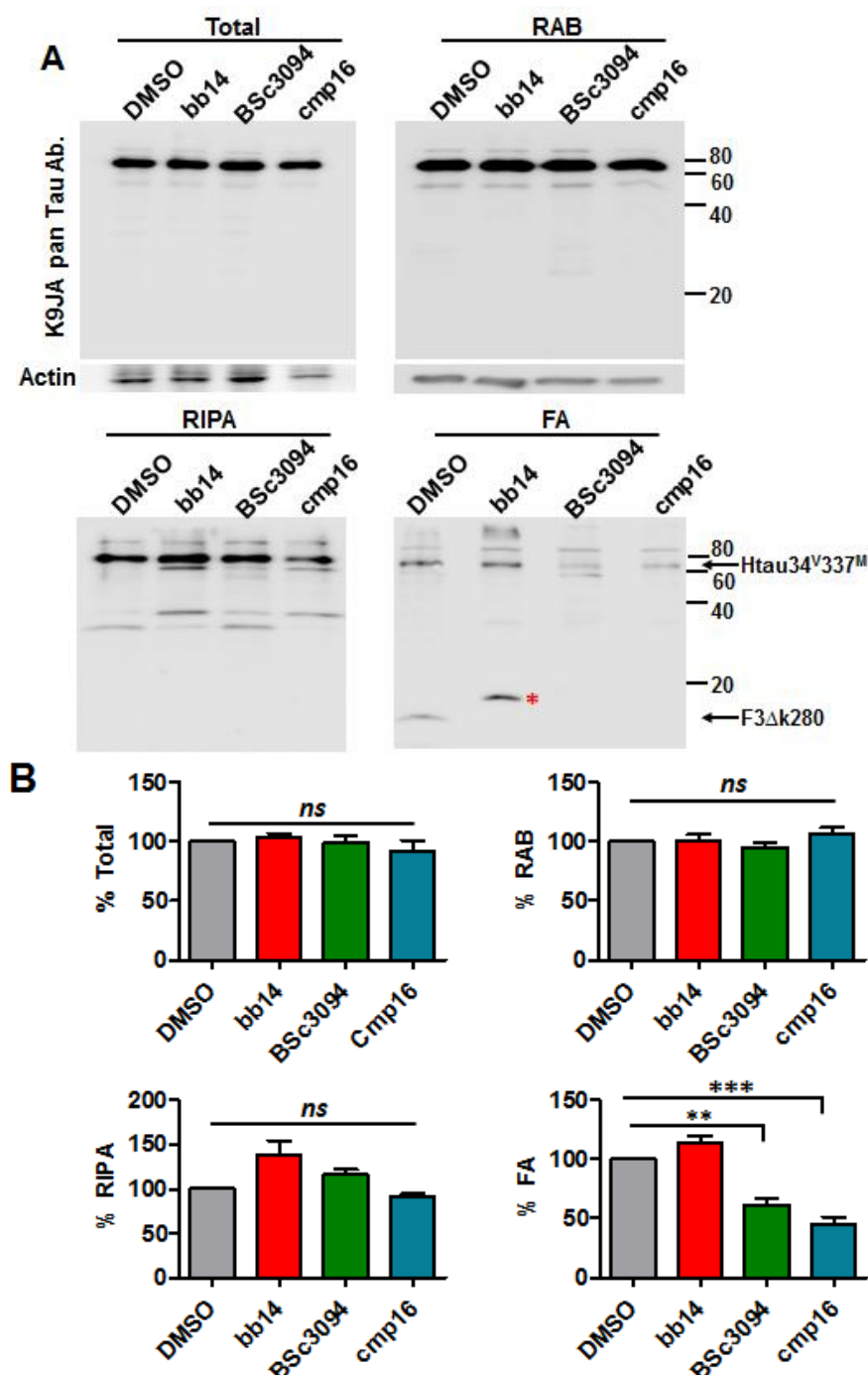


Figure 3.22: Sequential extraction of Tau from synchronized pro-aggregant animals after treatment with aggregation inhibitor compounds. Soluble Tau fraction (RAB), detergent soluble fraction (RIPA) and detergent insoluble fraction made soluble by 70% formic acid (FA) were immunoblotted using pan Tau antibody, which recognizes both the full-length V337M Tau and the repeat fragments F3 Δ K280/ F3 Δ K280PP. Anti-actin antibody was used as an internal control. **(A):** There is a slight decrease in the insoluble Tau extracted with formic acid (FA-blot) upon BSc3094 (25 μ M) and cmp16 (100 μ M) treatment but not a significant difference after bb14 (50 μ M) treatment. However, treatment with all the three compounds led to

disappearance of F3ΔK280 fragment. Asterisk in red (*) may be a proteolytic fragment of Tau. **(B)**: Quantification of the total, soluble, detergent soluble and detergent insoluble Tau from the pro-aggregant strain after 50 μM bb14, 25 μM BSc3094 and 100 μM cmp16 treatment. Equal amount of protein was loaded and immunoblotted with K9JA pan tau antibody, using actin as a loading control. For the quantification lane intensities were normalized against the untreated (DMSO). BSc3094 and cmp16 lead to approximately 40% and 50% decrease in the insoluble Tau respectively (One-Way ANOVA, ** $p < 0.01$, *** $p < 0.001$).

Treated pro-aggregant worms showed more thrashes per minute than the control 1% DMSO treated worms. The compounds ameliorated the phenotype to different extents and at different concentrations. 50μM bb14, 25μM BSc3094 and 100μM cmp16 treated worms produced 3 times, 6 times and 3 times more thrashes per minute respectively than the control 1% DMSO treated counterparts (**Fig 3.21**). We used these particular concentrations to perform the biochemistry after the compound treatment in order to look at the insoluble tau levels. To perform biochemistry, the culture conditions were extended to 6-well polystyrene plates and allowed to grow the worms in the presence or absence of compounds until day 3 of adulthood before lysing them for protein extraction. At the biochemical level, compound treatment reduced the Tau aggregates. In addition, no F3ΔK280 appeared in the formic acid fraction (**Fig 3.22 A**). BSc3094 reduced the insoluble tau by ~40% and cmp16 by ~50% (**Fig 3.22 B**).

3.19 Methylene blue

Methylene blue (MB) is a tricyclic phenothiazine drug (see **figure 3.23 A for structure**) (Wainwright and Amaral, 2005). It has been in use for almost 120 years as a medical drug as well as a staining reagent (Schirmer et al., 2011), however, it has been recently shown to reduce the aggregation of tau and thereby slow down the disease (Hattori et al., 2008; Wischik et al., 1996). We tested this compound on the pro-aggregant strain. We first treated wild type worms with MB and found no difference in the thrash rates between the treated and the untreated worms (**Fig 3.23 B**). However, MB treatment led to a partial amelioration of phenotype in pro-aggregant animals and the treated worms showed ~2 times more thrashes per minute at 25 μM concentration than the untreated worms (**Fig 2.23 C**). It should be noted that at higher concentrations MB started to crystallize in solution. So we continued with 25 μM MB concentration for biochemical analysis to look at the Tau

aggregates in the FA fraction (**Fig 3.23 D**). At the biochemical level, MB treatment altered the tau solubility and reduced detergent insoluble tau by ~35% (**Fig 3.23 E**).

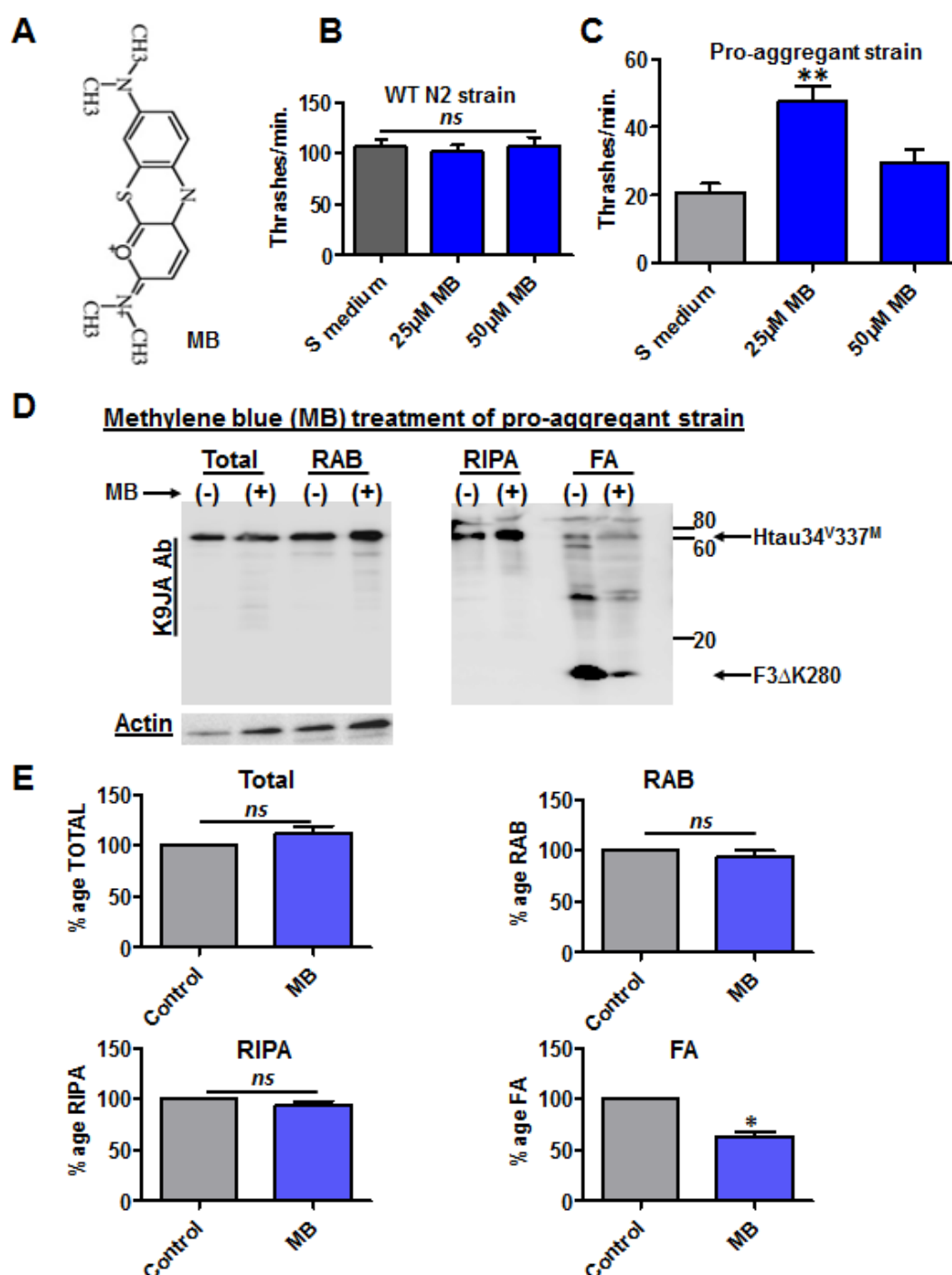


Figure 3.23: Methylene Blue treatment leads to partial amelioration of phenotype along with reduction in detergent insoluble tau. Total Tau, soluble Tau fraction (RAB), detergent soluble fraction (RIPA) and detergent insoluble fraction made soluble by 70% formic acid (FA) were immunoblotted using pan Tau antibody, which recognizes the repeat domains and hence detects both the full-length V337M Tau and the repeat fragments F3ΔK280/ F3ΔK280PP. Anti-actin antibody was used as an internal control. **(A):** Chemical structure of Methylene Blue (MB). **(B):** Bar diagram plotting the thrashing rates of synchronized day-3-old adult wild type N2 animals either untreated (S medium) as control or treated with 25 µM and 50 µM MB. MB had no effect on the wild type N2 strain. **(C):** Bar diagram plotting the thrashing rates of synchronized

day-3-old adult pro-aggregant animals either untreated (S medium) as control or treated with 25 μ M and 50 μ M MB. The error bars denote the SEM. MB at 25 μ M increased the thrash rates by ~ 2.5 times. Higher concentrations of MB led to its precipitation and were not effective. Unpaired *t* test was implemented for comparisons (** stands for $p < 0.01$ in the comparison between untreated pro-aggregant (S medium) and compound treated pro-aggregant at the best concentration. **(D)**: Sequential extraction of Tau from synchronized pro-aggregant animals after treatment with MB. Insoluble Tau species in the formic acid fraction (FA) decrease after Methylene Blue treatment (25 μ M). **(E)**: Quantification of the total, soluble, detergent soluble and detergent insoluble Tau from the pro-aggregant strain after Methylene Blue treatment. Equal amount of protein was loaded and immunoblotted with K9JA pan tau antibody. For the quantification lane intensities were normalized against the untreated sample. MB treatment leads to approximately 35% decrease in the insoluble Tau (Paired *t* test, $*p < 0.05$).

3.20 Trehalose treatment ameliorates the phenotype of pro-aggregant line, decreases the aggregation load by inducing autophagy

The disaccharide trehalose has been reported to induce autophagy and hence enhance the clearance of autophagy substrates like mutant huntingtin and the A30P and A53T mutants of alpha-synuclein, associated with Huntington disease (HD) and Parkinson disease (PD), respectively (Sarkar et al., 2007a). Though it is controversial whether tau protein is a proteasomal substrate (David et al., 2002; Mori et al., 1987; Zhang et al., 2005) or not (Brown et al., 2005; Delobel et al., 2005; Feuillet et al., 2005), recent evidence show that the amount of tau aggregates increase by blocking the macroautophagy, pointing towards the role of autophagy in the clearance of tau aggregates (Wang et al., 2009). Furthermore, trehalose treatment reduced the amount of sarkosyl insoluble Tau in a tet-on N2a cell model and reduced the overall Tau levels in primary neurons (Kruger et al., 2011). Thereby we tested this disaccharide in our pro-aggregant strain to see if there is an amelioration of phenotype. The worms were treated in liquid cultures supplied with 200 mM trehalose starting at L1 larval stage. The adults were analyzed at day 3 of adulthood for locomotion using the thrash assay as readout. Trehalose led to a partial amelioration of the uncoordinated phenotype and the trehalose treated worms showed ~ 2 times more thrashes per minute than their untreated counterparts (**Fig 3.24 B**). Then the worms were analyzed biochemically to examine the levels of tau aggregates on trehalose treatment (**Fig 3.24 C**). Upon sequential extraction of tau, it was found that trehalose treatment resulted in a profound decrease ($\sim 50\%$) in the detergent insoluble tau (**Fig**

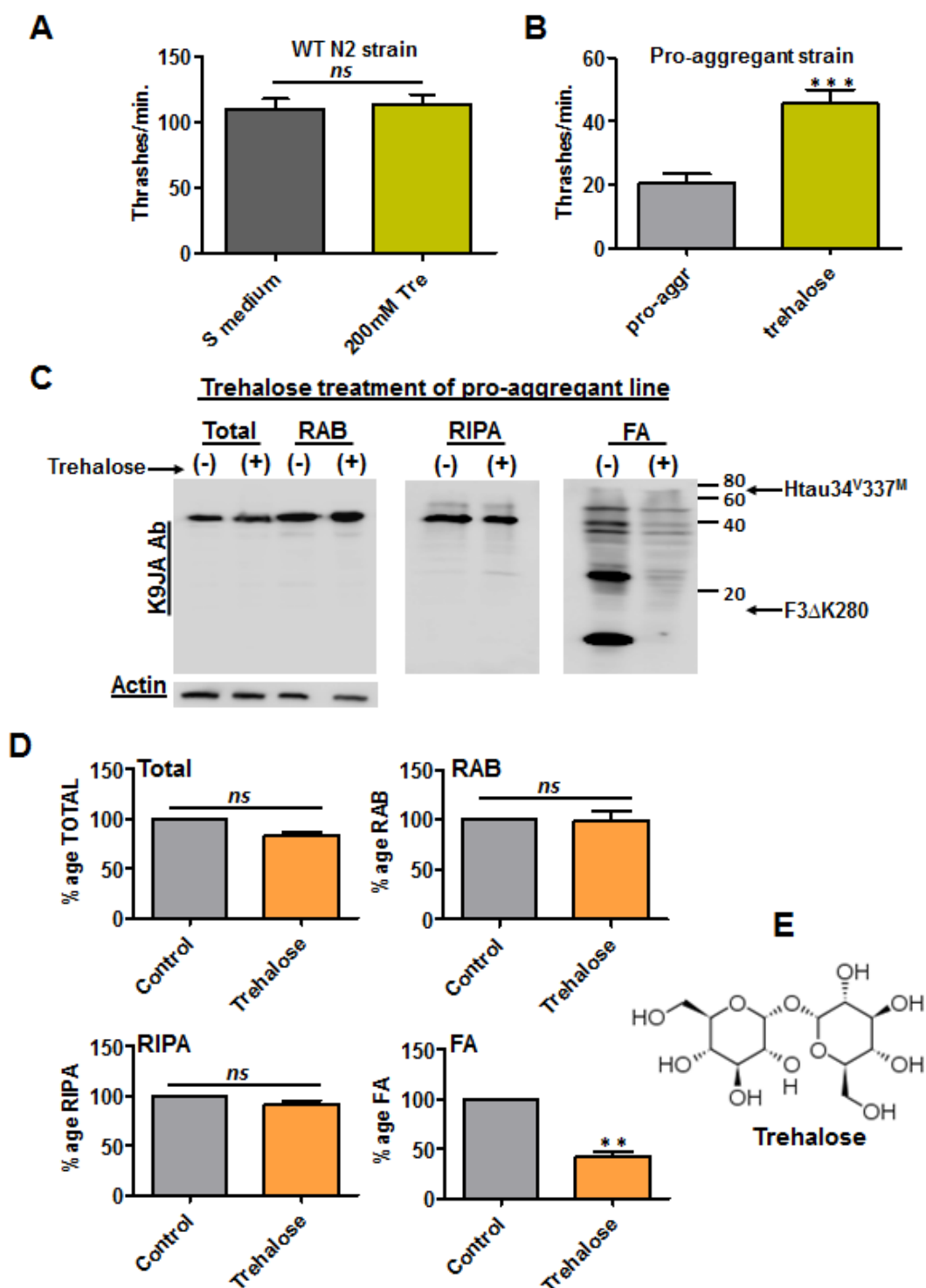


Figure 3.24: Trehalose treatment leads to partial amelioration of phenotype along with reduction in detergent insoluble tau. Total Tau, soluble Tau fraction (RAB), detergent soluble fraction (RIPA) and detergent insoluble fraction made soluble by 70% formic acid (FA) were immunoblotted using pan Tau antibody, which recognizes both the full-length V337M Tau and the repeat fragments F3ΔK280/ F3ΔK280PP. Anti-actin antibody was used as an internal control. **(A):** Bar diagram plotting the thrashing rates of synchronized day-3-old adult wild type N2 animals either untreated S medium as control or treated with 200 mM trehalose. Trehalose had no effect on the wild type N2 strain. **(B):** Bar diagram plotting the thrashing rates of synchronized day-3-old adult pro-aggregant animals either untreated S medium as control or treated with 200 mM trehalose. The error bars denote the SEM. 200 mM trehalose treated pro-aggregant worms showed ~2 fold thrashes than their counterparts in the S-medium. Unpaired *t* test was implemented for comparisons (***** stands for $p < 0.001$ in the comparison between untreated pro-aggregant (S medium) and

trehalose treated pro-aggregant. **(C)**: Sequential extraction of Tau from synchronized pro-aggregant animals after treatment with trehalose. **(D)**: Quantification of the total, soluble, detergent soluble and detergent insoluble Tau from the pro-aggregant strain after trehalose treatment. Equal amount of protein was loaded and immunoblotted with K9JA pan tau antibody. For the quantification lane intensities were normalized against the untreated sample. Trehalose treatment led to approximately 50% decrease in the insoluble tau (Paired *t* test, ** $p < 0.01$). **(E)**: Chemical structure of trehalose.

3.24 D). These results clearly show that the solubilizing property of trehalose is not limited to a specific protein as shown also earlier (Arora et al., 2004; Liu et al., 2005; Tanaka et al., 2004) but is able to solubilize the tau aggregates as well.

Next we examined whether the decrease in the tau aggregates was due to an increase in the autophagy level induced by trehalose as reported earlier (Sarkar et al., 2007a). A flux experiment was performed to look at the level of LGG2 (Alberti et al., 2010), *C. elegans* ortholog of human MAP1-LC3 (a marker of autophagy) (Rubinsztein et al., 2009). We decided to use the lysosomotropic chemical NH_4Cl to neutralize the lysosomal pH and hence block the degradation of LGG2. By blocking its degradation, we could compare the LGG2 levels in the trehalose treated and the untreated worms. To determine the saturating concentration of NH_4Cl that was needed to block the lysosomal degradation, we did a concentration dependent treatment of worms with NH_4Cl for 8 hrs and later checked for the LGG2 levels. It was found that NH_4Cl at 150 mM concentration led to the highest accumulation of LGG2 and beyond 150mM concentration there was again a decrease in the accumulation of LGG2 (**Fig 3.25 A**). So we decided to use 150 mM NH_4Cl concentration.

Next we allowed synchronized day 1 old adults to grow in liquid cultures in 6-well polystyrene plates supplemented with 200 mM trehalose until day 3 of adulthood, at which day they were treated with NH_4Cl for 8 hrs to block the degradation of LGG2. Worms treated with both 150 mM NH_4Cl and 200 mM trehalose showed a huge accumulation of LGG2 compared to the worms treated either with NH_4Cl alone or with trehalose alone (**Fig 3.25 B**). It is important to mention here that *lgg-1* and *lgg-2* are two *C. elegans* homologues of yeast Atg8 (ubiquitin-like protein present on autophagosomal membranes) (Ichimura et al., 2000). Both LGG-1 and LGG-2 localize to autophagosomes, display a similar expression pattern and are known to act synergistically in autophagy-induced

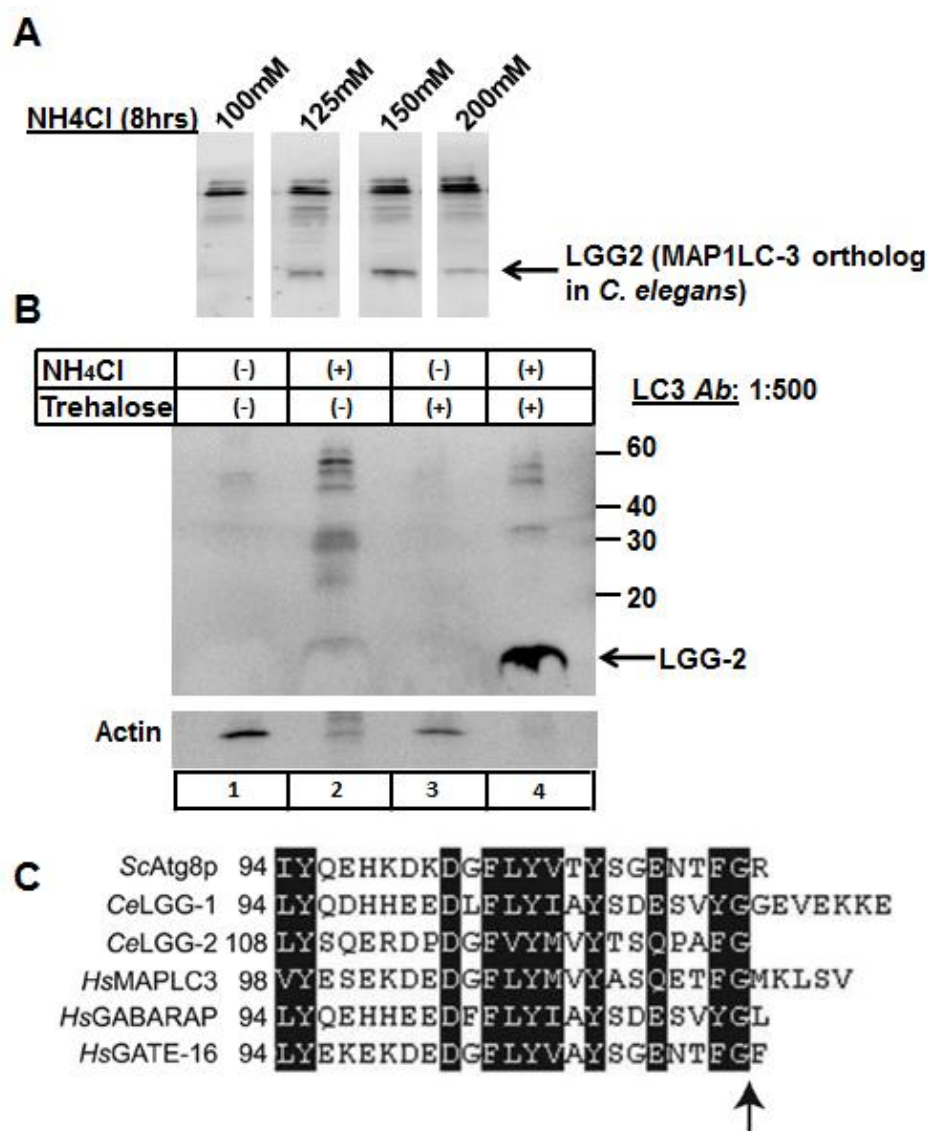


Figure 3.25: Trehalose increases the autophagy level. (A): NH₄Cl (a lysosomotropic chemical) inhibits the lysosomal degradation by neutralizing their acidic pH, leading to the accumulation of non-degraded products. Shown here is the concentration dependent effect of NH₄Cl on autophagy as seen by the increase in the levels of LGG-2. Equal amount of protein was loaded and immunoblotted with antibody against mouse LC3. NH₄Cl at 150 mM showed the highest accumulation of LGG2 levels and was therefore used for the subsequent flux experiment. (B): Trehalose treatment in combination with NH₄Cl (lane 4) leads to an additional accumulation of LGG2 compared to the NH₄Cl alone (lane 2). No LGG-2 accumulation was seen in the untreated worms (lane 1) and the worms treated with trehalose alone (lane 3). (C): Figure shows the sequence alignment of amino acids from the C-terminal segments of LGG-1 and LGG-2 and their homologues. The conserved residues are shaded in black and the arrow indicates the cleavage site in Atg8p and MAPLC3 [adapted from (Alberti et al., 2010)].

conditions, namely dauer formation, starvation and aging. Therefore, both can be used as autophagic markers. However, LGG-2 is more closely related to human MAP1LC-3 and was shown to be recognized by human LC3 antibody (see Fig 3.25 C for sequence homology) (Alberti et al., 2010). We used the human-LC3 antibody in

our experiments to determine the levels of LGG-2, which in turn served as an autophagy marker in *C. elegans*.

This result confirms that trehalose induces autophagy in *C. elegans*, which would in turn lead to the clearance of tau aggregates. As a result of which, the toxic protein aggregate load in the pro-aggregant strain would be reduced which would explain the amelioration of uncoordinated phenotype upon trehalose treatment. Furthermore, since tau in our *C. elegans* model is highly phosphorylated at multiple sites including the KXGS motif (see 12E8 panel_figure 3.14), it is reasonable to consider that the results from trehalose treatment in our *C. elegans* tau model lend support to the earlier findings that tau phosphorylated at the repeat domains is degraded by macroautophagy (Wang et al., 2009).

4 Discussion

Aggregation of proteins has been associated with a number of diseases. Tau, a highly conserved microtubule-associated protein (Cambiagno et al., 1995; Goedert et al., 1996a; Goedert et al., 1989), is predominantly expressed in neurons where its primary role is to support the neurite outgrowth and axonal transport by way of stabilizing the microtubules. Tau is an important protein from various disease points of view in that it undergoes a transition from a highly soluble state to an insoluble aggregated state. In fact, this pathological aggregation of Tau is one of the hallmarks of Alzheimer disease and a group of diseases called tauopathies. In this study we have addressed the issue of aggregation-mediated toxicity of Tau in a well-described model organism, *C. elegans*. Our *C. elegans* model system is based on the expression of FL V337M Tau and the repeat fragment with Δ K280 mutation that is endowed with a tendency to form seeds which lead to an accelerated aggregation and hence an early appearance of a severe uncoordinated phenotype. The results will be discussed below:

4.1 Phenotypic characterization of *C. elegans* Tau-transgenic lines

In this study we have described *C. elegans* Tau-transgenic lines based on Tau aggregation. In order to achieve this we co-expressed two combinations of Tau transgenes. One that co-expresses a full length V337M Tau (Kraemer et al, 2003) along with an aggregation prone repeat fragment F3 Δ K280 and the other that co-expresses full length V337M Tau along with an anti-aggregant repeat fragment F3 Δ K280PP containing two proline substitutions that prevent aggregation (von Bergen et al., 2001). In other words, the two lines only differ in the presence of a pro-aggregant or an anti-aggregant F3 fragment. When we look at the properties of these two repeat fragments F3 Δ K280 and F3 Δ K280PP, they are the same when it comes to the functional aspects like microtubule interaction (both have very poor binding) or phosphorylation sites (both contain the same phosphorylation sites) (Khlistunova et al., 2006; Wang et al., 2007). However, they only differ in their aggregation

propensity, therefore, this allowed us to attribute the phenotypic differences in the two lines solely to Tau aggregation and decouple it from the other functional aspects of these repeat fragments (phosphorylation, microtubule binding). The first thing we observed was a severe uncoordinated movement (using thrash assay as readout) visible already at the first day of adulthood only in the pro-aggregant animals. This uncoordinated phenotype was progressive and resulted in almost complete paralysis at day 7 of adulthood making it difficult to analyze their thrashes (**Fig 3.4**). The anti-aggregant animals did not show an uncoordinated phenotype in the early days of adulthood. However, later in their life (after day 5 of adulthood), anti-aggregant animals developed a rather mild phenotype. This can be explained by the fact that the expression of full length V337M Tau can produce an age dependent uncoordinated phenotype in *C. elegans* as described before (Kraemer et al., 2003). At the same time, the early onset of the phenotype already at the first day of adulthood in pro-aggregant animals shows certain advantages over previously published Tauopathy models of *C. elegans* (Brandt et al., 2009; Kraemer et al., 2003; Miyasaka et al., 2005) in that the age-related natural decline in proteostasis (Ben-Zvi et al., 2009; David et al., 2010; Dillin and Cohen, 2011) can be uncoupled from the Tau-mediated toxicity. We are also sure that the phenotype shown by the pro-aggregant worms is not due to a disturbance in important genome loci that might have happened in the course of integrating the transgenes because a combination of the same pro-aggregation transgenes in an extrachromosomal array showed a similar effect. Moreover, RNAi directed against the pro-aggregation fragment F3ΔK280 partially suppressed the phenotype (**Fig 3.9**). This argues that the toxicity solely comes as a result of the co-expression of the highly amyloidogenic F3 fragment.

Experiments in collaboration with the Baumeister lab (Chronis Fattouros) showed that the pro-aggregant animals possess three more prominent phenotypic defects namely, neuronal abnormalities, synaptic dysfunction and mitochondrial transport defects which will be discussed below:

Neuronal loss is a prominent feature of many neurodegenerative disorders and many mammalian models of tauopathy can recapitulate this phenotype (Obulesu et al., 2011). Neuronal dysfunction in our *C. elegans* tauopathy model was seen as

discontinuities in dorsal and ventral nerve cords, incomplete commissures and gaps in the axons (**Fig 3.13**); however, we saw all these morphological abnormalities occurred in the neurons in the absence of neuronal loss. There could be several reasons why there was not an apparent neuronal loss in our model system. First, the short life-span of *C. elegans* which gives a relatively short time frame to follow up the neuronal loss compared to the other model systems. Secondly, it could be that the neuronal dysfunction in the absence of neuronal loss, as seen in our model system, is more important during the early phase of AD and other tauopathies. Recent progress in the pathogenesis of tauopathies has indeed shown that mice develop characteristic symptoms resembling the human diseases without neuronal loss. It has been suggested that the physical changes that happen to the neurons in the absence of neurodegeneration underlie cognitive decline (Yankner et al., 2008). Same sort of results have surfaced earlier, whereby various animal models of Huntington's disease, spinobulbar muscular atrophy (SBMA) and tauopathy develop the characteristic human disease symptoms in the absence of neuronal loss (Brandt et al., 2009; Eckermann et al., 2007; Katsuno et al., 2002; Mangiarini et al., 1996; Miyasaka et al., 2005; Parker et al., 2001; Turmaine et al., 2000; Van der Jeugd et al., 2012). Furthermore, healthy brain aging is characterized by fine structural changes such as synaptic deterioration, neuronal sprouting, and restructuring rather than neuronal loss (Yankner et al., 2008) and these findings were further consolidated by the results in a recent work from aging *C. elegans* nervous system (Toth et al., 2012). This means it is the finer structural changes rather than a neuronal loss that may promote neuronal dysfunction in neurodegenerative diseases and our tauopathy model can successfully recapitulate these phenomena.

A loss of pre-synaptic marker SNB-1 in our model system (**3.17**) gives a clear indication that the neurons are not functioning properly. It is worthwhile to mention that synaptic dysfunction does not necessarily correlate with the neuronal loss as has been shown in the previous studies (D'Amelio et al., 2011; Hoover et al., 2010; Van der Jeugd et al., 2012). Pro-aggregant *C. elegans* expressing highly aggregating Tau species in their neurons have a relatively lower number of synapses (fewer SNB-1 puncta) and weaker synapses as seen by lower puncta intensity. It is important to note that a perfect correlation of the SNB-1 puncta with the presence of synapses has

been demonstrated already (Jin, 2002; Nonet, 1999). These observations suggest that the expression of aggregation prone Tau species in *C. elegans* neurons leads to synaptic dysfunction. These findings correlate well with the recent observation from a mouse model of tauopathy, whereby the expression of a pro-aggregant but not anti-aggregant full length Tau led to a spinal loss in the absence of neuronal loss (Van der Jeugd et al., 2012).

As we know that mitochondria play diverse roles in a cell but the most important function that sets them apart from the other sub-cellular organelles is their capacity to generate energy currency for the cell in the form of adenosine triphosphate (ATP), which gives them the name “power houses of the cell”. Their proper distribution, shape, size, anchorage, turnover and transport are thus essential for the survival of the cell; in particular the post-mitotic cells like neurons. Therefore, it is reasonable to think that a perturbation in any of these parameters could underlie neurodegeneration (Court and Coleman, 2012; De Vos et al., 2008; Ittner et al., 2008; Roy et al., 2005; Schon and Przedborski, 2011). Two parameters were examined in our system: mitochondrial distribution and transport. The mitochondrial distribution was examined in the DA9 tail neuron, the cell body of which is located on the ventral side of the body near vulva and extends a dendrite that runs anteroventrally and an axon vertically up towards the dorsal cord which further runs anteriop dorsally after making a turn. The distal part of the axon depicts a specific synaptic pattern made *en passant*. Since synapses are the highly active components of a neuron that has high energy demands, mitochondria accumulate and colocalize with these regions (Klassen et al., 2010). The pro-aggregation animals have proportionally less fluorescent puncta corresponding to tagged mitochondria in the distal axonal segment of the DA9 tail neuron (**Fig 3.18**). The puncta seemed to have accumulated near the cell body. These results point towards three possibilities which are: first, there is a disruption in the normal mitochondrial transport to the most distal synapses; secondly, synapses themselves are lost, thereby no mitochondria could be found and thirdly, the expression of aggregation prone Tau species in the neurons led to the retraction of axons. In order to differentiate between these possibilities, mitochondrial transport by time lapse imaging was examined. The results show that indeed the axonal transport of mitochondria is impaired in the pro-aggregant

animals expressing the highly amyloidogenic Tau species (**Fig 3.19**). Although, the pro- and the anti-aggregant animals do not differ much in the instantaneous particle velocity, however, the particles make frequent pauses in the pro-aggregant animals. Mitochondrial particles make short bursts of displacements followed by pauses, appearing as if they are trying to squeeze in through a mesh but are experiencing strong resistance. This shows that there is a traffic jam in the neuronal processes and the supply of cargo material and energy to the growth cones is disrupted. With the result that the high energy demands of the growth cones are not met, making the cell processes vulnerable. It would be interesting to examine if the Tau aggregation inhibitor compounds are able to counteract these phenotypic characteristics.

Furthermore, we also observed that the pro-aggregant animals propagated slowly compared to the other animals. *C. elegans* has a short life cycle and is able to grow in liquid cultures with *E. coli* as food source. Each animal is capable of producing hundreds of progenies in a few days. As a matter of fact, if the *E. coli* food source is limited, the animals will rapidly consume the *E. coli* which will result in a decrease in the OD of wells. This decrease in OD was used as readout for survival or fecundity of our Tau-transgenic *C. elegans*. Pro-aggregant animals significantly differed in finishing the limited *E. coli* food source until the 2nd day of incubation; however, this difference became insignificant after the 2nd day (**Fig 3.5**). It has been shown that certain compounds that decrease *C. elegans* growth, survival or fecundity produce a dose dependent delay in food clearance (Voisine et al., 2007). One explanation for the lack of difference after the 2nd day of incubation would be that, the decrease in optical density (OD) associated with the consumption of *E. coli* after the 2nd day of incubation is compensated by the fecal matter egested overtime by an increasing population or by some sort of bacterial growth.

4.2 Pro-aggregation strain shows appearance of higher oligomeric Tau species along with accelerated aggregation at an early age

The reason behind these phenotypic changes in *C. elegans* upon expression of aggregation prone Tau species will be described in this section. Tau is a highly

soluble protein under physiological conditions (Wille et al., 1992), yet aggregates in various neurodegenerative diseases. The accumulation of detergent insoluble Tau aggregates in the pro-aggregant animals were observed very early starting at the first day of adulthood (roughly 60 hrs. post-hatching) (**Fig 3.8**), which coincided with the appearance of other phenotypic defects like severe uncoordinated motion, morphological changes in the neurons, synaptic dysfunction, and impaired mitochondrial transport. The presence of aggregates only in the pro-aggregation strain at the first day of adulthood could not be due to an overall higher tau expression levels in this strain compared to the others, since both pro- and anti-aggregant animals show the same level of Tau expression. Even if the FL V337M strain and the anti-aggregant strain are compared, the total Tau levels in the anti-aggregant strain is definitely higher because the anti-aggregant strain co-expresses two Tau species (full-length V337M Tau and F3ΔK280PP) while the FL V337M expresses only the full-length V337M Tau, yet the two strains do not differ in their phenotype. This means it is the higher β -propensity of the Tau species in pro-aggregation strain rather than the overall protein levels that induce protein aggregation and the accompanied toxicity. From these results we can infer that the highly amyloidogenic Tau species are toxic which is in accordance with the recent reports of mouse models as well (Sydow et al., 2011).

The role of aggregation in the pathogenesis of the disease is still under debate, while some believe it to be protective as it may take away the more toxic oligomeric species; others contradict this view (Ballatore et al., 2007; Brunden et al., 2008; Caughey and Lansbury, 2003; Congdon and Duff, 2008; Morris et al., 2011; Obulesu et al., 2011; Oddo et al., 2006; Sahara et al., 2008; Santacruz et al., 2005; Spires-Jones et al., 2011). We believe that aggregates can be tolerated by a cell unto a certain threshold level. However, once this threshold level is crossed, it can no longer be protective. The cell cannot simply afford to disown the big garbage lying somewhere in it, so it has to find some measures to get rid of this garbage. This can be done by allocating molecular chaperones to the aggregation site in order to dissolve them or target them for degradation. Besides this, an accelerated aggregation as seen in the pro-aggregation animals can have many more consequences for a cell. It can sequester some of the important endogenous proteins in the cell as has been

suggested by the previous studies (Olzscha et al., 2011) leading to a breakdown of protein homeostasis and an overall cellular dysfunction. The newly synthesized polypeptide chains may not find enough molecular chaperones to assist them for proper folding and this may trigger a new chain of misfolding in the cell leading to a severe proteostasis breakdown.

On the other hand, we believe that there is an equilibrium existing between monomers, oligomers and higher Tau aggregates. The presence of a highly amyloidogenic Tau species like F3ΔK280 in pro-aggregant animals, enhances the rate at which this equilibrium is reached which further means that all sorts of intermediate Tau species including highly toxic oligomeric species start accumulating and are free to exert their toxic effects by influencing a number of molecular pathways in the cell. Indeed, the pro-aggregant strain showed the accumulation of higher oligomers of roughly 220 KDa (**Fig 3.16**) which could not be fully solubilized by high salt buffer and remained in the worm debris. However, these higher oligomers could be solubilized by using SDS which means that they represent some high molecular weight Tau oligomers capable of interacting with the membrane proteins.

4.3 Pro-aggregation Tau species reduce the lifespan in *C. elegans*

The accumulation of damaged protein aggregates can perturb the cell's capacity for proteostasis and provoke aging. Increased protein aggregation can lead to the sequestration of many important proteins including some heat-shock factors, which might ultimately result in cellular dysfunction (Olzscha et al., 2011). More and more molecular chaperones become engaged with these aggregates in an effort to dissolve them or direct them for degradation. This may result in a chaperone crisis in the cell. With less molecular chaperones available to attend to their newly synthesized polypeptide clients, a malicious cycle of further protein misfolding and aggregation may get triggered (Balch et al., 2008; Bence et al., 2001; David et al., 2010; Gidalevitz et al., 2006). In our case, pro-aggregant animals accumulate Tau aggregates early starting at the first day of adulthood. This would mean a severe homeostatic disturbance in the cell which might lead to their premature death. The appearance of Tau aggregates in the other Tau-transgenic lines (FL V337M line and anti-aggregant

line) at a later stage might offer a possible explanation for their relatively shorter life-span compared to the wild-type N2 strain which was only moderately affected (**Fig 3.6**). Similar findings have been reported in a *Drosophila* tauopathy model whereby Tau expression led to a decrease in their life-span (Wittmann et al., 2001).

It would be interesting to see if the Tau aggregates are maintained soluble by reducing the *daf-2*/insulin/IGF-1 signaling, which triggers the expression of many cell-protective proteins and pathways (Henis-Korenblit et al., 2010; Lee et al., 2003; Melendez et al., 2003; Murphy et al., 2003) that protect from proteostasis breakdown. A decrease in insulin-signaling was recently shown to also prevent the structural damage to the neurons in *C. elegans* which may explain their longer life-span (Toth et al., 2012). Of equal interest would be to examine if the phenotype of the anti-aggregant strain gets worse when crossed in a *daf-16* deficient background with increased insulin-signaling and a shorter life-span or in *hsf-1* deficient background with lower expression of cell-protective proteins (Hsu et al., 2003).

4.4 Full-length V337M Tau but not the seeding F3ΔK280 fragment is highly phosphorylated in the pro-aggregation strain

Phosphorylation of Tau and its implications in AD and other Tauopathies is a highly controversial subject. There are contradictory reports from different studies employing different model systems that have emerged in recent years. As an example, a Tau-transgenic *Drosophila* model showed a high correlation between the severity of neurodegeneration and Tau phosphorylation with age (Wittmann et al., 2001). Furthermore, overexpression of *shaggy*, the fly homolog of glycogen synthase kinase-3 β (GSK-3 β) and a potent kinase for Tau phosphorylation, exacerbated the neurodegeneration. This was associated with an increase in Tau phosphorylation and appearance of filamentous Tau aggregates (Jackson et al., 2002). Overexpression of GSK-3 β also deteriorated the Tau-induced neurodegeneration in a *C. elegans* tauopathy model (Miyasaka et al., 2005). In contradiction to this, overexpression of GSK-3 β improved the motor neuron defects and axonopathy in a Tau-transgenic

mouse model, in spite of the fact that GSK-3 β increases Tau phosphorylation (Brownlee et al., 1997; Lucas et al., 2001; Spittaels et al., 2000).

We examined the phosphorylation status of Tau in our Tau-transgenic worms at two stages: 1 day-old adult stage (**Fig 3.8**) and 7 day old adult stage (**Fig 3.14**). In 1-day old adults, there was no major difference in the phosphorylation of soluble Tau in the FL V337M Tau line, pro-aggregant and anti-aggregant line. Since the FL V337M Tau line and the anti-aggregant line did not accumulate detergent soluble and detergent insoluble Tau at this stage, there was no way that we could see phosphorylation in the fractions of these two lines. However, the pro-aggregant line showed phosphorylation of Tau in all the three fractions (RAB, RIPA and FA) at the KXGS motif (12E8 epitope) and the S396 and S404 sites (PHF-1 epitope). Interesting to note is that only full-length V337M Tau was phosphorylated not the F3 Δ K280 fragment as recognized by the 12E8 antibody. Furthermore, biochemical analysis of the phosphorylation status of Tau in 7 day-old adults showed that Tau is phosphorylated in the other lines as well, although not to the extent as it is in the pro-aggregant line. Again it was only the full-length V337M Tau that was phosphorylated at the KXGS motif as was the case in 1 day-old adult pro-aggregation line. Interestingly, a faint signal was recognized by 12E8 antibody (shown in **Fig 3.15** by green asterisk) corresponding to F3 Δ K280PP fragment in the soluble RAB fraction of anti-aggregant line. It is important to note that the aggregation of highly amyloidogenic F3 Δ K280 fragment, which is expressed in our pro-aggregant line, was shown to have no correlation with the degree of phosphorylation at KXGS motifs (Khlistunova et al., 2006) and at the same time phosphorylation at KXGS motifs inhibits the processing of repeat domain K18 Δ K280 and thereby slows down the aggregation of Tau (unpublished data from our lab). From these results, we can infer two things: first, the seed formation by a highly amyloidogenic Tau fragment like F3 Δ K280 may mask this phosphorylation site, however, the same site is free to be phosphorylated in anti-aggregant Tau fragment like F3 Δ K280PP. Second, an amyloidogenic fragment F3 Δ K280 is highly toxic to the neurons even though it is not phosphorylated while a non-amyloidogenic fragment F3 Δ K280PP which becomes phosphorylated but is unable to aggregate can be tolerated by the neurons. To put it in simple terms, phosphorylation in the flanking

regions of full-length Tau may not be a primary event in the pathogenesis of tauopathy. However, the fact that we observed some higher soluble (**Fig 3.14_AT8 panel**) and insoluble oligomers (**Fig 3.14_PHF-1 panel**) only in the pro-aggregant animals, do not exclude the possibility that phosphorylation plays a role in Tau-induced toxicity. Whether phosphorylation follows aggregation or vice versa remains an enigmatic question. It is known that both, too much as well as too little phosphorylation could be detrimental (Mandelkow and Mandelkow, 2012). In the former case, more tau can get detached from the microtubules and is available to aggregate. In the latter case, more Tau is going to bind to microtubules thereby, setting up a competition to other microtubule binding proteins. What we can say is that there is a right balance between the function of kinases and phosphatases in a cell, which regulate the phosphorylation of Tau and any disturbance in this balance, might be toxic for the cell.

4.5 Inhibitor compounds of Tau aggregation protect against Tau-induced toxicity

The ultimate aim of studying the mechanism of Tau-induced toxicity in lower organisms is to eventually use them for drug testing. If a drug shows positive results, it could be followed up in higher animals and eventually promoted for clinical trials. *C. elegans* offers many advantages when it comes to drug testing. The drugs can be tested in liquid cultures which enhance the drug delivery into the worm through all the three entry routes described (Choy et al., 2006; Perkins et al., 1986; Smith and Campbell, 1996). The fact that the drugs are tested in the context of the whole organism, any off-target effects due to their interaction with a wide range of proteins in the cell can be nullified. Furthermore, drugs which pass the initial *in vitro* tests may not be active *in vivo* because they may not enter the cells, may get selectively transported out, or may be rapidly metabolized when tested in whole organisms (Mazanetz and Fischer, 2007). This emphasizes the need to have a disease model which can allow a rapid, high throughput *in vivo* drug testing which may not be offered by the higher animal models like transgenic mice.

In this study, thrashe assay, an undulatory movement shown by the worms when placed in a drop of liquid, was used as readout to screen compounds some of which have been proven to be effective against Tau aggregation. Methylene blue (MB) and two other compounds bb14, BSc3094 belonging to the Rhodanine and phenylthiazolyl-hydrazide class of compounds respectively were tested initially. The compounds can partially ameliorate the uncoordinated phenotype of pro-aggregation animals by reducing the Tau aggregates. The compound treatment led to the disappearance of the seed forming repeat fragment F3ΔK280 from the detergent insoluble Tau aggregates, which means that the extent of Tau aggregation is dramatically reduced by compound treatment (**Fig 3.22**). Important to mention is that in order for compounds to be essentially effective they need to be administered from the early larval stages, so as to inhibit even the initial formation of toxic oligomeric Tau species. MB, bb14 and BSc3094 have recently been demonstrated to have protective effects in various cell and animals models (Bulic et al., 2007; Bulic et al., 2010; Hattori et al., 2008; Medina and Wandosell, 2011; Pickhardt et al., 2007; Schirmer et al., 2011; Wischik et al., 1996). Using the results from MB, bb14 and BSc3094 treatment as proof of principle, we tested another compound on our *C. elegans* tauopathy model namely; compound 16 (cmp16). Cmp16 belongs to the ATPZ class of compounds and the treatment with this compound showed protection against Tau aggregation-induced toxicity. This ATPZ Tau inhibitor has been shown to block Tau aggregation in vitro (Ballatore et al., 2010). Cmp16 also has a potential to cross the blood brain barrier making it a good candidate to be promoted for studies in higher animal models. It is possible that the bacteria in the culture, which serve as food for worms, could metabolize the compounds and alter their chemical structure. However, the use of dead bacteria as food source together with the fact that a significant improvement in the Tau aggregation-induced phenotype after treatment was observed, rules out any such possibility.

4.6 Trehalose induces autophagy and relieves the worms from Tau-aggregation induced toxicity

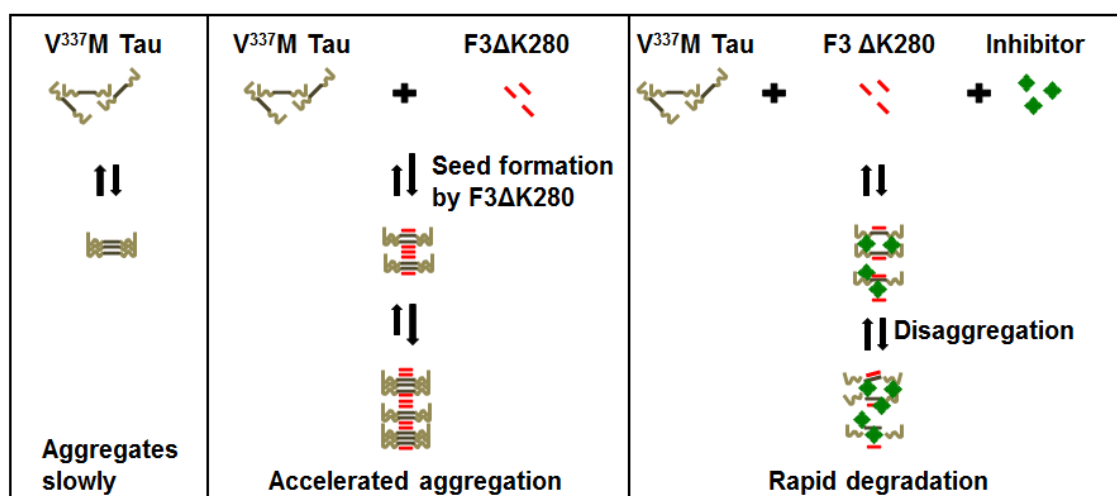
Aggregation of Tau, an otherwise highly soluble protein under physiological conditions, is a characteristic feature of several neurodegenerative diseases including AD. Autophagy plays a cardinal role in the cellular protein quality control and this is particularly important in post-mitotic cells like neurons, where the cell cannot reduce the total damaged protein and organelle load by redistribution to daughter cells. Besides homeostasis, autophagy also plays an important role in the remodeling of neuronal structures required to support neuronal plasticity (Wong and Cuervo, 2010). Keeping these things in mind and besides the fact that our tauopathy *C. elegans* model expresses Tau transgenes in the nervous system, any efforts to restore autophagy levels may prove to be protective. Here we show that, trehalose treatment can mitigate Tau aggregation- induced toxic effects through autophagy mediated reduction of Tau aggregate burden in our *C. elegans* model of tauopathy. Treatment of pro-aggregation worms with trehalose from the early embryonic stages ameliorates the Tau-induced uncoordinated phenotype (**Fig 3.24**). Studies have pointed out a role for autophagy in the clearance of protein aggregates for a number of proteins, including β -amyloid, α -synuclein, ataxin-3, prion protein and huntingtin (Casarejos et al., 2011; Heiseke et al., 2009; Majumdar et al., 2011; Pickford et al., 2008; Riedel et al., 2010; Sarkar et al., 2007b; Spilman et al., 2010; Webb et al., 2003). As far as the degradation pathway of Tau is concerned, it has been studied in systems based on Tau overexpression and the results are controversial. While some advocate for the proteasomal pathway (Carrettiero et al., 2009; Dickey et al., 2008; Shimura et al., 2004; Zhang et al., 2005), others argue that autophagy plays a major role (Berger et al., 2006; Hamano et al., 2008; Wang et al., 2009). However, a recent study focused on the endogenous Tau in primary neurons and found that the induction of autophagy can reduce endogenous Tau levels (Kruger et al., 2011). In this study, we show that trehalose can induce autophagy in *C. elegans*, as seen by an increased level of LGG-2 (MAP1LC3 ortholog in *C. elegans*) in autophagy flux experiment (**Fig 3.25**), and reduce the level of detergent insoluble Tau aggregates (**Fig 3.24**). This observation is in agreement with the previous reports, namely that trehalose induces

autophagy through an mTOR-independent pathway in cancer cell lines (Sarkar et al., 2007a). Furthermore, an FDA approved drug that increases autophagy in a TOR-dependent manner has also been shown to be protective against Tau pathology in fly and mouse models as well (Berger et al., 2006; Caccamo et al., 2010).

Additionally, trehalose was shown to be protective by inducing autophagy-mediated degradation of Tau aggregates in a tet-on N2a cell model of Tau aggregation. The same study reported that trehalose can inhibit protein aggregation *in vitro* as well (Kruger et al., 2011). Besides inducing autophagy, trehalose is known to act as a chaperone and stabilize the proteins in their native confirmation *in vitro* protecting them from aggregation (Hammarstrom et al., 2003; Singer and Lindquist, 1998). Therefore, by inducing autophagy and inhibiting aggregation at the same time, trehalose may offer a dual protection and being a disaccharide that can easily pass the blood brain barrier along with the fact that an increased autophagy may be protective against various protein misfolding diseases including AD, makes trehalose a promising candidate for treating these diseases.

An interesting future perspective would be to examine if the neuronal defects seen in our Tau-transgenic model can be improved by inducing autophagy (for example by trehalose) or by epigenetical studies using a *C. elegans* mutant with an over-activated pathway for lysosomal biogenesis (Settembre et al., 2011).

We finally arrive at the model shown below:



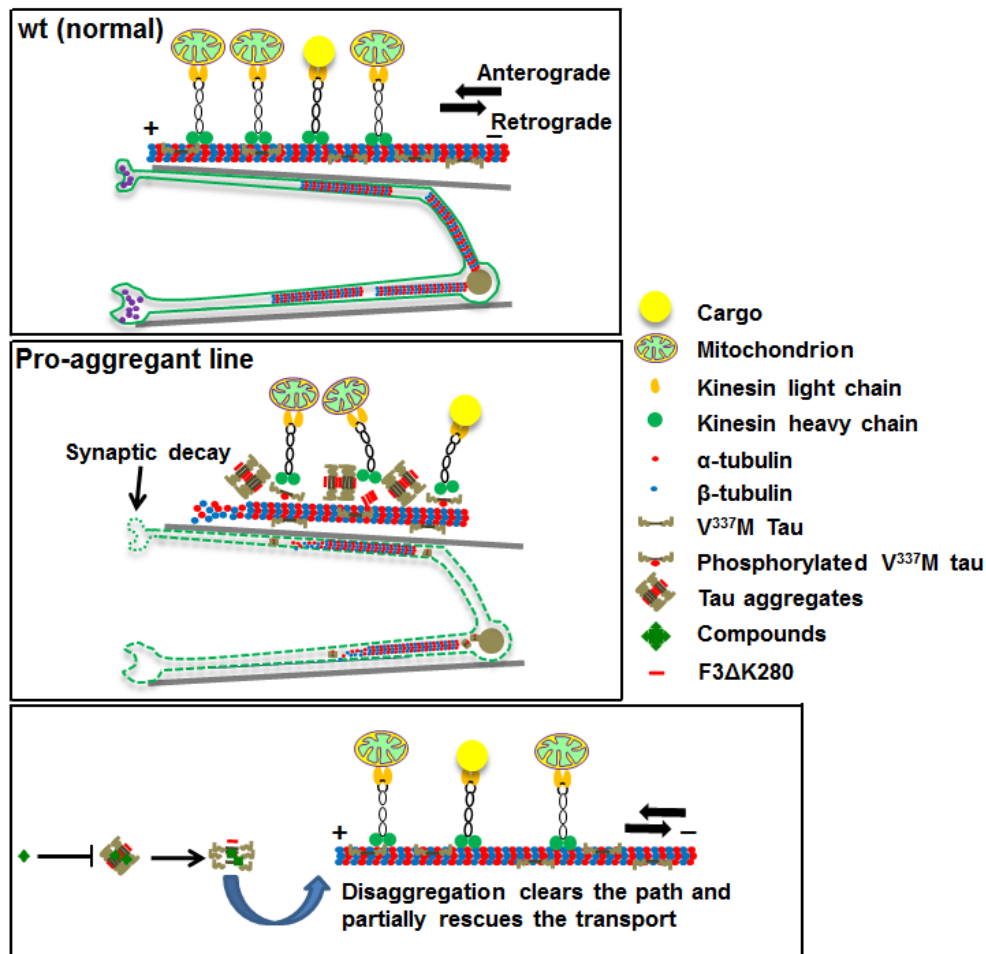


Figure 4.1: Tau is a highly soluble protein under physiological conditions; however, under pathological conditions it can aggregate and form PHFs. We propose that the aggregation is a multi-step process which proceeds through nucleation step with nuclei acting as foundation stones and that there is an equilibrium existing between the soluble and the insoluble tau. The nucleation step seems to be the rate limiting step. Under physiological conditions, a high activation energy is required to cross this barrier, thereby, shifting the equilibrium towards the elongation process. In the *in vitro* experiments, this activation energy can be brought down by the addition of polymerizing agents like heparin. While the aggregation of full-length tau in a cell can be accelerated by the proteolysis of the full-length tau which results in the release of highly aggregating species like the repeat domain (K18) and its proteolytic fragments (F2 and F3) with a high nucleation property. Once the foundation stone is laid, the nuclei can elongate very fast by adding to them the free tau molecules in the cell and at the same time may also sequester other proteins in the cell. We propose in our model that the presence of F3Δk280 brings down the activation energy needed for the full-length tau (V337M) to cross the nucleation barrier. This leads to the acceleration of the aggregation of full-length tau and a high abundance of toxic species (right panel). In a normal wild type worm, the neuronal transport including that of synaptic vesicles, mitochondria and other important factors required for a normal synaptic transmission is maintained by a balanced activity and turn over of the microtubules and the associated MAP proteins (left upper panel). The presence of aggregates, however, hinders this normal transport either by themselves or by the sequestration of the endogenous MAP proteins and other factors required for the microtubule stabilization and turnover. The sequestration may also provoke the cell to increase the expression of the endogenous MAPs which will increase the amount of MAP protein bound to microtubules, leaving no binding sites for the motor proteins that carry out transport (left middle panel). This impairment in transport will lead to the starvation and blockage of the synaptic transmission at the synapses which will ultimately lead to the neuronal death. Antiaggregation-compounds restore the normal transport partially either by decelerating the aggregation process or by breaking down the aggregates to easily degradable species (left bottom panel).

5 Summary

Proteins under certain conditions polymerize to form soluble oligomers, which eventually lead to insoluble fibrillar or amorphous aggregates. This may lead to an obstruction of the cell and a reduced availability of the protein for normal functions. Tau is one example; under normal conditions, Tau is a highly soluble protein that binds and stabilizes axonal microtubules (Binder et al., 1985). However, Tau gets modified posttranslationally and forms highly ordered fibrillar aggregates which accumulate as neurofibrillary tangles in AD and other neurodegenerative tauopathies (Mandelkow and Mandelkow, 2012). In this study we have generated transgenic *C. elegans* lines in which full-length V337M Tau is co-expressed with different fragments of the Tau repeat domain in the nervous system. The repeat fragments differ by two point mutations in the hexapeptide motifs, which determine whether they can adopt a beta structure conformation and hence aggregate or not. The “pro-aggregant” *C. elegans* line co-expresses full-length V337M Tau along with the aggregation prone repeat fragment F3ΔK280. By contrast, the anti-aggregant line co-expresses full-length V337M Tau along with the repeat fragment F3ΔK280PP, which cannot aggregate due to the presence of two beta-sheet breaking prolines. The project was aimed at a better understanding of the role of Tau aggregation on cell toxicity and dysfunction in the context of a whole organism. An additional aim was to explore the potential for drug screening against Tau aggregation in a cost effective manner. The results are summarized as follows:

- (i) The pro-aggregant animals show a severe uncoordinated phenotype (paralysis) starting at the first day of adulthood which is due to a defective pre-synaptic transmission. The nervous system of the pro-aggregant animals shows abnormalities in the form of neuronal gaps and defective axonal mitochondrial transport. By contrast, the control anti-aggregant animals show a rather mild phenotype.
- (ii) The pro-aggregant animals accumulate detergent soluble and detergent insoluble Tau aggregates starting at the first day of adulthood (roughly 60 hrs. after hatching) while anti-aggregant animals do not. The presence of Tau aggregates in pro-aggregant animals at such an early age allows one to attribute this phenotype to

the presence of Tau protein and to distinguish it from age-related breakdown of proteostasis. Besides this, soluble and insoluble oligomeric Tau species of roughly 220 kDa appear in the pro-aggregant animals as shown by biochemical analysis. As a result, the pro-aggregant animals suffer from stress due to misfolded protein accumulation. This is the likely cause for decreased microtubule stabilization, defective axonal transport, and ultimately neuronal dysfunction.

(iii) Tau is extensively phosphorylated in the pro-aggregant animals at most of the sites found in the AD brain. Higher order soluble oligomeric Tau species (high salt soluble RAB fraction) of roughly 220 kDa were detected by AT8 antibody (pSer202 and pThr205 epitope) only in the pro-aggregant animals. These intermediate oligomers are thought to be the most toxic species. The pro-aggregant animals also developed detergent insoluble Tau oligomeric species of roughly 100 kDa detected by PHF-1 antibody (pSer396 and pSer404 epitope). The results show that human Tau can undergo post-translational modification in *C. elegans* to a disease state.

(iv) The severe uncoordinated phenotype in this animal model allowed us to test compounds against Tau aggregation. Several compounds can ameliorate the phenotype by reducing the Tau aggregates. This illustrates the usefulness of the *C. elegans* model as a fast and cost-effective tool for assessing potential drugs for Tau pathology.

6 Bibliography

Alberti, A., Michelet, X., Djeddi, A., and Legouis, R. (2010). The autophagosomal protein LGG-2 acts synergistically with LGG-1 in dauer formation and longevity in *C. elegans*. *Autophagy* 6.

Alonso, A.C., Grundke-Iqbal, I., and Iqbal, K. (1996). Alzheimer's disease hyperphosphorylated tau sequesters normal tau into tangles of filaments and disassembles microtubules. *Nat Med* 2, 783-787.

Alonso, A.C., Zaidi, T., Grundke-Iqbal, I., and Iqbal, K. (1994). Role of abnormally phosphorylated tau in the breakdown of microtubules in Alzheimer disease. *Proc Natl Acad Sci U S A* 91, 5562-5566.

Alzheimer, A., Stelzmann, R.A., Schnitzlein, H.N., and Murtagh, F.R. (1995). An English translation of Alzheimer's 1907 paper, "Über eine eigenartige Erkrankung der Hirnrinde". *Clin Anat* 8, 429-431.

Andreadis, A., Brown, W.M., and Kosik, K.S. (1992). Structure and novel exons of the human tau gene. *Biochemistry* 31, 10626-10633.

Aronov, S., Aranda, G., Behar, L., and Ginzburg, I. (2002). Visualization of translated tau protein in the axons of neuronal P19 cells and characterization of tau RNP granules. *J Cell Sci* 115, 3817-3827.

Arora, A., Ha, C., and Park, C.B. (2004). Inhibition of insulin amyloid formation by small stress molecules. *FEBS Lett* 564, 121-125.

Arrasate, M., Perez, M., Armas-Portela, R., and Avila, J. (1999). Polymerization of tau peptides into fibrillar structures. The effect of FTDP-17 mutations. *FEBS Lett* 446, 199-202.

Askanas, V., and Engel, W.K. (2008). Inclusion-body myositis: muscle-fiber molecular pathology and possible pathogenic significance of its similarity to Alzheimer's and Parkinson's disease brains. *Acta Neuropathol* 116, 583-595.

Augustinack, J.C., Schneider, A., Mandelkow, E.M., and Hyman, B.T. (2002). Specific tau phosphorylation sites correlate with severity of neuronal cytopathology in Alzheimer's disease. *Acta Neuropathol* 103, 26-35.

Balch, W.E., Morimoto, R.I., Dillin, A., and Kelly, J.W. (2008). Adapting proteostasis for disease intervention. *Science* 319, 916-919.

- Ballatore, C., Brunden, K.R., Piscitelli, F., James, M.J., Crowe, A., Yao, Y., Hyde, E., Trojanowski, J.Q., Lee, V.M., and Smith, A.B., 3rd (2010). Discovery of brain-penetrant, orally bioavailable aminothienopyridazine inhibitors of tau aggregation. *J Med Chem* 53, 3739-3747.
- Ballatore, C., Hyde, E., Deiches, R.F., Lee, V.M., Trojanowski, J.Q., Huryn, D., and Smith, A.B., 3rd (2007). Paclitaxel C-10 carbamates: potential candidates for the treatment of neurodegenerative tauopathies. *Bioorg Med Chem Lett* 17, 3642-3646.
- Bancher, C., Grundke-Iqbal, I., Iqbal, K., Fried, V.A., Smith, H.T., and Wisniewski, H.M. (1991). Abnormal phosphorylation of tau precedes ubiquitination in neurofibrillary pathology of Alzheimer disease. *Brain Res* 539, 11-18.
- Barghorn, S., Zheng-Fischhofer, Q., Ackmann, M., Biernat, J., von Bergen, M., Mandelkow, E.M., and Mandelkow, E. (2000). Structure, microtubule interactions, and paired helical filament aggregation by tau mutants of frontotemporal dementias. *Biochemistry* 39, 11714-11721.
- Baron, U., Freundlieb, S., Gossen, M., and Bujard, H. (1995). Co-regulation of two gene activities by tetracycline via a bidirectional promoter. *Nucleic Acids Res* 23, 3605-3606.
- Baumann, K., Mandelkow, E.M., Biernat, J., Piwnica-Worms, H., and Mandelkow, E. (1993). Abnormal Alzheimer-like phosphorylation of tau-protein by cyclin-dependent kinases cdk2 and cdk5. *FEBS Lett* 336, 417-424.
- Ben-Zvi, A., Miller, E.A., and Morimoto, R.I. (2009). Collapse of proteostasis represents an early molecular event in *Caenorhabditis elegans* aging. *Proc Natl Acad Sci U S A* 106, 14914-14919.
- Benaroudj, N., Tarcsa, E., Cascio, P., and Goldberg, A.L. (2001). The unfolding of substrates and ubiquitin-independent protein degradation by proteasomes. *Biochimie* 83, 311-318.
- Bence, N.F., Sampat, R.M., and Kopito, R.R. (2001). Impairment of the ubiquitin-proteasome system by protein aggregation. *Science* 292, 1552-1555.
- Berger, Z., Ravikumar, B., Menzies, F.M., Oroz, L.G., Underwood, B.R., Pangalos, M.N., Schmitt, I., Wullner, U., Evert, B.O., O'Kane, C.J., *et al.* (2006). Rapamycin alleviates toxicity of different aggregate-prone proteins. *Hum Mol Genet* 15, 433-442.
- Biernat, J., Gustke, N., Drewes, G., Mandelkow, E.M., and Mandelkow, E. (1993).

Phosphorylation of Ser262 strongly reduces binding of tau to microtubules: distinction between PHF-like immunoreactivity and microtubule binding. *Neuron* 11, 153-163.

Biernat, J., Mandelkow, E.M., Schroter, C., Lichtenberg-Kraag, B., Steiner, B., Berling, B., Meyer, H., Mercken, M., Vandermeeren, A., Goedert, M., *et al.* (1992). The switch of tau protein to an Alzheimer-like state includes the phosphorylation of two serine-proline motifs upstream of the microtubule binding region. *EMBO J* 11, 1593-1597.

Binder, L.I., Frankfurter, A., and Rebhun, L.I. (1985). The distribution of tau in the mammalian central nervous system. *J Cell Biol* 101, 1371-1378.

Blair, J.E., Ikeo, K., Gojobori, T., and Hedges, S.B. (2002). The evolutionary position of nematodes. *BMC Evol Biol* 2, 7.

Braak, H., and Braak, E. (1991). Neuropathological staging of Alzheimer-related changes. *Acta Neuropathol* 82, 239-259.

Braak, H., and Braak, E. (1994). Morphological criteria for the recognition of Alzheimer's disease and the distribution pattern of cortical changes related to this disorder. *Neurobiology of aging* 15, 355-356; discussion 379-380.

Bramblett, G.T., Goedert, M., Jakes, R., Merrick, S.E., Trojanowski, J.Q., and Lee, V.M. (1993). Abnormal tau phosphorylation at Ser396 in Alzheimer's disease recapitulates development and contributes to reduced microtubule binding. *Neuron* 10, 1089-1099.

Brandt, R., Gergou, A., Wacker, I., Fath, T., and Hutter, H. (2009). A *Caenorhabditis elegans* model of tau hyperphosphorylation: induction of developmental defects by transgenic overexpression of Alzheimer's disease-like modified tau. *Neurobiology of aging* 30, 22-33.

Brandt, R., Hundelt, M., and Shahani, N. (2005). Tau alteration and neuronal degeneration in tauopathies: mechanisms and models. *Biochim Biophys Acta* 1739, 331-354.

Brandt, R., Lee, G., Teplow, D.B., Shalloway, D., and Abdel-Ghany, M. (1994). Differential effect of phosphorylation and substrate modulation on tau's ability to promote microtubule growth and nucleation. *J Biol Chem* 269, 11776-11782.

Brenner, S. (1973). The genetics of behaviour. *Br Med Bull* 29, 269-271.

Brenner, S. (1974). The genetics of *Caenorhabditis elegans*. *Genetics* 77, 71-94.

- Brion, J.P., Couck, A.M., Passareiro, E., and Flament-Durand, J. (1985). Neurofibrillary tangles of Alzheimer's disease: an immunohistochemical study. *J Submicrosc Cytol* 17, 89-96.
- Brown, M.R., Bondada, V., Keller, J.N., Thorpe, J., and Geddes, J.W. (2005). Proteasome or calpain inhibition does not alter cellular tau levels in neuroblastoma cells or primary neurons. *J Alzheimers Dis* 7, 15-24.
- Brownlees, J., Irving, N.G., Brion, J.P., Gibb, B.J., Wagner, U., Woodgett, J., and Miller, C.C. (1997). Tau phosphorylation in transgenic mice expressing glycogen synthase kinase-3beta transgenes. *Neuroreport* 8, 3251-3255.
- Brunden, K.R., Trojanowski, J.Q., and Lee, V.M. (2008). Evidence that non-fibrillar tau causes pathology linked to neurodegeneration and behavioral impairments. *J Alzheimers Dis* 14, 393-399.
- Buee, M., Rossignol, M., Jauneau, A., Ranjeva, R., and Becard, G. (2000). The pre-symbiotic growth of arbuscular mycorrhizal fungi is induced by a branching factor partially purified from plant root exudates. *Mol Plant Microbe Interact* 13, 693-698.
- Bulic, B., Pickhardt, M., Khlistunova, I., Biernat, J., Mandelkow, E.M., Mandelkow, E., and Waldmann, H. (2007). Rhodanine-based tau aggregation inhibitors in cell models of tauopathy. *Angew Chem Int Ed Engl* 46, 9215-9219.
- Bulic, B., Pickhardt, M., Mandelkow, E.M., and Mandelkow, E. (2010). Tau protein and tau aggregation inhibitors. *Neuropharmacology* 59, 276-289.
- Bulic, B., Pickhardt, M., Schmidt, B., Mandelkow, E.M., Waldmann, H., and Mandelkow, E. (2009). Development of tau aggregation inhibitors for Alzheimer's disease. *Angew Chem Int Ed Engl* 48, 1740-1752.
- Butner, K.A., and Kirschner, M.W. (1991). Tau protein binds to microtubules through a flexible array of distributed weak sites. *J Cell Biol* 115, 717-730.
- Byerly, L., Cassada, R.C., and Russell, R.L. (1976a). The life cycle of the nematode *Caenorhabditis elegans*. I. Wild-type growth and reproduction. *Dev Biol* 51, 23-33.
- Byerly, L., Scherer, S., and Russell, R.L. (1976b). The life cycle of the nematode *Caenorhabditis elegans*. II. A simplified method for mutant characterization. *Dev Biol* 51, 34-48.
- Caccamo, A., Majumder, S., Richardson, A., Strong, R., and Oddo, S. (2010). Molecular interplay between mammalian target of rapamycin (mTOR), amyloid-beta, and Tau: effects on cognitive impairments. *J Biol Chem* 285, 13107-13120.

- Caceres, A., and Kosik, K.S. (1990). Inhibition of neurite polarity by tau antisense oligonucleotides in primary cerebellar neurons. *Nature* 343, 461-463.
- Caceres, A., Potrebic, S., and Kosik, K.S. (1991). The effect of tau antisense oligonucleotides on neurite formation of cultured cerebellar macroneurons. *J Neurosci* 11, 1515-1523.
- Cai, X.D., Golde, T.E., and Younkin, S.G. (1993). Release of excess amyloid beta protein from a mutant amyloid beta protein precursor. *Science* 259, 514-516.
- Cambiazio, V., Gonzalez, M., and Maccioni, R.B. (1995). DMAP-85: a tau-like protein from *Drosophila melanogaster* larvae. *J Neurochem* 64, 1288-1297.
- Campion, D., Dumanchin, C., Hannequin, D., Dubois, B., Belliard, S., Puel, M., Thomas-Anterion, C., Michon, A., Martin, C., Charbonnier, F., *et al.* (1999). Early-onset autosomal dominant Alzheimer disease: prevalence, genetic heterogeneity, and mutation spectrum. *Am J Hum Genet* 65, 664-670.
- Canu, N., and Calissano, P. (2003). In vitro cultured neurons for molecular studies correlating apoptosis with events related to Alzheimer disease. *Cerebellum* 2, 270-278.
- Canu, N., Dus, L., Barbato, C., Ciotti, M.T., Brancolini, C., Rinaldi, A.M., Novak, M., Cattaneo, A., Bradbury, A., and Calissano, P. (1998). Tau cleavage and dephosphorylation in cerebellar granule neurons undergoing apoptosis. *J Neurosci* 18, 7061-7074.
- Cardozo, C., and Michaud, C. (2002). Proteasome-mediated degradation of tau proteins occurs independently of the chymotrypsin-like activity by a nonprocessive pathway. *Arch Biochem Biophys* 408, 103-110.
- Carrettiero, D.C., Hernandez, I., Neveu, P., Papagiannakopoulos, T., and Kosik, K.S. (2009). The cochaperone BAG2 sweeps paired helical filament- insoluble tau from the microtubule. *J Neurosci* 29, 2151-2161.
- Casarejos, M.J., Solano, R.M., Gomez, A., Perucho, J., de Yebenes, J.G., and Mena, M.A. (2011). The accumulation of neurotoxic proteins, induced by proteasome inhibition, is reverted by trehalose, an enhancer of autophagy, in human neuroblastoma cells. *Neurochem Int* 58, 512-520.
- Cassada, R.C., and Russell, R.L. (1975). The dauerlarva, a post-embryonic developmental variant of the nematode *Caenorhabditis elegans*. *Dev Biol* 46, 326-342.

- Caughey, B., and Lansbury, P.T. (2003). Protofibrils, pores, fibrils, and neurodegeneration: separating the responsible protein aggregates from the innocent bystanders. *Annu Rev Neurosci* 26, 267-298.
- Chapin, S.J., and Bulinski, J.C. (1991). Non-neuronal 210 x 10(3) Mr microtubule-associated protein (MAP4) contains a domain homologous to the microtubule-binding domains of neuronal MAP2 and tau. *J Cell Sci* 98 (Pt 1), 27-36.
- Chartier-Harlin, M.C., Crawford, F., Houlden, H., Warren, A., Hughes, D., Fidani, L., Goate, A., Rossor, M., Roques, P., Hardy, J., *et al.* (1991). Early-onset Alzheimer's disease caused by mutations at codon 717 of the beta-amyloid precursor protein gene. *Nature* 353, 844-846.
- Chen, N., Harris, T.W., Antoshechkin, I., Bastiani, C., Bieri, T., Blasiar, D., Bradnam, K., Canaran, P., Chan, J., Chen, C.K., *et al.* (2005). WormBase: a comprehensive data resource for *Caenorhabditis* biology and genomics. *Nucleic Acids Res* 33, D383-389.
- Chiti, F., and Dobson, C.M. (2006). Protein misfolding, functional amyloid, and human disease. *Annu Rev Biochem* 75, 333-366.
- Choy, R.K., Kemner, J.M., and Thomas, J.H. (2006). Fluoxetine-resistance genes in *Caenorhabditis elegans* function in the intestine and may act in drug transport. *Genetics* 172, 885-892.
- Ciechanover, A. (2001). Linking ubiquitin, parkin and synphilin-1. *Nat Med* 7, 1108-1109.
- Citron, M., Oltersdorf, T., Haass, C., McConlogue, L., Hung, A.Y., Seubert, P., Vigo-Pelfrey, C., Lieberburg, I., and Selkoe, D.J. (1992). Mutation of the beta-amyloid precursor protein in familial Alzheimer's disease increases beta-protein production. *Nature* 360, 672-674.
- Clark, L.N., Poorkaj, P., Wszolek, Z., Geschwind, D.H., Nasreddine, Z.S., Miller, B., Li, D., Payami, H., Awert, F., Markopoulou, K., *et al.* (1998). Pathogenic implications of mutations in the tau gene in pallido-ponto-nigral degeneration and related neurodegenerative disorders linked to chromosome 17. *Proc Natl Acad Sci U S A* 95, 13103-13107.
- Claverie, J.M. (2001). Gene number. What if there are only 30,000 human genes? *Science* 291, 1255-1257.
- Cohen, F.E., and Kelly, J.W. (2003). Therapeutic approaches to protein-misfolding diseases. *Nature* 426, 905-909.

- Coleman, P.D., and Yao, P.J. (2003). Synaptic slaughter in Alzheimer's disease. *Neurobiology of aging* 24, 1023-1027.
- Congdon, E.E., and Duff, K.E. (2008). Is tau aggregation toxic or protective? *J Alzheimers Dis* 14, 453-457.
- Couchie, D., Mavilia, C., Georgieff, I.S., Liem, R.K., Shelanski, M.L., and Nunez, J. (1992). Primary structure of high molecular weight tau present in the peripheral nervous system. *Proc Natl Acad Sci U S A* 89, 4378-4381.
- Court, F.A., and Coleman, M.P. (2012). Mitochondria as a central sensor for axonal degenerative stimuli. *Trends Neurosci* 35, 364-372.
- Cuervo, A.M., and Dice, J.F. (2000). Age-related decline in chaperone-mediated autophagy. *J Biol Chem* 275, 31505-31513.
- D'Amelio, M., Cavallucci, V., Middei, S., Marchetti, C., Pacioni, S., Ferri, A., Diamantini, A., De Zio, D., Carrara, P., Battistini, L., *et al.* (2011). Caspase-3 triggers early synaptic dysfunction in a mouse model of Alzheimer's disease. *Nat Neurosci* 14, 69-76.
- D'Souza, I., Poorkaj, P., Hong, M., Nochlin, D., Lee, V.M., Bird, T.D., and Schellenberg, G.D. (1999). Missense and silent tau gene mutations cause frontotemporal dementia with parkinsonism-chromosome 17 type, by affecting multiple alternative RNA splicing regulatory elements. *Proc Natl Acad Sci U S A* 96, 5598-5603.
- David, D.C., Layfield, R., Serpell, L., Narain, Y., Goedert, M., and Spillantini, M.G. (2002). Proteasomal degradation of tau protein. *J Neurochem* 83, 176-185.
- David, D.C., Ollikainen, N., Trinidad, J.C., Cary, M.P., Burlingame, A.L., and Kenyon, C. (2010). Widespread protein aggregation as an inherent part of aging in *C. elegans*. *PLoS Biol* 8, e1000450.
- Dawson, H.N., Cantillana, V., Jansen, M., Wang, H., Vitek, M.P., Wilcock, D.M., Lynch, J.R., and Laskowitz, D.T. (2010). Loss of tau elicits axonal degeneration in a mouse model of Alzheimer's disease. *Neuroscience* 169, 516-531.
- De Vos, K.J., Grierson, A.J., Ackerley, S., and Miller, C.C. (2008). Role of axonal transport in neurodegenerative diseases. *Annu Rev Neurosci* 31, 151-173.
- Delobel, P., Leroy, O., Hamdane, M., Sambo, A.V., Delacourte, A., and Buee, L. (2005). Proteasome inhibition and Tau proteolysis: an unexpected regulation. *FEBS Lett* 579, 1-5.

- Derkinderen, P., Scales, T.M., Hanger, D.P., Leung, K.Y., Byers, H.L., Ward, M.A., Lenz, C., Price, C., Bird, I.N., Perera, T., *et al.* (2005). Tyrosine 394 is phosphorylated in Alzheimer's paired helical filament tau and in fetal tau with c-Abl as the candidate tyrosine kinase. *J Neurosci* 25, 6584-6593.
- Dice, J.F. (1990). Peptide sequences that target cytosolic proteins for lysosomal proteolysis. *Trends Biochem Sci* 15, 305-309.
- Dickey, C.A., Kamal, A., Lundgren, K., Klosak, N., Bailey, R.M., Dunmore, J., Ash, P., Shoraka, S., Zlatkovic, J., Eckman, C.B., *et al.* (2007). The high-affinity HSP90-CHIP complex recognizes and selectively degrades phosphorylated tau client proteins. *J Clin Invest* 117, 648-658.
- Dickey, C.A., Koren, J., Zhang, Y.J., Xu, Y.F., Jinwal, U.K., Birnbaum, M.J., Monks, B., Sun, M., Cheng, J.Q., Patterson, C., *et al.* (2008). Akt and CHIP coregulate tau degradation through coordinated interactions. *Proc Natl Acad Sci U S A* 105, 3622-3627.
- DiFiglia, M., Sapp, E., Chase, K.O., Davies, S.W., Bates, G.P., Vonsattel, J.P., and Aronin, N. (1997). Aggregation of huntingtin in neuronal intranuclear inclusions and dystrophic neurites in brain. *Science* 277, 1990-1993.
- Dillin, A., and Cohen, E. (2011). Ageing and protein aggregation-mediated disorders: from invertebrates to mammals. *Philos Trans R Soc Lond B Biol Sci* 366, 94-98.
- Dixit, R., Ross, J.L., Goldman, Y.E., and Holzbaur, E.L. (2008). Differential regulation of dynein and kinesin motor proteins by tau. *Science* 319, 1086-1089.
- Dolan, P.J., and Johnson, G.V. (2010). The role of tau kinases in Alzheimer's disease. *Curr Opin Drug Discov Devel* 13, 595-603.
- Drechsel, D.N., Hyman, A.A., Cobb, M.H., and Kirschner, M.W. (1992). Modulation of the dynamic instability of tubulin assembly by the microtubule-associated protein tau. *Mol Biol Cell* 3, 1141-1154.
- Drewes, G., Ebner, A., Preuss, U., Mandelkow, E.M., and Mandelkow, E. (1997). MARK, a novel family of protein kinases that phosphorylate microtubule-associated proteins and trigger microtubule disruption. *Cell* 89, 297-308.
- Drewes, G., Lichtenberg-Kraag, B., Doring, F., Mandelkow, E.M., Biernat, J., Goris, J., Doree, M., and Mandelkow, E. (1992). Mitogen activated protein (MAP) kinase transforms tau protein into an Alzheimer-like state. *EMBO J* 11, 2131-2138.

Drewes, G., Mandelkow, E.M., Baumann, K., Goris, J., Merlevede, W., and Mandelkow, E. (1993). Dephosphorylation of tau protein and Alzheimer paired helical filaments by calcineurin and phosphatase-2A. *FEBS Lett* 336, 425-432.

Driscoll, M. (1995). Methods for the study of cell death in the nematode *Caenorhabditis elegans*. *Methods Cell Biol* 46, 323-353.

Drubin, D.G., and Kirschner, M.W. (1986). Tau protein function in living cells. *J Cell Biol* 103, 2739-2746.

Ebneth, A., Drewes, G., Mandelkow, E.M., and Mandelkow, E. (1999). Phosphorylation of MAP2c and MAP4 by MARK kinases leads to the destabilization of microtubules in cells. *Cell Motil Cytoskeleton* 44, 209-224.

Ebneth, A., Godemann, R., Stamer, K., Illenberger, S., Trinczek, B., and Mandelkow, E. (1998). Overexpression of tau protein inhibits kinesin-dependent trafficking of vesicles, mitochondria, and endoplasmic reticulum: implications for Alzheimer's disease. *J Cell Biol* 143, 777-794.

Eckermann, K., Mocanu, M.M., Khlistunova, I., Biernat, J., Nissen, A., Hofmann, A., Schonig, K., Bujard, H., Haemisch, A., Mandelkow, E., *et al.* (2007). The beta-propensity of Tau determines aggregation and synaptic loss in inducible mouse models of tauopathy. *J Biol Chem* 282, 31755-31765.

Ermekova, K.S., Zambrano, N., Linn, H., Minopoli, G., Gertler, F., Russo, T., and Sudol, M. (1997). The WW domain of neural protein FE65 interacts with proline-rich motifs in Mena, the mammalian homolog of *Drosophila* enabled. *J Biol Chem* 272, 32869-32877.

Esmali-Azad, B., McCarty, J.H., and Feinstein, S.C. (1994). Sense and antisense transfection analysis of tau function: tau influences net microtubule assembly, neurite outgrowth and neuritic stability. *J Cell Sci* 107 (Pt 4), 869-879.

Fatouros, C., Pir, G.J., Biernat, J., Koushika, S.P., Mandelkow, E., Mandelkow, E.M., Schmidt, E., and Baumeister, R. (2012). Inhibition of tau aggregation in a novel *Caenorhabditis elegans* model of tauopathy mitigates proteotoxicity. *Hum Mol Genet* 21, 3587-3603.

Feuillette, S., Blard, O., Lecourtois, M., Frebourg, T., Campion, D., and Dumanchin, C. (2005). Tau is not normally degraded by the proteasome. *J Neurosci Res* 80, 400-405.

- Fire, A., Xu, S., Montgomery, M.K., Kostas, S.A., Driver, S.E., and Mello, C.C. (1998). Potent and specific genetic interference by double-stranded RNA in *Caenorhabditis elegans*. *Nature* 391, 806-811.
- Fitch, D.H. (2005). Introduction to nematode evolution and ecology. *WormBook*, 1-8.
- Foster, N.L., Wilhelmsen, K., Sima, A.A., Jones, M.Z., D'Amato, C.J., and Gilman, S. (1997). Frontotemporal dementia and parkinsonism linked to chromosome 17: a consensus conference. Conference Participants. *Ann Neurol* 41, 706-715.
- Friedhoff, P., von Bergen, M., Mandelkow, E.M., Davies, P., and Mandelkow, E. (1998). A nucleated assembly mechanism of Alzheimer paired helical filaments. *Proc Natl Acad Sci U S A* 95, 15712-15717.
- Gamblin, T.C., Berry, R.W., and Binder, L.I. (2003a). Modeling tau polymerization in vitro: a review and synthesis. *Biochemistry* 42, 15009-15017.
- Gamblin, T.C., Chen, F., Zambrano, A., Abrahama, A., Lagalwar, S., Guillozet, A.L., Lu, M., Fu, Y., Garcia-Sierra, F., LaPointe, N., *et al.* (2003b). Caspase cleavage of tau: linking amyloid and neurofibrillary tangles in Alzheimer's disease. *Proc Natl Acad Sci U S A* 100, 10032-10037.
- Garcia-Sierra, F., Wischik, C.M., Harrington, C.R., Luna-Munoz, J., and Mena, R. (2001). Accumulation of C-terminally truncated tau protein associated with vulnerability of the perforant pathway in early stages of neurofibrillary pathology in Alzheimer's disease. *J Chem Neuroanat* 22, 65-77.
- Garcia, M.L., and Cleveland, D.W. (2001). Going new places using an old MAP: tau, microtubules and human neurodegenerative disease. *Curr Opin Cell Biol* 13, 41-48.
- Garg, S., Timm, T., Mandelkow, E.M., Mandelkow, E., and Wang, Y. (2011). Cleavage of Tau by calpain in Alzheimer's disease: the quest for the toxic 17 kD fragment. *Neurobiology of aging* 32, 1-14.
- Gatz, M., Pedersen, N.L., Berg, S., Johansson, B., Johansson, K., Mortimer, J.A., Posner, S.F., Viitanen, M., Winblad, B., and Ahlbom, A. (1997). Heritability for Alzheimer's disease: the study of dementia in Swedish twins. *J Gerontol A Biol Sci Med Sci* 52, M117-125.
- Geddes, A.J., Parker, K.D., Atkins, E.D., and Beighton, E. (1968). "Cross-beta" conformation in proteins. *J Mol Biol* 32, 343-358.

Georgieff, I.S., Liem, R.K., Mellado, W., Nunez, J., and Shelanski, M.L. (1991). High molecular weight tau: preferential localization in the peripheral nervous system. *J Cell Sci* 100 (Pt 1), 55-60.

Giacobini, E. (2000). Cholinesterase inhibitors stabilize Alzheimer's disease. *Annals of the New York Academy of Sciences* 920, 321-327.

Gidalevitz, T., Ben-Zvi, A., Ho, K.H., Brignull, H.R., and Morimoto, R.I. (2006). Progressive disruption of cellular protein folding in models of polyglutamine diseases. *Science* 311, 1471-1474.

Glenner, G.G., and Wong, C.W. (1984a). Alzheimer's disease and Down's syndrome: sharing of a unique cerebrovascular amyloid fibril protein. *Biochem Biophys Res Commun* 122, 1131-1135.

Glenner, G.G., and Wong, C.W. (1984b). Alzheimer's disease: initial report of the purification and characterization of a novel cerebrovascular amyloid protein. *Biochem Biophys Res Commun* 120, 885-890.

Goedert, M., Baur, C.P., Ahringer, J., Jakes, R., Hasegawa, M., Spillantini, M.G., Smith, M.J., and Hill, F. (1996a). PTL-1, a microtubule-associated protein with tau-like repeats from the nematode *Caenorhabditis elegans*. *J Cell Sci* 109 (Pt 11), 2661-2672.

Goedert, M., and Jakes, R. (1990). Expression of separate isoforms of human tau protein: correlation with the tau pattern in brain and effects on tubulin polymerization. *EMBO J* 9, 4225-4230.

Goedert, M., Jakes, R., Crowther, R.A., Cohen, P., Vanmechelen, E., Vandermeeren, M., and Cras, P. (1994). Epitope mapping of monoclonal antibodies to the paired helical filaments of Alzheimer's disease: identification of phosphorylation sites in tau protein. *Biochem J* 301 (Pt 3), 871-877.

Goedert, M., Jakes, R., Spillantini, M.G., Hasegawa, M., Smith, M.J., and Crowther, R.A. (1996b). Assembly of microtubule-associated protein tau into Alzheimer-like filaments induced by sulphated glycosaminoglycans. *Nature* 383, 550-553.

Goedert, M., and Spillantini, M.G. (2001). Tau gene mutations and neurodegeneration. *Biochem Soc Symp*, 59-71.

Goedert, M., Spillantini, M.G., Cairns, N.J., and Crowther, R.A. (1992a). Tau proteins of Alzheimer paired helical filaments: abnormal phosphorylation of all six brain isoforms. *Neuron* 8, 159-168.

Goedert, M., Spillantini, M.G., and Crowther, R.A. (1992b). Cloning of a big tau microtubule-associated protein characteristic of the peripheral nervous system. *Proc Natl Acad Sci U S A* 89, 1983-1987.

Goedert, M., Spillantini, M.G., Jakes, R., Rutherford, D., and Crowther, R.A. (1989a). Multiple isoforms of human microtubule-associated protein tau: sequences and localization in neurofibrillary tangles of Alzheimer's disease. *Neuron* 3, 519-526.

Goedert, M., Spillantini, M.G., Potier, M.C., Ulrich, J., and Crowther, R.A. (1989b). Cloning and sequencing of the cDNA encoding an isoform of microtubule-associated protein tau containing four tandem repeats: differential expression of tau protein mRNAs in human brain. *EMBO J* 8, 393-399.

Goedert, M., Wischik, C.M., Crowther, R.A., Walker, J.E., and Klug, A. (1988). Cloning and sequencing of the cDNA encoding a core protein of the paired helical filament of Alzheimer disease: identification as the microtubule-associated protein tau. *Proc Natl Acad Sci U S A* 85, 4051-4055.

Goldbaum, O., Oppermann, M., Handschuh, M., Dabir, D., Zhang, B., Forman, M.S., Trojanowski, J.Q., Lee, V.M., and Richter-Landsberg, C. (2003). Proteasome inhibition stabilizes tau inclusions in oligodendroglial cells that occur after treatment with okadaic acid. *J Neurosci* 23, 8872-8880.

Gong, C.X., Grundke-Iqbal, I., Damuni, Z., and Iqbal, K. (1994). Dephosphorylation of microtubule-associated protein tau by protein phosphatase-1 and -2C and its implication in Alzheimer disease. *FEBS Lett* 341, 94-98.

Gong, C.X., Lidsky, T., Wegiel, J., Zuck, L., Grundke-Iqbal, I., and Iqbal, K. (2000). Phosphorylation of microtubule-associated protein tau is regulated by protein phosphatase 2A in mammalian brain. Implications for neurofibrillary degeneration in Alzheimer's disease. *J Biol Chem* 275, 5535-5544.

Goode, B.L., and Feinstein, S.C. (1994). Identification of a novel microtubule binding and assembly domain in the developmentally regulated inter-repeat region of tau. *J Cell Biol* 124, 769-782.

Gordon, P., Hingula, L., Krasny, M.L., Swienkowski, J.L., Pokrywka, N.J., and Raley-Susman, K.M. (2008). The invertebrate microtubule-associated protein PTL-1 functions in mechanosensation and development in *Caenorhabditis elegans*. *Dev Genes Evol* 218, 541-551.

Gotz, J., Probst, A., Spillantini, M.G., Schafer, T., Jakes, R., Burki, K., and Goedert, M. (1995). Somatodendritic localization and hyperphosphorylation of tau protein in

transgenic mice expressing the longest human brain tau isoform. *EMBO J* 14, 1304-1313.

Greenberg, S.G., and Davies, P. (1990). A preparation of Alzheimer paired helical filaments that displays distinct tau proteins by polyacrylamide gel electrophoresis. *Proc Natl Acad Sci U S A* 87, 5827-5831.

Grundke-Iqbal, I., Iqbal, K., Quinlan, M., Tung, Y.C., Zaidi, M.S., and Wisniewski, H.M. (1986a). Microtubule-associated protein tau. A component of Alzheimer paired helical filaments. *J Biol Chem* 261, 6084-6089.

Grundke-Iqbal, I., Iqbal, K., Tung, Y.C., Quinlan, M., Wisniewski, H.M., and Binder, L.I. (1986b). Abnormal phosphorylation of the microtubule-associated protein tau (tau) in Alzheimer cytoskeletal pathology. *Proc Natl Acad Sci U S A* 83, 4913-4917.

Gu, Y., Oyama, F., and Ihara, Y. (1996). Tau is widely expressed in rat tissues. *J Neurochem* 67, 1235-1244.

Guo, H., Albrecht, S., Bourdeau, M., Petzke, T., Bergeron, C., and LeBlanc, A.C. (2004). Active caspase-6 and caspase-6-cleaved tau in neuropil threads, neuritic plaques, and neurofibrillary tangles of Alzheimer's disease. *Am J Pathol* 165, 523-531.

Gustke, N., Trinczek, B., Biernat, J., Mandelkow, E.M., and Mandelkow, E. (1994). Domains of tau protein and interactions with microtubules. *Biochemistry* 33, 9511-9522.

Guthrie, C.R., Greenup, L., Leverenz, J.B., and Kraemer, B.C. (2011). MSUT2 is a determinant of susceptibility to tau neurotoxicity. *Hum Mol Genet* 20, 1989-1999.

Guthrie, C.R., Schellenberg, G.D., and Kraemer, B.C. (2009). SUT-2 potentiates tau-induced neurotoxicity in *Caenorhabditis elegans*. *Hum Mol Genet* 18, 1825-1838.

Haass, C., Schlossmacher, M.G., Hung, A.Y., Vigo-Pelfrey, C., Mellon, A., Ostaszewski, B.L., Lieberburg, I., Koo, E.H., Schenk, D., Teplow, D.B., *et al.* (1992). Amyloid beta-peptide is produced by cultured cells during normal metabolism. *Nature* 359, 322-325.

Hamano, T., Gendron, T.F., Causevic, E., Yen, S.H., Lin, W.L., Isidoro, C., Deture, M., and Ko, L.W. (2008). Autophagic-lysosomal perturbation enhances tau aggregation in transfectants with induced wild-type tau expression. *Eur J Neurosci* 27, 1119-1130.

Hammarstrom, P., Wiseman, R.L., Powers, E.T., and Kelly, J.W. (2003). Prevention of transthyretin amyloid disease by changing protein misfolding energetics. *Science* 299, 713-716.

- Hanger, D.P., Byers, H.L., Wray, S., Leung, K.Y., Saxton, M.J., Seereeram, A., Reynolds, C.H., Ward, M.A., and Anderton, B.H. (2007). Novel phosphorylation sites in tau from Alzheimer brain support a role for casein kinase 1 in disease pathogenesis. *J Biol Chem* 282, 23645-23654.
- Harada, A., Oguchi, K., Okabe, S., Kuno, J., Terada, S., Ohshima, T., Sato-Yoshitake, R., Takei, Y., Noda, T., and Hirokawa, N. (1994). Altered microtubule organization in small-calibre axons of mice lacking tau protein. *Nature* 369, 488-491.
- Hardy, J., and Allsop, D. (1991). Amyloid deposition as the central event in the aetiology of Alzheimer's disease. *Trends Pharmacol Sci* 12, 383-388.
- Hardy, J., and Singleton, A. (2008). The HapMap: charting a course for genetic discovery in neurological diseases. *Arch Neurol* 65, 319-321.
- Hartig, W., Stieler, J., Boerema, A.S., Wolf, J., Schmidt, U., Weissfuss, J., Bullmann, T., Strijkstra, A.M., and Arendt, T. (2007). Hibernation model of tau phosphorylation in hamsters: selective vulnerability of cholinergic basal forebrain neurons - implications for Alzheimer's disease. *Eur J Neurosci* 25, 69-80.
- Hasegawa, M., Smith, M.J., and Goedert, M. (1998). Tau proteins with FTDP-17 mutations have a reduced ability to promote microtubule assembly. *FEBS Lett* 437, 207-210.
- Hattori, M., Sugino, E., Minoura, K., In, Y., Sumida, M., Taniguchi, T., Tomoo, K., and Ishida, T. (2008). Different inhibitory response of cyanidin and methylene blue for filament formation of tau microtubule-binding domain. *Biochem Biophys Res Commun* 374, 158-163.
- Heiseke, A., Aguib, Y., Riemer, C., Baier, M., and Schatzl, H.M. (2009). Lithium induces clearance of protease resistant prion protein in prion-infected cells by induction of autophagy. *J Neurochem* 109, 25-34.
- Henis-Korenblit, S., Zhang, P., Hansen, M., McCormick, M., Lee, S.J., Cary, M., and Kenyon, C. (2010). Insulin/IGF-1 signaling mutants reprogram ER stress response regulators to promote longevity. *Proc Natl Acad Sci U S A* 107, 9730-9735.
- Himmler, A. (1989). Structure of the bovine tau gene: alternatively spliced transcripts generate a protein family. *Mol Cell Biol* 9, 1389-1396.
- Himmler, A., Drechsel, D., Kirschner, M.W., and Martin, D.W., Jr. (1989). Tau consists of a set of proteins with repeated C-terminal microtubule-binding domains and variable N-terminal domains. *Mol Cell Biol* 9, 1381-1388.

- Hirokawa, N. (1993a). Axonal transport and the cytoskeleton. *Curr Opin Neurobiol* 3, 724-731.
- Hirokawa, N. (1993b). Mechanism of axonal transport. Identification of new molecular motors and regulations of transports. *Neurosci Res* 18, 1-9.
- Hirokawa, N. (1994). Microtubule organization and dynamics dependent on microtubule-associated proteins. *Curr Opin Cell Biol* 6, 74-81.
- Hirokawa, N., Funakoshi, T., Sato-Harada, R., and Kanai, Y. (1996). Selective stabilization of tau in axons and microtubule-associated protein 2C in cell bodies and dendrites contributes to polarized localization of cytoskeletal proteins in mature neurons. *J Cell Biol* 132, 667-679.
- Hodgkin, J. (1988). Sex determination. Right gene, wrong chromosome. *Nature* 336, 712.
- Hong, M., Zhukareva, V., Vogelsberg-Ragaglia, V., Wszolek, Z., Reed, L., Miller, B.I., Geschwind, D.H., Bird, T.D., McKeel, D., Goate, A., *et al.* (1998). Mutation-specific functional impairments in distinct tau isoforms of hereditary FTDP-17. *Science* 282, 1914-1917.
- Hoover, B.R., Reed, M.N., Su, J., Penrod, R.D., Kotilinek, L.A., Grant, M.K., Pitstick, R., Carlson, G.A., Lanier, L.M., Yuan, L.L., *et al.* (2010). Tau mislocalization to dendritic spines mediates synaptic dysfunction independently of neurodegeneration. *Neuron* 68, 1067-1081.
- Horiguchi, T., Uryu, K., Giasson, B.I., Ischiropoulos, H., Lightfoot, R., Bellmann, C., Richter-Landsberg, C., Lee, V.M., and Trojanowski, J.Q. (2003). Nitration of tau protein is linked to neurodegeneration in tauopathies. *Am J Pathol* 163, 1021-1031.
- Horowitz, P.M., Patterson, K.R., Guillozet-Bongaarts, A.L., Reynolds, M.R., Carroll, C.A., Weintraub, S.T., Bennett, D.A., Cryns, V.L., Berry, R.W., and Binder, L.I. (2004). Early N-terminal changes and caspase-6 cleavage of tau in Alzheimer's disease. *J Neurosci* 24, 7895-7902.
- Hsu, A.L., Murphy, C.T., and Kenyon, C. (2003). Regulation of aging and age-related disease by DAF-16 and heat-shock factor. *Science* 300, 1142-1145.
- Hutton, M., Lendon, C.L., Rizzu, P., Baker, M., Froelich, S., Houlden, H., Pickering-Brown, S., Chakraborty, S., Isaacs, A., Grover, A., *et al.* (1998). Association of missense and 5'-splice-site mutations in tau with the inherited dementia FTDP-17. *Nature* 393, 702-705.

Ichimura, Y., Kirisako, T., Takao, T., Satomi, Y., Shimonishi, Y., Ishihara, N., Mizushima, N., Tanida, I., Kominami, E., Ohsumi, M., *et al.* (2000). A ubiquitin-like system mediates protein lipidation. *Nature* 408, 488-492.

Ikegami, S., Harada, A., and Hirokawa, N. (2000). Muscle weakness, hyperactivity, and impairment in fear conditioning in tau-deficient mice. *Neurosci Lett* 279, 129-132.

Illenberger, S., Zheng-Fischhofer, Q., Preuss, U., Stamer, K., Baumann, K., Trinczek, B., Biernat, J., Godemann, R., Mandelkow, E.M., and Mandelkow, E. (1998). The endogenous and cell cycle-dependent phosphorylation of tau protein in living cells: implications for Alzheimer's disease. *Mol Biol Cell* 9, 1495-1512.

Ingelson, M., Vanmechelen, E., and Lannfelt, L. (1996). Microtubule-associated protein tau in human fibroblasts with the Swedish Alzheimer mutation. *Neurosci Lett* 220, 9-12.

Iqbal, K., Alonso, A.C., Gong, C.X., Khatoon, S., Singh, T.J., and Grundke-Iqbal, I. (1994a). Mechanism of neurofibrillary degeneration in Alzheimer's disease. *Mol Neurobiol* 9, 119-123.

Iqbal, K., Alonso Adel, C., Chen, S., Chohan, M.O., El-Akkad, E., Gong, C.X., Khatoon, S., Li, B., Liu, F., Rahman, A., *et al.* (2005). Tau pathology in Alzheimer disease and other tauopathies. *Biochim Biophys Acta* 1739, 198-210.

Iqbal, K., Alonso Adel, C., and Grundke-Iqbal, I. (2008). Cytosolic abnormally hyperphosphorylated tau but not paired helical filaments sequester normal MAPs and inhibit microtubule assembly. *J Alzheimers Dis* 14, 365-370.

Iqbal, K., Grundke-Iqbal, I., Zaidi, T., Merz, P.A., Wen, G.Y., Shaikh, S.S., Wisniewski, H.M., Alafuzoff, I., and Winblad, B. (1986). Defective brain microtubule assembly in Alzheimer's disease. *Lancet* 2, 421-426.

Iqbal, K., Zaidi, T., Bancher, C., and Grundke-Iqbal, I. (1994b). Alzheimer paired helical filaments. Restoration of the biological activity by dephosphorylation. *FEBS Lett* 349, 104-108.

Irminger-Finger, I., Laymon, R.A., and Goldstein, L.S. (1990). Analysis of the primary sequence and microtubule-binding region of the *Drosophila* 205K MAP. *J Cell Biol* 111, 2563-2572.

Ishiguro, K., Shiratsuchi, A., Sato, S., Omori, A., Arioka, M., Kobayashi, S., Uchida, T., and Imahori, K. (1993). Glycogen synthase kinase 3 beta is identical to tau protein

kinase I generating several epitopes of paired helical filaments. *FEBS Lett* 325, 167-172.

Ishihara, T., Hong, M., Zhang, B., Nakagawa, Y., Lee, M.K., Trojanowski, J.Q., and Lee, V.M. (1999). Age-dependent emergence and progression of a tauopathy in transgenic mice overexpressing the shortest human tau isoform. *Neuron* 24, 751-762.

Ittner, L.M., Fath, T., Ke, Y.D., Bi, M., van Eersel, J., Li, K.M., Gunning, P., and Gotz, J. (2008). Parkinsonism and impaired axonal transport in a mouse model of frontotemporal dementia. *Proc Natl Acad Sci U S A* 105, 15997-16002.

Ittner, L.M., Ke, Y.D., Delerue, F., Bi, M., Gladbach, A., van Eersel, J., Wolfing, H., Chieng, B.C., Christie, M.J., Napier, I.A., *et al.* (2010). Dendritic function of tau mediates amyloid-beta toxicity in Alzheimer's disease mouse models. *Cell* 142, 387-397.

Jackson, G.R., Wiedau-Pazos, M., Sang, T.K., Wagle, N., Brown, C.A., Massachi, S., and Geschwind, D.H. (2002). Human wild-type tau interacts with wingless pathway components and produces neurofibrillary pathology in *Drosophila*. *Neuron* 34, 509-519.

Jeganathan, S., von Bergen, M., Brutlach, H., Steinhoff, H.J., and Mandelkow, E. (2006). Global hairpin folding of tau in solution. *Biochemistry* 45, 2283-2293.

Jin, Y. (2002). Synaptogenesis: insights from worm and fly. *Curr Opin Neurobiol* 12, 71-79.

Kampers, T., Friedhoff, P., Biernat, J., Mandelkow, E.M., and Mandelkow, E. (1996). RNA stimulates aggregation of microtubule-associated protein tau into Alzheimer-like paired helical filaments. *FEBS Lett* 399, 344-349.

Kampers, T., Pangalos, M., Geerts, H., Wiech, H., and Mandelkow, E. (1999). Assembly of paired helical filaments from mouse tau: implications for the neurofibrillary pathology in transgenic mouse models for Alzheimer's disease. *FEBS Lett* 451, 39-44.

Karsten, S.L., Sang, T.K., Gehman, L.T., Chatterjee, S., Liu, J., Lawless, G.M., Sengupta, S., Berry, R.W., Pomakian, J., Oh, H.S., *et al.* (2006). A genomic screen for modifiers of tauopathy identifies puromycin-sensitive aminopeptidase as an inhibitor of tau-induced neurodegeneration. *Neuron* 51, 549-560.

Katsuno, M., Adachi, H., Kume, A., Li, M., Nakagomi, Y., Niwa, H., Sang, C., Kobayashi, Y., Doyu, M., and Sobue, G. (2002). Testosterone reduction prevents

phenotypic expression in a transgenic mouse model of spinal and bulbar muscular atrophy. *Neuron* 35, 843-854.

Kawarabayashi, T., Younkin, L.H., Saido, T.C., Shoji, M., Ashe, K.H., and Younkin, S.G. (2001). Age-dependent changes in brain, CSF, and plasma amyloid (beta) protein in the Tg2576 transgenic mouse model of Alzheimer's disease. *J Neurosci* 21, 372-381.

Keck, S., Nitsch, R., Grune, T., and Ullrich, O. (2003). Proteasome inhibition by paired helical filament-tau in brains of patients with Alzheimer's disease. *J Neurochem* 85, 115-122.

Keller, J.N., Hanni, K.B., and Markesbery, W.R. (2000). Impaired proteasome function in Alzheimer's disease. *J Neurochem* 75, 436-439.

Kelly, J.W., and Balch, W.E. (2003). Amyloid as a natural product. *J Cell Biol* 161, 461-462.

Kelly, S.M., Pabit, S.A., Kitchen, C.M., Guo, P., Marfatia, K.A., Murphy, T.J., Corbett, A.H., and Berland, K.M. (2007). Recognition of polyadenosine RNA by zinc finger proteins. *Proc Natl Acad Sci U S A* 104, 12306-12311.

Kenessey, A., Nacharaju, P., Ko, L.W., and Yen, S.H. (1997). Degradation of tau by lysosomal enzyme cathepsin D: implication for Alzheimer neurofibrillary degeneration. *J Neurochem* 69, 2026-2038.

Kennedy, S., Wang, D., and Ruvkun, G. (2004). A conserved siRNA-degrading RNase negatively regulates RNA interference in *C. elegans*. *Nature* 427, 645-649.

Kenyon, C., Chang, J., Gensch, E., Rudner, A., and Tabtiang, R. (1993). A *C. elegans* mutant that lives twice as long as wild type. *Nature* 366, 461-464.

Khlistunova, I., Biernat, J., Wang, Y., Pickhardt, M., von Bergen, M., Gazova, Z., Mandelkow, E., and Mandelkow, E.M. (2006). Inducible expression of Tau repeat domain in cell models of tauopathy: aggregation is toxic to cells but can be reversed by inhibitor drugs. *J Biol Chem* 281, 1205-1214.

King, M.E., Kan, H.M., Baas, P.W., Erisir, A., Glabe, C.G., and Bloom, G.S. (2006). Tau-dependent microtubule disassembly initiated by prefibrillar beta-amyloid. *J Cell Biol* 175, 541-546.

Kishi, M., Pan, Y.A., Crump, J.G., and Sanes, J.R. (2005). Mammalian SAD kinases are required for neuronal polarization. *Science* 307, 929-932.

- Kisselev, A.F., Akopian, T.N., and Goldberg, A.L. (1998). Range of sizes of peptide products generated during degradation of different proteins by archaeal proteasomes. *J Biol Chem* 273, 1982-1989.
- Kisselev, A.F., Akopian, T.N., Woo, K.M., and Goldberg, A.L. (1999). The sizes of peptides generated from protein by mammalian 26 and 20 S proteasomes. Implications for understanding the degradative mechanism and antigen presentation. *J Biol Chem* 274, 3363-3371.
- Klassen, M.P., Wu, Y.E., Maeder, C.I., Nakae, I., Cueva, J.G., Lehrman, E.K., Tada, M., Gengyo-Ando, K., Wang, G.J., Goodman, M., *et al.* (2010). An Arf-like small G protein, ARL-8, promotes the axonal transport of presynaptic cargoes by suppressing vesicle aggregation. *Neuron* 66, 710-723.
- Kopke, E., Tung, Y.C., Shaikh, S., Alonso, A.C., Iqbal, K., and Grundke-Iqbal, I. (1993). Microtubule-associated protein tau. Abnormal phosphorylation of a non-paired helical filament pool in Alzheimer disease. *J Biol Chem* 268, 24374-24384.
- Kosik, K.S. (1992). Alzheimer's disease: a cell biological perspective. *Science* 256, 780-783.
- Kosik, K.S., and Finch, E.A. (1987). MAP2 and tau segregate into dendritic and axonal domains after the elaboration of morphologically distinct neurites: an immunocytochemical study of cultured rat cerebrum. *J Neurosci* 7, 3142-3153.
- Kosik, K.S., Kowall, N.W., and McKee, A. (1989). Along the way to a neurofibrillary tangle: a look at the structure of tau. *Ann Med* 21, 109-112.
- Kosik, K.S., and Shimura, H. (2005). Phosphorylated tau and the neurodegenerative foldopathies. *Biochim Biophys Acta* 1739, 298-310.
- Kraemer, B., and Schellenberg, G.D. (2007). Using *Caenorhabditis elegans* models of neurodegenerative disease to identify neuroprotective strategies. *Int Rev Neurobiol* 77, 219-246.
- Kraemer, B.C., Zhang, B., Leverenz, J.B., Thomas, J.H., Trojanowski, J.Q., and Schellenberg, G.D. (2003). Neurodegeneration and defective neurotransmission in a *Caenorhabditis elegans* model of tauopathy. *Proc Natl Acad Sci U S A* 100, 9980-9985.
- Kruger, U., Wang, Y., Kumar, S., and Mandelkow, E.M. (2011). Autophagic degradation of tau in primary neurons and its enhancement by trehalose. *Neurobiology of aging*.

- Laemmli, U.K. (1970). Cleavage of structural proteins during the assembly of the head of bacteriophage T4. *Nature* 227, 680-685.
- Lai, C.H., Chou, C.Y., Ch'ang, L.Y., Liu, C.S., and Lin, W. (2000). Identification of novel human genes evolutionarily conserved in *Caenorhabditis elegans* by comparative proteomics. *Genome Res* 10, 703-713.
- Landy, A. (1989). Dynamic, structural, and regulatory aspects of lambda site-specific recombination. *Annu Rev Biochem* 58, 913-949.
- Lasagna-Reeves, C.A., Castillo-Carranza, D.L., Sengupta, U., Clos, A.L., Jackson, G.R., and Kaye, R. (2011). Tau oligomers impair memory and induce synaptic and mitochondrial dysfunction in wild-type mice. *Mol Neurodegener* 6, 39.
- Lebouvier, T., Scales, T.M., Hanger, D.P., Geahlen, R.L., Lardeux, B., Reynolds, C.H., Anderton, B.H., and Derkinderen, P. (2008). The microtubule-associated protein tau is phosphorylated by Syk. *Biochim Biophys Acta* 1783, 188-192.
- Lee, G. (1993). Non-motor microtubule-associated proteins. *Curr Opin Cell Biol* 5, 88-94.
- Lee, G. (2005). Tau and src family tyrosine kinases. *Biochim Biophys Acta* 1739, 323-330.
- Lee, G., Cowan, N., and Kirschner, M. (1988). The primary structure and heterogeneity of tau protein from mouse brain. *Science* 239, 285-288.
- Lee, G., Newman, S.T., Gard, D.L., Band, H., and Panchamoorthy, G. (1998). Tau interacts with src-family non-receptor tyrosine kinases. *J Cell Sci* 111 (Pt 21), 3167-3177.
- Lee, G., Thangavel, R., Sharma, V.M., Litersky, J.M., Bhaskar, K., Fang, S.M., Do, L.H., Andreadis, A., Van Hoesen, G., and Ksiezak-Reding, H. (2004). Phosphorylation of tau by fyn: implications for Alzheimer's disease. *J Neurosci* 24, 2304-2312.
- Lee, S.S., Lee, R.Y., Fraser, A.G., Kamath, R.S., Ahringer, J., and Ruvkun, G. (2003). A systematic RNAi screen identifies a critical role for mitochondria in *C. elegans* longevity. *Nat Genet* 33, 40-48.
- Lee, V.M., Goedert, M., and Trojanowski, J.Q. (2001). Neurodegenerative tauopathies. *Annu Rev Neurosci* 24, 1121-1159.

- Lee, V.M., Wang, J., and Trojanowski, J.Q. (1999). Purification of paired helical filament tau and normal tau from human brain tissue. *Methods Enzymol* 309, 81-89.
- LeVine, H., 3rd (1993). Thioflavine T interaction with synthetic Alzheimer's disease beta-amyloid peptides: detection of amyloid aggregation in solution. *Protein Sci* 2, 404-410.
- Lewis, J.A., and Fleming, J.T. (1995). Basic culture methods. *Methods Cell Biol* 48, 3-29.
- Lewis, S.A., Wang, D.H., and Cowan, N.J. (1988). Microtubule-associated protein MAP2 shares a microtubule binding motif with tau protein. *Science* 242, 936-939.
- Li, X., Kumar, Y., Zempel, H., Mandelkow, E.M., Biernat, J., and Mandelkow, E. (2011). Novel diffusion barrier for axonal retention of Tau in neurons and its failure in neurodegeneration. *EMBO J* 30, 4825-4837.
- Lichtenberg-Kraag, B., Mandelkow, E.M., Biernat, J., Steiner, B., Schroter, C., Gustke, N., Meyer, H.E., and Mandelkow, E. (1992). Phosphorylation-dependent epitopes of neurofilament antibodies on tau protein and relationship with Alzheimer tau. *Proc Natl Acad Sci U S A* 89, 5384-5388.
- Lindwall, G., and Cole, R.D. (1984). The purification of tau protein and the occurrence of two phosphorylation states of tau in brain. *J Biol Chem* 259, 12241-12245.
- Link, C.D. (1995). Expression of human beta-amyloid peptide in transgenic *Caenorhabditis elegans*. *Proc Natl Acad Sci U S A* 92, 9368-9372.
- Liu, F., Iqbal, K., Grundke-Iqbal, I., and Gong, C.X. (2002a). Involvement of aberrant glycosylation in phosphorylation of tau by cdk5 and GSK-3beta. *FEBS Lett* 530, 209-214.
- Liu, F., Zaidi, T., Iqbal, K., Grundke-Iqbal, I., Merkle, R.K., and Gong, C.X. (2002b). Role of glycosylation in hyperphosphorylation of tau in Alzheimer's disease. *FEBS Lett* 512, 101-106.
- Liu, R., Barkhordarian, H., Emadi, S., Park, C.B., and Sierks, M.R. (2005). Trehalose differentially inhibits aggregation and neurotoxicity of beta-amyloid 40 and 42. *Neurobiol Dis* 20, 74-81.
- Liu, Y., Xia, J., Ma, D., Faber, D.S., and Fischer, I. (1997). Tau-like proteins in the nervous system of goldfish. *Neurochem Res* 22, 1511-1516.

- Loomis, P.A., Howard, T.H., Castleberry, R.P., and Binder, L.I. (1990). Identification of nuclear tau isoforms in human neuroblastoma cells. *Proc Natl Acad Sci U S A* 87, 8422-8426.
- Lopez Salon, M., Morelli, L., Castano, E.M., Soto, E.F., and Pasquini, J.M. (2000). Defective ubiquitination of cerebral proteins in Alzheimer's disease. *J Neurosci Res* 62, 302-310.
- LoPresti, P., Szuchet, S., Papasozomenos, S.C., Zinkowski, R.P., and Binder, L.I. (1995). Functional implications for the microtubule-associated protein tau: localization in oligodendrocytes. *Proc Natl Acad Sci U S A* 92, 10369-10373.
- Lu, Q., Soria, J.P., and Wood, J.G. (1993). p44mpk MAP kinase induces Alzheimer type alterations in tau function and in primary hippocampal neurons. *J Neurosci Res* 35, 439-444.
- Lucas, J.J., Hernandez, F., Gomez-Ramos, P., Moran, M.A., Hen, R., and Avila, J. (2001). Decreased nuclear beta-catenin, tau hyperphosphorylation and neurodegeneration in GSK-3beta conditional transgenic mice. *EMBO J* 20, 27-39.
- Lund, J., Tedesco, P., Duke, K., Wang, J., Kim, S.K., and Johnson, T.E. (2002). Transcriptional profile of aging in *C. elegans*. *Curr Biol* 12, 1566-1573.
- Lundquist, E.A., Reddien, P.W., Hartwig, E., Horvitz, H.R., and Bargmann, C.I. (2001). Three *C. elegans* Rac proteins and several alternative Rac regulators control axon guidance, cell migration and apoptotic cell phagocytosis. *Development* 128, 4475-4488.
- MacMorris, M., Kumar, M., Lasda, E., Larsen, A., Kraemer, B., and Blumenthal, T. (2007). A novel family of *C. elegans* snRNPs contains proteins associated with trans-splicing. *RNA* 13, 511-520.
- Maeda, I., Kohara, Y., Yamamoto, M., and Sugimoto, A. (2001). Large-scale analysis of gene function in *Caenorhabditis elegans* by high-throughput RNAi. *Curr Biol* 11, 171-176.
- Maji, S.K., Ogorzalek Loo, R.R., Inayathullah, M., Spring, S.M., Vollers, S.S., Condrón, M.M., Bitan, G., Loo, J.A., and Teplow, D.B. (2009a). Amino acid position-specific contributions to amyloid beta-protein oligomerization. *J Biol Chem* 284, 23580-23591.
- Maji, S.K., Perrin, M.H., Sawaya, M.R., Jessberger, S., Vadodaria, K., Rissman, R.A., Singru, P.S., Nilsson, K.P., Simon, R., Schubert, D., *et al.* (2009b). Functional amyloids

as natural storage of peptide hormones in pituitary secretory granules. *Science* 325, 328-332.

Maji, S.K., Wang, L., Greenwald, J., and Riek, R. (2009c). Structure-activity relationship of amyloid fibrils. *FEBS Lett* 583, 2610-2617.

Majumdar, A., Capetillo-Zarate, E., Cruz, D., Gouras, G.K., and Maxfield, F.R. (2011). Degradation of Alzheimer's amyloid fibrils by microglia requires delivery of CLC-7 to lysosomes. *Mol Biol Cell* 22, 1664-1676.

Mandelkow, E. (1999). Alzheimer's disease. The tangled tale of tau. *Nature* 402, 588-589.

Mandelkow, E.M., Drewes, G., Biernat, J., Gustke, N., Van Lint, J., Vandenheede, J.R., and Mandelkow, E. (1992). Glycogen synthase kinase-3 and the Alzheimer-like state of microtubule-associated protein tau. *FEBS Lett* 314, 315-321.

Mandelkow, E.M., and Mandelkow, E. (1998). Tau in Alzheimer's disease. *Trends in cell biology* 8, 425-427.

Mandelkow, E.M., and Mandelkow, E. (2012). Biochemistry and cell biology of tau protein in neurofibrillary degeneration. *Cold Spring Harb Perspect Med* 2, a006247.

Mangiarini, L., Sathasivam, K., Seller, M., Cozens, B., Harper, A., Hetherington, C., Lawton, M., Trotter, Y., Lehrach, H., Davies, S.W., *et al.* (1996). Exon 1 of the HD gene with an expanded CAG repeat is sufficient to cause a progressive neurological phenotype in transgenic mice. *Cell* 87, 493-506.

Masters, C.L., Multhaup, G., Simms, G., Pottgiesser, J., Martins, R.N., and Beyreuther, K. (1985). Neuronal origin of a cerebral amyloid: neurofibrillary tangles of Alzheimer's disease contain the same protein as the amyloid of plaque cores and blood vessels. *EMBO J* 4, 2757-2763.

Matsudaira, P.T., and Burgess, D.R. (1978). SDS microslab linear gradient polyacrylamide gel electrophoresis. *Anal Biochem* 87, 386-396.

Mattson, M.P. (2004). Pathways towards and away from Alzheimer's disease. *Nature* 430, 631-639.

Mazanetz, M.P., and Fischer, P.M. (2007). Untangling tau hyperphosphorylation in drug design for neurodegenerative diseases. *Nat Rev Drug Discov* 6, 464-479.

- McDermott, J.B., Aamodt, S., and Aamodt, E. (1996). *ptl-1*, a *Caenorhabditis elegans* gene whose products are homologous to the tau microtubule-associated proteins. *Biochemistry* 35, 9415-9423.
- Medina, M., and Wandosell, F. (2011). Deconstructing GSK-3: The Fine Regulation of Its Activity. *Int J Alzheimers Dis* 2011, 479249.
- Melendez, A., Talloczy, Z., Seaman, M., Eskelinen, E.L., Hall, D.H., and Levine, B. (2003). Autophagy genes are essential for dauer development and life-span extension in *C. elegans*. *Science* 301, 1387-1391.
- Mello, C., and Fire, A. (1995). DNA transformation. *Methods Cell Biol* 48, 451-482.
- Mello, C.C., Kramer, J.M., Stinchcomb, D., and Ambros, V. (1991). Efficient gene transfer in *C.elegans*: extrachromosomal maintenance and integration of transforming sequences. *EMBO J* 10, 3959-3970.
- Miklossy, J., Taddei, K., Suva, D., Verdile, G., Fonte, J., Fisher, C., Gnjec, A., Ghika, J., Suard, F., Mehta, P.D., *et al.* (2003). Two novel presenilin-1 mutations (Y256S and Q222H) are associated with early-onset Alzheimer's disease. *Neurobiology of aging* 24, 655-662.
- Minniti, A.N., Rebolledo, D.L., Grez, P.M., Fadic, R., Aldunate, R., Volitakis, I., Cherny, R.A., Opazo, C., Masters, C., Bush, A.I., *et al.* (2009). Intracellular amyloid formation in muscle cells of Abeta-transgenic *Caenorhabditis elegans*: determinants and physiological role in copper detoxification. *Mol Neurodegener* 4, 2.
- Miyasaka, T., Ding, Z., Gengyo-Ando, K., Oue, M., Yamaguchi, H., Mitani, S., and Ihara, Y. (2005). Progressive neurodegeneration in *C. elegans* model of tauopathy. *Neurobiol Dis* 20, 372-383.
- Mocanu, M.M., Nissen, A., Eckermann, K., Khlistunova, I., Biernat, J., Drexler, D., Petrova, O., Schonig, K., Bujard, H., Mandelkow, E., *et al.* (2008). The potential for beta-structure in the repeat domain of tau protein determines aggregation, synaptic decay, neuronal loss, and coassembly with endogenous Tau in inducible mouse models of tauopathy. *J Neurosci* 28, 737-748.
- Mori, H., Kondo, J., and Ihara, Y. (1987). Ubiquitin is a component of paired helical filaments in Alzheimer's disease. *Science* 235, 1641-1644.
- Morishima-Kawashima, M., Hasegawa, M., Takio, K., Suzuki, M., Titani, K., and Ihara, Y. (1993). Ubiquitin is conjugated with amino-terminally processed tau in paired helical filaments. *Neuron* 10, 1151-1160.

Morishima-Kawashima, M., Hasegawa, M., Takio, K., Suzuki, M., Yoshida, H., Watanabe, A., Titani, K., and Ihara, Y. (1995). Hyperphosphorylation of tau in PHF. *Neurobiology of aging* 16, 365-371; discussion 371-380.

Morishima, M., and Ihara, Y. (1994). Posttranslational modifications of tau in paired helical filaments. *Dementia* 5, 282-288.

Morita, T., and Sobue, K. (2009). Specification of neuronal polarity regulated by local translation of CRMP2 and Tau via the mTOR-p70S6K pathway. *J Biol Chem* 284, 27734-27745.

Morris, M., Maeda, S., Vossel, K., and Mucke, L. (2011). The many faces of tau. *Neuron* 70, 410-426.

Mucke, L., Masliah, E., Yu, G.Q., Mallory, M., Rockenstein, E.M., Tatsuno, G., Hu, K., Kholodenko, D., Johnson-Wood, K., and McConlogue, L. (2000). High-level neuronal expression of abeta 1-42 in wild-type human amyloid protein precursor transgenic mice: synaptotoxicity without plaque formation. *J Neurosci* 20, 4050-4058.

Munch, G., Deuther-Conrad, W., and Gasic-Milenkovic, J. (2002). Glycoxidative stress creates a vicious cycle of neurodegeneration in Alzheimer's disease--a target for neuroprotective treatment strategies? *J Neural Transm Suppl*, 303-307.

Murphy, C.T., McCarroll, S.A., Bargmann, C.I., Fraser, A., Kamath, R.S., Ahringer, J., Li, H., and Kenyon, C. (2003). Genes that act downstream of DAF-16 to influence the lifespan of *Caenorhabditis elegans*. *Nature* 424, 277-283.

Murrell, J., Farlow, M., Ghetti, B., and Benson, M.D. (1991). A mutation in the amyloid precursor protein associated with hereditary Alzheimer's disease. *Science* 254, 97-99.

Nacharaju, P., Lewis, J., Easson, C., Yen, S., Hackett, J., Hutton, M., and Yen, S.H. (1999). Accelerated filament formation from tau protein with specific FTDP-17 missense mutations. *FEBS Lett* 447, 195-199.

Nakata, T., and Hirokawa, N. (2003). Microtubules provide directional cues for polarized axonal transport through interaction with kinesin motor head. *J Cell Biol* 162, 1045-1055.

Nelson, P.T., Stefansson, K., Gulcher, J., and Saper, C.B. (1996). Molecular evolution of tau protein: implications for Alzheimer's disease. *J Neurochem* 67, 1622-1632.

Neve, R.L., Harris, P., Kosik, K.S., Kurnit, D.M., and Donlon, T.A. (1986). Identification of cDNA clones for the human microtubule-associated protein tau and

chromosomal localization of the genes for tau and microtubule-associated protein 2. *Brain Res* 387, 271-280.

Newton, C.R., Graham, A. (1997) *PCR*, 2nd edn. pp. 75-84, BIOS Scientific Publishers, Oxford

Nixon, R.A., Wegiel, J., Kumar, A., Yu, W.H., Peterhoff, C., Cataldo, A., and Cuervo, A.M. (2005). Extensive involvement of autophagy in Alzheimer disease: an immuno-electron microscopy study. *J Neuropathol Exp Neurol* 64, 113-122.

Nonet, M.L. (1999). Visualization of synaptic specializations in live *C. elegans* with synaptic vesicle protein-GFP fusions. *J Neurosci Methods* 89, 33-40.

Novak, M., Kabat, J., and Wischik, C.M. (1993). Molecular characterization of the minimal protease resistant tau unit of the Alzheimer's disease paired helical filament. *Embo J* 12, 365-370.

Obulesu, M., Venu, R., and Somashekhar, R. (2011). Tau mediated neurodegeneration: an insight into Alzheimer's disease pathology. *Neurochem Res* 36, 1329-1335.

Oddo, S., Billings, L., Kesslak, J.P., Cribbs, D.H., and LaFerla, F.M. (2004). Abeta immunotherapy leads to clearance of early, but not late, hyperphosphorylated tau aggregates via the proteasome. *Neuron* 43, 321-332.

Oddo, S., Vasilevko, V., Caccamo, A., Kitazawa, M., Cribbs, D.H., and LaFerla, F.M. (2006). Reduction of soluble Abeta and tau, but not soluble Abeta alone, ameliorates cognitive decline in transgenic mice with plaques and tangles. *J Biol Chem* 281, 39413-39423.

Olzscha, H., Schermann, S.M., Woerner, A.C., Pinkert, S., Hecht, M.H., Tartaglia, G.G., Vendruscolo, M., Hayer-Hartl, M., Hartl, F.U., and Vabulas, R.M. (2011). Amyloid-like aggregates sequester numerous metastable proteins with essential cellular functions. *Cell* 144, 67-78.

Papasozomenos, S.C. (1989). Tau protein immunoreactivity in dementia of the Alzheimer type: II. Electron microscopy and pathogenetic implications. Effects of fixation on the morphology of the Alzheimer's abnormal filaments. *Lab Invest* 60, 375-389.

Papasozomenos, S.C., and Binder, L.I. (1987). Phosphorylation determines two distinct species of Tau in the central nervous system. *Cell Motil Cytoskeleton* 8, 210-226.

- Park, S.Y., and Ferreira, A. (2005). The generation of a 17 kDa neurotoxic fragment: an alternative mechanism by which tau mediates beta-amyloid-induced neurodegeneration. *J Neurosci* 25, 5365-5375.
- Parker, J.A., Connolly, J.B., Wellington, C., Hayden, M., Dausset, J., and Neri, C. (2001). Expanded polyglutamines in *Caenorhabditis elegans* cause axonal abnormalities and severe dysfunction of PLM mechanosensory neurons without cell death. *Proc Natl Acad Sci U S A* 98, 13318-13323.
- Perkins, L.A., Hedgecock, E.M., Thomson, J.N., and Culotti, J.G. (1986). Mutant sensory cilia in the nematode *Caenorhabditis elegans*. *Dev Biol* 117, 456-487.
- Petrucelli, L., Dickson, D., Kehoe, K., Taylor, J., Snyder, H., Grover, A., De Lucia, M., McGowan, E., Lewis, J., Prihar, G., *et al.* (2004). CHIP and Hsp70 regulate tau ubiquitination, degradation and aggregation. *Hum Mol Genet* 13, 703-714.
- Pickford, F., Masliah, E., Britschgi, M., Lucin, K., Narasimhan, R., Jaeger, P.A., Small, S., Spencer, B., Rockenstein, E., Levine, B., *et al.* (2008). The autophagy-related protein beclin 1 shows reduced expression in early Alzheimer disease and regulates amyloid beta accumulation in mice. *J Clin Invest* 118, 2190-2199.
- Pickhardt, M., Larbig, G., Khlistunova, I., Coksezen, A., Meyer, B., Mandelkow, E.M., Schmidt, B., and Mandelkow, E. (2007). Phenylthiazolyl-hydrazide and its derivatives are potent inhibitors of tau aggregation and toxicity in vitro and in cells. *Biochemistry* 46, 10016-10023.
- Poorkaj, P., Bird, T.D., Wijsman, E., Nemens, E., Garruto, R.M., Anderson, L., Andreadis, A., Wiederholt, W.C., Raskind, M., and Schellenberg, G.D. (1998). Tau is a candidate gene for chromosome 17 frontotemporal dementia. *Ann Neurol* 43, 815-825.
- Porat, Y., Abramowitz, A., and Gazit, E. (2006). Inhibition of amyloid fibril formation by polyphenols: structural similarity and aromatic interactions as a common inhibition mechanism. *Chem Biol Drug Des* 67, 27-37.
- Rapoport, M., Dawson, H.N., Binder, L.I., Vitek, M.P., and Ferreira, A. (2002). Tau is essential to beta -amyloid-induced neurotoxicity. *Proc Natl Acad Sci U S A* 99, 6364-6369.
- Reed, L.A., Grabowski, T.J., Schmidt, M.L., Morris, J.C., Goate, A., Solodkin, A., Van Hoesen, G.W., Schelper, R.L., Talbot, C.J., Wragg, M.A., *et al.* (1997). Autosomal dominant dementia with widespread neurofibrillary tangles. *Ann Neurol* 42, 564-572.

- Reed, L.A., Schmidt, M.L., Wszolek, Z.K., Balin, B.J., Soontornniyomkij, V., Lee, V.M., Trojanowski, J.Q., and Schelper, R.L. (1998). The neuropathology of a chromosome 17-linked autosomal dominant parkinsonism and dementia ("pallido-ponto-nigral degeneration"). *J Neuropathol Exp Neurol* 57, 588-601.
- Reynolds, M.R., Berry, R.W., and Binder, L.I. (2007). Nitration in neurodegeneration: deciphering the "Hows" "nYs". *Biochemistry* 46, 7325-7336.
- Riedel, M., Goldbaum, O., Schwarz, L., Schmitt, S., and Richter-Landsberg, C. (2010). 17-AAG induces cytoplasmic alpha-synuclein aggregate clearance by induction of autophagy. *PLoS One* 5, e8753.
- Rissman, R.A., Poon, W.W., Blurton-Jones, M., Oddo, S., Torp, R., Vitek, M.P., LaFerla, F.M., Rohn, T.T., and Cotman, C.W. (2004). Caspase-cleavage of tau is an early event in Alzheimer disease tangle pathology. *J Clin Invest* 114, 121-130.
- Rizzu, P., Joosse, M., Ravid, R., Hoogeveen, A., Kamphorst, W., van Swieten, J.C., Willemsen, R., and Heutink, P. (2000). Mutation-dependent aggregation of tau protein and its selective depletion from the soluble fraction in brain of P301L FTDP-17 patients. *Hum Mol Genet* 9, 3075-3082.
- Roberson, E.D., Searce-Levie, K., Palop, J.J., Yan, F., Cheng, I.H., Wu, T., Gerstein, H., Yu, G.Q., and Mucke, L. (2007). Reducing endogenous tau ameliorates amyloid beta-induced deficits in an Alzheimer's disease mouse model. *Science* 316, 750-754.
- Rogaev, E.I., Sherrington, R., Rogaeva, E.A., Levesque, G., Ikeda, M., Liang, Y., Chi, H., Lin, C., Holman, K., Tsuda, T., *et al.* (1995). Familial Alzheimer's disease in kindreds with missense mutations in a gene on chromosome 1 related to the Alzheimer's disease type 3 gene. *Nature* 376, 775-778.
- Rohn, T.T., Rissman, R.A., Davis, M.C., Kim, Y.E., Cotman, C.W., and Head, E. (2002). Caspase-9 activation and caspase cleavage of tau in the Alzheimer's disease brain. *Neurobiol Dis* 11, 341-354.
- Roy, H., Ling, J., Alfonzo, J., and Ibba, M. (2005). Loss of editing activity during the evolution of mitochondrial phenylalanyl-tRNA synthetase. *J Biol Chem* 280, 38186-38192.
- Rubin, G.M., Yandell, M.D., Wortman, J.R., Gabor Miklos, G.L., Nelson, C.R., Hariharan, I.K., Fortini, M.E., Li, P.W., Apweiler, R., Fleischmann, W., *et al.* (2000). Comparative genomics of the eukaryotes. *Science* 287, 2204-2215.

- Rubinsztein, D.C., Cuervo, A.M., Ravikumar, B., Sarkar, S., Korolchuk, V., Kaushik, S., and Klionsky, D.J. (2009). In search of an "autophagometer". *Autophagy* 5, 585-589.
- Sabo, S.L., Ikin, A.F., Buxbaum, J.D., and Greengard, P. (2001). The Alzheimer amyloid precursor protein (APP) and FE65, an APP-binding protein, regulate cell movement. *J Cell Biol* 153, 1403-1414.
- Sahara, N., Maeda, S., and Takashima, A. (2008). Tau oligomerization: a role for tau aggregation intermediates linked to neurodegeneration. *Curr Alzheimer Res* 5, 591-598.
- Samuelson, A.V., Klimczak, R.R., Thompson, D.B., Carr, C.E., and Ruvkun, G. (2007). Identification of *Caenorhabditis elegans* genes regulating longevity using enhanced RNAi-sensitive strains. *Cold Spring Harb Symp Quant Biol* 72, 489-497.
- Santacruz, K., Lewis, J., Spires, T., Paulson, J., Kotilinek, L., Ingelsson, M., Guimaraes, A., DeTure, M., Ramsden, M., McGowan, E., *et al.* (2005). Tau suppression in a neurodegenerative mouse model improves memory function. *Science* 309, 476-481.
- Santambrogio, L., and Cuervo, A.M. (2011). Chasing the elusive mammalian microautophagy. *Autophagy* 7, 652-654.
- Sapir, T., Frotscher, M., Levy, T., Mandelkow, E.M., and Reiner, O. (2012). Tau's role in the developing brain: implications for intellectual disability. *Hum Mol Genet* 21, 1681-1692.
- Sarkar, S., Davies, J.E., Huang, Z., Tunnacliffe, A., and Rubinsztein, D.C. (2007a). Trehalose, a novel mTOR-independent autophagy enhancer, accelerates the clearance of mutant huntingtin and alpha-synuclein. *J Biol Chem* 282, 5641-5652.
- Sarkar, S., Perlstein, E.O., Imarisio, S., Pineau, S., Cordenier, A., Maglathlin, R.L., Webster, J.A., Lewis, T.A., O'Kane, C.J., Schreiber, S.L., *et al.* (2007b). Small molecules enhance autophagy and reduce toxicity in Huntington's disease models. *Nat Chem Biol* 3, 331-338.
- Sato, Y., Naito, Y., Grundke-Iqbal, I., Iqbal, K., and Endo, T. (2001). Analysis of N-glycans of pathological tau: possible occurrence of aberrant processing of tau in Alzheimer's disease. *FEBS Lett* 496, 152-160.
- Schirmer, R.H., Adler, H., Pickhardt, M., and Mandelkow, E. (2011). "Lest we forget you--methylene blue...". *Neurobiology of aging* 32, 2325 e2327-2316.

- Schneider, A., Biernat, J., von Bergen, M., Mandelkow, E., and Mandelkow, E.M. (1999). Phosphorylation that detaches tau protein from microtubules (Ser262, Ser214) also protects it against aggregation into Alzheimer paired helical filaments. *Biochemistry* 38, 3549-3558.
- Schneider, A., and Mandelkow, E. (2008). Tau-based treatment strategies in neurodegenerative diseases. *Neurotherapeutics* 5, 443-457.
- Schon, E.A., and Przedborski, S. (2011). Mitochondria: the next (neurode)generation. *Neuron* 70, 1033-1053.
- Schultheis, C., Brauner, M., Liewald, J.F., and Gottschalk, A. (2011). Optogenetic analysis of GABAB receptor signaling in *Caenorhabditis elegans* motor neurons. *J Neurophysiol* 106, 817-827.
- Schulze, E., and Kirschner, M. (1987). Dynamic and stable populations of microtubules in cells. *J Cell Biol* 104, 277-288.
- Seglen, P.O., and Gordon, P.B. (1982). 3-Methyladenine: specific inhibitor of autophagic/lysosomal protein degradation in isolated rat hepatocytes. *Proc Natl Acad Sci U S A* 79, 1889-1892.
- Seitz, A., Kojima, H., Oiwa, K., Mandelkow, E.M., Song, Y.H., and Mandelkow, E. (2002). Single-molecule investigation of the interference between kinesin, tau and MAP2c. *EMBO J* 21, 4896-4905.
- Selkoe, D.J. (1994). Normal and abnormal biology of the beta-amyloid precursor protein. *Annu Rev Neurosci* 17, 489-517.
- Settembre, C., Di Malta, C., Polito, V.A., Garcia Arencibia, M., Vetrini, F., Erdin, S., Erdin, S.U., Huynh, T., Medina, D., Colella, P., *et al.* (2011). TFEB links autophagy to lysosomal biogenesis. *Science* 332, 1429-1433.
- Seubert, P., Mawal-Dewan, M., Barbour, R., Jakes, R., Goedert, M., Johnson, G.V., Litersky, J.M., Schenk, D., Lieberburg, I., Trojanowski, J.Q., *et al.* (1995). Detection of phosphorylated Ser262 in fetal tau, adult tau, and paired helical filament tau. *J Biol Chem* 270, 18917-18922.
- Seubert, P., Vigo-Pelfrey, C., Esch, F., Lee, M., Dovey, H., Davis, D., Sinha, S., Schlossmacher, M., Whaley, J., Swindlehurst, C., *et al.* (1992). Isolation and quantification of soluble Alzheimer's beta-peptide from biological fluids. *Nature* 359, 325-327.

- Shankar, G.M., Bloodgood, B.L., Townsend, M., Walsh, D.M., Selkoe, D.J., and Sabatini, B.L. (2007). Natural oligomers of the Alzheimer amyloid-beta protein induce reversible synapse loss by modulating an NMDA-type glutamate receptor-dependent signaling pathway. *J Neurosci* 27, 2866-2875.
- Sherrington, R., Rogaev, E.I., Liang, Y., Rogaeva, E.A., Levesque, G., Ikeda, M., Chi, H., Lin, C., Li, G., Holman, K., *et al.* (1995). Cloning of a gene bearing missense mutations in early-onset familial Alzheimer's disease. *Nature* 375, 754-760.
- Shimura, H., Miura-Shimura, Y., and Kosik, K.S. (2004a). Binding of tau to heat shock protein 27 leads to decreased concentration of hyperphosphorylated tau and enhanced cell survival. *J Biol Chem* 279, 17957-17962.
- Shimura, H., Schwartz, D., Gygi, S.P., and Kosik, K.S. (2004b). CHIP-Hsc70 complex ubiquitinates phosphorylated tau and enhances cell survival. *J Biol Chem* 279, 4869-4876.
- Shoji, M., Golde, T.E., Ghiso, J., Cheung, T.T., Estus, S., Shaffer, L.M., Cai, X.D., McKay, D.M., Tintner, R., Frangione, B., *et al.* (1992). Production of the Alzheimer amyloid beta protein by normal proteolytic processing. *Science* 258, 126-129.
- Shuman, S. (1991). Recombination mediated by vaccinia virus DNA topoisomerase I in *Escherichia coli* is sequence specific. *Proc Natl Acad Sci U S A* 88, 10104-10108.
- Shuman, S. (1994). Novel approach to molecular cloning and polynucleotide synthesis using vaccinia DNA topoisomerase. *J Biol Chem* 269, 32678-32684.
- Sieburth, D., Ch'ng, Q., Dybbs, M., Tavazoie, M., Kennedy, S., Wang, D., Dupuy, D., Rual, J.F., Hill, D.E., Vidal, M., *et al.* (2005). Systematic analysis of genes required for synapse structure and function. *Nature* 436, 510-517.
- Simmer, F., Tijsterman, M., Parrish, S., Koushika, S.P., Nonet, M.L., Fire, A., Ahringer, J., and Plasterk, R.H. (2002). Loss of the putative RNA-directed RNA polymerase RRF-3 makes *C. elegans* hypersensitive to RNAi. *Curr Biol* 12, 1317-1319.
- Singer, M.A., and Lindquist, S. (1998). Multiple effects of trehalose on protein folding in vitro and in vivo. *Mol Cell* 1, 639-648.
- Smith, H., and Campbell, W.C. (1996). Effect of ivermectin on *Caenorhabditis elegans* larvae previously exposed to alcoholic immobilization. *J Parasitol* 82, 187-188.
- Sontag, E., Nunbhakdi-Craig, V., Lee, G., Bloom, G.S., and Mumby, M.C. (1996). Regulation of the phosphorylation state and microtubule-binding activity of Tau by protein phosphatase 2A. *Neuron* 17, 1201-1207.

Soto, C. (2003). Unfolding the role of protein misfolding in neurodegenerative diseases. *Nat Rev Neurosci* 4, 49-60.

Spillantini, M.G., Bird, T.D., and Ghetti, B. (1998a). Frontotemporal dementia and Parkinsonism linked to chromosome 17: a new group of tauopathies. *Brain Pathol* 8, 387-402.

Spillantini, M.G., Goedert, M., Crowther, R.A., Murrell, J.R., Farlow, M.R., and Ghetti, B. (1997). Familial multiple system tauopathy with presenile dementia: a disease with abundant neuronal and glial tau filaments. *Proc Natl Acad Sci U S A* 94, 4113-4118.

Spillantini, M.G., Murrell, J.R., Goedert, M., Farlow, M.R., Klug, A., and Ghetti, B. (1998b). Mutation in the tau gene in familial multiple system tauopathy with presenile dementia. *Proc Natl Acad Sci U S A* 95, 7737-7741.

Spilman, P., Podlitskaya, N., Hart, M.J., Debnath, J., Gorostiza, O., Bredesen, D., Richardson, A., Strong, R., and Galvan, V. (2010). Inhibition of mTOR by rapamycin abolishes cognitive deficits and reduces amyloid-beta levels in a mouse model of Alzheimer's disease. *PLoS One* 5, e9979.

Spires-Jones, T.L., Kopeikina, K.J., Koffie, R.M., de Calignon, A., and Hyman, B.T. (2011). Are tangles as toxic as they look? *J Mol Neurosci* 45, 438-444.

Spittaels, K., Van den Haute, C., Van Dorpe, J., Geerts, H., Mercken, M., Bruynseels, K., Lasrado, R., Vandezande, K., Laenen, I., Boon, T., *et al.* (2000). Glycogen synthase kinase-3 β phosphorylates protein tau and rescues the axonopathy in the central nervous system of human four-repeat tau transgenic mice. *J Biol Chem* 275, 41340-41349.

Squier, T.C. (2001). Oxidative stress and protein aggregation during biological aging. *Exp Gerontol* 36, 1539-1550.

Stamer, K., Vogel, R., Thies, E., Mandelkow, E., and Mandelkow, E.M. (2002). Tau blocks traffic of organelles, neurofilaments, and APP vesicles in neurons and enhances oxidative stress. *J Cell Biol* 156, 1051-1063.

Stanford, P.M., Shepherd, C.E., Halliday, G.M., Brooks, W.S., Schofield, P.W., Brodaty, H., Martins, R.N., Kwok, J.B., and Schofield, P.R. (2003). Mutations in the tau gene that cause an increase in three repeat tau and frontotemporal dementia. *Brain* 126, 814-826.

Steiner, B., Mandelkow, E.M., Biernat, J., Gustke, N., Meyer, H.E., Schmidt, B., Mieskes, G., Soling, H.D., Drechsel, D., Kirschner, M.W., *et al.* (1990).

Phosphorylation of microtubule-associated protein tau: identification of the site for Ca²⁺(+)-calmodulin dependent kinase and relationship with tau phosphorylation in Alzheimer tangles. *Embo J* 9, 3539-3544.

Stiernagle, T. (2006). Maintenance of *C. elegans*. *WormBook*, 1-11.

Sulston, J.E., Schierenberg, E., White, J.G., and Thomson, J.N. (1983). The embryonic cell lineage of the nematode *Caenorhabditis elegans*. *Dev Biol* 100, 64-119.

Sultan, A., Nessler, F., Violet, M., Begard, S., Loyens, A., Talahari, S., Mansuroglu, Z., Marzin, D., Sergeant, N., Humez, S., *et al.* (2011). Nuclear tau, a key player in neuronal DNA protection. *J Biol Chem* 286, 4566-4575.

Sun, L., Liu, S.Y., Zhou, X.W., Wang, X.C., Liu, R., Wang, Q., and Wang, J.Z. (2003). Inhibition of protein phosphatase 2A- and protein phosphatase 1-induced tau hyperphosphorylation and impairment of spatial memory retention in rats. *Neuroscience* 118, 1175-1182.

Suzuki, N., Cheung, T.T., Cai, X.D., Odaka, A., Otvos, L., Jr., Eckman, C., Golde, T.E., and Younkin, S.G. (1994). An increased percentage of long amyloid beta protein secreted by familial amyloid beta protein precursor (beta APP717) mutants. *Science* 264, 1336-1340.

Sydow, A., Van der Jeugd, A., Zheng, F., Ahmed, T., Balschun, D., Petrova, O., Drexler, D., Zhou, L., Rune, G., Mandelkow, E., *et al.* (2011). Tau-induced defects in synaptic plasticity, learning, and memory are reversible in transgenic mice after switching off the toxic Tau mutant. *J Neurosci* 31, 2511-2525.

Tabara, H., Grishok, A., and Mello, C.C. (1998). RNAi in *C. elegans*: soaking in the genome sequence. *Science* 282, 430-431.

Tabert, M.H., Liu, X., Doty, R.L., Serby, M., Zamora, D., Pelton, G.H., Marder, K., Albers, M.W., Stern, Y., and Devanand, D.P. (2005). A 10-item smell identification scale related to risk for Alzheimer's disease. *Ann Neurol* 58, 155-160.

Tanaka, M., Machida, Y., Niu, S., Ikeda, T., Jana, N.R., Doi, H., Kurosawa, M., Nekooki, M., and Nukina, N. (2004). Trehalose alleviates polyglutamine-mediated pathology in a mouse model of Huntington disease. *Nat Med* 10, 148-154.

Telford, M.J. (2004). Animal phylogeny: back to the coelomata? *Curr Biol* 14, R274-276.

- Thies, E., and Mandelkow, E.M. (2007). Missorting of tau in neurons causes degeneration of synapses that can be rescued by the kinase MARK2/Par-1. *J Neurosci* 27, 2896-2907.
- Timmons, L., Court, D.L., and Fire, A. (2001). Ingestion of bacterially expressed dsRNAs can produce specific and potent genetic interference in *Caenorhabditis elegans*. *Gene* 263, 103-112.
- Timmons, L., and Fire, A. (1998). Specific interference by ingested dsRNA. *Nature* 395, 854.
- Tofaris, G.K., Layfield, R., and Spillantini, M.G. (2001). alpha-synuclein metabolism and aggregation is linked to ubiquitin-independent degradation by the proteasome. *FEBS Lett* 509, 22-26.
- Tonoki, A., Kuranaga, E., Tomioka, T., Hamazaki, J., Murata, S., Tanaka, K., and Miura, M. (2009). Genetic evidence linking age-dependent attenuation of the 26S proteasome with the aging process. *Mol Cell Biol* 29, 1095-1106.
- Toth, M.L., Melentijevic, I., Shah, L., Bhatia, A., Lu, K., Talwar, A., Naji, H., Ibanez-Ventoso, C., Ghose, P., Jevince, A., *et al.* (2012). Neurite Sprouting and Synapse Deterioration in the Aging *Caenorhabditis elegans* Nervous System. *J Neurosci* 32, 8778-8790.
- Touitou, R., Richardson, J., Bose, S., Nakanishi, M., Rivett, J., and Allday, M.J. (2001). A degradation signal located in the C-terminus of p21WAF1/CIP1 is a binding site for the C8 alpha-subunit of the 20S proteasome. *EMBO J* 20, 2367-2375.
- Turmaine, M., Raza, A., Mahal, A., Mangiarini, L., Bates, G.P., and Davies, S.W. (2000). Nonapoptotic neurodegeneration in a transgenic mouse model of Huntington's disease. *Proc Natl Acad Sci U S A* 97, 8093-8097.
- Umeyama, T., Okabe, S., Kanai, Y., and Hirokawa, N. (1993). Dynamics of microtubules bundled by microtubule associated protein 2C (MAP2C). *J Cell Biol* 120, 451-465.
- Uptain, S.M., and Lindquist, S. (2002). Prions as protein-based genetic elements. *Annu Rev Microbiol* 56, 703-741.
- Uversky, V.N. (2008). Amyloidogenesis of natively unfolded proteins. *Curr Alzheimer Res* 5, 260-287.
- Van der Jeugd, A., Hochgrafe, K., Ahmed, T., Decker, J.M., Sydow, A., Hofmann, A., Wu, D., Messing, L., Balschun, D., D'Hooze, R., *et al.* (2012). Cognitive defects are

reversible in inducible mice expressing pro-aggregant full-length human Tau. *Acta Neuropathol* 123, 787-805.

van Swieten, J., and Spillantini, M.G. (2007). Hereditary frontotemporal dementia caused by Tau gene mutations. *Brain Pathol* 17, 63-73.

van Swieten, J.C., Stevens, M., Rosso, S.M., Rizzu, P., Joosse, M., de Koning, I., Kamphorst, W., Ravid, R., Spillantini, M.G., Niermeijer, *et al.* (1999). Phenotypic variation in hereditary frontotemporal dementia with tau mutations. *Ann Neurol* 46, 617-626.

Vanier, M.T., Neuville, P., Michalik, L., and Launay, J.F. (1998). Expression of specific tau exons in normal and tumoral pancreatic acinar cells. *J Cell Sci* 111 (Pt 10), 1419-1432.

Vassar, P.S., and Culling, C.F. (1959). Fluorescent stains, with special reference to amyloid and connective tissues. *Arch Pathol* 68, 487-498.

Voisine, C., Varma, H., Walker, N., Bates, E.A., Stockwell, B.R., and Hart, A.C. (2007). Identification of potential therapeutic drugs for huntington's disease using *Caenorhabditis elegans*. *PLoS One* 2, e504.

von Bergen, M., Barghorn, S., Li, L., Marx, A., Biernat, J., Mandelkow, E.M., and Mandelkow, E. (2001). Mutations of tau protein in frontotemporal dementia promote aggregation of paired helical filaments by enhancing local beta-structure. *J Biol Chem* 276, 48165-48174.

von Bergen, M., Barghorn, S., Muller, S.A., Pickhardt, M., Biernat, J., Mandelkow, E.M., Davies, P., Aebi, U., and Mandelkow, E. (2006). The core of tau-paired helical filaments studied by scanning transmission electron microscopy and limited proteolysis. *Biochemistry* 45, 6446-6457.

von Bergen, M., Friedhoff, P., Biernat, J., Heberle, J., Mandelkow, E.M., and Mandelkow, E. (2000). Assembly of tau protein into Alzheimer paired helical filaments depends on a local sequence motif ((306)VQIVYK(311)) forming beta structure. *Proc Natl Acad Sci U S A* 97, 5129-5134.

Wainwright, M., and Amaral, L. (2005). The phenothiazinium chromophore and the evolution of antimalarial drugs. *Trop Med Int Health* 10, 501-511.

Waldemar, G., Dubois, B., Emre, M., Georges, J., McKeith, I.G., Rossor, M., Scheltens, P., Tariska, P., and Winblad, B. (2007). Recommendations for the diagnosis and management of Alzheimer's disease and other disorders associated with dementia: EFNS guideline. *Eur J Neurol* 14, e1-26.

- Wang, D., Kennedy, S., Conte, D., Jr., Kim, J.K., Gabel, H.W., Kamath, R.S., Mello, C.C., and Ruvkun, G. (2005). Somatic misexpression of germline P granules and enhanced RNA interference in retinoblastoma pathway mutants. *Nature* 436, 593-597.
- Wang, J.Z., Gong, C.X., Zaidi, T., Grundke-Iqbal, I., and Iqbal, K. (1995). Dephosphorylation of Alzheimer paired helical filaments by protein phosphatase-2A and -2B. *J Biol Chem* 270, 4854-4860.
- Wang, J.Z., Grundke-Iqbal, I., and Iqbal, K. (1996). Glycosylation of microtubule-associated protein tau: an abnormal posttranslational modification in Alzheimer's disease. *Nat Med* 2, 871-875.
- Wang, Y., Kruger, U., Mandelkow, E., and Mandelkow, E.M. (2010). Generation of tau aggregates and clearance by autophagy in an inducible cell model of tauopathy. *Neurodegener Dis* 7, 103-107.
- Wang, Y., Martinez-Vicente, M., Kruger, U., Kaushik, S., Wong, E., Mandelkow, E.M., Cuervo, A.M., and Mandelkow, E. (2009). Tau fragmentation, aggregation and clearance: the dual role of lysosomal processing. *Hum Mol Genet* 18, 4153-4170.
- Wang, Y.P., Biernat, J., Pickhardt, M., Mandelkow, E., and Mandelkow, E.M. (2007). Stepwise proteolysis liberates tau fragments that nucleate the Alzheimer-like aggregation of full-length tau in a neuronal cell model. *Proc Natl Acad Sci U S A* 104, 10252-10257.
- Webb, J.L., Ravikumar, B., Atkins, J., Skepper, J.N., and Rubinsztein, D.C. (2003). Alpha-Synuclein is degraded by both autophagy and the proteasome. *J Biol Chem* 278, 25009-25013.
- Weimer, R.M., Richmond, J.E., Davis, W.S., Hadwiger, G., Nonet, M.L., and Jorgensen, E.M. (2003). Defects in synaptic vesicle docking in unc-18 mutants. *Nat Neurosci* 6, 1023-1030.
- Weingarten, M.D., Lockwood, A.H., Hwo, S.Y., and Kirschner, M.W. (1975). A protein factor essential for microtubule assembly. *Proc Natl Acad Sci U S A* 72, 1858-1862.
- Weisberg, R.A., Enquist, L.W., Foeller, C., and Landy, A. (1983). Role for DNA homology in site-specific recombination. The isolation and characterization of a site affinity mutant of coliphage lambda. *J Mol Biol* 170, 319-342.
- White, J. (1988). The Anatomy. In *The nematode C. elegans* (ed. W.B. Wood), pp.81-122, Cold Spring Harbor, New York.

- Wickner, S., Maurizi, M.R., and Gottesman, S. (1999). Posttranslational quality control: folding, refolding, and degrading proteins. *Science* 286, 1888-1893.
- Wille, H., Drewes, G., Biernat, J., Mandelkow, E.M., and Mandelkow, E. (1992). Alzheimer-like paired helical filaments and antiparallel dimers formed from microtubule-associated protein tau in vitro. *J Cell Biol* 118, 573-584.
- Williamson, R., Scales, T., Clark, B.R., Gibb, G., Reynolds, C.H., Kellie, S., Bird, I.N., Varndell, I.M., Sheppard, P.W., Everall, I., *et al.* (2002). Rapid tyrosine phosphorylation of neuronal proteins including tau and focal adhesion kinase in response to amyloid-beta peptide exposure: involvement of Src family protein kinases. *J Neurosci* 22, 10-20.
- Winston, W.M., Molodowitch, C., and Hunter, C.P. (2002). Systemic RNAi in *C. elegans* requires the putative transmembrane protein SID-1. *Science* 295, 2456-2459.
- Wischik, C.M., Edwards, P.C., Lai, R.Y., Roth, M., and Harrington, C.R. (1996). Selective inhibition of Alzheimer disease-like tau aggregation by phenothiazines. *Proc Natl Acad Sci U S A* 93, 11213-11218.
- Wischik, C.M., Novak, M., Edwards, P.C., Klug, A., Tichelaar, W., and Crowther, R.A. (1988a). Structural characterization of the core of the paired helical filament of Alzheimer disease. *Proc Natl Acad Sci U S A* 85, 4884-4888.
- Wischik, C.M., Novak, M., Thogersen, H.C., Edwards, P.C., Runswick, M.J., Jakes, R., Walker, J.E., Milstein, C., Roth, M., and Klug, A. (1988b). Isolation of a fragment of tau derived from the core of the paired helical filament of Alzheimer disease. *Proc Natl Acad Sci U S A* 85, 4506-4510.
- Wisniewski, T., Ghiso, J., and Frangione, B. (1991). Peptides homologous to the amyloid protein of Alzheimer's disease containing a glutamine for glutamic acid substitution have accelerated amyloid fibril formation. *Biochem Biophys Res Commun* 179, 1247-1254.
- Wittmann, C.W., Wszolek, M.F., Shulman, J.M., Salvaterra, P.M., Lewis, J., Hutton, M., and Feany, M.B. (2001). Tauopathy in *Drosophila*: neurodegeneration without neurofibrillary tangles. *Science* 293, 711-714.
- Wong, E., and Cuervo, A.M. (2010). Autophagy gone awry in neurodegenerative diseases. *Nat Neurosci* 13, 805-811.
- Wood, W.B. (1988). Determination of pattern and fate in early embryos of *Caenorhabditis elegans*. *Dev Biol (N Y 1985)* 5, 57-78.

Wszolek, Z.K., Tsuboi, Y., Ghetti, B., Pickering-Brown, S., Baba, Y., and Cheshire, W.P. (2006). Frontotemporal dementia and parkinsonism linked to chromosome 17 (FTDP-17). *Orphanet J Rare Dis* 1, 30.

Yan, S.D., Chen, X., Schmidt, A.M., Brett, J., Godman, G., Zou, Y.S., Scott, C.W., Caputo, C., Frappier, T., Smith, M.A., *et al.* (1994). Glycated tau protein in Alzheimer disease: a mechanism for induction of oxidant stress. *Proc Natl Acad Sci U S A* 91, 7787-7791.

Yankner, B.A., Lu, T., and Loerch, P. (2008). The aging brain. *Annu Rev Pathol* 3, 41-66.

Yin, H.S., Chou, H.C., and Chiu, M.M. (1995). Changes in the microtubule proteins in the developing and transected spinal cords of the bullfrog tadpole: induction of microtubule-associated protein 2c and enhanced levels of Tau and tubulin in regenerating central axons. *Neuroscience* 67, 763-775.

Yoshida, H., and Ihara, Y. (1993). Tau in paired helical filaments is functionally distinct from fetal tau: assembly incompetence of paired helical filament-tau. *J Neurochem* 61, 1183-1186.

Zempel, H., Thies, E., Mandelkow, E., and Mandelkow, E.M. (2010). Abeta oligomers cause localized Ca(2+) elevation, missorting of endogenous Tau into dendrites, Tau phosphorylation, and destruction of microtubules and spines. *J Neurosci* 30, 11938-11950.

Zhang, J.Y., Liu, S.J., Li, H.L., and Wang, J.Z. (2005). Microtubule-associated protein tau is a substrate of ATP/Mg(2+)-dependent proteasome protease system. *J Neural Transm* 112, 547-555.

Zheng-Fischhofer, Q., Biernat, J., Mandelkow, E.M., Illenberger, S., Godemann, R., and Mandelkow, E. (1998). Sequential phosphorylation of Tau by glycogen synthase kinase-3beta and protein kinase A at Thr212 and Ser214 generates the Alzheimer-specific epitope of antibody AT100 and requires a paired-helical-filament-like conformation. *Eur J Biochem* 252, 542-552.

7 Appendix

7.1 Abbreviations

A β	Amyloid- β peptide
ABAD	A β -binding alcohol dehydrogenase
ACTH	Adrenocorticotrophic hormone
AD	Alzheimer's disease
ADDLs	A β -derived diffusible ligands
ADP	Adenosine diphosphate
ALS	Amyotrophic lateral sclerosis
AMP	Adenosine monophosphate
ANOVA	Analysis of variance
APOE	Apolipoprotein E
APP	Amyloid precursor protein
APS	Ammonium persulfate
ATP	Adenosine triphosphate
ATPZ	Aminothienopyridazine
BBB	Blood brain barrier
BCA	Bicinchoninic acid
BMB	Bromophenol blue
BRSK	Brain specific kinase
BSA	Bovine serum albumin
CaCl ₂	Calcium chloride
CAST	Calpastatin
CD	Circular dichroism spectroscopy
CDK	Cyclin dependent kinase
CHAP	(3-[(3-Cholamidopropyl) dimethylammonio]-1-propane sulfonate)
CHIP	Carboxyl terminus of Hsp70-interacting protein
CHO	Chinese hamster ovary
Cmp16	Compound 16
CNS	Central nervous system
CREB	cAMP response element binding protein

CSF	Cerebrospinal fluid
Da	Dalton
DDPAC	Disinhibition-dementia-parkinsonism-amyotrophy complex
DIV	Days <i>in vitro</i>
DMSO	Dimethylsulfoxide
DNA	Deoxyribonucleic acid
DTT	Dithiothreitol
ECL	Enhanced chemiluminescence light
EDTA	Ethylene diamine tetraacetic acid
EF	Endotoxin free
EGTA	Ethylene glycol tetraacetic acid
ER	Endoplasmic reticulum
EthD	Ethidium homodimer
FA	Formic acid
FAD	Familial Alzheimer's disease
FBS	Fetal bovine serum
FL-Tau	Full-length Tau
FL V337M Tau	Full-length Tau with V337M mutation
FTDP-17	Frontotemporal dementia and parkinsonism linked to chromosome 17
FUdR	Floxuridine (5-fluorodeoxyuridine)
GFP	Green fluorescent protein
GRK	G-protein coupled receptor kinase
GSK-3 β	Glycogen synthase kinase 3 β
GSS	Gerstmann-Scheinker-Sträussler syndrome
HBSS	Hank's buffered salt solution
HCl	Hydrochloric acid
HClO ₄	Perchloric acid
HD	Huntington disease
HFIP	1,1,1,3,3,3-hexafluoro-2-propanol
H ₂ O ₂	Hydrogen peroxide

HPLC	High pressure liquid chromatography
Hsc70	Heat shock cognate 70
<i>hsf-1</i>	Heat shock factor 1
Hsp70	Heat shock protein 70
IGF-1	Insulin-like growth factor 1
IPTG	Isopropyl β -D-1-thiogalactopyranoside
kDa	Kilo-Dalton
LB	Luria-Bertani
LDH	Lactate dehydrogenase
MAP	Microtubule associated protein
MAPK	Mitogen activated protein kinase
MAPT	Microtubule associated protein Tau
MARK	Microtubule-affinity regulating kinase
MB	Methylene blue
MBq	Megabecquerel
MCS	Multiple cloning site
MEM	Modified essential medium
mg	Miligram
MgCl ₂	Magnesium chloride
MHC	Major histocompatibility complex
ml	Mililitre
mM	Milimolar
mRNA	Messenger ribonucleic acid
Mr	Apparent relative molecular weight
MSTD	Familial multiple system tauopathy with presenile dementia
mt	Mitochondria
MT	Microtubule
MTT	3-(4,5-dimethylthiazol-2-yl)-2,5-diphenyltetrazolium bromide
MW	Molecular weight
N2	Normal wild-type laboratory

	<i>C. elegans</i> strain
NaCl	Sodium chloride
NADH	Nicotinamide adenine dinucleotide
NADPH	Nicotinamide adenine dinucleotide phosphate
NaF	Sodium fluoride
NaHCO ₃	Sodium bicarbonate
NaN ₃	Sodium nitrite
NaOCl	Sodium hypochlorite
Na ₃ VO ₄	Sodium vandate
NFTs	Neurofibrillary tangles
ng	Nanogram
NGM	Nematode growth medium
NH ₄ Cl	Ammonium chloride
NH ₄ HCO ₃	Ammonium bicarbonate
nm	Nanometre
nM	Nanomolar
NMDA	N-methyl-D-aspartate
NP40	Nonyl phenoxypolyethoxylethanol
OA	Okadaic acid
OD	Optical density
PARP	Poly (ADP) ribose polymerase
PBS	Phosphate buffered saline
PCR	Polymerase chain reaction
PD	Parkinson's disease
PDC	Parkinson-dementia complex
PDPKs	Proline directed protein kinases
PHF	Paired helical filament
PKA	Cyclic AMP-dependent protein kinase A
pmol	Picomolar
PMSF	Phenylmethylsulfonylfluoride
PNS	Peripheral nervous system
PPND	Pallid-ponto-nigral degeneration

PS	Presenilins
PSA	Puromycin sensitive aminopeptidase
p-Tau	Phospho-Tau
PTH	Phenylthiohydantoin
PVDF	Polyvinylidene fluoride
RAB	Release assay buffer
RIPA buffer	Radioimmunoprecipitation assay buffer
RNAi	Ribonucleic acid interference
rpm	Revolutions/rotations per minute
SAD	Sporadic Alzheimer's disease
SADK	Synapses of Amphids Defective Family Kinases
SDS	Sodium dodecyl sulfate
SDS-PAGE	SDS-polyacrylamide gel electrophoresis
SFKs	Src Family kinases
SNB	Synaptobrevin
SP	Senile plaques
SW-PCR	Single worm polymerase chain reaction
TAE	Tris-Acetate-EDTA buffer
Tau	Tubulin-associated unit
TBST	Tris buffer saline containing tween
Tg	Transgenic
ThS	Thioflavin S
ThT	Thioflavin T
U/mg	Units per milligram
UV	Ultraviolet
WLB	Worm lysis buffer
w/v	Weight/volume
Wt	Wildtype
3xTg	Triple transgenic
3R	3 repeat Tau domain
4R	4 repeat Tau domain
B-Me	β -mercaptoethanol

Δ	Deletion
μg	Microgram
μl	Microlitre
μM	Micromolar
μm	Micrometre

7.2 Protein sequences

Protein sequence of Tau (longest isoform in CNS, 441 residues)

```

1  maepqrqefev medhagtygl gdrkdqggyt mhqdqegdtd aglkesplqt ptedgseepg
61  setsdakstp taedvtaplv degapgkqaa aqphteipeg ttaeeagigd tpsledeaag
121 hvtqarmvsk skdgtgsddk kakgadggtk iatprgaapp gqkgqanatr ipaktppapk
181 tppssgeppk sgdrsgyssp gspgtpgsrs rtpsltppt repkkvavvr tppkspssak
241 srlqtapvpm pdlknvkski gstenlkhqp gggkvqiink kldlsnvqsk cgskdni khv
301 pgggsvqivy kpvdlskvts kcsglnihh kpgggqvevk sekldfkdrv qskigsldni
361 thvpgggnkk iethkltfre nakaktdhga eivykspvvs gdt sprhlsn vsstgsidmv
421 dspqlatlad evsaslakqg l

```

(Genbank accession no: NP_005901) (Goedert et al., 1989a)

Protein sequence of hTau40ΔK280

```

1      MAEPRQEFEV MEDHAGTYGL GDRKDQGGYT MHQDQEGDTD
      AGLKESPLQT
51     PTEDGSEEPG SETSDAKSTP TAEDVTAPLV DEGAPGKQAA AQPHTEIPEG
101    TTAAEEAGIGD TPSLEDEAAG HVTQARMVSK SKDGTGSDDK
      KAKGADGGTK
151    IATPRGAAPP GQKGQANATR IPAKTPPAPK TPPSSGEPPK SGDRSGYSSP
201    GSPGTPGSRS RTPSLTPPT REPKKVAVVR TPPKSPSSAK SRLQTAPVPM
251    PDLKNVSKI GSTENLKHQP GGGKVQIINK LDLSNVQSKC GSKDNIKHVP
301    GGGSQIVYK PVDLSKVTSK CGSLGNIHHK PGGGQVEVKS
      EKLDKDRVQ
351    SKIGSLDNIT HVPGGGNKKI ETHKLTREN AKAKTDHGAE IVYKSPVVS
401    DTSRHLNSV SSTGSIDMVD SPQLATLADE VSASLAKQGL *

```

Protein sequence of anti-aggregant hTau40ΔK280PP

1 MAEPRQEFV MEDHAGTYGL GDRKDQGGYT MHQDQEGDTD
 AGLKESPLQT
 51 PTEDGSEEPG SETSDAKSTP TAEDVTAPLV DEGAPGKQAA AQPHTEIPEG
 101 TTAEAEAGIGD TPSLEDEAAG HVTQARMVSK SKDGTGSDDK
 KAKGADGKTK
 151 IATPRGAAPP GQKGQANATR IPAKTPPAPK TPPSSGEPPK SGDRSGYSSP
 201 GSPGTPGSRs RTPSLPTPPT REPKKVAVVR TPPKSPSSAK SRLQTAPVPM
 251 PDLKNVSKI GSTENLKHQP GGGK**VQPINK** LDLSNVQSKC GSKDNIKHVP
 301 GGG**VQPVYK** PVDLSKVTSK CGSLGNIHHK PGGGQVEVKS EKLDKDRVQ
 351 SKIGSLDNIT HVPGGGNKKI ETHKLTFRN AKAKTDHGAE IVYKSPVVS
 401 DTSRHLNSV SSTGSIDMVD SPQLATLADE VSASLAKQGL *

Protein sequence of pro-aggregant repeat domain K18ΔK280

1 MQTAPVPMPD LKNVSKIGS TENLKHQPGG GK**VQIINK**LD LSNVQSKCGS
 51 KDNIKHVP GG GS**VQIVYK**PV DLSKVTSKCG SLGNIHHKPG GGQVEVKSEK
 101 LDFKDRVQSK IGSLDNITHV PGGGNKKIE*

Protein sequence of anti-aggregant repeat domain K18ΔK280PP

1 MQTAPVPMPD LKNVSKIGS TENLKHQPGG GK**VQPINK**LD LSNVQSKCGS
 51 KDNIKHVP GG GS**VQPVYK**PV DLSKVTSKCG SLGNIHHKPG GGQVEVKSEK
 101 LDFKDRVQSK IGSLDNITHV PGGGNKKIE*

Protein sequence of pro-aggregant repeat fragment F3ΔK280

1 MSKIGSTENL KHQPGGGK**VQ IINK**LDLSNV QSKCGSKDNI KHVPGGGS**VQ**
 51 **IVYK**PVDLSK VTSKCGSLGN IHHKPGGGQV EVKSEKLDFK DRVQSKIGSL
 101 DNI*

Protein sequence of pro-aggregant repeat fragment F3ΔK280PP

1 MSKIGSTENL KHQPGGGK**VQ PINK**LDLSNV QSKCGSKDNI KHVPGGGS**VQ**
 51 **PVYK**PVDLSK VTSKCGSLGN IHHKPGGGQV EVKSEKLDFK DRVQSKIGSL
 101 DNI*

7.3 Oligonucleotide sequences

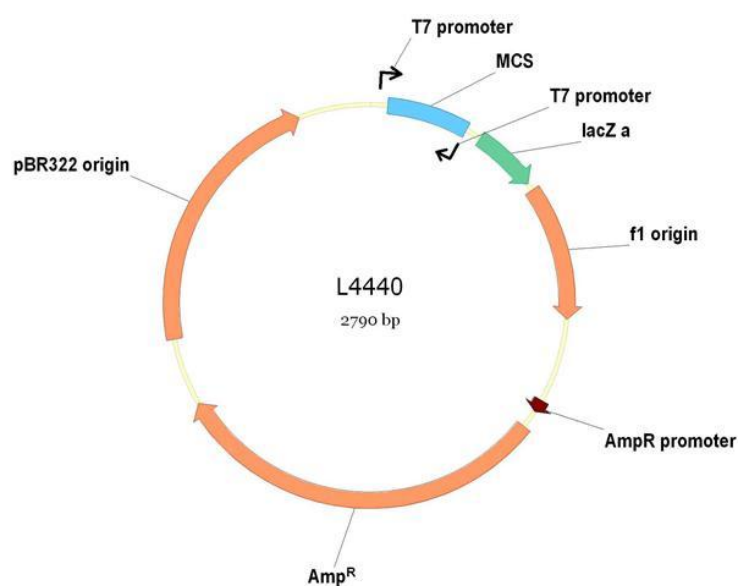
Unc N-t	GGGCTGCTCATCTAATCTTTTGTCATTTTGTC
Unc C-t	CGGCATCCGCTTACAGACAAG
NcoKpn K18 Nt	CCATGGTACCATGCAGACAGCCCCCGTG
K18 EcoRI Ct	GAATTCCTATTCAATCTTTTTATTTCCTCCGCC
Unc-25 XbaI Nt	CTCTAGAAAAAACACCCACTTTTGTATCTCAAA TTTGCACTTATTAAG
Unc-25 NcoI Ct	CCCATGGGGCGGTGAACTGAGCTTTTCCC TATTCC
F3 NcoKpn Nt	CCCATGGTACCATGTCCAAGATCGGCTCCA CTGAG
F3 EcoRI Ct	GGAATTCCTAGATATTGTCCAGGGACCCAA TCTTC
Ht40 KpnNco Nt	GGGTACCATGGCTGAGCCCCGCCAG
Ht40 EcoRI Ct	GGAATTCTCACAAACCCTGCTTGGCCAGG
Htau SpeI Ct	AACTAGTCTCACAAACCCTGCTTGGCCAGG
Ht40 EcoRIEagI	CCGGCCGAATTCTCACAAACCCTGCTTGGCC AGG
K18 EcoRIEagI	CCGGCCGAATTCCTATTCAATCTTTTTATTTC CTCCGCC
F3 EcoRIEagI	CCGGCCGAATTCCTAGATATTGTCCAGGGA CCCAATCTTC
K18 Nt pRab	GTGCCCATGCCAGACCTGAA
pRab Ct	GGGAACAAAAGCTGGCGTTA
K18 Nt Punc	GTGCCCATGCCAGACCTGAA
Punc25 Ct	AAATTTGTTATCCGCGGCCG
Paex3 1	ATCACACGGAAATCTGTTTT
(pCJ151 Fwd)	
Paex3 2	TCTCTCCCTCTATTGATTTG
Paex3 3	AAATATTGGATGTCGTGGGA
Paex3 4	CCAGTCAAATGAAGTCCAAA
Paex3 5	TAATTTCTTCTGTTCCGTTT

Paex3 6	GGATAGGTACATTGGTGCAA
Paex3 7 (pCJ151 Rev)	CCGTTACGAAACAGACTGAT
ECFP KpnNco Fwd	CGGTACCATGGTGAGCAAGGGCGAGGAG
ECFP NdXhEcEag Rev	CCGGCCGAATTCCTCGAGCATATGCTTGT ACAGCTCGTCCATGCCGAG
Ptl-1A NdeI fwd	CCATATGTCAACCCCTCAATCAGAGCCTGGA TCCG
Ptl-1A NheI rev	GGCTAGCTCAGCGATTGAATATAAAATCAG GAGAAAGAGGATAAATGGC
Ptl-1B NheI rev	GGCTAGCTCAATTATTGTGGCCGTCATCATT TTTGGTCGAC
Ptl1-1	TTCCGGTTCAGGTTCCGGGC
Ptl1-2	TCGAATCTCCTCCTCGAGAACAAG
Ptl1-3	TCGAGCTCTCTCGGAGCGATATC
Ptl1-4	AGTACACCAAGACAAACTGCTTCAAC
Ptl1-5	ATCGAAAACAGGAAGCTAGATTTTTC
Ptl1-6	ACTATCTTCACGTCAGACTTTGCTGG
Ptl1-7	AGTCAAAAATTGAACTGGAAAGCC
Ptl-1A Rpt NdeI	CCATATGGGAAGAATGAACGCCAAAGGTT AACGCCAAATTTGTAAAT
Ptl1 s	GAAGGAGATATACATATGGGAAGAATGACGC CAAAGG
Ptl1 as	CCTTTGGCGTCATTCTTCCCATATGTATAT CTCCTTC
Paex-3 SpeI fwd	GACTAGTAGCTTAGCTTCCACAAAACTGCCG
Htau BamHI fwd	GGGATCCATGGCTGAGCCCCGCCAG
Htau XhoIBamHI rev	CGGATCCCTCGAGTCACAAACCCTGCTTGGC CAGG
Htau40attB1 fwd	GGGGACAAAGTTTGTACAAAAAAGCAGGCT CCACCATGGCTGAGCCCCGCCAG
Htau40attB2 rev	GGGGACCACTTTGTACAAGAAAGCTGGGTAT CACAAACCCTGCTTGGCCAGG

F3attB1 fwd	GGGGACAAGTTTGTACAAAAAAGCAGGC TCCACCATGTCCAAGATCGGCTCCACTGAG
F3attB1 rev	GGGGACCACTTTGTACAAGAAAGCTGGG TACTAGATATTGTCCAGGGACCCAATCTTC
Stop del s	CATGGACGAGCTTTATAAGGCAAGCGGCCG CATGGCTGAG
Stop del as	CTCAGCCATGCGGCCGCTTGCCTTATAAAGC TCGTCCATG
Ht40 NotI Fwd	GGCGGCCGCATGGCTGAGCCCCGCCAG
Ht40 XbaEcoRV rev	TATCTAGAGATATCGGATCCGTGATCAC AAACCCTGCTTGGCCAG
CFP KpnNco fwd	CGGTACCATGGTGAGCAAGGGCGAGGAG
F3 XbaEcoRV rev	CGATATCTAGACTAGATATTGTCCAGGGACCC AATCTTC
F3 SalI rev	GATATCGTCGACTGACTAGATATTGTCCAGG GACCCAATCTTC
Mt-F3 ClaI Fwd	ATCGATGGCCCCATACTCCCTCCTCGTGACTC GGCTCCAAAAGGCGCTCGGCGTGCGGCAATACCACG TGGCCTCCGTGCTCTGTCAACGGGCCAAGGTGGCGAT GTCCTCCAAGATCGG
SP-F3 ClaI Fwd	CCGCATCGATATGAAGCTCTCCCTGGTGGCCG CGATGCTGCTGCTGCTCAGCGCGGCGGGCCGAGT CCAAGATCGGCTCCACTG
F3-KDEL SalI rev	CCAGTCTAGAGATATCGTCGACGGATCCTGAC TACAACTCATCTTTGATATTGTCCAGGGAC CCAAT
SP-K18 ClaI fwd	CCGCATCGATATGAAGCTCTCCCTGGTGGC CGCGATGCTGCTGCTGCTCAGCGCGGCGCGGGC CGAGCGACAGCCCCCGTGCCCATG
K18-KDEL SalI rev	CCAGTCTAGAGATATCGTCGACGGATCCTGA

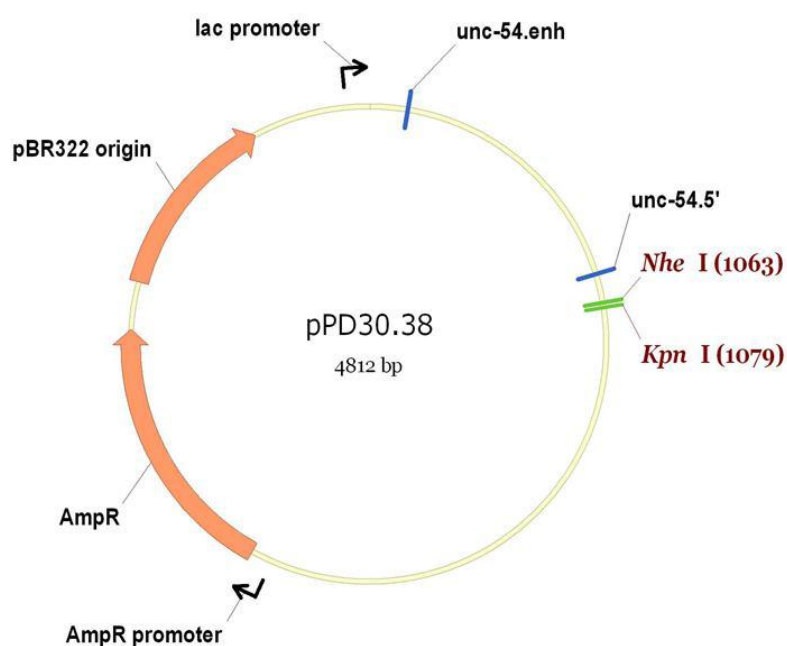
	CTACAACTCATCTTTTTCAATCTTTTTATTTCCTCCGCC AGG
Mt-K18 ClaI fwd	ATCGATGGCCCCATACTCCCTCCTCGTGAC TCGGCTCCAAAAGGCGCTCGGCGTGCGGCAATACCA CGTGGCCTCCGTGCTCTGTCAACGGGCCAAGGTGGCG GTCCCAGACAGCCCC
K18 SalI rev	GATATCGTCGACTGACTATTCAATCTTTTTATT TCCTCCGCCAGG
K18-KDEL XbaI rev	CTTATCTAGAAGCCTACAACTCATCTTTTTCAAT CTTTTTATTTCCTCC
Mt-signal SalI Fwd	CCGTCGACACCATGGCCCCATACTCCCTCCT CGTG
K18 XbaI rev	CTTATCTAGAAGCCTATTCAATCTTTTTATTTC CTCCGCCAGGG
SP-signal SalI Fwd	CCGTCGACACCATGAAGCTCTCCCTGGTGGCCG
F3 XbaI rev	CTTATCTAGAAGCCTAGATATTGTCCAGGGAC CCAATCTTCG
F3-KDEL XbaI rev	CTTATCTAGAAGCCTACAACTCATCTTTGATA TTGTCCAGGGACC
K18 SalI fwd	CCGTCGACACCATGTCCAAGATCGGCTCCA CTGAG

2.1.6 Vectors



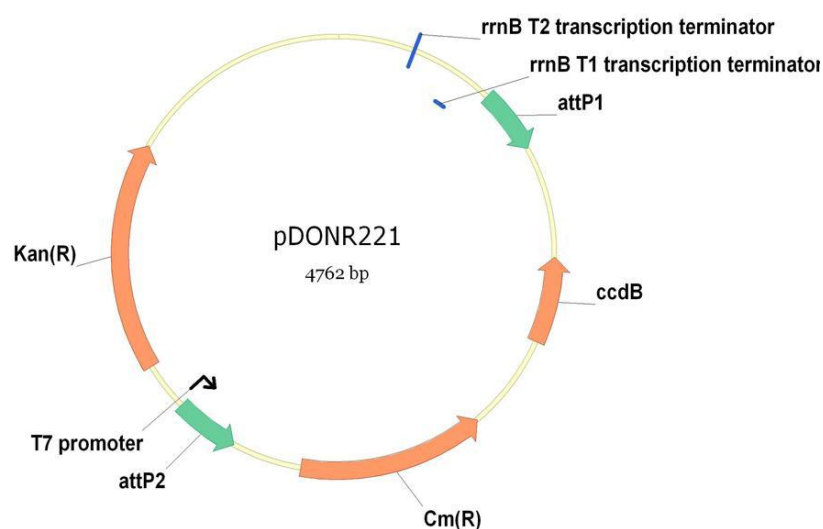
Plasmid-map of RNAi feeding vector L4440.

Note the multiple cloning site (MCS) between the two convergent T7 promoters. The T7 promoters drive expression of sense and antisense insert sequence (Timmons and Fire, 1998).

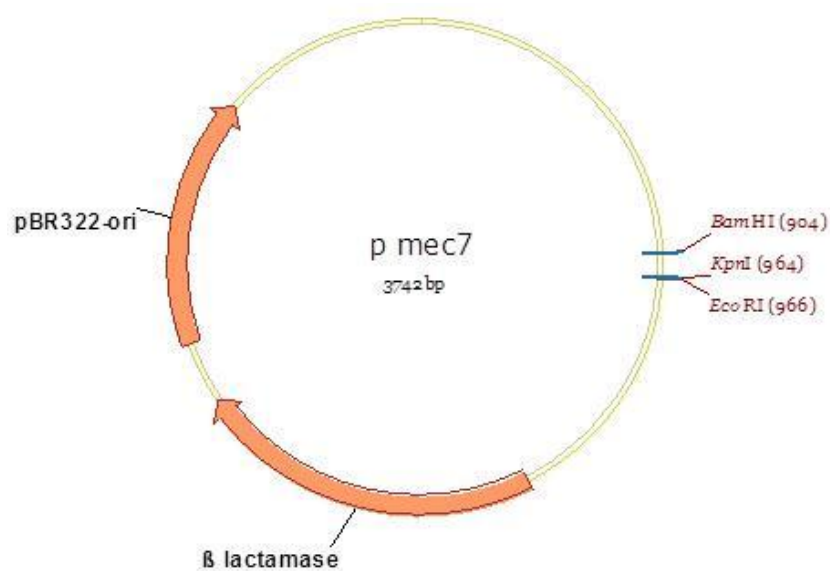


Plasmid-map of pPD30.38.

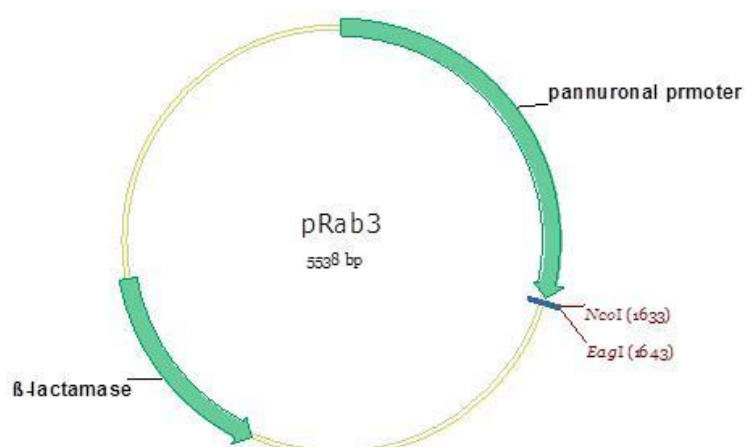
C. elegans expression vector containing body wall muscle specific promoter unc-54. NheI and KpnI restriction sites for the insertion of tau are highlighted (Mello and Fire, 1995).



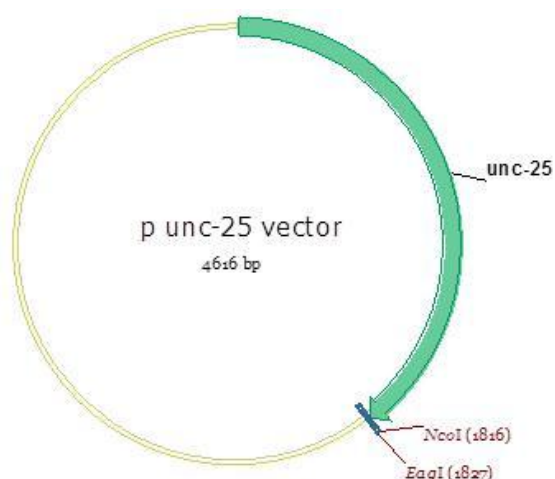
Plasmid-map of pDONR221. Entry vector for Gateway® cloning (Invitrogen, Karlsruhe, Germany).



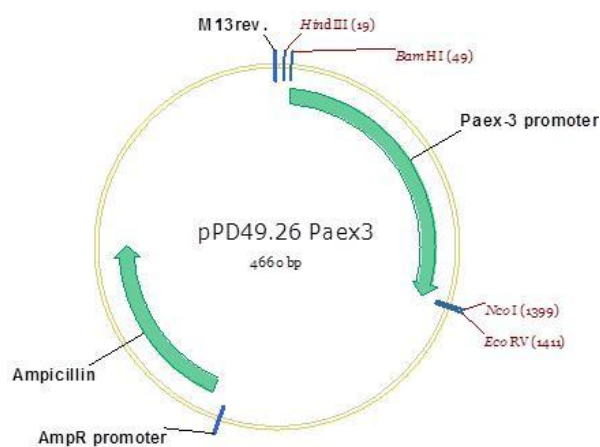
***C. elegans* expression vector containing mechanosensory neuron specific mec7 promoter** (gift of Dr. Sandhya P. Koushika, NCBS, TIFR, Bangalore, India). KpnI and EcoRI restriction sites for the insertion of genomic sequence of Tau are highlighted.



***C. elegans* expression vector containing pan neuronal rab3 promoter** (gift of Dr. Sandhya P. Koushika, NCBS, TIFR, Bangalore, India). NcoI and EagI restriction sites for the insertion of genomic sequence of Tau are highlighted.



***C. elegans* expression vector containing motor neuron specific unc-25 promoter** (gift of Dr. Sandhya P. Koushika, NCBS, TIFR, Bangalore, India). NcoI and EagI restriction sites for the insertion of genomic sequence of Tau are highlighted.



***C. elegans* expression vector containing pan neuronal aex-3 promoter** (gift of Dr. Daniele Bano, DZNE, Bonn, Germany). NcoI and EcoRV restriction sites for the insertion of genomic sequence of Tau are highlighted.

List of figures

Figure 1.1	Pathological hallmarks of Alzheimer's disease	4
Figure 1.2	Tau isoforms generated by alternative splicing of a single human Tau gene	9
Figure 1.3	Tau gene mutations in FTDP-17	11
Figure 1.4	Tau phosphorylation sites	14
Figure 1.5	Tau hypothesis of AD	16
Figure 1.6	Proteocleavage sites on Tau	17
Figure 1.7	Amyloid cascade hypothesis of AD	21
Figure 1.8	Life-cycle of hermaphrodite <i>C. elegans</i> at 22°C	26
Figure 1.9	The two cladistics trees suggested by recent evolutionary analyses	28
Figure 2.1	Diagram illustrating epitopes of Tau antibodies	36
Figure 2.2	Schematic view of TOPO blunt end ligation	46
Figure 2.3	Schematic view of the BR and LR reaction occurring during the Gateway™ cloning	49
Figure 3.1	Single worm PCR analysis to detect the presence of transgenes	66
Figure 3.2	Tau expression by immunoblotting using K9JA pan Tau antibody	67
Figure 3.3	Western blot of total lysates from L4 larvae and 5 day old adult worms using 2.5% perchloric acid extraction	69
Figure 3.4	Locomotion defects upon pan-neuronal expression of pro-aggregant human Tau transgenes	70
Figure 3.5	Food clearance assay	71
Figure 3.6	Aging graph of <i>C. elegans</i>	72
Figure 3.7	Panneuronal expression of FL Tau v337M along with F3ΔK280 leads to deposition of aggregates in <i>C. elegans</i>	73
Figure 3.8	Insoluble Tau aggregates accumulate in the pro-aggregant strain starting at day 1 of adulthood	75
Figure 3.9	RNAi against Tau ameliorates the phenotype in pro-aggregant animals	76

Figure 3.10	Tau solubility using two step protocol	77
Figure 3.11	Sequential extraction of Tau from 7-day-old adult animals using the old Protocol	78
Figure 3.12	Sequential extraction of Tau from 7-day-old adult animals using the modified Protocol	79
Figure 3.13	Pro-aggregant animals show structural defects in the GABAergic and cholinergic motor neurons	80
Figure 3.14	Pro-aggregation strain shows pronounced hyperphosphorylation of Tau	82
Figure 3.15	Blot from soluble and insoluble tau showing extra bands common to all as detected by 12E8 antibody	83
Figure 3.16	Sarkosyl extraction of Tau from synchronized 9-day old adult worms	85
Figure 3.17	Pro-aggregant animals display defective presynaptic structures and organization already at early adulthood	87
Figure 3.18	Mitochondria mislocalize to the proximal axonal segment of the DA9 neuron in pro-aggregation strain	89
Figure 3.19	Pro-aggregant Tau transgenic worms show defective mitochondrial transport in the axons of mechanosensory neurons	91
Figure 3.20	Compound treatment of wild-type N2 strain	93
Figure 3.21	Treatment of pro-aggregation strain with the anti-aggregation compounds can ameliorate the phenotype	94
Figure 3.22	Sequential extraction of Tau from synchronized pro-aggregant animals after treatment with aggregation inhibitor compounds	95
Figure 3.23	Methylene blue treatment leads to partial amelioration of phenotype along with reduction in detergent insoluble Tau	97
Figure 3.24	Trehalose treatment leads to partial amelioration of phenotype along with reduction in detergent insoluble Tau	99
Figure 3.25	Trehalose increases the autophagy level	101

Figure 4.1	Model figure	116
------------	--------------	-----

Table 1	Human diseases associated with formation of extracellular amyloid deposits or intracellular inclusions with amyloid-like characteristics	2
---------	--	---

Inhibition of tau aggregation in a novel *Caenorhabditis elegans* model of tauopathy mitigates proteotoxicity

Chronis Fatouros^{1,2,4,5,†}, Ghulam Jeelani Pir^{6,7,†}, Jacek Biernat^{6,7},
Sandhya Padmanabhan Koushika⁹, Eckhard Mandelkow^{6,7,8}, Eva-Maria Mandelkow^{6,7,8},
Enrico Schmidt^{1,2,4,†,¶} and Ralf Baumeister^{1,2,3,4,*,†}

¹Faculty of Biology, Institute of Biology III, ²Faculty of Medicine, Center for Biochemistry and Molecular Cell Research (ZBMZ) and ³Center for Biological Signalling Studies (BIOS) and Freiburg Center for Advanced Studies (FRIAS), University of Freiburg, 79104 Freiburg, Germany, ⁴Center for Biological Systems Analysis (ZBSA), 79104 Freiburg, Germany, ⁵International Max Planck Research School for Molecular and Cell Biology (IMPRS-MCB), Freiburg, Germany, ⁶German Center for Neurodegenerative Diseases (DZNE), 53175 Bonn, Germany, ⁷Max Planck Institute for Neurological Research (MPINF), 50931 Cologne, Germany, ⁸CAESAR Research Center, 53175 Bonn, Germany and ⁹Department of Biological Sciences, Tata Institute of Fundamental Research, Homi Bhabha Road, Mumbai 400 005, India

Received February 21, 2012; Revised and Accepted May 14, 2012

Increased Tau protein amyloidogenicity has been causatively implicated in several neurodegenerative diseases, collectively called tauopathies. In pathological conditions, Tau becomes hyperphosphorylated and forms intracellular aggregates. The deletion of K280, which is a mutation that commonly appears in patients with frontotemporal dementia with Parkinsonism linked to chromosome 17, enhances Tau aggregation propensity (pro-aggregation). In contrast, introduction of the I277P and I308P mutations prevents β -sheet formation and subsequent aggregation (anti-aggregation). In this study, we created a tauopathy model by expressing pro- or anti-aggregant Tau species in the nervous system of *Caenorhabditis elegans*. Animals expressing the highly amyloidogenic Tau species showed accelerated Tau aggregation and pathology manifested by severely impaired motility and evident neuronal dysfunction. In addition, we observed that the axonal transport of mitochondria was perturbed in these animals. Control animals expressing the anti-aggregant combination had rather mild phenotype. We subsequently tested several Tau aggregation inhibitor compounds and observed a mitigation of Tau proteotoxicity. In particular, a novel compound that crosses the blood–brain barrier of mammals proved effective in ameliorating the motility as well as delaying the accumulation of neuronal defects. Our study establishes a new *C. elegans* model of Tau aggregation-mediated toxicity and supports the emerging notion that inhibiting the nucleation of Tau aggregation can be neuroprotective.

INTRODUCTION

Aggregation of mutant or even wild-type, hyperphosphorylated Tau is a common factor in the course of several

neurodegenerative diseases collectively called tauopathies (1–5). An unresolved debate in the field focuses on the role of terminal Tau aggregates termed neurofibrillary tangles for the pathogenesis of the disease. It is still unclear whether

*To whom correspondence should be addressed at: Institute of Biology III, Schaezlestrasse 1, D-79104 Freiburg, Germany. Tel: +49 7612038350; Fax: +49 761203831; Email: baumeister@celegans.de

[†]These authors contributed equally to this paper.

[¶]Present address: Center for Proteomic Chemistry, Novartis Pharma AG, Basel, Switzerland.

these are the cause of neuronal toxicity, or whether they result from an effort of the cell to sequester the more toxic oligomers that could disrupt various cellular functions, such as axonal transport (4,6,7). A deluge of recent evidence points to the pre-tangle oligomers with high propensity to aggregate as being the instigating factor of toxicity, not only for Tau (reviewed in 7), but also for amyloid-beta or Huntingtin (8,9). Their continuous presence in the cell is detrimental, although no correlation was detected between neuronal toxicity and the formation of tangles which can persist even after expression of transgenic Tau has been switched off (10–14).

An experimental approach to uncouple the aggregation-mediated toxicity of Tau from other functions involves the Δ K280 pro-aggregation mutation which is found in patients with FDTP-17 (15) and the respective anti-aggregation mutations I277P and I308P in the hexapeptide motifs. These substitutions prevent the formation of a β -sheet structure and thus hinder aggregation (10–13,16). These studies have shown that the pro-aggregant Tau species is very toxic, whereas at a similar expression level the anti-aggregant species is not (16). Moreover, the F3 Δ K280 fragment of Tau (amino acids 258–360) has been shown to act as a nucleation agent, and leads to accelerated toxicity by promoting the aggregation of both mutant and wild-type Tau (17).

The *C. elegans* system presents numerous practical advantages, especially for high-throughput screening approaches (18–21). As a result, transgenic strains expressing various human Tau mutations have been studied as disease models by several groups (22–27). However, a common theme in these previously published tauopathy models is that they develop a significant proteotoxicity phenotype at a rather advanced age. Specifically, it has been shown that expression of hyperphosphorylated, mutated Tau protein, and also wild-type Tau, can lead to progressive accumulation of structural damage such as axonal breaks in the GABAergic motor neurons and age-dependent defects in locomotion (25). Additionally, expression of different Tau mutants (P301L and V337M) in the *C. elegans* nervous system was reported to result in Tau pathology (24). Kraemer *et al.* used their tauopathy model to perform a mutagenesis screen, uncovering two new factors that participate in the pathological cascade, namely SUT-1 and SUT-2 (22,26,28). The latter was shown in a follow-up study to have a direct homologue in humans (MSUT-2), whose knock-down also alleviated Tau pathology in a mammalian cell culture model (28). These seminal contributions served as proof of principle, showing that human Tau mutants can indeed recapitulate neuron-related phenotypes in the worm, and that insights gained in such a time and cost-effective model can have relevance for understanding the disease in humans. Importantly, studying human Tau mutants in *C. elegans* has the advantage of avoiding interference with endogenous Tau, since the only Tau homologue in the worm, PTL-1, is expressed only in a small subset of neurons (29,30).

Here, we take advantage of the well-documented molecular dissection of Tau aggregation-mediated toxicity (11,13,16) and establish a *C. elegans* model of tauopathy based on the highly amyloidogenic Δ K280 Tau mutation. We strove to achieve a strong toxicity phenotype that could be attributed to the process of accelerated aggregation already in young

adult worms. For this purpose, we introduced a pan-neuronally expressed pro-aggregant F3 Δ K280 Tau fragment (encompassing the repeat domain of Tau) in the full-length (FL) Tau V337M strain CK10 (22), using the anti-aggregant F3 Δ K280-PP transgene as a control. Pro-aggregant Tau led to substantially increased toxicity in the worms. This recapitulated the main aspects of tauopathy known from mammalian models of the disease (4,6,13), manifested by uncoordinated movement from the first day of adulthood, axonal defects such as gaps and varicosities in motor neurons, impaired pre-synaptic areas and perturbed axonal transport of mitochondria. The anti-aggregant combination caused only a mild phenotype with a significantly reduced level of morphological abnormalities. We also showed that the levels of rapidly aggregating Tau in the pro-aggregant worms are increased. Treating the worms with methylene blue (MB), an aggregation inhibitor of the phenothiazine class (31,32), resulted in beneficial effects. We also demonstrated that the treatment of the pro-aggregant transgenic strains with a novel Tau aggregation inhibitor, a compound belonging to the aminothienopyridazine (ATPZ) class (compound #16 in reference 33, hereafter referred to as cmp16), ameliorated the motility phenotype, reflected also by a reduced extent of the progressive accumulation of neuronal morphological abnormalities.

RESULTS

Rapid deposition of Tau aggregates in the nervous system of *C. elegans* led to early onset of uncoordinated phenotype

Our first aim was to create a novel tauopathy model in the nematode *C. elegans* that allows distinction of pathological mechanisms specifically induced by aggregation of the Tau protein. For this purpose, we focused on the well-characterized Δ K280 mutation (10–13), which specifically leads to aggregation-mediated toxicity. We generated transgenic strains expressing chromosomally integrated versions of the amyloidogenic F3 Δ K280 fragment of human Tau [derived from the repeat domain of Tau Δ K280 (16,17)] from the *rab-3* promoter, to achieve pan-neuronal expression. In one set of *C. elegans* strains, we expressed the pathological FDTP-17 mutant Δ K280, which enhances aggregation, whereas the other set harbours, in addition to Δ K280, the proline substitutions I277P and I308P (PP), which act as β -sheet breakers and prevent aggregation (15). We obtained two independently integrated lines for each mutant, which we then backcrossed to wild-type N2 worms 10 times each, to get rid of possible background mutations caused by the insertion events. Our hypothesis was that the strains carrying integrated transgenes of the pro-aggregant F3 Δ K280 (*byIs161*, *byIs193*) would result in a more pronounced phenotype than that of the strains expressing the anti-aggregant F3 Δ K280-PP transgenes (*byIs162*, *byIs194*). However, the locomotion phenotype of day 1 adult animals of these single-transgenic strains was very similar (Supplementary Material, Fig. S1A), which could be the consequence of the nucleation process being too slow compared with the short lifespan of the animals. We therefore crossed each of these strains with CK10, a previously characterized strain that expresses pan-neuronal FL Tau V337M (23,24). We hypothesized that

co-generating FL mutant Tau and the F3ΔK280 fragment should potentiate nucleation of aggregation and result in increased toxicity. Indeed, strongly defective locomotion phenotype developed at day 1 of adulthood for both strains expressing FL Tau plus F3ΔK280 (BR5485 pro-aggr. line 1 mean speed \pm standard deviation (SD) = 70.6 ± 17.9 μ m/s and BR5706 pro-aggr. line 2 speed = 60.8 ± 22.3 μ m/s), compared with both the anti-aggregant strains expressing FL Tau plus F3ΔK280-PP (BR5486 anti-aggr line 1 speed = 103.5 ± 29.5 μ m/s and BR6427 anti-aggr line 2 speed = 108.7 ± 27.5 μ m/s; Fig. 1A). The latter strains did not exhibit obvious locomotion defects (Supplementary Material, Movies S1–S3).

We verified with western blot analysis that the independently integrated transgene arrays are expressed at similar levels in both sets of strains (Fig. 1B and C). We also performed antibody staining to confirm that Tau is properly expressed in the nervous system (Fig. 1D–F). Since the two independent strains for each transgene combination had similar phenotype and comparable expression levels, we decided to further analyse one strain from each set, namely the pro-aggregant line 1 (with the *byIs161* transgene) and the anti-aggregant line 1 (with the *byIs162* transgene).

In order to quantitate aggregate formation, we applied thioflavin-S (ThS) staining, which detects amyloid deposits (34,35) on synchronous young adult populations of worms, including worms expressing just the transformation marker as control. We observed extensive ThS staining at the nerve ring of the pro-aggregant strain (mean number of aggregates = 14.6, range = 1–64), whereas the anti-aggregant strain showed only minimal staining (mean = 2.2, range: 0–6), similar to negative controls (mean = 0.7, range = 0–2). Representative images are shown in Figure 1G–I and quantification is shown in Supplementary Material, Figure S1B. We next extracted Tau aggregates from these worms, using formic acid (FA) (Fig. 2A). The pro-aggregant F3ΔK280 fragment appeared only in the detergent insoluble fraction (FA fraction), whereas the anti-aggregant F3ΔK280-PP appeared solely in the soluble RAB fraction (Fig. 2A, upper panel), suggesting that the pro-aggregation construct indeed preferably aggregated. In addition, only FL Tau V337M was phosphorylated at the KXGS motif (Fig. 2A, mid panel, 12E8), S396 and S404 (PHF-1 epitope) (Fig. 2A, lower panel, PHF-1). We then extracted Tau from 7-day-old worms and detected both detergent-soluble and -insoluble aggregates even in the CK10 strain (FL Tau V337M) as reported earlier (24). However, the pro-aggregant strain displayed approximately four times more aggregated Tau (Fig. 2B). We conclude that F3ΔK280 fragment is capable of accelerating the aggregation of FL Tau, and this process can be monitored in the short lifespan of *C. elegans*, causing an easily distinguishable phenotype.

Hyperphosphorylation of Tau is complex and has been suggested to play a role in its toxicity (36–39) even in the absence of higher order aggregates (40,41), whereas other studies have shown a dissociation of hyperphosphorylation and toxicity (42,43). Therefore, we wanted to determine the phosphorylation status of the sequentially extracted Tau from our transgenic strains. Both the soluble and insoluble Tau from all three Tau transgenic strains were phosphorylated at various sites and the CP13, AT8 and AT100 epitopes revealed

reduced phosphorylation in the CK10 strain compared with the pro-aggregant strain and least levels of phosphorylation in the anti-aggregant strain (Supplementary Material, Fig. S2). Overall, Tau, both in the soluble and in the insoluble fractions, was phosphorylated to a higher degree in the pro-aggregant strain compared with the other two strains.

In order to add further support to our hypothesis that the locomotion defect phenotype that we described was caused by Tau aggregation-mediated toxicity and not by unknown neighbourhood effects of the transgene insertion event, we performed RNAi against Tau after crossing the strains into a neuronal RNAi sensitizing mutant background [strain *eri-1(mg366)IV;lin-15B(n744)X* (44)]. The motility of the pro-aggregant worms was considerably enhanced upon applying RNAi against F3ΔK280 (speed = 70.7 ± 17 μ m/s for RNAi-treated versus 40.3 ± 17 for control), whereas the anti-aggregant worms showed no difference upon treatment (Supplementary Material, Fig. S1C). In addition, introducing a non-integrated extrachromosomal array expressing F3ΔK280 also reduced the motility of the FL Tau V337M strain (by ~30%), whereas an F3ΔK280-PP extrachromosomal array did not (Supplementary Material, Fig. S1D). These experiments suggested that the phenotypic differences observed are indeed due to the differential aggregation propensities of the Tau fragments and were not caused by transgene insertion. In summary, we conclude that expression of the highly amyloidogenic combination of Tau species leads to rapid formation of aggregates and overt toxicity in *C. elegans*, manifested by uncoordinated locomotion, whereas the anti-aggregant combination does not.

Accelerated aggregation of Tau caused morphological abnormalities in the motor neurons of *C. elegans*

We next hypothesized that the locomotion phenotype is caused by damage in the motor neurons, since the transgenes are expressed in the whole nervous system, and neuronal structural defects have been demonstrated in previous neurodegenerative *C. elegans* models (24,25). We first looked at the GABAergic motor neurons, using the *juls73::[Punc-25::gfp]III* reporter (45) and measured the number of axonal discontinuities (gaps) in the ventral and dorsal cords of the animals during larval stages as well as during adulthood (representative example of a wild-type young adult animal is shown in Fig. 3A). In wild-type animals, the development of the nervous system is mostly completed in the L3 stage. Correspondingly, GFP-stained processes show no gaps and have continuous dorsal and ventral cords (Fig. 3D). In contrast, we observed severe developmental defects in the pro-aggregant strain (BR5707) that manifest as increased numbers of persistent gaps in both the ventral and dorsal neural cords (mean \pm SD = 2.7 ± 1.4 gaps at the L3 stage). Gaps were still visible at the L4 stage (Fig. 3D). At day 1 of adulthood, we observed 1.32 ± 0.8 gaps in the cords of the pro-aggregant strain (example of a young adult in Fig. 3C). In contrast, the anti-aggregant strain (BR5674) did not show comparable morphological defects during development (Fig. 3D), and as young adults (example in Fig. 3B), they showed very few, if any, gaps (mean \pm SD = 0.13 ± 0.3). The number of axonal gaps in the pro-aggregant strain rose with age, so that by day 5 of

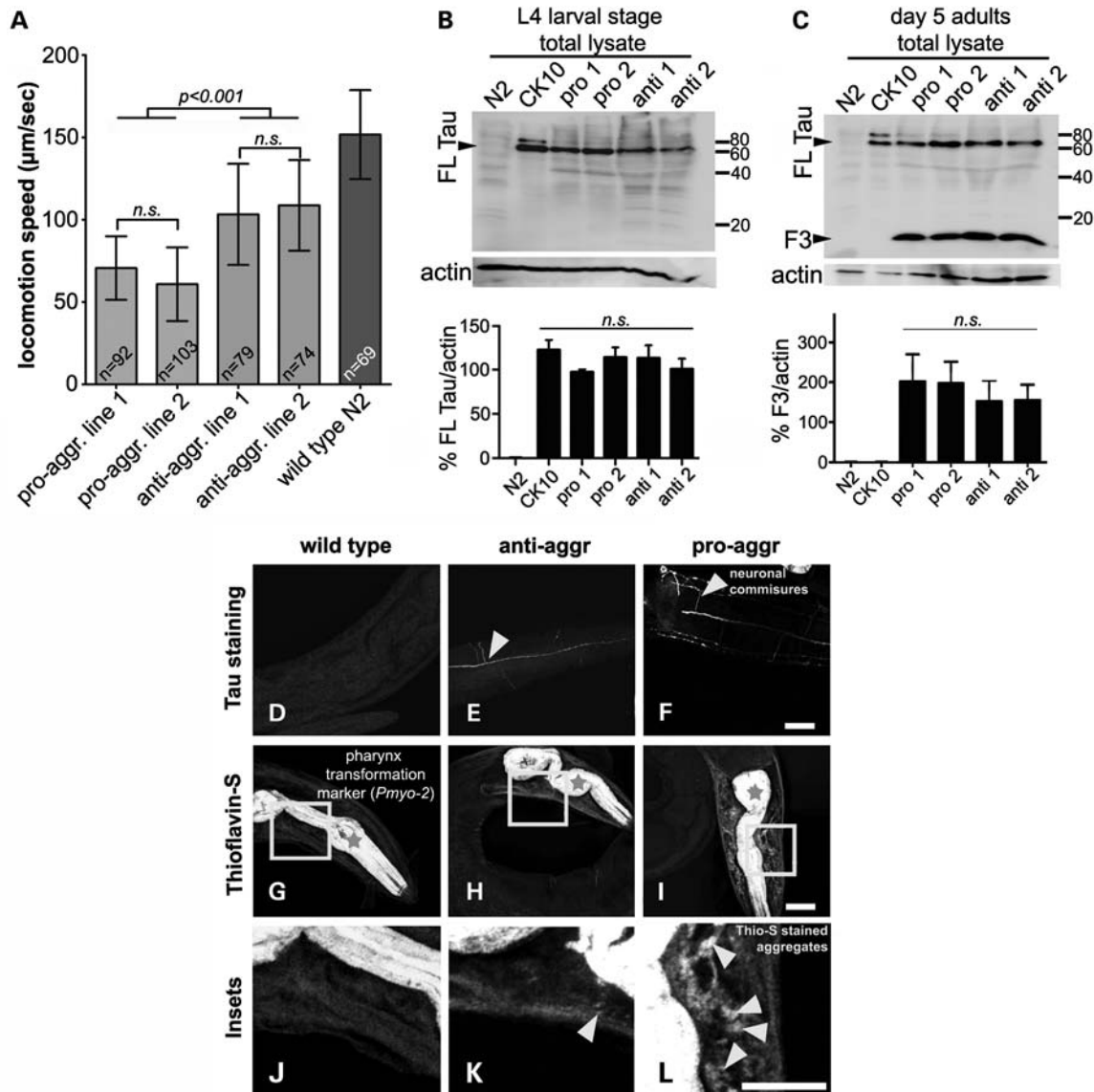


Figure 1. Pan-neuronal expression of pro-aggregant human Tau transgenes resulted in the deposition of aggregates and locomotion defects. **(A)** Mean locomotion speed of day 1 adult animals from strains carrying independently integrated transgene arrays with pro- or anti-aggregant Tau. N2 wild-type strain serves as control. Error bars denote SD. One-way ANOVA with Tukey's test was applied for comparisons (*n.s.*, non-significant). **(B)** Western blot of total lysates from synchronized L4 larvae. The blots were probed with the K9JA antibody (upper panel), which recognizes the Tau repeat domain (RD) and thus detects both the FL Tau and the F3 fragment. An anti-actin antibody was used as loading control (lower panel). L4 larvae extracts did not show the F3 fragment but total levels of Tau expression were similar among all the different transgenic lines (normalization to actin)—quantification shown in the graph below the blot. The error bars denote SEM from three repetitions of the experiment, and differences were considered non-significant ($P > 0.05$) after performing one-way ANOVA. **(C)** Western blot of total lysates from synchronized day-5-old adults. Both the FL Tau and the F3 fragment were detected with the K9JA antibody. The independently integrated strains express the F3 fragment at comparable levels (normalization to actin)—quantification shown in the graph below the blot. The error bars denote SEM from three repetitions of the experiment, and differences were considered non-significant ($P > 0.05$) after performing one-way ANOVA. **(D–F)** Tau expression detected with anti-Tau K9JA antibody. Neuronal structures were stained in the anti-aggregant (E) and pro-aggregant (F) Tau transgenic strains (marked with arrowheads). Only background staining is observed in non-transgenic controls (D). **(G–I)** Maximal intensity projections (MIP) of worms stained with ThS to image Tau aggregates in the nerve ring. The strong signal in the pharynx of the animals (marked with an asterisk) derives from the transformation marker (*Pmyo-2::gfp*). Wild-type strain (transformation marker only) in (G) shows only background staining, the anti-aggregant strain (H) shows very few spots and the pro-aggregant strain in (I) shows extensive decoration, with spots around the nerve ring area. **(J–L)** Zoom of the marked area of (G)–(I), corresponding to the dotted rectangle region. Grey arrowheads point to individual ThS-stained Tau aggregates. Scale bars: 20 μm .

adulthood almost 100% of the worms showed axonal gaps (3.1 ± 0.9) (Fig. 3D). By that age, the anti-aggregant strain showed a reduced number of gaps (1.1 ± 0.9), which was not very different from wild-type (0.5 ± 0.4) (Fig. 3D). To corroborate this result, we also looked at the cholinergic

motor neurons, which provide the activating signals to the neuromuscular junctions in coordination with the GABAergic inhibitory neurons on the opposite side (46). For this purpose, we introduced an extrachromosomal array to mark the cholinergic neurons [*Punc-129::mCherry*] and examined the ventral

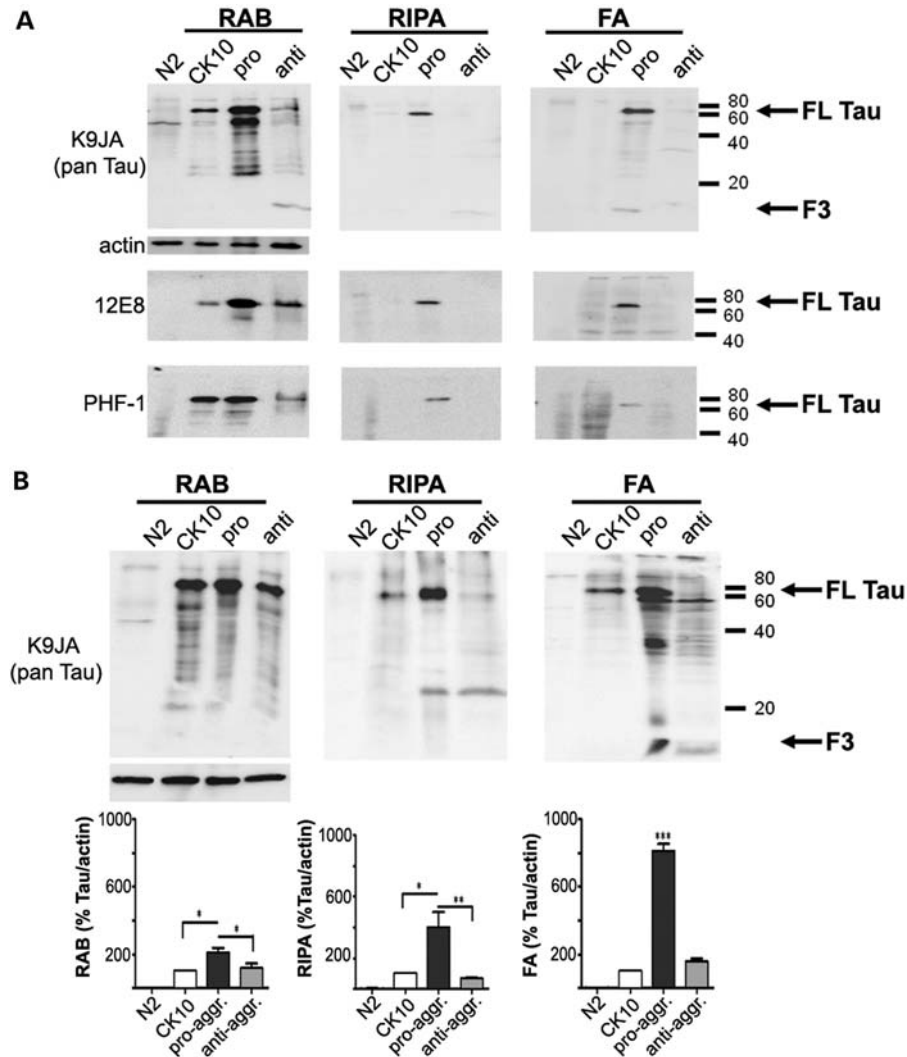


Figure 2. Sequential extraction revealed increased accumulation of insoluble Tau in the pro-aggregant strain. (A) After sequential extraction of Tau from day 1 adult transgenic *C. elegans* strains (with laboratory wild-type N2 strain as control), only the pro-aggregant strain (lane 3) shows the detergent-soluble (RIPA) and the detergent-insoluble tau aggregates, which were solubilized with 70% FA. FL Tau V337M, but not the F3ΔK280 fragment, is phosphorylated at the KXGS motif (12E8 panel) and the S396 and S404 epitopes (PHF-1 panel). In the pro-aggregant strain, F3ΔK280 appears only in the detergent-insoluble fraction (lane 3 of the FA fraction in the top panel). In contrast, F3ΔK280-PP in the anti-aggregant strain appears solely in the soluble fraction (lane 4 of the RAB fraction, top panel). (B) Sequential extraction of Tau from day 7 adult animals. Equal amount of protein was loaded and normalized against the CK10 sample. The pro-aggregant shows ~2-fold soluble (RAB blot), 4-fold detergent-soluble (RIPA blot) and 8-fold detergent-insoluble Tau (FA blot), as quantified from three independent experiments (one-way ANOVA, * $P < 0.05$, ** $P < 0.01$, *** $P < 0.001$). These data corroborate the notion that Tau displays increased aggregation when combined with the amyloidogenic F3ΔK280 fragment in the pro-aggregant strain, whereas combination with the non-amyloidogenic F3ΔK280-PP fragment, or FL Tau V337M alone, does not aggregate to such extent.

and dorsal cords of young adult animals for morphological abnormalities. The wild-type reporter strain (BR6061) and the anti-aggregant strain (BR6089) showed rare occurrence of gaps (wild-type: $2.3 \pm 0.5\%$ animals with gaps, $8.5 \pm 3.2\%$ in anti-aggregant) (Fig. 3E and Supplementary Material, Fig. S3). In contrast, the pro-aggregant strain showed frequent occurrence of gaps ($27.8 \pm 4.8\%$ of day 1 adult animals), similar to those observed in the GABAergic neurons (Fig. 3E and Supplementary Material, Fig. S3). From these data, we conclude that the continued expression of FL Tau V337M and F3ΔK280 is toxic for the neurons and as a consequence, the development of the nervous system is perturbed. The continuous rise of the number of gaps later in adulthood

suggests that progressive axonal degeneration follows the initial developmental defects. Combination of FL Tau V337M with the non-amyloidogenic F3ΔK280-PP produced only mild defects which only in day 5 old animals became statistically distinguishable from wild-type.

The pro-aggregant strain had defective accumulation of synaptobrevin-1 in the pre-synaptic termini, indicating impaired presynaptic transmission

Aberrant phosphorylation and aggregation of Tau have been linked to axonal transport problems, synaptic malfunction and degeneration (6). In order to examine synapse morphology

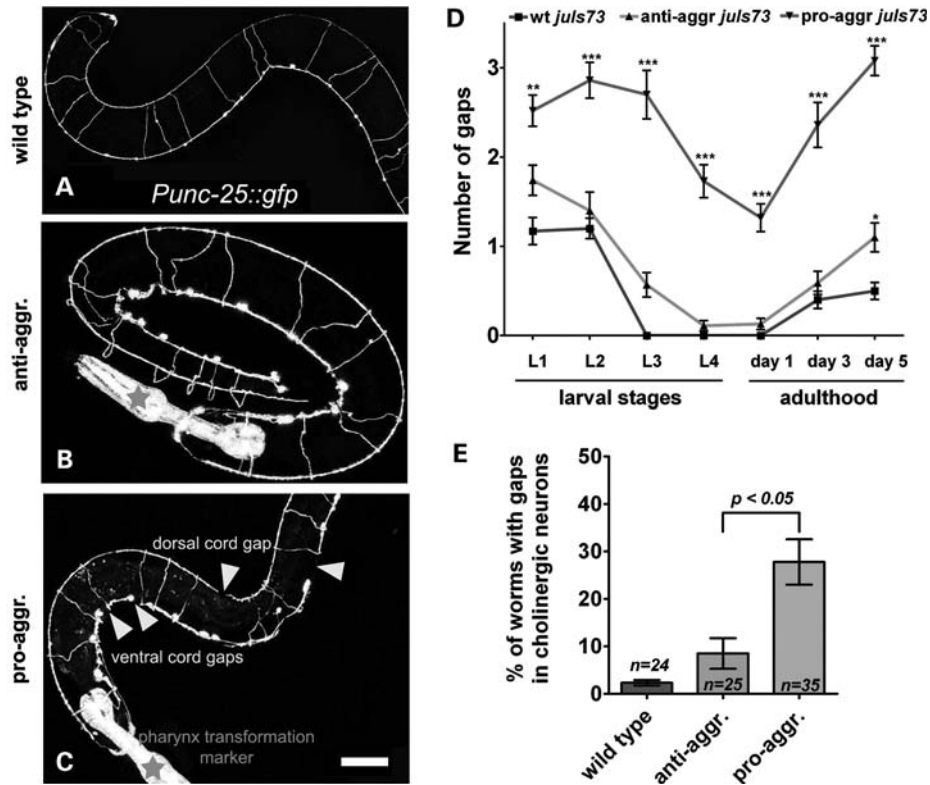


Figure 3. Morphological abnormalities accumulated in the motor neurons of the pro-aggregant Tau transgenic worms. (A–C) Maximum intensity projections (MIP) of (A) wild-type with *Punc-25::gfp* reporter staining GABAergic motor neurons, day 1 adult. Intact ventral and dorsal cords are observed. (B) Anti-aggregant GABAergic reporter strain, day 1 adult. No gaps are observed. (C) Pro-aggregant GABAergic reporter strain, day 1 adult. Arrowheads point to axonal gaps along the ventral or dorsal cord. Asterisks denote the pharynx, which expresses the transformation marker *Pmyo-2::GFP*. Scale bar: 20 μ m. (D) The graph plotting the average number of gaps occurring in the neural cords of the animals as a function of time during larval development and through adulthood. Increased numbers of defects during development as well as progressive increase of gaps during adulthood were observed for the pro-aggregant strain (two-way ANOVA with Dunn's test, $*P < 0.05$, $**P < 0.01$, $***P < 0.001$) Error bars denote SEM. Thirty worms were scored per strain and per time point. (E) Percentage of day 1 adult worms showing axonal gaps in the cholinergic motor neurons (*Punc-129::mCherry* reporter). Three times more pro-aggregant animals have axonal gaps compared with anti-aggregant animals. Error bars denote SD.

in Tau-expressing worms, we used the reporter gene *nIs52::[Punc-47::snb-1::gfp]* as a marker (47) that expresses GFP fused to synaptobrevin-1 from the motor neuron-specific *unc-47* promoter. For quantitation, we focused on analysing the dorsal neural cord at the posterior gonadal arm (Fig. 4A–C). In the wild-type strain, SNB-1::GFP formed a regular pattern of puncta along the neural cord (Fig. 4D) as described before (48). This pattern was similar to that of the anti-aggregant strain (BR5793, Fig. 4E). In contrast, the pro-aggregant strain (BR5792) displayed a discontinuous punctate pattern and staining was generally more diffuse in pre-synaptic areas, which we take as an indicator for synaptic transport defects or potentially synaptic loss (Fig. 4F). In older animals, this phenotypic pattern deteriorated further (Supplementary Material, Fig. S4A–F). We quantitated the mean of the fluorescence intensity in SNB-1::GFP puncta from 25 animals of each genotype (Fig. 4G–I) and found that the puncta intensity of the pro-aggregant strain was reduced (mean intensity \pm SD = 1022 ± 330 arbitrary units, AU) compared with both wild-type (1410 ± 300 AU) and anti-aggregant (1292 ± 400 AU) strains (Fig. 4J). Moreover, the density of puncta (number of puncta per 50 μ m) was also reduced (Fig. 4K). Specifically, pro-aggregant worms had 8.9 ± 5.1 puncta per 50 μ m, whereas wild-type had 14.1 ± 3.3

and the anti-aggregants had 12.5 ± 3.5 . This indicated that SNB-1 failed to properly accumulate at the presynaptic termini of young adult pro-aggregant worms. At day 5 of adulthood, reduction of puncta numbers was already seen in wild-type and anti-aggregant strains compared with young adults. However, the staining loss was more pronounced for the pro-aggregant strain (Supplementary Material, Fig. S4J). Since previous experiments performed by others (48,49) suggested a correlation of SNB-1 puncta with the presence of synapses, we are confident that our marker staining faithfully represents the alterations of presynaptic structures.

This finding suggests that synaptic transmission may be negatively affected. In order to test neurotransmission in the individual strains, we performed aldicarb and levamisole sensitivity assays with day 1 adult animals (50). Worms with functional neurotransmitter release should be sensitive to both substances and become paralysed due to muscle hypercontraction (50). Resistance to aldicarb can arise from either a pre- or a post-synaptic perturbation, whereas resistance to levamisole typically indicates a post-synaptic defect (50). Animals of the pro-aggregant strain displayed a mild resistance to aldicarb, producing a paralysis profile intermediate between the sensitive wild-type N2 and the resistant *rab-3(js49)* strain, which we used as controls (Fig. 5A).

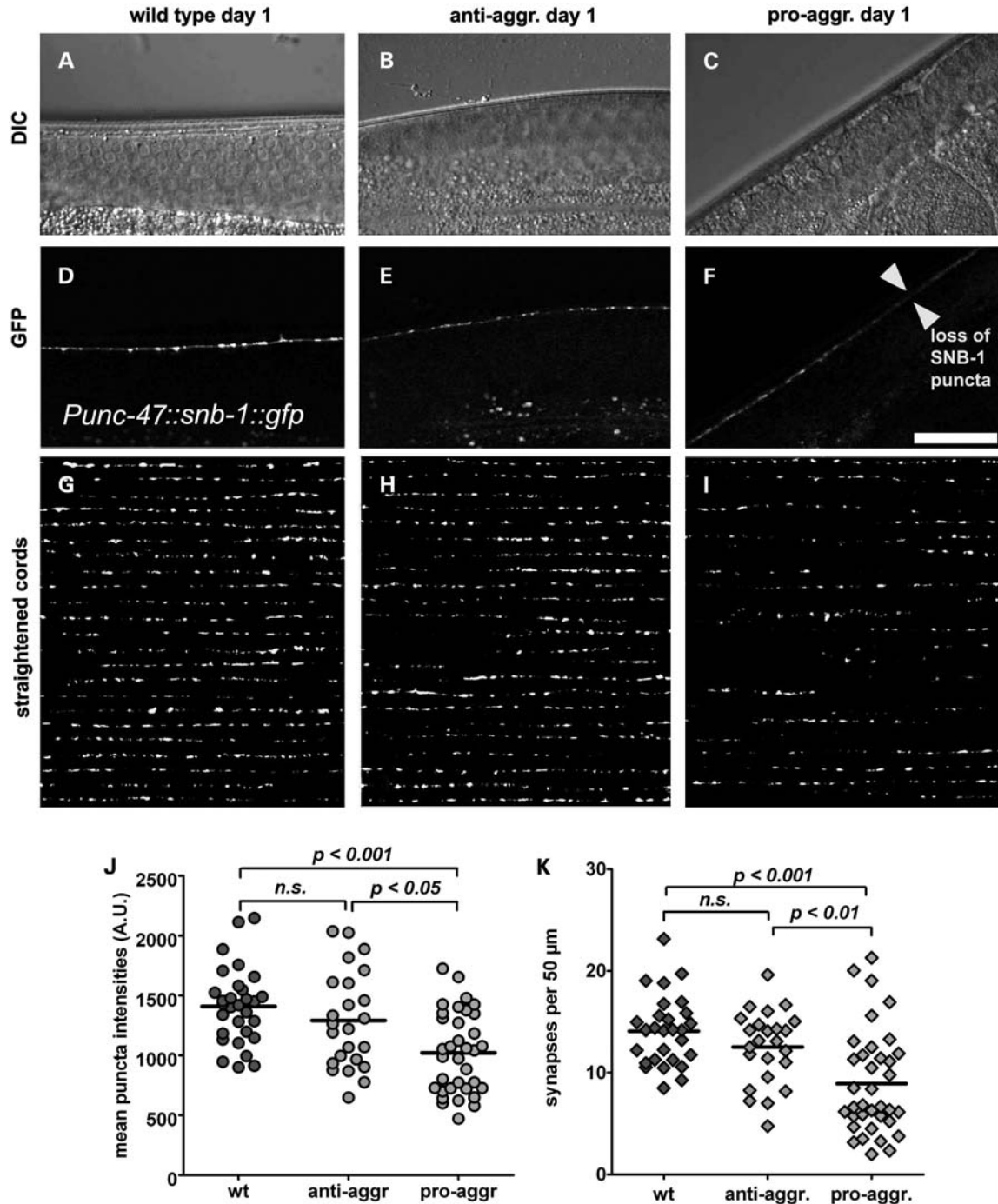


Figure 4. Defective presynaptic accumulation and organization of synaptobrevin-1 puncta in the pro-aggregant strain. (A–C) DIC images of the dorsal neural cord above the posterior gonadal arm of (A) wild-type animals, (B) anti-aggregant and (C) pro-aggregant strains expressing the *Punc-47::snb-1::gfp* reporter. Day 1 adults are shown. (D–F) MIP of the SNB-1::GFP fluorescent puncta (pre-synaptic termini) along the dorsal neural cord corresponding to the regions shown in the DIC pictures above. Note that for the pro-aggregation example, the SNB-1::GFP puncta are weaker and more diffuse (region between the arrowheads). (G–I) Panel showing a compilation of 23 straightened dorsal cord segments (after binary thresholding) of day 1 adult animals expressing *Punc-47::snb-1::gfp*. (G) Wild-type, (H) anti-aggregant strain, (I) pro-aggregant strain. (J) Scatter plot of the mean fluorescent intensity of SNB-1::GFP puncta (arbitrary units), as measured from the MIP images for each animal. The line denotes the mean. The Kruskal–Wallis ANOVA (non-parametric) with Dunn's *post hoc* test was used for comparisons. (K) Scatter plot showing the number of SNB-1::GFP puncta (synapses) per 50 μm of dorsal cord, calculated from the same images that were used for the puncta intensity quantification graph in (J). The Kruskal–Wallis ANOVA with Dunn's *post hoc* test was used for comparisons. Pre-synaptic SNB-1 puncta in the pro-aggregant strain often show diffuse structure and are less in numbers.

The anti-aggregant strain also displayed mild resistance to aldicarb, although animals typically became paralysed earlier than pro-aggregants (Fig. 5A, the small difference between

anti-aggregant and pro-aggregant strains was not statistically significant). All the transgenic strains were sensitive to levamisole and indistinguishable from wild-type (Fig. 5B).

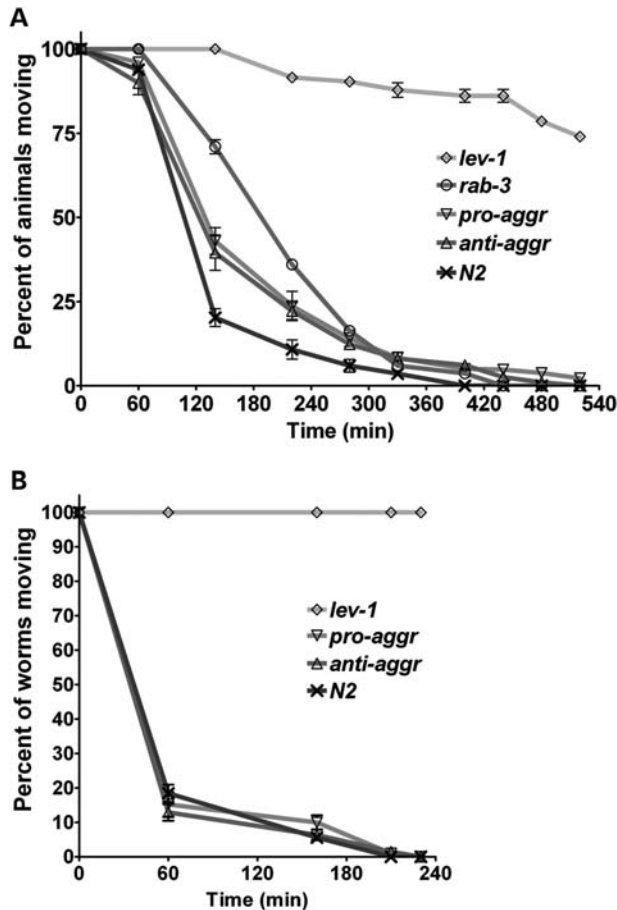


Figure 5. Tau expression resulted in mild resistance against aldicarb-induced paralysis but did not change the levamisole sensitivity. **(A)** Time course of aldicarb-induced paralysis. The percentage of worms still moving on 1 mM aldicarb plates after being touched with a metal wire is plotted as a function of time. The *lev-1(x21)* strain is strongly resistant to aldicarb, whereas the *rab-3(js49)* is mildly resistant and wild-type N2 is sensitive (50). Both the pro- and anti-aggregant strains displayed slight resistance to aldicarb. Two-way ANOVA with the Bonferroni correction was applied for comparisons and produced $P < 0.001$ for both the pro- and anti-aggregants compared with N2 for the time points of 140, 220 and 280 min. Error bars denote SEM calculated from three repetitions of the experiment (blind test). **(B)** Time course of levamisole-induced paralysis. The percentage of worms still moving on 0.2 mM levamisole plates after being touched with a metal wire is plotted as a function of time. The *lev-1(x21)* strain is strongly resistant to levamisole and did not paralyze. The different Tau transgenic strains paralysed fast, at the same rate as wild-type (N2), indicating levamisole sensitivity.

Taken together, these experiments suggest that both anti- and pro-aggregant strains may display pre-synaptic defects. This corresponds to the observed SNB-1 puncta defect at the pre-synaptic termini of the pro-aggregant strain. We conclude that expression of amyloidogenic Tau fragments in combination with FL Tau V337M perturbs proper presynaptic organization in this *C. elegans* tauopathy model.

The pro-aggregant Tau strain showed mislocalized mitochondria in the DA9 motor neuron

Mitochondrial transport problems have been suggested to contribute to the progression of pathology in most mammalian

neurodegeneration models, so we examined whether our tauopathy model recapitulates the neuronal mitochondria mislocalization phenotype (6,51–53). For this purpose, we took advantage of the *wyEx2709* [*Pitr-1::TOM-20^{1-54aa}::yfp*] reporter strain (54), which labels mitochondria only in the DA9 neuron close to the posterior end of the animal. The soma of the DA9 neuron is located at the ventral side near the anus and extends a dendrite anteroventrally and an axon towards the dorsal cord which then extends antiodorsally. This region typically displays a regular distribution of mitochondrial particles (54) (Fig. 6A), extending to the distal axonal segment. The vertical axonal part is synaptic and has few mitochondria (54). We crossed *WyEx2709* into the pro-aggregant strain (resulting in strain BR6011) and discovered that this regular mitochondrial distribution was distorted. Few or no mitochondrial particles were detected in the distal axonal segment (example in Fig. 6C), whereas the anti-aggregant strain (BR6012) showed only a moderate perturbation (example in Fig. 6B). Almost 60% of the axonal mitochondria accumulated in the proximal region and typically did not reach the more distal parts of the axon in the animals of the pro-aggregant strain. In contrast, only 32 and 45% of the axonal mitochondrial population was localized to the proximal axonal segment of wild-type and anti-aggregant strain, respectively (Fig. 6D and Supplementary Material, Fig. S5). It is unclear whether this mislocalization arose from a severe transport problem or from axonal retraction, reminiscent of the axonal gaps in Figure 3. In summary, the results shown so far further support the notion that a highly amyloidogenic Tau species is detrimental for neurons, whereas the non-amyloidogenic species does not cause severe problems.

Axonal transport was perturbed in mechanosensory neurons of the pro-aggregant Tau transgenic worms

We reasoned that aggregation-prone Tau species might affect axonal transport properties which, for example, may alter the motility of mitochondria. The strain *jsIs609* expresses GFP with a mitochondrial localization signal (MLS) in the six mechanosensory neurons of *C. elegans*. We crossed this strain with our Tau mutants, creating the pro-aggregant (BR6174) and the anti-aggregant (BR6175) mitochondrial marker strains. To quantify mitochondrial movements, we performed single-plane live imaging of the middle axonal segment of the PLML or PLMR neurons in immobilized worms, for ~8–10 min per time lapse (see Materials and Methods). For analysis, we selected in each animal the PLM axon closer to the microscope objective. We chose these posterior neurons for two reasons: (i) analysis of the axons of the other mechanosensory neurons is frequently obscured by gut autofluorescence or the GFP transformation markers used, and (ii) with our anaesthetic-free immobilization protocol we get animals that can still slightly move their heads and have a pumping pharynx—both may affect the quality of data acquisitions. We collected time lapse acquisitions from 20 animals of each strain—representative examples of which are shown as kymographs in Figure 7A–C and as movies in the Supplementary Material, Movies S4–S6. We manually tracked each moving GFP particle with ImageJ and extracted the instantaneous velocity values of continuously moving particles (Fig. 7D). The velocity

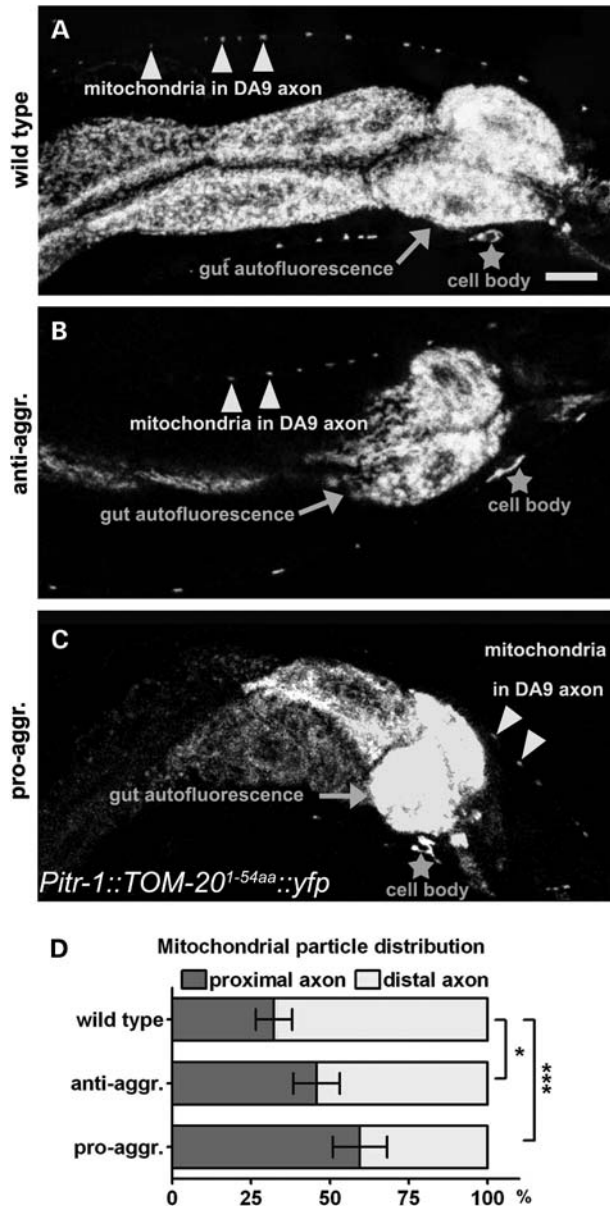


Figure 6. In the pro-aggregant strain, mitochondria mislocalized to the proximal axonal segment of the DA9 neuron. (A) MIP of the YFP fluorescence from the tail region of a *Pitr-1::TOM-20^{gal-54}::yfp* wild-type reporter worm, showing the distribution of labelled mitochondrial particles along the DA9 neuron. The cell body (denoted by an asterisk) is located ventrally, extending a dendrite anterior-ventrally and an axon to the anterior dorsal cord (arrowheads point to representatively labelled mitochondria). The strongly fluorescent mass in the middle is the autofluorescence of the gut. Scale bar: 10 μ m. (B) MIP of the YFP fluorescence from the tail region of a representative animal with anti-aggregant Tau. YFP-labelled mitochondria (arrowheads) are distributed along the dorsal axon, similar to wild-type. (C) MIP of the YFP fluorescence from the tail region of a pro-aggregant animal. Note the altered distribution of YFP labelled mitochondria along the DA9 neuron (the arrowheads point to mitochondria in the proximal axon; the distal segment is devoid of puncta). (D) Stacked bar diagram showing the distributions (percentage) of mitochondrial YFP particles in the proximal and distal axonal segments (the axon was arbitrarily divided in two parts of equal length for this analysis; see also Supplementary Material, Fig. S5). In wild-type, ~60% of the axonal mitochondria are located in the distal part of the axon, whereas in the pro-aggregant strain, mitochondria cluster preferentially (60%) in the proximal part of the axon. The anti-aggregant strain shows an intermediate phenotype. Fifteen to 20 animals from each strain were used for quantification and error bars denote SD. χ^2 test with Yates's correction was used for comparisons.

of mitochondrial transport in the pro-aggregant strain was lower than in wild-type (mean \pm SD = 171 ± 111 versus 256 ± 117 nm/s), whereas the anti-aggregant strain (194 ± 131 nm/s) did not substantially differ from wild-type (Fig. 7D). In addition, a striking difference in the mitochondrial pausing frequency was observed between pro-aggregant and the other two strains, with approximately four times more frequent pause events for the pro- compared with the anti-aggregant (Fig. 7E). This suggests that mitochondrial transport in the axons of this strain is perturbed. The mitochondrial flux (number of moving mitochondria per minute) was slightly reduced in both Tau transgenics (Fig. 7F), and the ratio of mobile to stationary mitochondria was also lower, particularly in the pro-aggregants (Fig. 7F), although these differences proved to be not statistically significant. The range of track lengths we recorded for the pro-aggregants was from 1 to 33.1 μ m (mean = 6.31 μ m), whereas for the anti-aggregants we recorded a range from 1.6 to 87.2 μ m (mean = 14.39 μ m); for the wild-type, these values ranged from 2.7 to 87.3 μ m (mean = 19.2 μ m) (Fig. 7G). Taken together, the track length of mitochondria in a given time lapse was smaller in the pro-aggregant strain. In summary, we found that several phenotypic criteria tested allow us to distinguish between pro-aggregant and anti-aggregant Tau transgenic strains. Therefore, our *C. elegans* model indicates that amyloidogenic properties of Tau block axonal transport of mitochondria.

A novel Tau aggregation inhibitor compound ameliorated the phenotype of the pro-aggregant strains and mitigated neurotoxicity

The pathology we observed in *C. elegans* is reminiscent of the cellular pathology observed in mammalian tauopathy models. Aiming to see whether we can ameliorate the phenotype, we set out to test small molecule compounds that have already been shown to have Tau anti-aggregation properties *in vitro*. As a proof of principle, we first tested the efficacy of MB, a Tau aggregation inhibitor with potential cognition-enhancing effects (55,56). We supplemented the growth medium of synchronized L1 larvae (pro-aggregant strain) with 25 μ M MB and measured their locomotion speed as day 1 young adults. This treatment led to 15% amelioration of locomotion (Supplementary Material, Fig. S6A). Higher MB concentrations were not effective. At the biochemical level, MB treatment altered Tau solubility, shifting the equilibrium towards more soluble Tau and reduced detergent-insoluble Tau by ~35% in the pro-aggregant strain (Fig. 8A, quantitation in 8B), consistent with its anti-aggregation properties (31). We then applied, in the 96-well liquid culture format, the two most promising hit compounds obtained in a mammalian cell model of Tau toxicity (57), namely the phenylthiazolyl-hydrazide derivatives Bsc3094 and bb14, and observed a similar amelioration effect in locomotion (Supplementary Material, Fig. S6B). Bsc3094 resulted in 40% decrease in the detergent-insoluble Tau (FA fraction) in pro-aggregant animals, but there was no apparent change in the detergent-insoluble monomeric Tau after bb14 treatment (Fig. 8C, quantitation in 8D).

The successful treatment using a small molecule served as a proof of principle, suggesting that the *C. elegans* tauopathy

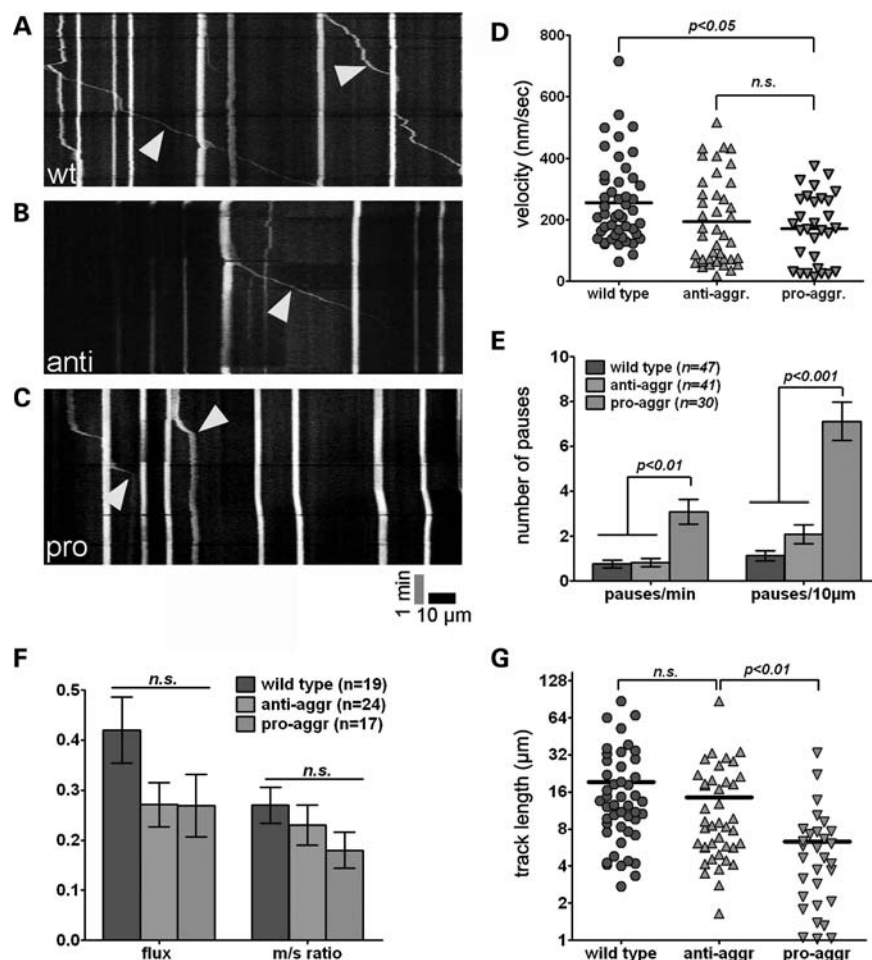


Figure 7. Mitochondrial transport was perturbed in axons of mechanosensory neurons in the pro-aggregant Tau transgenic worms. (A–C) Representative kymographs of PLM axons from day 1 adult animals of the pro-, anti-aggregant and wild-type strain derived from time lapse imaging are shown. Vertical lines represent stationary/docked mitochondria, and oblique lines (denoted by arrowheads) represent the tracks of moving mitochondria. The slope of this track is an indicator of velocity. Anterograde movements: the slope declines to the right, in retrograde movements to the left. The kymograph space and time scale is shown at the bottom. (A) Wild-type: Two mitochondrial particles were recorded to move anterograde (arrowheads), making only short intervening pauses. (B) Anti-aggregant strain: Note the oblique line in the middle which shows the track of a fast moving mitochondrial particle (arrowhead). (C) Pro-aggregant strain: Note that the two particles in motion make long pauses (oblique lines become vertical, denoted by arrowheads) and their track displacement is rather limited. (D) Scatter plot of the mean velocities of mitochondrial particles that were manually tracked from 20 time lapse videos that were analysed for each strain. Instantaneous velocity values that were < 10 nm/s were not included in the calculation of the means for this plot, as these frames were classified as pause events that were separately analysed (see the next graph). (E) Bar diagram for the quantification of pausing frequency in relation to time and distance parameter. The number of pausing events is significantly increased in the pro-aggregant strain. Error bars denote SEM. (F) Stacked bar diagram showing the quantification of mitochondrial flux (number of mobile mitochondria/min) and the mobile/stationary ratio (m/s ratio). No statistically significant difference was observed between the transgenics, although the ratio was slightly reduced for the pro-aggregant worms. Error bars denote SEM. (G) Scatter plot of the mitochondrial track displacement length that was measured for each particle from the three different strains. The Y axis is in the \log_2 scale, and the line denotes the mean of each distribution. The mitochondria in the pro-aggregant worms typically covered shorter distances during comparable lengths of time lapse acquisitions (8–10 min for each time lapse). In summary, the axonal transport of mitochondria in pro-aggregant worms does not run smoothly due to increased pause events and subsequently shorter track distances, although instantaneous velocities *per se* are not substantially different from those seen in the anti-aggregant worms.

model we generated is well suited for the *in vivo* testing of compounds in high throughput. We next analysed the most prominent Tau aggregation inhibitor compound from a recently published *in vitro* screen (compound #16 in reference 33), which belongs to the ATPZ class of Tau inhibitors (5-amino-3-(4-chlorophenyl)-N-cyclopropyl-4-oxo-3,4-dihydrothieno[3,4-d]pyridazine-1-carboxamide, referred to as cmp16 for simplicity, structure shown in Fig. 9A). This compound prevents Tau fibril formation *in vitro*, and is able to

cross the mammalian blood–brain barrier, an attribute that makes it favourable for clinical applications (33). We incubated pro-aggregant L1 larvae with increasing concentrations of cmp16 until adulthood. At 100 μM , we observed improved locomotion of treated animals. These animals moved approximately 1.6 times faster than DMSO-treated controls (Fig. 9A). The compound did not have an effect on the other strains tested, suggesting that it acts specifically by reducing the toxicity of the amyloidogenic F3ΔK280 fragment

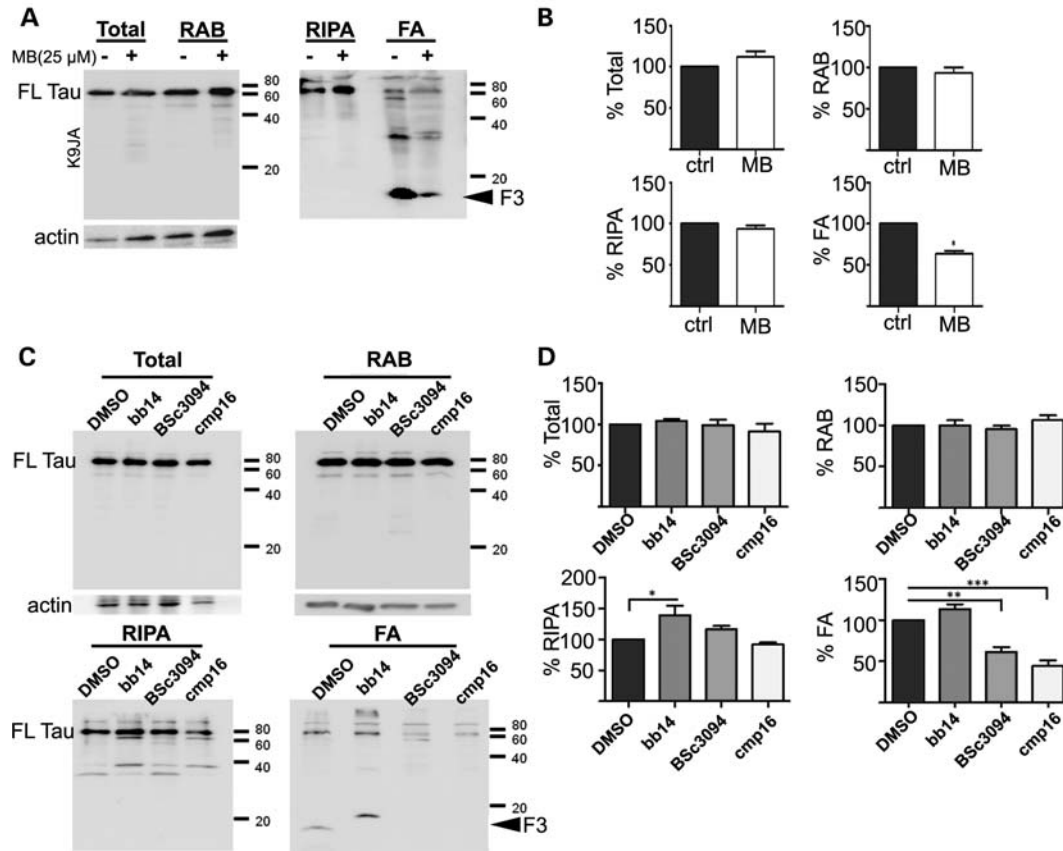


Figure 8. Tau aggregation inhibitors reduced detergent-insoluble Tau in the pro-aggregant Tau strain. Sequential extraction of Tau from synchronized pro-aggregant animals after treatment with aggregation inhibitor compounds. (A) Insoluble Tau species in the FA fraction decrease after MB treatment (25 μ M). (B) Quantification of the total, soluble, detergent-soluble and detergent-insoluble Tau from the pro-aggregant strain after 25 μ M MB treatment. Equal amount of protein was loaded, and for the quantification, signal intensities were normalized against the untreated sample. The experiment was repeated three times. MB treatment leads to $\sim 35\%$ decrease in the insoluble Tau (paired *t*-test, $*P < 0.05$, error bars denote SEM). (C) There is a slight decrease in the insoluble Tau extracted with FA (FA blot) upon BSc3094 (25 μ M) and cmp16 (100 μ M) treatment but no difference after bb14 (50 μ M) treatment. However, F3 Δ K280 becomes visible only in the control (DMSO only). (D) Quantification of the total, soluble, detergent-soluble and detergent-insoluble Tau from the pro-aggregant strain after bb14, BSc3094 and cmp16 treatment. Equal amounts of protein were loaded and, for the quantification signal intensities, were normalized against the untreated control (DMSO). The experiment was repeated three times. Compound bb14 leads to $\sim 25\%$ increase in the detergent soluble Tau. BSc3094 and cmp16 lead to ~ 40 and 50% decrease in the insoluble Tau, respectively (one-way ANOVA, $*P < 0.05$, $**P < 0.01$, $***P < 0.001$; error bars denote SEM).

(Supplementary Material, Fig. S6C). To visualize whether cmp16 is successful in reducing neural outgrowth defects, we also treated the pro-aggregant GABAergic reporter strain (described in Fig. 3), using the same conditions. For this purpose, we sampled animals at day 1, day 3 and day 5 of adulthood and counted the number of axonal discontinuities in the motor neurons. Treatment with cmp16 diminished the progressive accumulation of neurite gaps in the motor neurons of the pro-aggregant animals compared with the DMSO-treated controls (from 3.2 ± 1 gaps at day 5 of the DMSO-treated strains to 2.4 ± 1 gaps of the cmp16-treated strains, $P < 0.05$) (Fig. 9B). Lower accumulation of structural damage in neurons can be interpreted as a sign of reduced neurodegeneration (22,58). This phenotype correlated with a reduction of the insoluble Tau species by $\sim 50\%$ in animals, following cmp16 treatment (Fig. 8B and D). In summary, these data indicate that this novel Tau anti-aggregation compound may be neuroprotective.

DISCUSSION

In this study, we created and characterized a new tauopathy model in *C. elegans* by combining expression of FL Tau V337M (22) and the F3 fragment harbouring the FDTP-17 mutation Δ K280 (15). This model differs from previously described tauopathy models in *C. elegans* (24,25) since it is based on a well-characterized pathology basis and shows a robust toxicity phenotype. The latter appears already at day 1 of adulthood, which allows the uncoupling from age-related alterations of proteostasis (59–62). Importantly, using this model allowed us to focus on Tau aggregation-mediated toxicity and decouple this effect from Tau hyperphosphorylation or association with microtubules or membranes. To achieve this, we did not restrict ourselves to comparing phenotypes of transgenic versus non-transgenic animals, as was done in previous *C. elegans* Tau studies. Instead, we compared strains that all harboured FL Tau V337M, coexpressed either

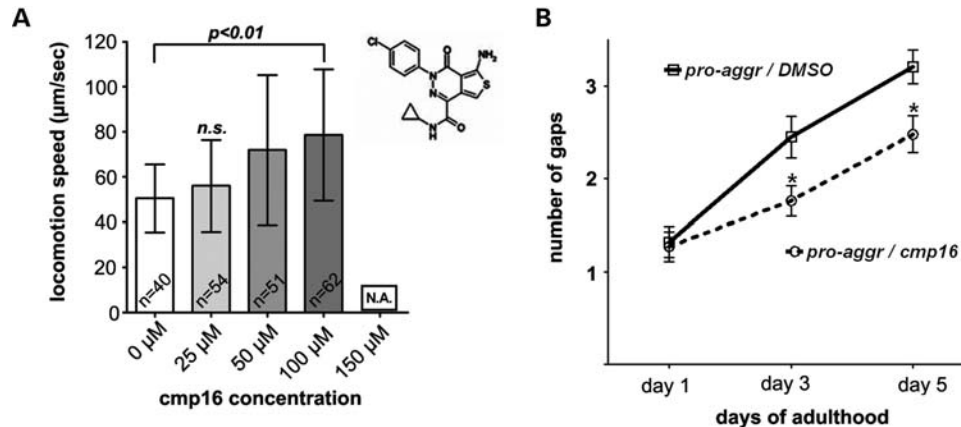


Figure 9. Tau aggregation inhibitor cmp16 partially suppressed the locomotion defect of the pro-aggregant strain and delayed the progressive accumulation of neuronal abnormalities. (A) Mean locomotion speed of synchronized day 1 adult animals treated with either 1% DMSO (solvent control) or a series of increasing concentrations of cmp16 (in 1% DMSO). The chemical structure of the compound is depicted next to the graph, and the error bars denote SD. Worms treated with 100 μ M cmp16 showed 1.6 times faster locomotion compared with DMSO-treated controls. Worms incubated with higher concentrations were not assayed (N.A.) due to compound precipitation and toxicity in the liquid cultures. (B) Time course graph plotting the number of axonal discontinuities in the GABAergic motor nervous system of synchronized worms treated with the Tau inhibitor cmp16 or 1% DMSO control, from L1 stage until the day of scoring (day 1, day 3 and day 5 of adulthood). Cmp16 treatment reduced the accumulation of neuronal morphological abnormalities. Error bars denote SEM from three repetitions of the experiment, with approximately 30 worms per group and time point. Two-way ANOVA with the Bonferroni correction was implemented for comparisons (* $P < 0.05$).

with a pro-aggregant F3 Δ K280 or with an anti-aggregant F3 Δ K280-PP fragment. These strains revealed significant phenotypic differences that will allow using them for modifier screening assays. These F3 fragments have been shown to differ only in their amyloidogenic propensity and not in other aspects, such as microtubule interaction (both have very poor binding) or phosphorylation patterns (both contain only a few phosphorylation sites in the repeat domain) (12,16). Consequently, this provides support that the toxicity which manifests itself through neuronal morphological abnormalities, loss of SNB-1 puncta and impaired mitochondrial transport correlates with the amyloidogenic potential of Tau moieties and this is in accordance with recent reports in mouse models (13).

Axonal transport of mitochondria is a vital process for neuronal physiology and it is not surprising that its perturbation is thought to contribute to the neurodegenerative demise (52,63–66). We probed axonal transport of mitochondria in our system with two approaches. First, we examined the localization of mitochondria along the axon of the DA9 tail neuron and found that there are proportionally less fluorescent puncta corresponding to tagged mitochondria in the distal axonal segment of the pro-aggregant strain. These mitochondrial accumulations that correspond to synapses made *en passant* along the DA9 neuron (54) suggest either a lack of supply of mitochondria to the most distal synapses, or they may be caused by a loss of synapses or axonal retraction. With the marker we used here we cannot distinguish between these possibilities, as we would need the co-expression of a soluble fluorescent protein to fill the axonal cytoplasm and discern its boundaries. However, the results obtained with the second method, time lapse imaging and tracking of moving mitochondria, support the interpretation that their transport is perturbed by the amyloidogenic Tau species. Although the instantaneous particle velocities are similar, the pausing frequencies in the

pro-aggregation animals show a significant increase. This is reminiscent of the differences between fast and slow axonal transport in mammalian neurons, which differ not by the motor-driven instantaneous speed, but by the intervening pauses (67). Many mitochondrial particles in these animals demonstrate a characteristic motion of short bursts of displacement followed by pauses, reminiscent of a traffic jam (68). We conclude that such a mitochondrial behaviour is unfavourable for the high energy demands of neurons.

The rapid occurrence of the neural toxicity phenotype already during development, and also its age-dependent progression, supports the notion that the accelerated formation of amyloidogenic oligomers within neurons is the causative toxicity factor. The robust locomotion defect that appears in our transgenic model makes this aspect a particularly suitable read-out for time- and cost-effective pharmacological or genetic screens to uncover specific modulators of Tau pathology. Several other neurodegeneration screens have been successfully performed before in *C. elegans*, as exemplified for Tau (22), amyloid-beta peptide (69,70), Huntingtin/polyQ (19,71) and spinal muscular atrophy (72) disease models. To demonstrate the value of our new model, we tested several compounds for which an efficacy against Tau aggregation has been suggested. These were MB, which was already tested in mouse models (56,73), BSc3094 and bb14, which demonstrated protective effects in cell culture models (57,74,75), and the ATPZ Tau inhibitor cmp16, which blocked Tau aggregation *in vitro* and has been shown to readily cross the blood–brain barrier of mice (33). We showed here that they are all capable of at least partially preventing or delaying Tau-mediated toxicity in *C. elegans*. At the biochemical level, we demonstrated a reduction of insoluble Tau after applying the compounds in liquid cultures. Concerning the bioavailability of the reported compounds, all of them have chemical structures such as benzene rings that

have been found enriched in molecules that can accumulate within *C. elegans* tissues (76). This lends support to our interpretation that these compounds reach the neurons of the worms and act on Tau species inhibiting their aggregation.

An important conclusion from this study is that, by inhibiting the aggregation process, neuronal damage can be thwarted. We achieved this in two ways: by expressing the F3Δ280-PP fragment, which does not allow accelerated aggregate formation, and by treating with compounds that have anti-aggregation capacities. This treatment is essentially effective if administered from the early larval stages onwards, to suppress even the initial formation of toxic oligomers. Actively preventing the aggregation process is a promising therapeutic avenue and encompasses a particularly active research field (75,77–80). Capitalizing on advances in structural and computational biology, researchers have recently developed non-natural amino acid inhibitors of Tau and polyQ aggregation (81,82). Moreover, the compound thioflavin-T, which is predominantly known as a staining reagent for aggregates, has been recently revisited and demonstrated to prevent widespread aggregation and proteotoxicity in worms (83). The fact that amyloidogenic intermediates share common structure (84) implies that compounds that are able to block the process in a non-protein-specific way can be effective in a wider range of protein folding disorders. In this study, we used MB, BSc3094 and bb14 as proof of principle and demonstrated that a new compound belonging to the ATPZ class can be protective against Tau aggregation-mediated toxicity. It would be interesting to know whether this compound has therapeutic potential by testing it in mouse models of tauopathies and, if proven effective, to promote it for clinical testing in an effort to curb the progression of this debilitating condition. Finally, this new *C. elegans* model of tauopathy can be exploited for high-throughput screening approaches to uncover novel modulators of neurodegeneration.

MATERIALS AND METHODS

Generation and maintenance of *C. elegans* strains

The following transgenic *C. elegans* strains were generated for this study: BR5270: *byIs161[Prab-3::F3ΔK280;Pmyo-2::mCherry]*, BR5271: *byIs162;[Prab-3::F3ΔK280(I277P)(I308P);Pmyo-2::mCherry]*, BR5944: *byIs193[Prab-3::F3ΔK280;Pmyo-2::mCherry]*, BR6516: *byIs194;[Prab-3::F3ΔK280(I277P)(I308P);Pmyo-2::mCherry]*, CK10: *bkIs10[Paex-3::h4R1 NTauV337M;Pmyo-2::gfp]* (provided by Brian Kraemer) (24), BR5485: *byIs161;bkIs10* (pro-aggregant line 1), BR5486: *byIs162;bkIs10* (anti-aggregant line 1), BR5706: *byIs193;bkIs10* (pro-aggregant line 2), BR6427: *byIs194;bkIs10* (anti-aggregant line 2), BR5625: *eri-1(mg366)IV;lin-15B(n744)X;byIs161;bkIs10* (pro-aggregant, neuronal RNAi-sensitized strain), BR5578: *eri-1(mg366)IV;lin-15B(n744)X;byIs162;bkIs10* (anti-aggregant, neuronal RNAi sensitized strain) and *juls73::[Punc-25::gfp]III* (provided by Erik Lundquist) (45), BR5674: *byIs162;bkIs10;juls73*, BR5707: *byIs161;bkIs10;juls73*, *nIs52::[Punc-47::snb-1::gfp]* (provided by Erik Jorgensen) (47), BR5792: *byIs161;bkIs10;nIs52*, BR5793: *byIs162;bkIs10;nIs52*, BR5960: *bkIs10;Ex1069[Pmyo-2::mCherry;Prab-3::F3ΔK280]*, BR5961: *bkIs10;Ex1070*

[Pmyo-2::mCherry;Prab-3::F3ΔK280(I277P)(I308P)] and *wyEx 2709::[Pitr-1::TOM-20^{1-54aa}::yfp;Podr-1::gfp]* (provided by Kang Shen) (54), BR6011: *byIs161;bkIs10;wyEx2709*, BR6012: *byIs162;bkIs10;wyEx2709*, BR6088: *byIs161;bkIs10;Ex[Punc-129::mCherry]*, BR6089: *byIs162;bkIs10;Ex[Punc-129::mCherry]* (provided by Stefan Eimer) and *jsIs609::[P-mec-4::MLS::gfp]*, BR6174: *byIs161;bkIs10;jsIs609*, BR6175: *byIs162;bkIs10;jsIs609*.

The following mutant strains were used in this study: BR4338: *eri-1(mg366)IV;lin-15B(n744)X* [sensitized strain for neuronal RNAi (44)], BR794: *lev-1(x21)IV*, NM791: *rab-3(js49)II* (as resistant controls for the aldicarb and levamisole assays).

General worm handling and generation of transgenic worms were performed according to standard procedures described previously (85). Worm cultures were maintained at 20°C unless otherwise mentioned. Integration of extra chromosomal arrays was achieved after subjecting L4 transgenic larvae to 30 Gy dosage of γ-irradiation and screening the F2 generation for clones that have 100% fluorescent marker penetrance. The stable lines obtained were subsequently backcrossed to laboratory N2 wild-type males for 10 rounds, to get rid of background mutations. The strains were typically thawed fresh from −80°C glycerol stocks every 4–5 months, to avoid (epi)genetic drift.

Sequential extraction of proteins

Synchronized worms were washed off NGM plates with M9 buffer. Dead animals and bacteria were removed by flotation on a 30% sucrose solution. The entire extraction procedure was carried out on ice and centrifugation steps were at 4°C except for the last step with 70% FA, which was performed at room temperature. To extract the different Tau fractions (86), worm pellets—after sucrose separation—were directly resuspended in an equal amount (w/v) of high-salt RAB buffer [100 mM 2-(N-morpholino) ethanesulfonic acid (MES), 1 mM EGTA, 0.5 mM MgSO₄, 20 mM NaF]. Worms were lysed by sonication (6 × 10 s, 10 s break) on ice, and homogenates were centrifuged at 40 000g for 40 min. The supernatant constitutes the RAB fraction. The pellet was re-extracted with 1 M sucrose in RAB buffer and centrifuged for 20 min at 40 000g, and the supernatant was discarded. The pellet was extracted with RIPA buffer (150 mM NaCl, 1% Nonidet P-40, 0.5% deoxycholate, 0.1% SDS, 50 mM Tris, pH 8.0) and centrifuged at 40 000g for 20 min. The supernatant is the RIPA fraction. The pellet, after a brief washing with RIPA buffer, was extracted with 70% FA and centrifuged at 13 000g for 15 min. The supernatant is the FA fraction. All buffers contained Complete Protease Inhibitor Mixture 3× (Sigma-Aldrich P8340, Hamburg, Germany) and 0.5 mM PMSF.

Immunohistochemistry

Antibody staining was done as described previously (87). To detect Tau and F3 fragment together, the K9JA antibody was used at 1:20 000 dilution. An Alexa 488 goat anti-rabbit antibody (1:5000) was used for detection. Imaging was

performed with a Nikon A1 CLEM confocal through a Plan Apo VC 60× Oil DIC N2 objective, using a 488 nm laser at 14% power and 120 PMT value.

Thioflavin S staining

ThS (Sigma-Aldrich, Hamburg, Germany) was used to stain aggregates as described previously (34,35), with the modification that the fixation procedure was performed according to the antibody-staining protocol to increase the permeability of the cuticle. ThS signal was visualized with a Plan Apo VC 60× Oil DIC N2 objective and a 488 nm laser at 25% power, 110 PMT. Z-stacks were acquired with 1.5× zoom, and the region between the first and the second pharyngeal bulb (where the nerve ring is located) was examined for the presence of ThS-positive staining. For quantification, the acquired images were thresholded at 600 arbitrary intensity units, and spots were counted using the NIS Elements 3.0 software (Nikon).

Live imaging

Images were acquired with a Nikon A1 CLEM confocal and a Nikon A1 CCD camera. Within each group of reporter strains, the laser power and PMT values were kept constant, always avoiding oversaturation. For immobilizing the animals on the slides, a suspension of 1% (v/v) solution of 0.1 µm diameter polystyrene beads (Polysciences Europe, Eppelheim, Germany) was used without the need for anaesthetics as described in Wasserman *et al.* (88). The worms become immobilized due to their inability to surpass friction between the beads and the underlying 8% agarose pad. Z-stacks of the posterior dorsal neural cord of *Punc-47::snb-1::gfp* reporter strains were collected with 30% GFP laser power, 150 PMT with a Plan Apo VC 60× WI DIC N2 objective and a 2× zoom factor. Imaging of the DA9 tail neuron to visualize the mitochondrial marker *Pitr-1::TOM-20^{1-54aa}::yfp* was performed with 30% power of a 514.5 nm laser, 140 PMT and a 1.68 zoom factor of a Plan Apo VC 60× WI DIC N2 objective. For time lapse imaging of the *Pmec-4::MLS:gfp* mitochondrial marker, a 488 nm laser at 13.5% power and 140 PMT was used, with a 1.5× zoom factor of a Plan Apo VC 60× WI DIC N2 objective and 1.3 airy unit pinhole size. For each time lapse video, an axonal region of the PLML or PLMR neuron was selected that could be observed in a single plane, and one frame was acquired every 2 s, for 8–10 min.

Quantitation of synapses

In all sampled animals, the dorsal cord segment above the posterior gonadal arm was imaged and Z-stacks were acquired for comparisons. The resulting files were analysed with the NIS Elements 3.0 software (Nikon). A region of interest was drawn around the neural cord, and a threshold was set at 600 intensity units, as well as at 0.5 µm diameter to select fluorescent puncta. Then the puncta number and the mean intensity for each punctum were calculated. The length of each imaged cord was measured as well, in order to extract the ratio of number of synapses per 50 µm. For the compilation of the

cumulative panels in Figure 4 and Supplementary Material, Figure S4, the ImageJ 'Straighten' function was applied to straighten the cords, using a line width of 50 pixels, and then the 'Threshold' function was performed, selecting the default B&W method and setting the threshold level at 600 arbitrary intensity units.

Aldicarb and levamisole assays

We performed aldicarb and levamisole assays as previously described (50,89), using plates with 1 mM aldicarb (Supelco Germany GmbH) and 0.2 mM levamisole (Fluka Analytical, Germany), respectively. The scoring of animals for paralysis was performed blind to the genotype with 30 animals per strains and the experiment was repeated three times.

Compound treatment

The compounds were applied in liquid culture in the 96-well plate format. OP50 bacteria were grown overnight at 37°C in LB medium, collected by centrifugation, frozen at –80°C and then resuspended in nematode S-medium (90), so that the OD₅₉₅ was 1.5 in four times diluted samples. Twenty microlitres of this suspension were added per well. Synchronized L1 larvae were resuspended in S-medium supplemented with 10 µg/ml fungizone and 10 µg/ml cholesterol (both from Sigma-Aldrich) in an appropriate volume so that there is approximately one worm per microlitre, and 20 µl was added per well. Finally, 40 µl of a 2× compound solution in S-medium was added per well, reaching a total volume of 80 µl. The final concentrations used in the experiments were 100 µM cmp16, 50 µM BSc3094 and 50 µM bb14 each in 1% DMSO. Worms cultured in 1% DMSO served as treatment control. Water-soluble MB was used at a final concentration of 25 µM, with H₂O as control. Plates were sealed with parafilm and incubated at 20°C for 4 days. The worms were then transferred to empty NGM plates to measure the locomotion speed by acquiring and analysing movies as described in Supplementary Material, Methods. For biochemical characterization, the same procedure was scaled up for the six-well plate format, having 5 ml of final volume added per well. Synchronized L1 larvae were added to the wells containing the compounds of interest, and when the worms became L4 larvae, 75 µM FuDR was added to prevent spawning of progeny. The worms were allowed to grow at 20°C with constant shaking until harvested for protein extraction.

Statistical analysis

For statistical analyses, the software GraphPad Prism 4.03 was used (GraphPad Software, Inc., LaJolla, CA, USA). One-way ANOVA was used for comparisons between three or more groups, with Tukey's *post hoc* test for comparisons between all groups. In case of non-parametric distributions, the Kruskal–Wallis ANOVA with Dunn's *post hoc* test was used. For the time course experiments with the drug treatments, two-way ANOVA with the Bonferroni correction was applied. For the comparison of mitochondrial distributions, Yates's χ^2 test was used. In all graphs, the error bars depict

the SD, unless otherwise mentioned. Differences at $P < 0.05$ were accepted as statistically significant.

SUPPLEMENTARY MATERIAL

Supplementary Material is available at *HMG* online.

AUTHORS' CONTRIBUTIONS

C.F. created the transgenic strains that were used in this study (excluding *jsIs609* and the ones provided by others as defined in Materials and Methods), performed all the imaging and phenotypic characterization experiments and co-wrote the paper. G.J.P. performed the cloning and all the biochemical experiments and contributed the relevant parts of Materials and Methods and Results sections. S.P.K. created the *jsIs609* strain in Michael L. Nonet's laboratory. E.M., E.-M.M., E.S. and R.B. proposed and supervised the study, co-wrote the paper and received the financial means to accomplish it.

ACKNOWLEDGEMENTS

We are grateful to the following people for providing strains and reagents crucial for this study: Brian Kraemer (VA Puget Sound Health Care System, Seattle, USA), Yishi Jin (University of California, San Diego, USA), Stefan Eimer (European Neuroscience Institute, Göttingen, Germany), Kang Shen (Stanford University, USA), Erik Lundquist (University of Kansas, USA), Erik Jorgensen (University of Utah, USA), Daniele Bano (DZNE, Bonn, Germany) and Peter Davies (Feinstein Institute for Medical Research, North Shore LIJ, USA). Senexis Limited (Babraham Research Campus, Cambridge, UK) kindly provided the Tau inhibitor cmp16. We also thank Malikmohamed Yousuf (ZBSA, Freiburg, Germany), Ursula Schäffer (ZBSA, Freiburg, Germany) and Yipeng Wang (DZNE, Bonn, Germany) for helpful discussions and comments.

Conflict of Interest statement. None declared.

FUNDING

E.M., E.-M.M. and R.B. were supported by MEMOSAD, a collaborative project receiving funds from the European Community's Seventh Framework Programme (FP7/2007-2011 under Grant Agreement No. 200611). Additional support was provided by DFB SFB592, BIOS and FRIAS (The German Excellence Initiative) to R.B. and Metlife Foundation (to E.M. and E.-M.M.). S.P.K. received funds from a grant of the Department of Biotechnology, Government of India.

REFERENCES

- Ballatore, C., Lee, V.M.-Y. and Trojanowski, J.Q. (2007) Tau-mediated neurodegeneration in Alzheimer's disease and related disorders. *Nat. Rev. Neurosci.*, **8**, 663–672.
- Congdon, E.E. and Duff, K.E. (2008) Is tau aggregation toxic or protective? *J. Alzheimers Dis.*, **14**, 453–457.
- Iqbal, K., Wang, X., Blanchard, J., Liu, F., Gong, C.-X. and Grundke-Iqbal, I. (2010) Alzheimer's disease neurofibrillary degeneration: pivotal and multifactorial. *Biochem. Soc. Trans.*, **38**, 962–966.
- Obulesu, M., Venu, R. and Somashekhar, R. (2011) Tau mediated neurodegeneration: an insight into Alzheimer's disease pathology. *Neurochem. Res.*, **36**, 1329–1335.
- Reiniger, L., Lukic, A., Linehan, J., Rudge, P., Collinge, J., Mead, S. and Brandner, S. (2011) Tau, prions and Abeta: the triad of neurodegeneration. *Acta Neuropathol.*, **121**, 5–20.
- Morris, M., Maeda, S., Vossell, K. and Mucke, L. (2011) The many faces of Tau. *Neuron*, **70**, 410–426.
- Spires-Jones, T.L., Kopeikina, K.J., Koffie, R.M., de Calignon, A. and Hyman, B.T. (2011) Are tangles as toxic as they look? *J. Mol. Neurosci.*, **45**, 438–444.
- Caughey, B. and Lansbury, P.T. (2003) Protofibrils, pores, fibrils, and neurodegeneration: separating the responsible protein aggregates from the innocent bystanders. *Annu. Rev. Neurosci.*, **26**, 267–298.
- Uversky, V.N. (2010) Mysterious oligomerization of the amyloidogenic proteins. *FEBS J.*, **277**, 2940–2953.
- Mocanu, M.-M., Nissen, A., Eckermann, K., Khlistunova, I., Biernat, J., Drexler, D., Petrova, O., Schonig, K., Bujard, H., Mandelkow, E. *et al.* (2008) The potential for beta-structure in the repeat domain of Tau protein determines aggregation, synaptic decay, neuronal loss, and coassembly with endogenous Tau in inducible mouse models of tauopathy. *J. Neurosci.*, **28**, 737–748.
- Eckermann, K., Mocanu, M.-M., Khlistunova, I., Biernat, J., Nissen, A., Hofmann, A., Schöning, K., Bujard, H., Haemisch, A., Mandelkow, E. *et al.* (2007) The beta-propensity of Tau determines aggregation and synaptic loss in inducible mouse models of tauopathy. *J. Biol. Chem.*, **282**, 31755–31765.
- Khlistunova, I., Biernat, J., Wang, Y., Pickhardt, M., von Bergen, M., Gazova, Z., Mandelkow, E. and Mandelkow, E.-M. (2006) Inducible expression of Tau repeat domain in cell models of tauopathy: aggregation is toxic to cells but can be reversed by inhibitor drugs. *J. Biol. Chem.*, **281**, 1205–1214.
- Sydow, A., Van der Jeugd, A., Zheng, F., Ahmed, T., Balschun, D., Petrova, O., Drexler, D., Zhou, L., Rune, G., Mandelkow, E. *et al.* (2011) Tau-induced defects in synaptic plasticity, learning, and memory are reversible in transgenic mice after switching off the toxic tau mutant. *J. Neurosci.*, **31**, 2511–2525.
- Santacruz, K., Lewis, J., Spire, T., Paulson, J., Kotilinek, L., Ingelsson, M., Guimaraes, A., DeTure, M., Ramsden, M., McGowan, E. *et al.* (2005) Tau suppression in a neurodegenerative mouse model improves memory function. *Science*, **309**, 476–481.
- von Bergen, M., Barghorn, S., Li, L., Marx, A., Biernat, J., Mandelkow, E.M. and Mandelkow, E. (2001) Mutations of tau protein in frontotemporal dementia promote aggregation of paired helical filaments by enhancing local beta-structure. *J. Biol. Chem.*, **276**, 48165–48174.
- Wang, Y.P., Biernat, J., Pickhardt, M., Mandelkow, E. and Mandelkow, E.-M. (2007) Stepwise proteolysis liberates tau fragments that nucleate the Alzheimer-like aggregation of full-length tau in a neuronal cell model. *Proc. Natl Acad. Sci. USA*, **104**, 10252–10257.
- Wang, Y., Martinez-Vicente, M., Kruger, U., Kaushik, S., Wong, E., Mandelkow, E.M., Cuervo, A.M. and Mandelkow, E. (2009) Tau fragmentation, aggregation and clearance: the dual role of lysosomal processing. *Hum. Mol. Genet.*, **18**, 4153–4170.
- Artal-Sanz, M., de Jong, L. and Tavernarakis, N. (2006) *Caenorhabditis elegans*: a versatile platform for drug discovery. *Biotechnol. J.*, **1**, 1405–1418.
- Voisine, C., Varma, H., Walker, N., Bates, E.A., Stockwell, B.R. and Hart, A.C. (2007) Identification of potential therapeutic drugs for huntington's disease using *Caenorhabditis elegans*. *PLoS ONE*, **2**, e504.
- Giacomotto, J. and Segalat, L. (2010) High-throughput screening and small animal models, where are we? *Br. J. Pharmacol.*, **160**, 204–216.
- Braungart, E., Gerlach, M., Riederer, P., Baumeister, R. and Hoener, M.C. (2004) *Caenorhabditis elegans* MPP+ model of Parkinson's disease for high-throughput drug screenings. *Neurodegener. Dis.*, **1**, 175–183.
- Kraemer, B.C. and Schellenberg, G.D. (2007) SUT-1 enables tau-induced neurotoxicity in *C. elegans*. *Hum. Mol. Genet.*, **16**, 1959–1971.
- Kraemer, B.C., Burgess, J.K., Chen, J.H., Thomas, J.H. and Schellenberg, G.D. (2006) Molecular pathways that influence human tau-induced pathology in *Caenorhabditis elegans*. *Hum. Mol. Genet.*, **15**, 1483–1496.
- Kraemer, B.C., Zhang, B., Leverenz, J.B., Thomas, J.H., Trojanowski, J.Q. and Schellenberg, G.D. (2003) Neurodegeneration and defective

- neurotransmission in a *Caenorhabditis elegans* model of tauopathy. *Proc. Natl Acad. Sci. USA*, **100**, 9980–9985.
25. Brandt, R., Gergou, A., Wacker, I., Fath, T. and Hutter, H. (2009) A *Caenorhabditis elegans* model of tau hyperphosphorylation: induction of developmental defects by transgenic overexpression of Alzheimer's disease-like modified tau. *Neurobiol. Aging*, **30**, 22–33.
 26. Guthrie, C.R., Schellenberg, G.D. and Kraemer, B.C. (2009) SUT-2 potentiates tau-induced neurotoxicity in *Caenorhabditis elegans*. *Hum. Mol. Genet.*, **18**, 1825–1838.
 27. Miyasaka, T., Ding, Z., Gengyo-Ando, K., Oue, M., Yamaguchi, H., Mitani, S. and Ihara, Y. (2005) Progressive neurodegeneration in *C. elegans* model of tauopathy. *Neurobiol. Dis.*, **20**, 372–383.
 28. Wheeler, J.M., Guthrie, C.R. and Kraemer, B.C. (2010) The role of MSUT-2 in tau neurotoxicity: a target for neuroprotection in tauopathy? *Biochem. Soc. Trans.*, **38**, 973–976.
 29. Goedert, M., Baur, C.P., Ahringer, J., Jakes, R., Hasegawa, M., Spillantini, M.G., Smith, M.J. and Hill, F. (1996) PTL-1, a microtubule-associated protein with tau-like repeats from the nematode *Caenorhabditis elegans*. *J. Cell Sci.*, **109**, 2661–2672.
 30. Gordon, P., Hingula, L., Krasny, M.L., Swienkowski, J.L., Pokrywka, N.J. and Raley-Susman, K.M. (2008) The invertebrate microtubule-associated protein PTL-1 functions in mechanosensation and development in *Caenorhabditis elegans*. *Dev. Genes Evol.*, **218**, 541–551.
 31. Taniguchi, S., Suzuki, N., Masuda, M., Hisanaga, S., Iwatsubo, T., Goedert, M. and Hasegawa, M. (2005) Inhibition of heparin-induced tau filament formation by phenothiazines, polyphenols, and porphyrins. *J. Biol. Chem.*, **280**, 7614–7623.
 32. Wischik, C.M., Edwards, P.C., Lai, R.Y., Roth, M. and Harrington, C.R. (1996) Selective inhibition of Alzheimer disease-like tau aggregation by phenothiazines. *Proc. Natl Acad. Sci. USA*, **93**, 11213–11218.
 33. Ballatore, C., Brunden, K.R., Piscitelli, F., James, M.J., Crowe, A., Yao, Y., Hyde, E., Trojanowski, J.Q., Lee, V.M. and Smith, A.B. III (2010) Discovery of brain-penetrant, orally bioavailable aminothienopyridazine inhibitors of tau aggregation. *J. Med. Chem.*, **53**, 3739–3747.
 34. Link, C.D. (1995) Expression of human beta-amyloid peptide in transgenic *Caenorhabditis elegans*. *Proc. Natl Acad. Sci. USA*, **92**, 9368–9372.
 35. Minniti, A.N., Rebolledo, D.L., Grez, P.M., Fadic, R., Aldunate, R., Volitakis, I., Cherny, R.A., Opazo, C., Masters, C., Bush, A.I. *et al.* (2009) Intracellular amyloid formation in muscle cells of Abeta-transgenic *Caenorhabditis elegans*: determinants and physiological role in copper detoxification. *Mol. Neurodegener.*, **4**, 2.
 36. Iqbal, K., Alonso Adel, C., Chen, S., Chohan, M.O., El-Akkad, E., Gong, C.X., Khatoon, S., Li, B., Liu, F., Rahman, A. *et al.* (2005) Tau pathology in Alzheimer disease and other tauopathies. *Biochim. Biophys. Acta*, **1739**, 198–210.
 37. Kosik, K.S. and Shimura, H. (2005) Phosphorylated tau and the neurodegenerative foldopathies. *Biochim. Biophys. Acta*, **1739**, 298–310.
 38. Augustinack, J.C., Schneider, A., Mandelkow, E.M. and Hyman, B.T. (2002) Specific tau phosphorylation sites correlate with severity of neuronal cytopathology in Alzheimer's disease. *Acta Neuropathol.*, **103**, 26–35.
 39. Paquet, D., Bhat, R., Sydow, A., Mandelkow, E.M., Berg, S., Hellberg, S., Falting, J., Distel, M., Koster, R.W., Schmid, B. *et al.* (2009) A zebrafish model of tauopathy allows *in vivo* imaging of neuronal cell death and drug evaluation. *J. Clin. Invest.*, **119**, 1382–1395.
 40. Kosmidis, S., Grammenoudi, S., Papanikolopoulou, K. and Skoulakis, E.M. (2010) Differential effects of Tau on the integrity and function of neurons essential for learning in *Drosophila*. *J. Neurosci.*, **30**, 464–477.
 41. Papanikolopoulou, K., Kosmidis, S., Grammenoudi, S. and Skoulakis, E.M. (2010) Phosphorylation differentiates tau-dependent neuronal toxicity and dysfunction. *Biochem. Soc. Trans.*, **38**, 981–987.
 42. Ambegaokar, S.S. and Jackson, G.R. (2011) Functional genomic screen and network analysis reveal novel modifiers of tauopathy dissociated from tau phosphorylation. *Hum. Mol. Genet.*, **20**, 4947–4977.
 43. Talmat-Amar, Y., Arribat, Y., Redt-Clouet, C., Feuillette, S., Bouge, A.L., Lecourtois, M. and Parmentier, M.L. (2011) Important neuronal toxicity of microtubule-bound Tau *in vivo* in *Drosophila*. *Hum. Mol. Genet.*, **20**, 3738–3745.
 44. Samuelson, A.V., Klimczak, R.R., Thompson, D.B., Carr, C.E. and Ruvkun, G. (2007) Identification of *Caenorhabditis elegans* genes regulating longevity using enhanced RNAi-sensitive strains. *Cold Spring Harb. Symp. Quant. Biol.*, **72**, 489–497.
 45. Lundquist, E.A., Reddien, P.W., Hartwig, E., Horvitz, H.R. and Bargmann, C.I. (2001) Three *C. elegans* Rac proteins and several alternative Rac regulators control axon guidance, cell migration and apoptotic cell phagocytosis. *Development*, **128**, 4475–4488.
 46. Schultheis, C., Brauner, M., Liewald, J.F. and Gottschalk, A. (2011) Optogenetic analysis of GABAB receptor signaling in *Caenorhabditis elegans* motor neurons. *J. Neurophysiol.*, **106**, 817–827.
 47. Weimer, R.M., Richmond, J.E., Davis, W.S., Hadwiger, G., Nonet, M.L. and Jorgensen, E.M. (2003) Defects in synaptic vesicle docking in unc-18 mutants. *Nat. Neurosci.*, **6**, 1023–1030.
 48. Nonet, M.L. (1999) Visualization of synaptic specializations in live *C. elegans* with synaptic vesicle protein-GFP fusions. *J. Neurosci. Methods*, **89**, 33–40.
 49. Jin, Y. (2002) Synaptogenesis: insights from worm and fly. *Curr. Opin. Neurobiol.*, **12**, 71–79.
 50. Mahoney, T.R., Luo, S. and Nonet, M.L. (2006) Analysis of synaptic transmission in *Caenorhabditis elegans* using an aldicarb-sensitivity assay. *Nat. Protoc.*, **1**, 1772–1777.
 51. Lasagna-Reeves, C.A., Castillo-Carranza, D.L., Sengupta, U., Clos, A.L., Jackson, G.R. and Kaye, R. (2011) Tau oligomers impair memory and induce synaptic and mitochondrial dysfunction in wild-type mice. *Mol. Neurodegener.*, **6**, 39.
 52. Schon, E.A. and Przedborski, S. (2011) Mitochondria: the next (neurode)generation. *Neuron*, **70**, 1033–1053.
 53. Thies, E. and Mandelkow, E.M. (2007) Misrouting of tau in neurons causes degeneration of synapses that can be rescued by the kinase MARK2/Par-1. *J. Neurosci.*, **27**, 2896–2907.
 54. Klassen, M.P., Wu, Y.E., Maeder, C.I., Nakae, I., Cueva, J.G., Lehrman, E.K., Tada, M., Gengyo-Ando, K., Wang, G.J., Goodman, M. *et al.* (2010) An Arf-like small G protein, ARL-8, promotes the axonal transport of presynaptic cargoes by suppressing vesicle aggregation. *Neuron*, **66**, 710–723.
 55. Deiana, S., Harrington, C.R., Wischik, C.M. and Riedel, G. (2009) Methylthioninium chloride reverses cognitive deficits induced by scopolamine: comparison with rivastigmine. *Psychopharmacology*, **202**, 53–65.
 56. Schirmer, R.H., Adler, H., Pickhardt, M. and Mandelkow, E. (2011) 'Lest we forget you - methylene blue ...'. *Neurobiol. Aging*, **32**, 2325.e7–2325.e16.
 57. Pickhardt, M., Larbig, G., Khlistunova, I., Coksezen, A., Meyer, B., Mandelkow, E.-M., Schmidt, B. and Mandelkow, E. (2007) Phenylthiazolyl-hydrazide and its derivatives are potent inhibitors of tau aggregation and toxicity *in vitro* and in cells. *Biochemistry*, **46**, 10016–10023.
 58. Earls, L.R., Hacker, M.L., Watson, J.D. and Miller, D.M. III (2010) Coenzyme Q protects *Caenorhabditis elegans* GABA neurons from calcium-dependent degeneration. *Proc. Natl Acad. Sci. USA*, **107**, 14460–14465.
 59. Ben-Zvi, A., Miller, E.A. and Morimoto, R.I. (2009) Collapse of proteostasis represents an early molecular event in *Caenorhabditis elegans* aging. *Proc. Natl Acad. Sci. USA*, **106**, 14914–14919.
 60. David, D.C., Ollikainen, N., Trinidad, J.C., Cary, M.P., Burlingame, A.L. and Kenyon, C. (2010) Widespread protein aggregation as an inherent part of aging in *C. elegans*. *PLoS Biol.*, **8**, e1000450.
 61. Dillin, A. and Cohen, E. (2011) Ageing and protein aggregation-mediated disorders: from invertebrates to mammals. *Philos. Trans. R. Soc. B Biol. Sci.*, **366**, 94–98.
 62. Cohen, E. and Dillin, A. (2008) The insulin paradox: aging, proteotoxicity and neurodegeneration. *Nat. Rev. Neurosci.*, **9**, 759–767.
 63. De Vos, K., Grierson, A., Ackerley, S. and Miller, C. (2008) Role of axonal transport in neurodegenerative diseases. *Annu. Rev. Neurosci.*, **31**, 151–173.
 64. Ittner, L.M., Fath, T., Ke, Y.D., Bi, M., van Eersel, J., Li, K.M., Gunning, P. and Götz, J. (2008) Parkinsonism and impaired axonal transport in a mouse model of frontotemporal dementia. *Proc. Natl Acad. Sci. USA*, **105**, 15997–16002.
 65. Roy, S., Zhang, B., Lee, V.M.-Y. and Trojanowski, J.Q. (2005) Axonal transport defects: a common theme in neurodegenerative diseases. *Acta Neuropathol.*, **109**, 5–13.
 66. Stamer, K., Vogel, R., Thies, E., Mandelkow, E. and Mandelkow, E.M. (2002) Tau blocks traffic of organelles, neurofilaments, and APP vesicles in neurons and enhances oxidative stress. *J. Cell Biol.*, **156**, 1051–1063.

67. Brown, A. (2003) Axonal transport of membranous and nonmembranous cargoes: a unified perspective. *J. Cell Biol.*, **160**, 817–821.
68. Mandelkow, E.M., Thies, E., Trinczek, B., Biernat, J. and Mandelkow, E. (2004) MARK/PAK1 kinase is a regulator of microtubule-dependent transport in axons. *J. Cell Biol.*, **167**, 99–110.
69. Wu, Y., Wu, Z., Butko, P., Christen, Y., Lambert, M.P., Klein, W.L., Link, C.D. and Luo, Y. (2006) Amyloid-beta-induced pathological behaviors are suppressed by Ginkgo biloba extract EGb 761 and ginkgolides in transgenic *Caenorhabditis elegans*. *J. Neurosci.*, **26**, 13102–13113.
70. Diomedea, L., Cassata, G., Fiordaliso, F., Salio, M., Ami, D., Natalello, A., Doglia, S.M., De Luigi, A. and Salmona, M. (2010) Tetracycline and its analogues protect *Caenorhabditis elegans* from beta amyloid-induced toxicity by targeting oligomers. *Neurobiol. Dis.*, **40**, 424–431.
71. Silva, M.C., Fox, S., Beam, M., Thakkar, H., Amaral, M.D. and Morimoto, R.I. (2011) A genetic screening strategy identifies novel regulators of the proteostasis network. *PLoS Genet.*, **7**, e1002438.
72. Sleight, J.N., Buckingham, S.D., Esmaili, B., Viswanathan, M., Cuppen, E., Westlund, B.M. and Sattelle, D.B. (2011) A novel *Caenorhabditis elegans* allele, *smn-1(cb131)*, mimicking a mild form of spinal muscular atrophy, provides a convenient drug screening platform highlighting new and pre-approved compounds. *Hum. Mol. Genet.*, **20**, 245–260.
73. Medina, D.X., Caccamo, A. and Oddo, S. (2011) Methylene blue reduces abeta levels and rescues early cognitive deficit by increasing proteasome activity. *Brain Pathol.*, **21**, 140–149.
74. Bulic, B., Pickhardt, M., Khlistunova, I., Biernat, J., Mandelkow, E.-M., Mandelkow, E. and Waldmann, H. (2007) Rhodanine-based tau aggregation inhibitors in cell models of tauopathy. *Angew. Chem. Int. Ed. Engl.*, **46**, 9215–9219.
75. Bulic, B., Pickhardt, M., Mandelkow, E.-M. and Mandelkow, E. (2010) Tau protein and tau aggregation inhibitors. *Neuropharmacology*, **59**, 276–289.
76. Burns, A.R., Wallace, I.M., Wildenhain, J., Tyers, M., Giaever, G., Bader, G.D., Nislow, C., Cutler, S.R. and Roy, P.J. (2010) A predictive model for drug bioaccumulation and bioactivity in *Caenorhabditis elegans*. *Nat. Chem. Biol.*, **6**, 549–557.
77. Cho, J.E. and Kim, J.R. (2011) Recent approaches targeting beta-amyloid for therapeutic intervention of Alzheimer's disease. *Recent Patents CNS Drug Discov.*, **6**, 222–233.
78. Schneider, A. and Mandelkow, E. (2008) Tau-based treatment strategies in neurodegenerative diseases. *Neurotherapeutics*, **5**, 443–457.
79. Voisine, C., Pedersen, J.S. and Morimoto, R.I. (2010) Chaperone networks: tipping the balance in protein folding diseases. *Neurobiol. Dis.*, **40**, 12–20.
80. Sirangelo, I. and Irace, G. (2010) Inhibition of aggregate formation as therapeutic target in protein misfolding diseases: effect of tetracycline and trehalose. *Expert Opin. Ther. Targets*, **14**, 1311–1321.
81. Landau, M., Sawaya, M.R., Faull, K.F., Laganowsky, A., Jiang, L., Sievers, S.A., Liu, J., Barrio, J.R. and Eisenberg, D. (2011) Towards a pharmacophore for amyloid. *PLoS Biol.*, **9**, e1001080.
82. Sievers, S.A., Karanickolas, J., Chang, H.W., Zhao, A., Jiang, L., Zirafi, O., Stevens, J.T., Münch, J., Baker, D. and Eisenberg, D. (2011) Structure-based design of non-natural amino-acid inhibitors of amyloid fibril formation. *Nature*, **475**, 96–100.
83. Alavez, S., Vantipalli, M.C., Zucker, D.J., Klang, I.M. and Lithgow, G.J. (2011) Amyloid-binding compounds maintain protein homeostasis during ageing and extend lifespan. *Nature*, **472**, 226–229.
84. Kayed, R., Head, E., Thompson, J.L., McIntire, T.M., Milton, S.C., Cotman, C.W. and Glabe, C.G. (2003) Common structure of soluble amyloid oligomers implies common mechanism of pathogenesis. *Science*, **300**, 486–489.
85. Nyamsuren, O., Faggionato, D., Loch, W., Schulze, E. and Baumeister, R. (2007) A mutation in CHN-1/CHIP suppresses muscle degeneration in *Caenorhabditis elegans*. *Dev. Biol.*, **312**, 193–202.
86. Ishihara, T., Hong, M., Zhang, B., Nakagawa, Y., Lee, M.K., Trojanowski, J.Q. and Lee, V.M. (1999) Age-dependent emergence and progression of a tauopathy in transgenic mice overexpressing the shortest human tau isoform. *Neuron*, **24**, 751–762.
87. Sandoval, G.M., Duerr, J.S., Hodgkin, J., Rand, J.B. and Ruvkun, G. (2006) A genetic interaction between the vesicular acetylcholine transporter VACHT/UNC-17 and synaptobrevin/SNB-1 in *C. elegans*. *Nat. Neurosci.*, **9**, 599–601.
88. Wasserman, S.M., Beverly, M., Bell, H.W. and Sengupta, P. (2011) Regulation of response properties and operating range of the AFD thermosensory neurons by cGMP signaling. *Curr. Biol.*, **21**, 353–362.
89. Gottschalk, A., Almedom, R.B., Schedletsky, T., Anderson, S.D., Yates, J.R. III and Schafer, W.R. (2005) Identification and characterization of novel nicotinic receptor-associated proteins in *Caenorhabditis elegans*. *EMBO J.*, **24**, 2566–2578.
90. Wood, W.B. (1988) Determination of pattern and fate in early embryos of *Caenorhabditis elegans*. *Dev. Biol.*, **5**, 57–78.

Acknowledgment

First of all, I would like to express my sincere thanks and regards to Prof. Dr. Eckhard Mandelkow for giving me an opportunity to conduct my Ph.D. thesis under his captivating, honest and able supervision. I sincerely thank Dr. Eva Maria Mandelkow for her able guidance, encouragement and fruitful discussions throughout this work. I wish to express my deep sense of gratitude to both Dr. Eckhard Mandelkow and to Dr. Eva Maria Mandelkow who inspite of their busy schedule, guided me and provided all the required facilities in the institute for successful completion of this work.

My earnest and deepest gratitude to Dr. Jacek Biernat for his generous support, technical advice and help during this work. I sincerely acknowledge his supportive advice. I express my gratitude to Dr. Alexander Marx, Dr. Katharina Tepper, Dr. Kevin Flynn, Dr. Marcus Pickhardt, Dr. Thomas Timm and Dr. Yipeng Wang for their interest, valuable hints, technical advice and help during this work.

A big thanks to Prof. Ralf Baumeister, Dr. Enrico Schmidt and Chronis Fatouros for their excellent and precious collaboration.

Special thanks to Dr. Satish Kumar, Dr. Subashchandrabose Chinnathambi, Dr. Syed Mubarak Hussain, Hans Zempel and Dr. Yatender Kumar for providing a stimulating and fun environment in which to learn and grow. Their companionship during the coffee sessions is something unforgettable.

Special thanks to Dr. Chanakya Nugoor, Dr. Sarvanan Paneerselvam, Dr. Sadasivam Jaganathan, and Dr Yusuf Akhtar for being great pals.

I also thank Sabrina Hubschmann, Ilka Lindner, and Julia Ludke for providing a great and fun environment.

I wish to thank my entire extended family and friends for providing a loving environment for me.

Lastly, and most importantly, I wish to thank my parents. They bore me, raised me, supported me, taught me, and loved me. To them I dedicate this thesis.

Pir Ghulam Jeelani

Declaration (Erklärung)

I declare that I have carried out this thesis by myself and have not used external help except where explicitly indicated. This thesis is not submitted to any other university. I did not make any earlier attempt to submit this work as a doctoral thesis.

Pir Ghulam Jeelani

October, 2012

Hamburg

Hiermit erkläre ich, dass ich die vorliegende Arbeit selbständig und ohne fremde Hilfe verfasst, andere als die angegebenen Quellen und Hilfsmittel nicht benutzt und die den verwendeten Werken wörtlich oder inhaltlich entnommenen Stellen als solche kenntlich gemacht habe. Ferner versichere ich, dass ich diese Dissertation noch an keiner anderen Universität eingereicht habe, um ein Promotionsverfahren eröffnen zu lassen. Hiermit erkläre ich auch, dass ich keine anderen früheren Versuche gemacht habe, die Arbeit zur Promotion einzureichen.

Pir Ghulam Jeelani

Oktober, 2012

Hamburg

German Center for Neurodegenerative Diseases (DZNE)

Ludwig-Erhard-Allee 2

53175 Bonn

05th October, 2012

Dr. Kevin Flynn

To whom so ever it may concern,

This letter is to certify that as a native English speaker I have read the PhD thesis entitled "*Caenorhabditis elegans* model of Tauopathy". This thesis is to be submitted to the University of Hamburg by Pir Ghulam Jeelani.

Yours Sincerely,



Kevin Flynn